UNIVERSIDADE D
COIMBRA

Thiago Brazeiro Carlos

Experimental and Numerical Analysis on the Structural Behaviour of RC Beams Strengthened with CFRP Laminates Under Fire Conditions

Tese de Doutoramento em Engenharia de Segurança ao Incêndio, orientada pelo Professor Doutor João Paulo Correia Rodrigues, pelo Professor Doutor Rogério Cattelan Antocheves de Lima e pelo Doutor Dhionis Dhima e apresentada ao Departamento de Engenharia Civil da Faculdade de Ciências e Tecnologia da Universidade de Coimbra.

Abril de 2019

UNIVERSIDADE D
COIMBRA

Thiago Brazeiro Carlos

EXPERIMENTAL AND NUMERICAL ANALYSIS ON THE STRUCTURAL BEHAVIOUR OF RC BEAMS STRENGTHENED WITH CFRP LAMINATES UNDER FIRE CONDITIONS

Tese de Doutoramento em Engenharia de Segurança ao Incêndio, orientada pelo Professor Doutor João Paulo Correia Rodrigues, pelo Professor Doutor Rogério Cattelan Antocheves de Lima e pelo Doutor Dhionis Dhima e apresentada ao Departamento de Engenharia Civil da Faculdade de Ciências e Tecnologia da Universidade de Coimbra.

Abril de 2019

ACKNOWLEDGEMENTS

I am sincerely grateful to my supervisors Professor João Paulo Correia Rodrigues, Professor Rogério Cattelan Antocheves de Lima and Doutor Dhionis Dhima for the splendid guidance, knowledge, patience, dedication, encouragement, friendship and valuable support provided over the last few years for the development of this research as well as assistance in many ways.

I would also like to thank the University of Coimbra for providing the necessary facilities and technical support.

I grateful acknowledge CNPq – National Council of Scientific and Technological Development, Brazil, for the PhD scholarship awarded that allowed me to materialize this great stage of my formation in one of the most important institutions in the world.

Thanks also to the S&P Clever Reinforcement Ibérica, Lda. for the supply and support of CFRP strengthening materials and the STAP, S.A. for the application of the fire protection materials on specimens. I thank TRIA, S.A. and ARGEX, S.A. for the supply of fire protection materials.

I would like to express my deep and sincere appreciation to my family, especially to my parents Fátima Regina Gomes Brazeiro and Benoni Cardoso Carlos, to my brother Jorge Brazeiro Carlos and to my grandmother Neusa Gomes Brazeiro for the unconditional support, perseverance, friendship, love and encouragement in the search for my ideals and in accomplishment of this PhD degree. They made great part of this adventure possible and showed me with love and optimism all the way to the end. Without them, none of this would be possible.

I dedicate this thesis to my grandfather James Brazeiro (*in memoriam*) as a small part of my acknowledgment of his goodness and unconditional sharing of love for humanity and nature and for the great moments in which he provided me as his grandson until his last days in this universe. He was my great example and will continue to shine in my life and memory forever.

Many wonderful people have still supported me on this journey. A special word of appreciation to all my friends and colleagues from Portugal and Brazil. To all those who contributed in some way to the conclusion of this important journey of my life, my immense and sincere thanks. They made a very important contribution to the success of my thesis.

Finally, I grateful thank the God.

ABSTRACT

The use of carbon fibre reinforced polymer (CFRP) laminates on strengthening and rehabilitation of reinforced concrete (RC), steel and timber structures has been widely used in the past few years due to the excellent mechanical performance, lightness, ease of application and corrosion resistance at ambient temperature of this composite material.

However, it is well known that CFRP strengthening systems are very vulnerable to high thermal exposure as well as the ones developed in a fire scenario. These systems can rapidly lose the effectiveness of their service conditions and lead the structure to collapse. In these systems, the bond between the CFRP and concrete is the most critical element. When exposed to high temperatures, the bond loses its mechanical properties and consequently the strengthening system collapses.

The increasing use of these systems on the strengthening of concrete structures, the possibility of fires in buildings, their thermal vulnerability and the gap in current fire design standards, have generated many concerns for the fire safety engineering society. Therefore, a better understanding of the thermomechanical response of CFRP-strengthened structures, especially RC beams, under thermal conditions is crucial, enabling a reliable safety design of those structures in fire situations. This PhD thesis and the consequent research intends to be an important contribution in this regard.

The main purpose of this research was to assess the flexural behaviour of RC beams externally strengthened with CFRP laminates under fire conditions. Other important goal of this investigation was to evaluate the effectiveness/influence of the different and new fire protection systems varying its thickness and to verify their practical applicability in strengthening systems in a fire situation. In order to achieve the objectives of this research, an experimental and numerical program have been carried out at the Department of Civil Engineering (DEC) of the University of Coimbra (UC), in Portugal.

In the experimental part, Single lap Shear Tests (SST) at elevated temperatures on twenty-one concrete blocks strengthened with CFRP laminates were performed. The SST tests were carried out to investigate the behaviour of the bond between concrete and CFRP at elevated temperatures in terms of bond strength, displacements and axial strains. The response of the bond was analysed under steady state conditions. First, the specimens were heated to the setpoint temperature and then they were loaded up to failure. The CFRP laminate was in both

type of tests assembled using the externally bonded reinforcement (EBR) technique. Reference tests at ambient temperature were also carried out.

To complete the experimental campaign, a great number of fire resistance (FR) tests were carried out on CFRP-strengthened RC beams thermally insulated with passive fire protection systems of vermiculite-perlite (VP), expanded clay (EC) aggregates and ordinary Portland (OP) cement-based mortars, in a fire scenario as real as possible. These tests were intended to study several parameters that might influence the structural response of these members in fire situations, such as, the critical temperature-time of debonding of the EBR strengthening system, collapse of the fire protection system and of the beam failure. The FR tests have been performed under transient state conditions with the specimens subjected to a serviceability loading. In addition, flexural tests at ambient temperature have been performed as reference.

Regarding the numerical phase, a large number of numerical simulations using a three-dimensional (3D) commercial finite element (FE) software package was performed. The numerical analyses made it possible to validate the developed FE models based on the results of the experimental tests and allowed to enlarge the research to other situations not tested experimentally in a future parametric study. A series of different parameters that have influence on the behaviour of RC beams strengthened with CFRP in a fire situation were simulated.

The fire resistance tests confirmed the limited fire behaviour of the CFRP-concrete bond in these systems and the need for their fire protection, which in turn is a critical zone and very sensitive to high temperatures. The results showed that the tested passive fire protection materials provided the integrity of strengthening for long periods of fire exposure. Moreover, tests carried out on new fire protection systems shown a good thermal performance during its serviceability period, especially for the systems composed by EC mortar. Despite the premature failure of the EC system, due to its low mechanical capacity, an excellent thermal behaviour was noticed by the mortar, which kept the temperatures practically constant at the CFRP-concrete interface and at the cross-section of the beam at a heating rate almost null while it still had integrity. This is a very relevant achievement in this investigation since these materials (if improved mechanically) can be a good and alternative solution to fire protection of the strengthening systems in building structures, providing integrity to the global element and safety for users in a fire event. Further investigation in this regard need to be performed to confirm this assumption. Concerning the SST tests, the results showed that approximately 40% of the bond strength was lost to temperatures near to the glass transition temperature (T_g) of the adhesive. However, despite the loss of bond strength with the increasing temperatures, a significant residual strength retention was still noticed for temperatures higher and much higher than the T_g (from + 15 ºC to + 65 ºC). Similar tendency was noticed on the fire tested CFRP-

strengthened RC beams, where the debonding of the strengthening system also occurred for temperatures above T_g of the adhesive. This bond behaviour noticed at temperatures significantly higher than the T_g was another important achievement of the current investigation, since it is a very relevant phenomenon in the effectiveness of the CFRP-strengthened concrete structures which needs to be taken into account for their fire design and a limited number of studies have been performed under these test and temperature conditions. In addition, the current research contributes to evidence and proof this important phenomenon developed in the CFRP-concrete bond at elevated temperatures, which is neglected by the standards that guide the fire design of concrete structures, such as EN 1992-1-2 (2004), ACI 440.2R-17 (2017) and Fib bulletin (2001) [1–3]. The results achieved in this thesis are fundamental to a better understanding of the CFRP-concrete bond behaviour at elevated temperatures, particularly concerning to its behaviour at temperatures above T_g of the adhesive. Moreover, it can be concluded that this phenomenon must be considered in the fire design of the CFRP strengthening systems and that the standards are quite conservative in this regard, where they merely define the critical temperature of the system by the T_g of the adhesive or, in an oversimply way, recommend not consider the effectiveness of the strengthening system in a fire situation. These reported experimental data are valuable and can be useful for the review and improvement of the mentioned standards or still for creating new rules, documents or calculation methods for guiding the fire design of these structures. Finally, the FE models developed were successfully validated and presented an excellent agreement with the experimental results, being able to reproduce the thermomechanical response of the tested beams with fairly good accuracy.

Keywords: Fire, Reinforced Concrete Structures, Beam, CFRP Strengthening, EBR Technique, Passive Protection, Glass Transition Temperature, Experimental Analysis, Numerical Modelling.

RESUMO

O uso de laminados de polímero reforçado com fibra de carbono (CFRP) no reforço e reabilitação de estruturas de betão armado, aço e madeira tem sido amplamente utilizado nos últimos anos devido ao seu excelente desempenho mecânico, leveza, facilidade de aplicação e resistência à corrosão sob condições de temperatura ambiente.

No entanto, é bem sabido que os sistemas de fortalecimento CFRP são muito vulneráveis à elevada exposição térmica, como aquelas desenvolvidas em um cenário real de incêndio. Esses sistemas podem rapidamente perder a eficácia de suas condições de serviço e levar a estrutura ao colapso. Nestes sistemas, a ligação entre o CFRP e o betão é a área mais crítico. Quando exposto a altas temperaturas, a ligação perde suas capacidades mecânicas e, consequentemente, o sistema de fortalecimento colapsa.

O uso crescente desses sistemas no reforço de estruturas de betão, a possibilidade de incêndios em edifícios, sua vulnerabilidade térmica e a lacuna nas normas atuais de projeto de incêndio têm gerado muitas preocupações para a sociedade de engenharia de segurança contra incêndios. Portanto, um melhor entendimento da resposta termomecânica de estruturas reforçadas com CFRP, especialmente vigas de betão armado, sob condições térmicas é crucial, permitindo projetar essas estruturas de forma segura para situações de incêndio. Essa tese de doutorado e a consequente pesquisa pretendem ser uma importante contribuição nesse sentido.

O principal objetivo desta pesquisa foi avaliar o comportamento à flexão de vigas de betão armado reforçadas externamente com laminados CFRP sob condições de incêndio. Outro objetivo importante desta investigação foi avaliar a eficácia/influência de diferentes e novos sistemas de proteção contra incêndio, variando sua espessura, e verificar sua aplicabilidade nos sistemas de reforço para uma situação de incêndio. Para atingir os objetivos desta pesquisa, um programa experimental e numérico foi desenvolvido no Departamento de Engenharia Civil (DEC) da Universidade de Coimbra (UC), em Portugal.

Na parte experimental, uma série de ensaios de cisalhamento único (SST) em vinte e um blocos de betão reforçados com laminados de CFRP a temperaturas elevadas foram realizados. Os ensaios SST foram realizados para investigar o comportamento ao fogo da ligação entre o betão e o CFRP em termos de resistência à tração, deslocamentos e deformações axiais. A resposta da ligação foi analisada em condições de estado estacionário. Primeiro, as amostras foram aquecidas até a temperatura nominal e, em seguida, foram carregadas até a falha. O laminado

de CFRP foi em ambos os tipos de ensaios colado usando a técnica de ligação externa (EBR). Ensaios de referência à temperatura ambiente também foram realizados.

Para completar o programa experimental, um grande número de ensaios de resistência ao fogo foram realizados em vigas reforçadas com CFRP, termicamente protegidas com sistemas passivos contra incêndio compostos por argamassas de vermiculita-perlita (VP), agregados de argila expandida (EC) e cimento Portland comum (OP) em uma configuração de ensaios que representasse um cenário de incêndio da forma mais fiel possível. Pretendeu-se com estes ensaios estudar vários parâmetros que pudessem influenciar a resposta estrutural destes elementos em situações de incêndio, como a temperatura crítica vs. tempo do colapso do sistema de reforço EBR, o colapso do sistema de proteção contra incêndio e a falha da viga. Os ensaios de resistência ao fogo foram realizados em condições de estado transitório com os provetes sujeitos a uma carga de serviço. Além disso, ensaios de flexão à temperatura ambiente foram realizados como referência.

Em relação à fase numérica, foi realizado um grande número de simulações numéricas utilizando um software comercial de elementos finitos tridimensionais (3D). As análises numéricas permitiram validar os modelos de elementos finitos desenvolvidos com base nos resultados dos ensaios experimentais e tornam possível a ampliação da pesquisa para outras situações não testadas experimentalmente em um futuro estudo paramétrico. Uma série de diferentes parâmetros que influenciam no comportamento das vigas de betão armado reforçadas com CFRP em situação de incêndio foram simulados.

Os ensaios de resistência ao fogo confirmaram o comportamento limitado ao fogo da ligação CFRP-betão e a necessidade de sua proteção contra incêndio, que por sua vez é uma zona crítica e muito sensível a altas temperaturas. Os resultados mostraram que os materiais passivos de proteção contra incêndio proporcionaram a integridade do reforço por longos períodos de exposição ao fogo. Além disso, os testes realizados nos novos sistemas de proteção contra incêndio mostraram um bom desempenho térmico durante seu período de manutenção, especialmente para os sistemas compostos por argamassa EC. Apesar da falha prematura do sistema EC, devido a sua baixa capacidade mecânica, um excelente comportamento térmico foi observado pela argamassa, que manteve as temperaturas praticamente constantes na interface CFRP-betão e na seção transversal da viga a uma taxa de aquecimento quase nula, enquanto ainda tinha integridade. Esta é uma conquista muito relevante desta investigação, uma vez que estes materiais (se melhorados mecanicamente) podem ser uma solução boa e alternativa para proteção contra incêndio dos sistemas de reforço em estruturas da construção civil, fornecendo integridade ao elemento global e segurança para os usuários em um eventual incêndio. Outras investigações a esse respeito precisam ser realizadas para confirmar essa suposição. Em relação

aos ensaios SST, os resultados mostraram que aproximadamente 40% da resistência mecânica da ligação foi perdida para temperaturas próximas à temperatura de transição vítrea (T_g) do adesivo. No entanto, apesar da perda da resistência mecânica da ligação com o aumento de temperatura, uma significativa retenção mecânica residual ainda foi notada para temperaturas superiores e excessivamente superiores a T_g (de + 15 ºC a + 65 ºC). Tendência semelhante foi notada nas vigas reforçadas com CFRP ensaiadas ao fogo, onde a falha do sistema de reforço também ocorreu para temperaturas superiores a T_g do adesivo. Este comportamento da ligação, observado a temperaturas significativamente mais altas do que a T_g, foi outra importante conquista desta investigação, uma vez que é um fenômeno muito relevante na eficácia das estruturas de concreto reforçadas com CFPP, que precisa ser levado em consideração para seu projeto de incêndio, e um número limitado de estudos tem sido realizados sob essas condições de teste e temperatura. Portanto, essa pesquisa contribui para evidenciar e confirmar esse importante fenômeno desenvolvido na ligação CFRP-betão a temperaturas elevadas, o que é negligenciado pelas normas que norteiam o dimensionamento e projeto de estruturas de concreto ao fogo, bem como a EN 1992-1-2 (2004), ACI 440.2R-17 (2017) e Fib bulletin (2001) [1–3]. Os resultados obtidos nesta tese são fundamentais para uma melhor compreensão do comportamento da ligação CFRP-betão a temperaturas elevadas, particularmente no que diz respeito ao seu comportamento a temperaturas superiores a T_g do adesivo. Além disso, pode-se concluir que este fenômeno deve ser considerado no projeto do fogo dos sistemas de reforço com CFPP e que os padrões são bastante conservadores a esse respeito, onde meramente definem a temperatura crítica do sistema pela T_g do adesivo ou, de uma maneira excessivamente simplista, recomendam desconsiderar a eficácia do sistema de reforço em uma situação de incêndio. Esses dados experimentais relatados são valiosos e podem ser úteis para a revisão e melhoria dos padrões mencionados ou ainda para a criação de novas regras, documentos ou métodos de cálculo para orientar o dimensionamento dessas estruturas em situação de incêndio. Por fim, os modelos de elementos finitos desenvolvidos foram validados com sucesso e apresentaram excelente compatibilidade com os resultados experimentais, sendo capazes de reproduzir a resposta termomecânica das vigas testadas com boa precisão.

Palavras-chave: Incêndio, Estruturas de Concreto Reforçadas, Vigas, Reforço CFRP, Técnica EBR, Proteção Passiva, Temperatura de Transição Vítrea, Análise Experimental, Modelagem Numérica.

TABLE OF CONTENTS

LIST OF FIGURES

CHAPTER 1:

CHAPTER 2:

CHAPTER 3:

CHAPTER 4:

CHAPTER 5:

APPENDIX A:

APPENDIX B:

LIST OF TABLES

CHAPTER 2:

CHAPTER 3:

CHAPTER 4:

CHAPTER 5:

NOTATION

RC	Reinforced Concrete
FRP	Fibre-Reinforced Polymers
CFRP	Carbon Fibre Reinforced Polymer
T_g	glass transition temperature
EBR	Externally Bonded Reinforcement
NSM	Near Surface Mounted
FE	finite element
DSC	Differential Scanning Calorimetry
DMA	Dynamic Mechanical Analysis
FR	Fire Resistance tests
SST	Single lap Shear Test
DST	Double lap Shear Test
OP	Ordinary Portland cement mortar
EC	Portland cement with Expanded Clay aggregates mortar
VP	Vermiculite-Perlite mortar
L	span of the beam
h	height of the beam cross-section
f_{cm}	mean value of the compressive strength (at 28 days) of the concrete at ambient temperature
P	applied load in the testing beams
P_{ult}	ultimate capacity of the beams at ambient temperature
P_{calc}	design value of the loadbearing capacity of the unstrengthened RC beam at ambient temperature
t	thickness of the fire protection material
tf_{cfrp}	time when the strengthening system failed
Tf_{CFRP}	temperature at the CFRP-concrete interface when the strengthening system failed
tf_{ps}	time when the fire protection system failed
tf_{beam}	final collapse time of the beam
Tf_{PS}	temperature at the CFRP-concrete interface when the fire protection system failed
c_p	specific heat of concrete
c_s	specific heat of steel reinforcement
$c_{p,vp}$	specific heat of VP mortar

$c_{p,ec}$	specific heat of EC mortar
$c_{p,op}$	specific heat of OP mortar
λ_{vp}	thermal conductivity of VP mortar
u	moisture content
ρ	concrete density
ρ_s	steel reinforcement density
TGA	Thermogravimetric Analyses
E_{cm}	Modulus of elasticity of concrete
f_{ctm}	Average tensile strength of concrete
$k_{c,t}(\theta)$	Reduction factor for the tensile strength of concrete at temperature θ
$k_{c,c}(\theta)$	Reduction factor for the compressive strength of concrete at temperature θ
$k_{Ec}(\theta)$	Reduction factor for the modulus of elasticity of concrete at temperature θ
v	Poisson's ratio of steel reinforcement
$k_{s,y}(\theta)$	Reduction factor for the yield stress of steel reinforcement at temperature θ
$k_{s,u}(\theta)$	Reduction factor for the ultimate tensile strength of steel reinforcement at temperature θ
$k_{Es}(\theta)$	Reduction factor for the modulus of elasticity of steel reinforcement at temperature θ
P_{NUM}	Maximum numerical load-carrying capacity of the beam
P_{EXP}	Maximum experimental load-carrying capacity of the beam
FR_{time}	Fire resistance time of the RC beam
$FR_{time,CFRP}$	Fire resistance time of the CFRP strengthening system
E'	Storage modulus curve

1 INTRODUCTION

This chapter summarizes the current state of knowledge on strengthening of reinforced concrete (RC) structures with fibre reinforced polymers (FRPs), specifically carbon fibres reinforced polymers (CFRPs). The problems and difficulties in this field, as well as the objectives and methods of this research are also described in this chapter.

The historical evolution of composites is briefly addressed at the beginning of the chapter, followed by a brief description of its constituent materials. Subsequently, CFRP composites are exclusively discussed in terms of their manufacturing forms and processes, their application techniques and examples of their use as a strengthening system in RC structures. In addition, the most important issues and challenges in the field of strengthening of RC structures that motivated the development of this PhD thesis are also discussed in this chapter, especially regarding to their fire behaviour, the main current normative documents for their fire design and the gaps in this field. Finally, the current objectives of this research and the methods used to achieve them are also detailed in Chapter 1.

1.1 Overview

The use of reinforced concrete is not so recent with its first known application dated of 1849, in France, but outside the civil construction. The use of RC in civil large-scale construction started only in the first half of the 20th century. Actually, after a better understanding of its behaviour, it quickly became the main and most widely used building material in structural applications.

Over the years, with the aging process of the reinforced concrete constructions, it was noticed that this material could present degradations. These degradations can be induced by the exposed environment, fires, seismic activity, errors in the execution, use of inadequate techniques and designs or even from the combination of these events. As a result, these effects have led many of the existing constructions to an inability in terms of structural safety. The facts stated above, along with the possible need for changes in their use, architectonic modifications or expansions, increase loadings, compliance with standards, preservation of historical heritage, among others, may result in structures that need to have their mechanical capacity re-established or increased. For this purpose, in view of the possibility of occurrence of these events, different structural strengthening techniques in reinforced concrete constructions have been implemented in the past few decades.

The addition of external steel reinforcements, either by simple bonding or by prestressing, was one of the techniques quite used in the past. However, materials susceptible to deterioration and which require maintenance (as well as the initial elements) are used in these techniques, especially steel. Until then, it was practically impossible to design strengthening systems that could simultaneously minimize the effects on the architecture, exhibit high durability and mechanical strength characteristics and easy and quick to apply, using traditional building materials. In order to establish a strengthening technique with a material that exhibited all these characteristics, composite materials have recently emerged as an excellent alternative.

A composite material is made from two or more different kinds of materials. When they are combined, they may become a new material which conjugates the best properties of each one of them [4]. The technology of fibre reinforced polymers (FRP) that results from the incorporation of reinforcing fibres in a polymer matrix is an excellent alternative solution between the composites (see Figure 1.1).

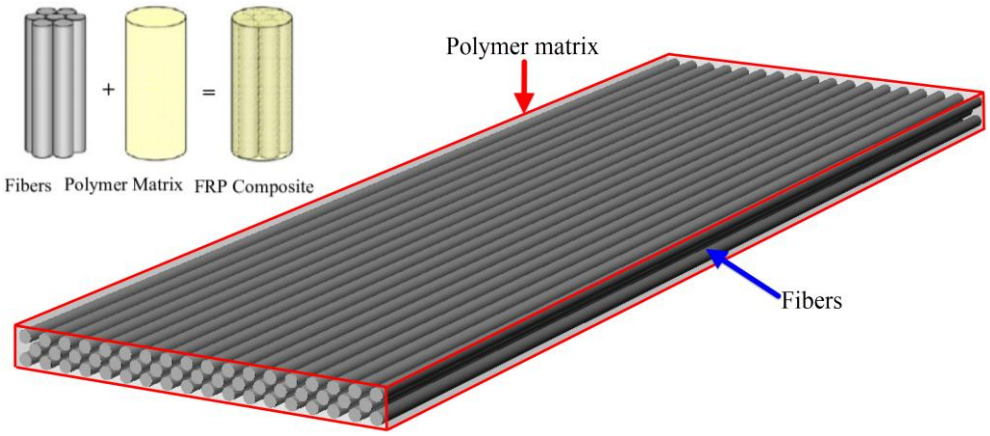

Figure 1.1 – Basic scheme of the incorporation of reinforcing fibres in a polymer matrix for the development of FRPs (adapted from [5,6])

The concept of composite materials has existed for several centuries, however, the interest in the use of FRP's in large-scale in civil construction occurred recently towards the end of the 20th century with the development of the plastics industry. In the 1940s, the use of fibre reinforced polymer was already in use for naval defence and aerospace industries (Figure 1.2a and Figure 1.2b, respectively) as the main promoters of the development of composite materials [7].

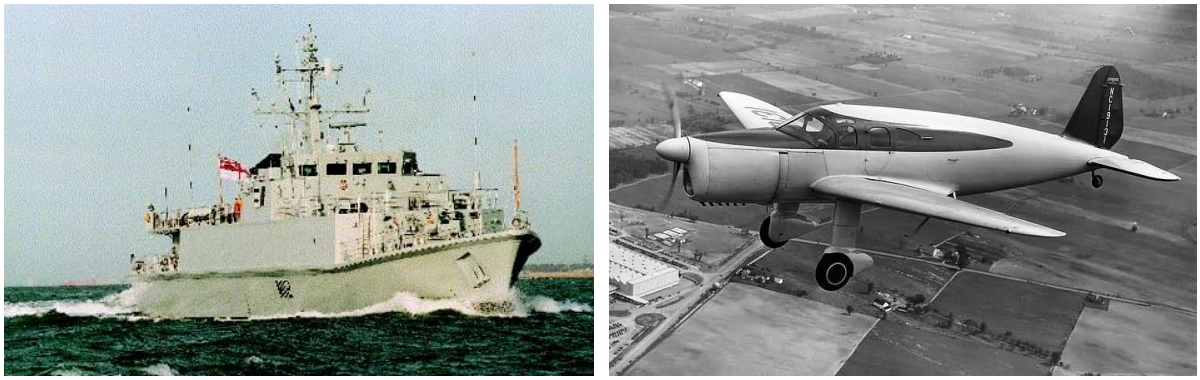

(a) **(b)**

Figure 1.2 – Applications of fibre reinforced polymers: (a) in the hull of military ships [8] and (b) in the body of an airplane (Fairchild F-4: first fibre-reinforced polymer plane, 1937) [9]

Still in the 40s, the oil industry had become one of the largest consumers of FRP's, both for offshore platform structural elements and for pipelines, where a high chemical resistance is essential [10]. In the early 50's, its application was extended to the chemical and automobile industries (Figure 1.3).

Figure 1.3 – Use of FRP composites in a car (Stout Scarab Experimental: first fiberglass-bodied car, 1946) [11]

In the 1960s, materials consisting of fibres of high elastic modulus and strength, namely "advanced composite materials", began to be produced. Among them, the carbon fibre reinforced polymer (CFRP) can be highlighted. However, the high price of these materials at that time did not allow their use outside the aerospace and military aviation industry [12].

Only in the 80's, new processes were developed to manufacture carbon fibres with excellent mechanical properties and at lower prices [13]. The technological evolution of manufacturing processes led to a reduction in FRP costs in the late 1980s and in the 1990s, accompanied the need to renovate infrastructures, with increasing functionality requirements. A growing acceptance of these materials in construction applications occurred after that, awakening work fronts in different locations, such as Japan (interested in pre-fabrication and prestressing), North America (motivated in solutions to durability problems) and Europe (concerned about the need for preservation of historical heritage). A series of international conferences to discuss specific aspects of the use of these composite materials in civil engineering began even in the 1990s. From this point onwards, diversified products have been developed, for both applications in repair works and in new constructions [14]. Figure 1.4a and Figure 1.4b presents examples of using FRP materials in important engineering works.

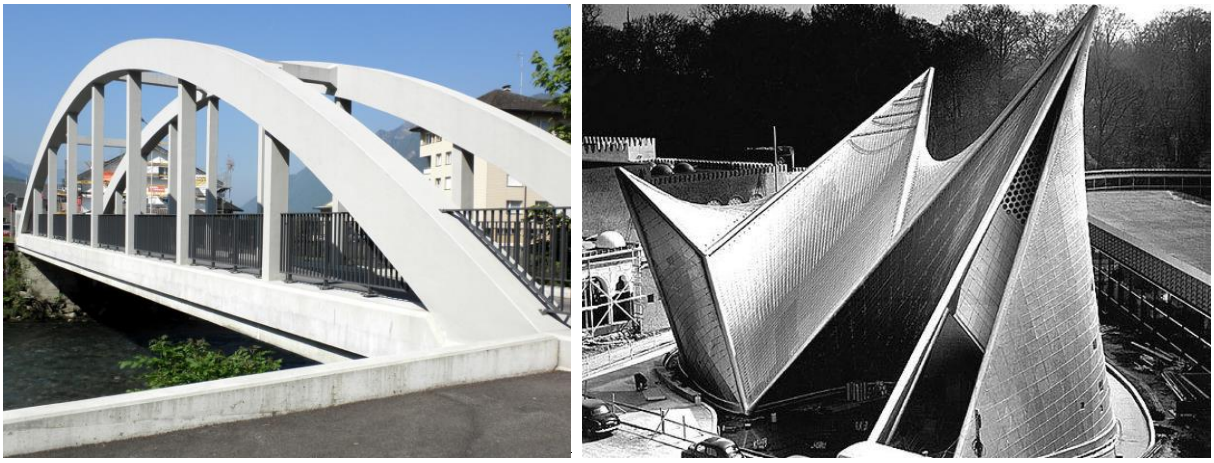

(a) **(b)**

Figure 1.4 – (a) Ibach Bridge: first structure strengthened with CFRP [15]; (b) American Pavillion in Brussels: use of glass fibre reinforced polymer (GFRP) as facade coating [16]

The CFRP has been largely used in the civil construction in the past few years as an excellent alternative for structural strengthening, overcoming to other composites due to their high modulus of elasticity and tensile strength, lightness, ease of application and corrosion and fatigue resistance. Figure 1.5 presents the stress-strain relationship of most used FRP composites in civil engineering and steel reinforcement. The respective curves reveal a linear behaviour until the rupture of all the FRP composites and that the CFRP is the one that presents higher tensile strength and modulus of elasticity closer to the one of steel [17].

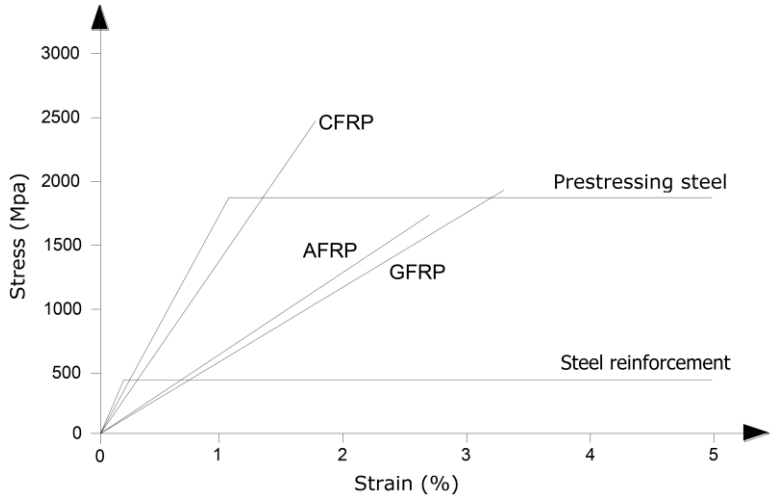

Figure 1.5 – Stress-strain relationship of different FRP composites and steel reinforcement (adapted from Sonnenschein *et al.* [17])

The segment of the strengthening of concrete structures has been one of the main reasons for using CFRP composite material. In this regard, the flexural and shear strengthening of reinforced concrete (RC) beams (Figure 1.6a and Figure 1.6b, respectively), flexural strengthening of slabs (Figure 1.6c) and strengthening to axial stress and confinement of columns (Figure 1.6d) can be highlighted.

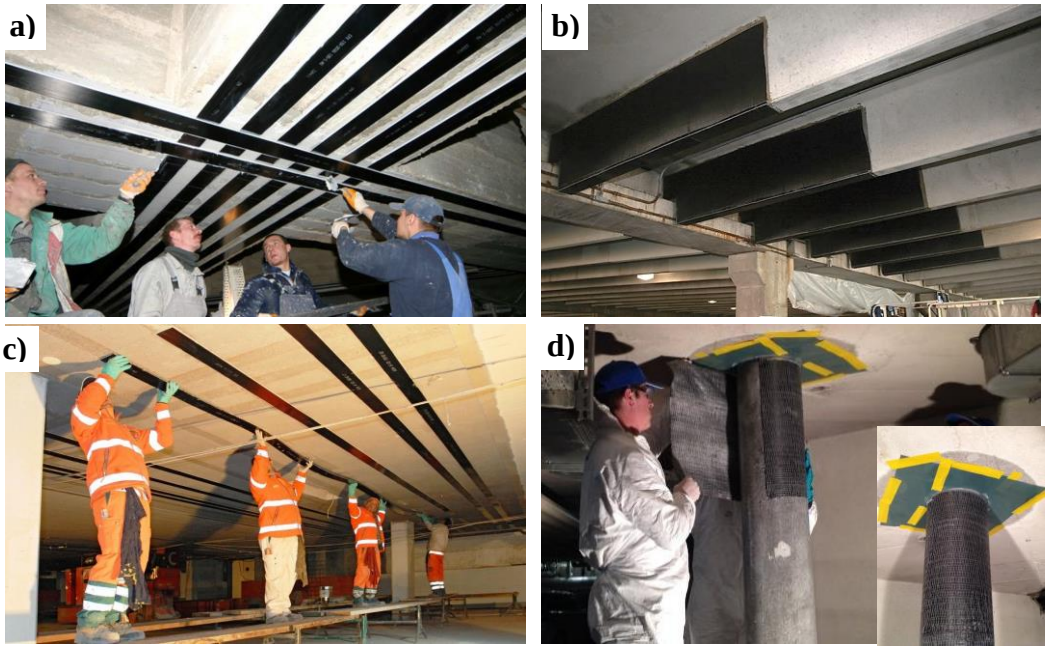

Figure 1.6 – (a) flexural strengthening of RC beams with CFRP laminates [18]; (b) partial shear strengthening of RC beams with CFRP sheets [19]; (c) flexural strengthening of slabs with CFRP laminates [20]; (d) strengthening to axial stress and confinement of columns with CFRP sheets [21]

The CFRP composite materials used in the strengthening of concrete structures arise mainly in the following forms: laminates, sheets, rods, rebars and wires/cables (Figure 1.7a-e, respectively).

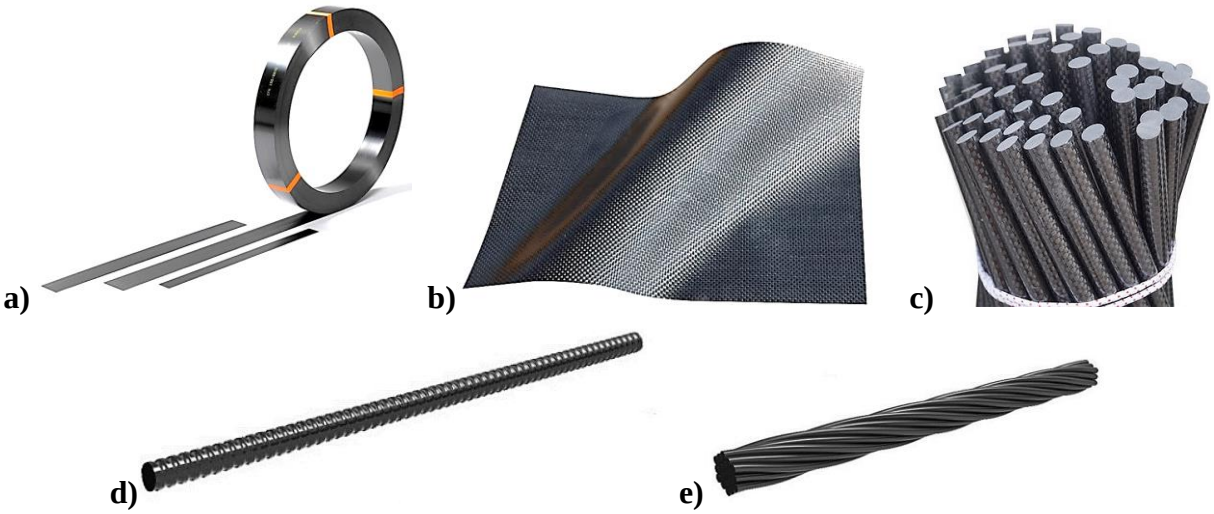

Figure 1.7 – Main forms of CFRP composite materials for using in strengthening concrete structures: (a) laminates [20], (b) sheets [22], (c) rods [23], (d) rebars [6] and (e) wires/cables [6]

The laminates in particular are the most common form used in structural strengthening applications. They result from the impregnation of a set of continuous strands or layers of fibres by a thermosetting resin, consolidated by a pultrusion fabrication process (see Figure 1.8) with control of the thickness and width of the composite [14].

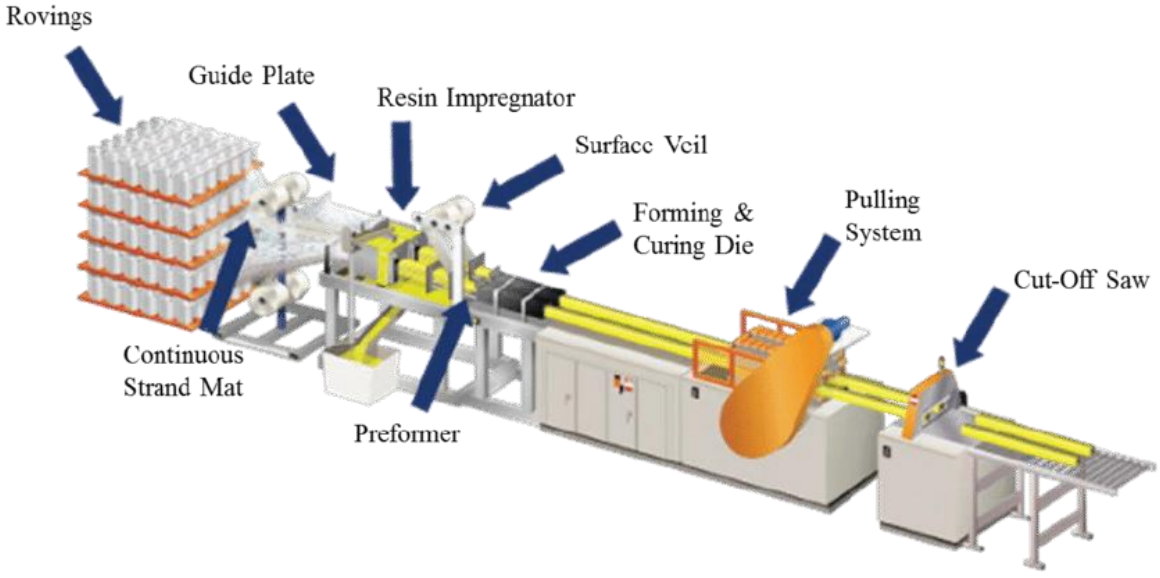

Figure 1.8 – CFRP laminates' pultrusion manufacture process [24]

The CFRP laminates are bonded to the concrete surface by an adhesive agent, generally a two-component epoxy resin. In this way, the tension may be transferred among the plans of the concrete-adhesive-composite interfaces.

In cases where it is intended to provide an additional flexural strength in the concrete structures (such as RC beams), there are two different techniques for the laminates bonding: externally bonded reinforcement (EBR) and the near surface mounted (NSM).

The EBR technique consists of bonding the strengthening material directly to the exposed concrete surface. Among the two techniques, EBR is the most used since it involves few means of preparation and application in comparison to the NSM and still presents a high performance. Figure 1.9 shows a typical EBR strengthening system for flexural strengthening of RC beams.

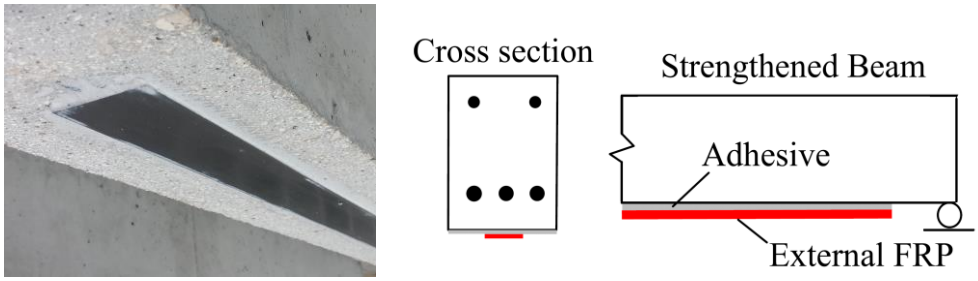

Figure 1.9 – EBR strengthening system: (a) typical application for flexural strengthening of an RC beam and (b) laminates positioning scheme in the beam's sections [25]

The NSM system is based on the bonding of the CFRP laminates inside grooves made in the concrete cover. According to [26], this technique presents some advantages compared to EBR, highlighting a higher resistance to CFRP debonding/pull-out phenomena, it has better protection against vandalism acts, reduction of the amount of CFRP employed and improvement on fire behaviour. However, despite the aforementioned EBR advantages, the NSM technique is often limited to the thickness of the concrete cover, which may make the method impractical in certain cases due to the need to create surface grooves. In addition, the execution of the grooves in the concrete consists of an invasive, more expensive and complex procedure than a simply surface treatment with sandblasting, water, or needle hammers used in the EBR technique. A typical NSM strengthening system for flexural strength of RC beams is presented in Figure 1.10.

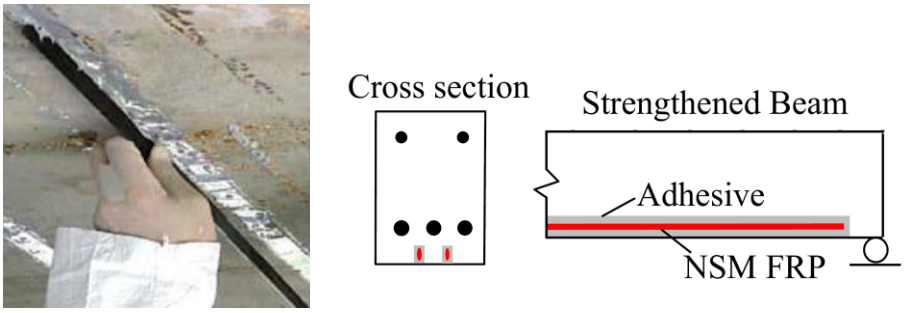

(a) **(b)**

Figure 1.10 – NSM strengthening system: (a) typical application for flexural strength of an RC structure (adapted from [14]) and (b) laminates positioning scheme in the beam's sections [25]

Although CFRPs present excellent performance at ambient temperature, their behaviour at high temperatures remains one of the main obstacles to their full acceptance as strengthening material, constituting one of its main disadvantages. In a fire situation, the bond between concrete and CFRP constitutes the most critical part in CFRP strengthening systems, it is very sensitive to the thermal exposure. The properties of the bond severely deteriorate when the temperature of the most susceptible material to thermal action (generally the adhesive resin) reaches the glass transition temperature (T_g). As a result of these detrimental conditions, a loss of strength of the strengthening system can lead the element and building structure to collapse.

These issues, along with increasing use of these materials over the years in civil construction, have generated concerns in the civil and scientific community regarding the behaviour of these systems under fire conditions, especially in RC structures. To date, several studies have been conducted to explain the fire behaviour of the strengthening systems. However, there is still much more be done, mainly concerning the assess of the CFRP-concrete bond behaviour at temperatures higher and much higher than the T_g. Few investigations have been carried out in this regard and have shown that the bond still present significant mechanical capacity at these temperature conditions. Moreover, this phenomenon is still neglected by the current standards. Further investigations are needed to confirm and evidence this relevant behaviour and to provide data to a future review or development of standards or documents for fire design of these structures under these conditions. The bond behaviour at this temperature conditions is studied in this thesis. Concerning the passive systems for fire protection of CFRP strengthening, the development of new systems has been suggested by the international scientific community over the years. However, this important issue needs to be investigated in further detail since to date a limited number of fire protection systems with good fire performance are found in the civil construction industry. In this regard, the current research proposed a large experimental campaign with a series of tests on new and potential high-performance fire protection systems

to fire protect the CFRP strengthening system, assessing its performance in terms of material composition and thickness under fire conditions. These materials must ensure a minimum fire resistance time to the protected structure in order to provide safe evacuation of such structures by users in a fire situation. The main scientific investigations reported to date on the fire behaviour of concrete structures strengthened with CFRP systems are discussed in detail in Chapter 2 of this thesis. The other difficulties and gaps currently found on this area are also addressed in the next section.

Finally, this research intends to contribute to the development of knowledge in the area, to present solutions for better and safer use of this type of structures in fire conditions.

1.2 Motivation

Carbon fibre reinforced polymers have been largely used on the strengthening and repair of reinforced concrete elements, especially on beams, due to their excellent flexural performance. In addition, this strengthening material presents other advantages such as lightness, easy application and corrosion resistance. However, when these elements are exposed to fire, other detrimental factors may arise due to high thermal exposure, rapidly affecting their physical-mechanical capabilities.

In civil construction when strengthening an RC beam with CFRP laminates, these elements are typically externally bonded to the concrete member by epoxy resins to provide additional flexural strength. These materials are known to enhance the behaviour of the elements at ambient temperature but in case of fire the same effect is not observed. According to some studies [27–30], the organic matrix of the fibre-reinforced polymers (FRP) decomposes when exposed to temperatures between 300 and 500 ºC.

The knowledge of the mechanical behaviour of the bond between the carbon fibre reinforced polymer strengthening system and the concrete at elevated temperatures is a key factor on the fire design of concrete structures. This fact becomes important in view of the mentioned increasing use of these materials over the years on strengthening and rehabilitation of concrete structures, making them reliable and safe in case of fire. The CFRP-concrete bond interface is a critical zone responsible for maintaining the effectiveness of the externally bonded reinforced (EBR)-strengthening system very vulnerable to elevated temperatures such as the ones developed in the event of fire. The failure of bond generally occurs at temperatures near or above the glass transition temperature of the adhesive. However, in some cases, this happens for temperatures below T_g. The T_g of the adhesive varies usually from 50 and 120 ºC [3,29–32], depending on the polymeric matrix of constituents and the type of resin, among others.

In the past, the development of research allowed the elaboration and implementation of standards for ambient temperature design of concrete structures that resulted in the elaboration of EN 1992-1-1 (2004) [33]. However, for fire design of CFRP-strengthened concrete elements, there is still a lack of research. Currently, the methods presented in EN 1992-1-2 (2004) [1] for fire design of concrete structures do not take into account the contribution of the CFRP strengthening on the flexural behaviour of these elements under fire conditions and do not have consistent methods for fire design. Furthermore, there are other important standards for specific design of externally bonded FRP systems for strengthening existing structures, such as ACI 440.2R-17 (2017) [3] and Fib bulletin 14 (2001) [2]. Both of them recognize the inefficiency of CFRP strengthening systems at elevated temperatures, but they do not define any calculation criteria or method that consider the contribution of the CFRP in the case of fire. The ACI and Fib documents [2,3] are overly conservative when they simply suggest that the fire verification of the structure may be conducted considering that the strengthening is non-existent, i.e., that the contribution of the resistance of the CFRP system to the service conditions verifications is not considered. Therefore, the development of new design methods for concrete structures strengthened with CFRP subjected to fire are urgently and absolutely necessary given the substantial current demand for their use in buildings and due to the inherent risks of a composite structural element when subjected to these limit conditions. This research intends to contribute to this purpose. The current investigation assesses a relevant phenomenon developed in the CFRP-concrete bond at elevated temperatures: the presence of mechanical capacity of the bond at temperatures higher or much higher than T_g (residual bond strength), since it is very important part in the fire design of the CFRP-strengthened system effectiveness (as reported in the literature) and is still neglected by the abovementioned standards. This research intends to provide valuable and useful experimental data for the review and improvement of the existing standards or still for creating new rules or documents for guiding the fire design of these structures.

Concerning the behaviour of CFRP-strengthened RC beams under fire conditions a few studies have been reported in the literature (see Section 2.2). However, most of the studies of experimental nature, did not take into account the interaction between a CFRP-strengthened beam and the surrounding building elements. The thermal and mechanical response of the beams when inserted in a building structure is different from when isolated. The contact between beam and slab plays an important role on the behaviour of the beam since it induces different ways of thermal interaction. In addition, the slab promotes an adiabatic surface, as it happens in a real situation. Moreover, it is still difficult to define which mechanisms lead to failure of the FRP strengthening systems and especially when this happens in a real structure. For this reason, the thermal-mechanical behaviour of CFRP strengthened elements at high temperatures and the various factors arising from their thermal exposure, such as the (i) failure

modes of the strengthening and fire protection systems, (ii) effectiveness and influence of new passive fire protection systems, (iii) fire behaviour of the bond, (iv) boundary conditions, (v) effects of the surrounding building elements, among others, need further investigation and this research addresses these issues.

The development of new passive systems for fire protection of CFRP strengthening systems has been suggested by the international scientific community over the years. However, this important issue still needs to be further investigated since to date a limited number of fire protection systems with good fire performance are found in the civil construction industry. The current research proposes a large experimental campaign in this regard, where a series of tests on new and potential high-performance fire protection systems is carried out to assess its performance under fire conditions. Three based mortar materials with different thickness levels are tested under fire conditions in this thesis.

Furthermore, a limited number of studies have focused on the bond behaviour of CFRP-concrete interface on strengthening systems at elevated temperatures using the EBR technique. Despite the investigations carried out over the years (as discussed in Section 2.1), many issues concerning the bond behaviour between concrete and CFRP strengthening systems at elevated temperatures remain unclear and need further investigation. Most of the previous studies have been performed for temperatures below, near or slightly above the T_g of the adhesive. A limited number of investigations have been carried out at temperatures significantly higher than T_g and have shown that the bond still had significant mechanical capacity under these conditions (residual bond strength). However, some divergences have been still noted from the authors in this regard. Thus, the thermal and mechanical response of the CFRP-concrete bond for temperatures higher and much higher than T_g needs further investigation. Furthermore, as mentioned above, the residual bond strength noticed for the CFRP-concrete interface temperatures above T_g is still neglected by the current standards that guide the fire design of these structures. Therefore, further investigations are needed to confirm and evidence this relevant bond behaviour at elevated temperatures and to provide data to a future review or development of standards, documents or calculation methods for fire design of these structures considering these conditions. The current research addresses these issues, particularly the CFRP-strengthening bond behaviour at this temperature conditions. In addition, it is important to note that the test specimens analysed in this investigation were made with particular materials and parameters (CFRP, adhesive, bonded length, T_g) that have not been studied before on other experimental works carried out by other authors. Finally, the tests were performed with a distinct method, procedure and conditions, in which a new test set-up was especially developed.

Based on the challenges discussed above, it is fundamental the development of a highly detailed research in the scientific field on the structural behaviour of RC beams strengthened with CFRP subjected to fire conditions. Therefore, it is hoped that this document will make an important contribution to the improvement, standardization and accuracy of the fire design of CFRP-strengthened concrete structures within the practical developments in the area of fire safety engineering.

1.3 Research Objectives

The overall purpose of this research was to investigate the flexural behaviour of RC beams EBR-strengthened with CFRP laminates under fire conditions, aiming to contribute to the advancement of technology and fire performance of buildings, to promote increased fire safety of structures, to provide valuable data for review and improvement of the standards relative to the fire design of the CFRP-strengthened concrete elements or to the creation of a new document or rules associated with these standards, fulfilling a gaps in this field. Another important goal of this investigation was to evaluate the effectiveness/influence of different fire protection systems varying its thickness and to verify their practical applicability in strengthening systems in a fire situation. In order to achieve the objectives of this research, a large experimental program and advanced numerical analyses were implemented and carried out at the Department of Civil Engineering (DEC) of the University of Coimbra (UC), in Portugal.

Concerning the experimental phase, Single lap Shear Tests (SST) at elevated temperatures on concrete blocks strengthened with CFRP laminates were performed. The SST tests were carried out to evaluate the behaviour of the bond between concrete and CFRP at elevated temperatures in terms of bond strength, displacements, axial strains and failure modes as function of temperature evolution. The response of the bond was analysed under steady state conditions. A total of twenty-one CFRP-strengthened concrete blocks were tested at different temperature series. The specimens were heated from ambient temperature (around 15 ºC) up to 165 ºC and after that they were loaded (under displacement control) up to failure. The CFRP laminate was in both type of tests assembled using the externally bonded reinforcement (EBR) technique.

To accomplish the experimental program, a great number of fire resistance (FR) tests were carried out on CFRP-strengthened RC beams thermally insulated with passive fire protection systems of vermiculite-perlite (VP), expanded clay (EC) aggregates and ordinary Portland (OP) cement-based mortars, in a quite real scenario. These tests were intended to study several parameters that have influence on the structural response of these members in fire, such as, the critical temperature-time of debonding of the EBR strengthening system, collapse of the fire

protection system and of the beam failure. The FR tests have been performed following the ISO 834 standard fire curve [34] under transient state conditions with the specimens being subjected to a serviceability loading and without axial restrictions. The experimental phase was conducted at the Materials and Structure Testing Laboratory (LEME) of UC.

Posteriorly, the advanced numerical phase included a huge amount of numerical simulations using a commercial finite element software package Abaqus/CAE (version 6.14-5) [35]. The numerical analyses made possible to validate the developed finite element (FE) models based on the experimental results.

Thus, the specific objectives of this research are:

- To contribute to a future revision of European Standard EN 1992-1-2 (2004) [1], relative to the fire design of the CFRP-strengthened concrete structures.

- To study the failure loads, failure modes, failure times and temperatures of the strengthening system, failure of the beams and of the passive fire protection system under flexural state and subjected to fire, by means of FR tests under transient state conditions.

- To analyse and characterize the behaviour of the bond between the CFRP and concrete at ambient and elevated temperatures in what concerns of bond strength, failure modes, axial strains and displacements, performing several Single lap Shear Tests under steady state conditions.

- To investigate the influence of the surrounding structure on the strengthened beams when they are subjected to fire. Thus, a large number of FR tests on CFRP-strengthened RC beams considering the interaction between the beams and a surrounding building slab were undertaken. The slab promoted an adiabatic surface, reproducing as faithful as possible the actual boundary conditions of a beam when it is inserted in a real concrete building structure.

- To evaluate the effectiveness and influence of the different fire protection systems, their thickness variation and to verify their practical applicability for protection of strengthening systems in a fire situation.

- To develop accurate finite element models capable of simulating the flexural behaviour of CFRP-strengthened concrete beams at ambient temperature and under fire conditions

and especially their interactions between the different surrounding elements and materials.

- To validate the developed numerical models by comparison with experimental results.

- To verify the predictions from the currently available design documents, such as EN 1992-1-2 (2004), ACI 440.2R-17 (2017) and Fib bulletin (2001) [1–3], by comparing them with the experimental and numerical results obtained from both ambient temperature and fire conditions.

- To provide valuable data for developing a suitable analytical guidance or new simplified calculation methods for fire design of CFRP-strengthened RC beams.

- To propose issues for good practice in the area of fire safety engineering, especially on strengthening of concrete beams with CFRP laminate strips looking for a better way to improve its fire performance.

1.4 Thesis Contents

This PhD thesis is organized into a total of 5 chapters and the contents of each chapter, except for this chapter, are briefly described as follows:

Chapter 2, Literature Review, presents the state-of-the-art of the most important experimental, numerical and analytical investigations conducted by previous researchers, describing and discussing the findings correlated to this PhD thesis.

Chapter 3, Experimental Investigation on Bond Behaviour Between CFRP and Concrete at Elevated Temperatures, presents a series of Single Lap Shear tests on EBR-CFRP-strengthened concrete blocks at ambient and elevated temperatures. Twenty-one SST tests were carried out to evaluate the temperature influence on CFRP-concrete bond behaviour. The test specimens, the test set-up, the test program, the testing procedures and the results in terms of bond strength, displacements, axial strains and failure modes as function of temperature evolution are addressed and discussed in the Chapter 3.

Chapter 4, Experimental Investigation on RC Beams EBR-strengthened with CFRP Laminates under Fire Conditions, addresses a series of flexural tests on simply supported EBR-CFRP-strengthened RC beams and unstrengthened RC beams at ambient temperature and under fire conditions. The use of different fire protection materials applied on the CFRP-strengthened

beams were also tested in order to assess their thermal performance and their influence on the strengthening system and on the beams when subjected to fire conditions. In addition, three different thicknesses in each protection system were tested. A building element was also adopted in the fire resistance tests to represent the thermal contact conditions and interactions between the materials in test as it occurs in the reality. The test specimens, the test set-up, the test program, the testing procedures and the results of this experimental investigation are presented and discussed in detail in this chapter.

Chapter 5, Numerical Investigation, reports on a numerical study concerning the flexural behaviour of simply supported CFRP-strengthened RC beams under fire conditions. The developed FE models to simulate the thermal and mechanical response of this elements were addressed in this chapter. The finite element software, the finite element mesh, the material modelling and analysis criteria, the boundary, loading and contact conditions, the analysis method and procedure and the validation of the FE models were also presented in this chapter. In addition, the results of the numerical analysis were duly discussed in Chapter 5.

Chapter 6, Conclusions and Future Work, provides an overview of the developed investigation and a summary of the most significant findings of this research. This chapter also presents suggestions for possible future researches on the fire behaviour of RC Beams EBR-strengthened with CFRP laminates. Considerations related to the use of CFRP-strengthened systems on RC beams, ethics and good practice for the EBR-CFRP strengthening construction are still addressed in this chapter, looking for a better way to improve the fire performance of this type of structures, such as the development of new materials and methods to design this.

Finally, Appendix A and Appendix B present additional information and results on the experimental phase of this investigation.

2 STATE OF THE ART

In this chapter, the current state-of-the-art on the RC beams strengthened with CFRP composite materials is carefully addressed. The most important experimental and numerical investigations in this area of knowledge, both for CFRP-concrete bond scale and for beam-strengthening element scale, are presented in detail and discussed below in terms of thermal and mechanical behaviour.

2.1 Bond Behaviour of CFRP-concrete Interface

2.1.1 Experimental investigations

A limited number of experimental studies were reported in the literature [36–43] regarding the behaviour of CFRP-concrete interface on strengthening systems at ambient and elevated temperatures, using the externally bonded reinforcement (EBR) technique.

Blontrock [36] performed Double lap Shear Tests (DST) on CFRP-strengthened concrete blocks (150 x 150 x 800 mm). The specimens were strengthened using the EBR technique and the T_g of the epoxy adhesive that bonds the CFRP laminates to the concrete members was quoted as 62 ºC (the test and estimation method used to obtain the T_g were not specified). The specimens were tested at ambient temperature (reference test), 40 ºC, 55 ºC and 70 ºC. The bond strength of the CFRP-concrete at 40 ºC, 55 ºC and 70 ºC presented a retention of 141%, 124% and 82% of the value at ambient temperature, respectively. A rapid loss of bond strength for temperatures above T_g was observed. Despite this, a significant residual strength retention was noticed even at temperatures exceeding T_g. The authors attributed the thermal stresses induced by the different thermal expansion coefficient of the materials, CFRP and concrete, to justify the strength increase to temperatures below T_g (40 ºC and 55 ºC) and decrease for temperatures above T_g (70 ºC). The post-curing phenomena of the adhesive due to excessive heating exposure time on the tested specimens can be the reason for this behaviour, but this hypothesis cannot be confirmed since the authors did not report information on the heating period. The failure mode of the specimens occurred due to the concrete substrate rupture at ambient temperature and due to adhesive failure along the bond interface at elevated temperatures.

Double lap Shear Tests (Figure 2.1) carried out by Klamer et al. [37] presented a similarity with the ones performed by Blontrock [36]. The specimens were bonded according to the EBR

technique and subjected to temperatures of 20 ºC (ambient temperature), 50 ºC and 75 ºC. The T_g was quoted as 62 ºC and the test and estimation method used to obtain this temperature were not specified.

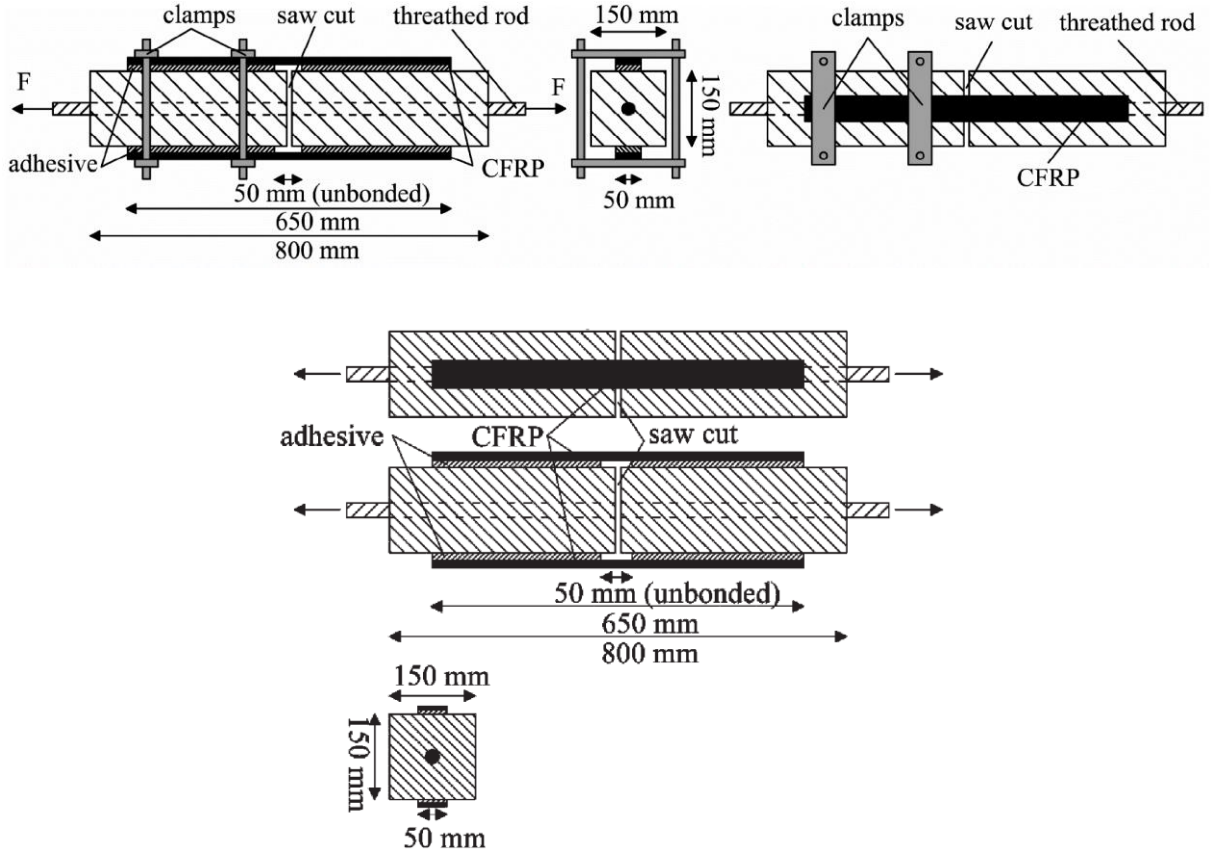

Figure 2.1 – Double-lap Shear Test Setup [37]

A low increase of the bond strength for temperatures below the T_g (about 110% of bond strength retention at 50 ºC) and a moderate loss of bond strength for temperatures above the T_g (about 63% of residual strength retention at 75 ºC) were noticed (Figure 2.2 – Series A). Similar tendencies were reported by Klamer [38] in an experimental investigation that included DST tests at temperatures ranging from –20 ºC to 90 ºC. The results also revealed an increase of the strength retention at temperatures below T_g (increase of about 9% at 50 ºC) and a loss at temperatures above T_g (loss of about 16% at 70 ºC), considering 20 ºC as a reference temperature. The characteristics of the epoxy adhesive was the same used in Klamer et al. [37].

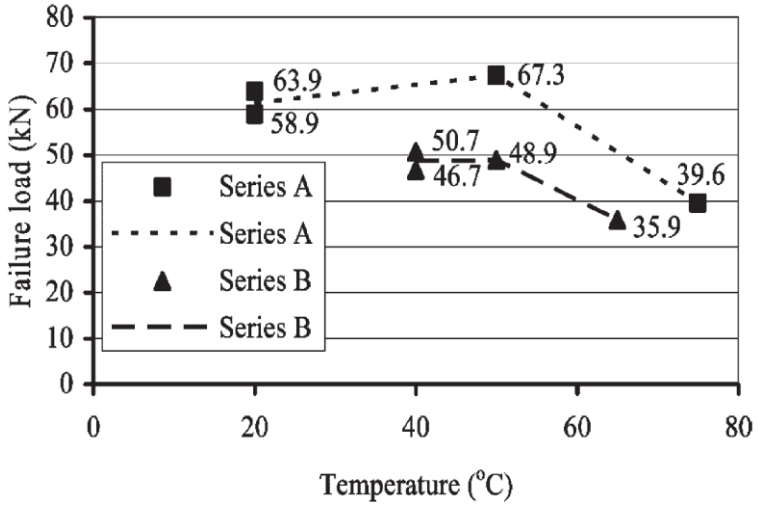

Figure 2.2 – Failure loads of the double-lap shear test specimens (series A and B) [37]

The failure modes were similar as observed in the work by Blontrock [36], where specimens tested at temperatures from -20 ºC till 50 ºC failed in the concrete substrate (Figure 2.3a) and the specimens subjected at temperatures higher than 50 ºC failed at the adhesive (Figure 2.3b). The same behaviour was verified in Klamer et al. [37].

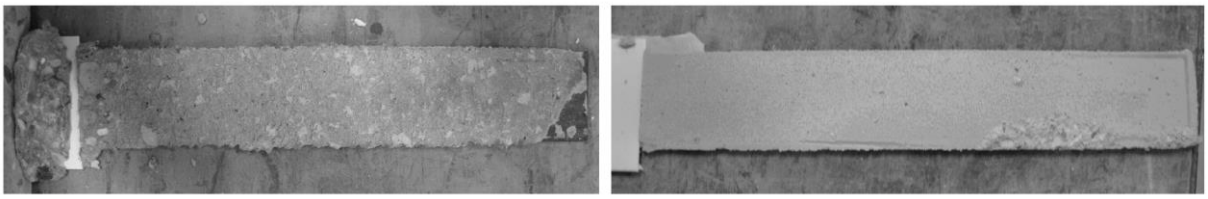

(a) **(b)**

Figure 2.3 – Failure modes in the (a) concrete at 20 ºC and (b) adhesive at 70 ºC [38]

Similarly, Firmo et al. [39] conduced DST tests on concrete blocks strengthened with externally bonded CFRP laminates. Geometry and detail of instrumentation of test specimens are presented in Figure 2.4. The specimens were subjected to temperatures of 20 ºC (ambient temperature), 55 ºC, 90 ºC and 120 ºC. The T_g of the adhesive, determined by Dynamic Mechanical Analyses (DMA) and based on the storage modulus curve (E'), was estimated at 47 ºC.

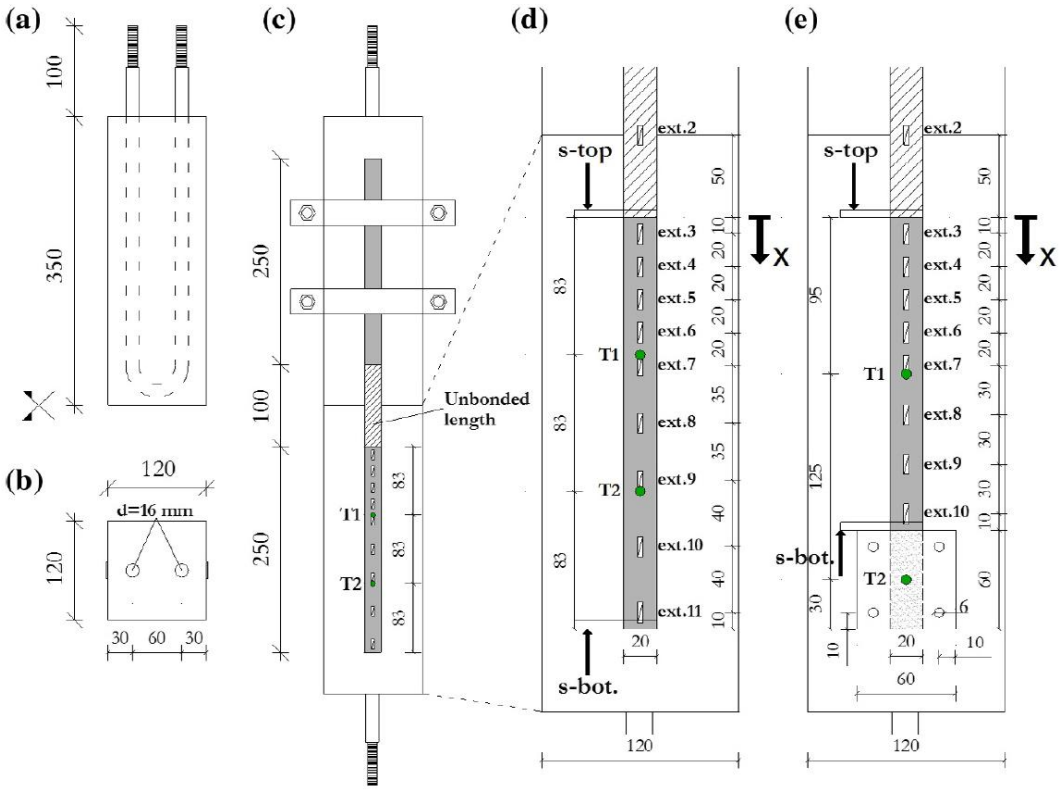

Figure 2.4 – Geometry of test specimens (a-c) and detail of instrumentation of (d) series S1 and (e) series S1A, dimensions in mm [39]

Figure 2.5 shows that the increasing temperature caused consistent reduction of bond strength. The heating for temperatures of 55 ºC (above T_g) induced a small loss of bond strength, around 10% when compared to ambient temperature. In addition, a residual bond strength retention at temperatures much higher than T_g (32% at 90 ºC and 23% at 120 ºC) were noticed. In addition, the influence of mechanical anchorage on the ends of the laminates was investigated (Series-S1A), as well as the effect of the different test procedures, namely tests under steady state and transient conditions (Series-S2). The use of mechanical anchorage in the specimens provided significantly higher bond strength between 56% and 139% compared with the ones without anchorage (Series-S1). The obtained results were similar for both steady state and transient conditions.

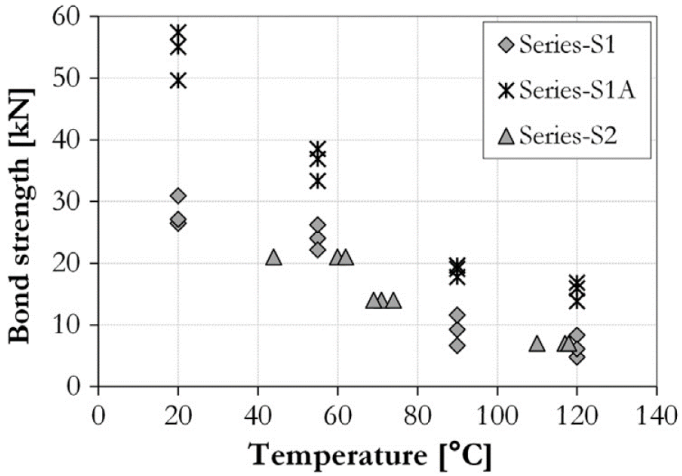

Figure 2.5 – Bond strength vs. temperature for all test series [39]

Concerning the failure modes, for series S1 and S2, concrete substrate failure occurred at ambient temperature and the adhesive failure occurred at elevated temperatures, as can be seen in Figure 2.6a and Figure 2.6b, respectively. For specimens with mechanical anchorage (S1A), a shear failure at the anchorage zone at ambient temperature (Figure 2.6c) and an adhesive failure at the area of bonded length at elevated temperatures (Figure 2.6d) were observed.

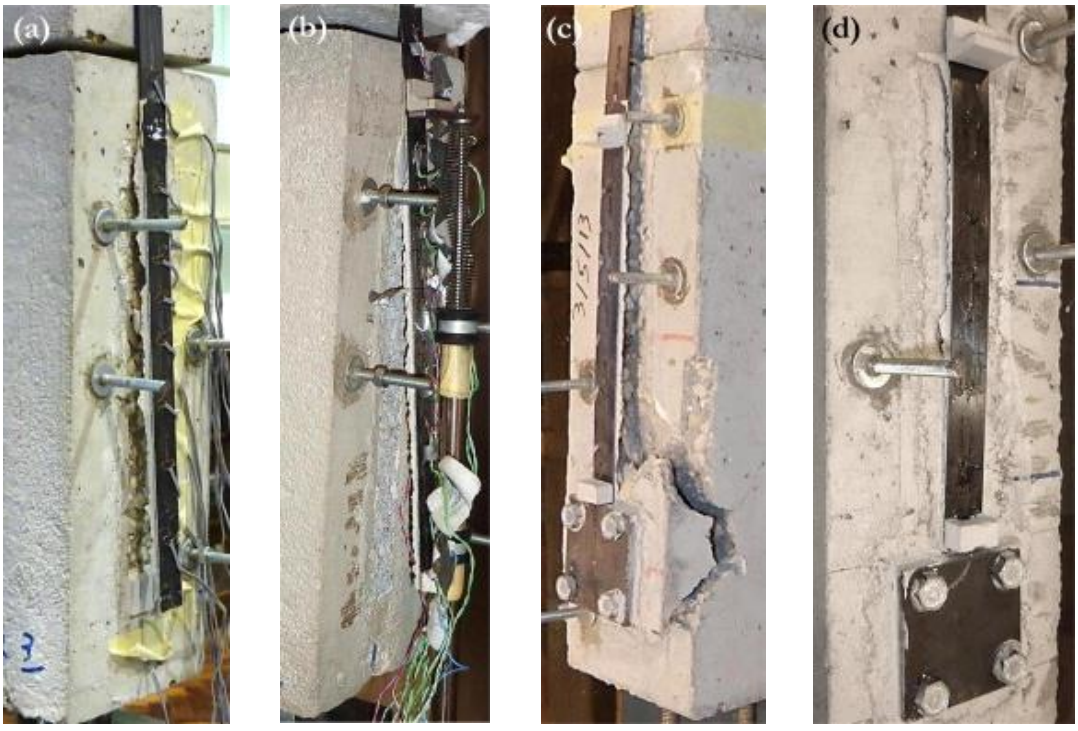

Figure 2.6 – Failure modes for series S1 at (a) 20 ºC and (b) 55 ºC; Failure modes for series S1A at (c) 20 ºC and (d) 55 ºC [39]

Ferrier [40] has also recently investigated the temperature variations on concrete blocks externally bonded with CFRP laminates. Double lap Shear Tests were carried out heating the specimens to different levels of temperatures between –20 ºC to 120 ºC. Considering the temperature of 20 ºC as a reference, the test results demonstrated a continuous decrease of the bond strength with temperature increasing. However, an expressive retention was noticed at temperatures above T_g (between 70 and 80% from temperature range of 50 to 110 ºC. Moreover, decreases were observed for very low temperatures (–20 ºC). The T_g was quoted as 58 ºC.

Wu et al. [41] studied the CFRP-concrete bond behaviour at temperatures ranging from 26 ºC to 60 ºC. Double lap Shear Tests were carried out on concrete blocks (100 x 100 x 450 mm) strengthened with CFRP sheets using the EBR technique (see Figure 2.7). Two types of epoxy adhesives were used, an ordinary and a thermo-resisting one. The ordinary and the thermo-resisting adhesive used to bond the CFRP have an estimated T_g of 34 ºC and 40 ºC, respectively. The type of test and the estimation method for determining T_g were not reported.

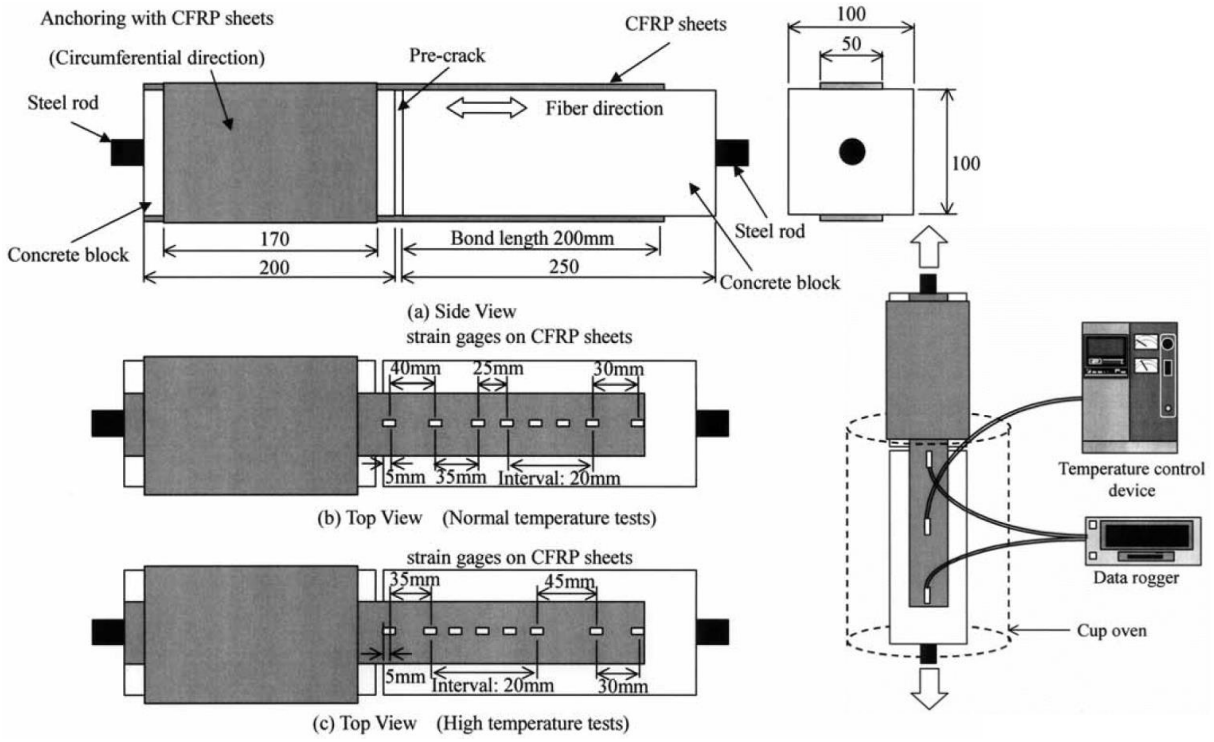

Figure 2.7 – Specimen's details and DST test setup [41]

The bond strength showed a consistent decrease with temperature increasing for both types of adhesive (Figure 2.8). Despite the decreasing of the bond strength, a bond strength retention of 40% at a temperature of 50 ºC (above T_g) was obtained for specimens with the ordinary adhesive and of 85% for specimens with the thermo-resisting adhesive. At 60 ºC, the specimens tested

with the thermo-resisting adhesive presented a significant bond strength retention of around 50%. The temperature increase changed the failure mode from concrete substrate at ambient temperature to adhesive (in the bonding interface area) at elevated temperature.

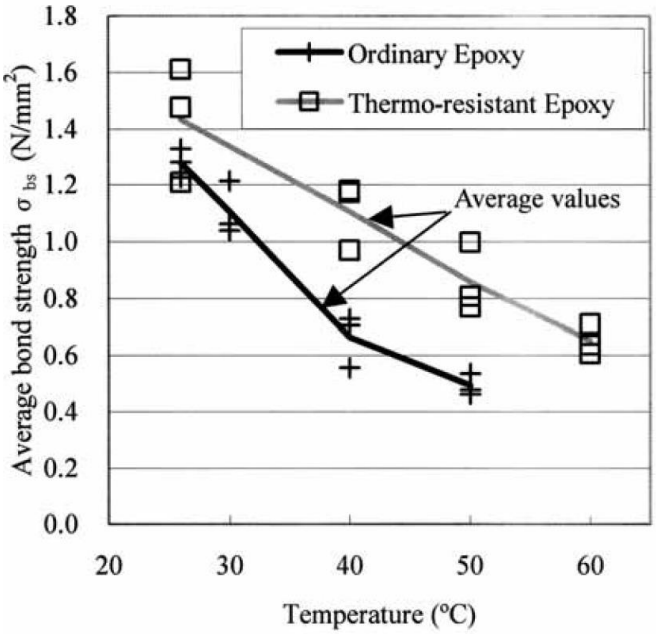

Figure 2.8 – Average bond strength under different temperatures [41]

Gamage et al. [42] conduced SST tests on ten concrete blocks (130 x 130 x 300 mm) EBR-strengthened with CFRP sheets bonded using epoxy adhesive. The T_g of the adhesive was not reported and neither was the type of test and the estimation method to obtain it. The specimens were heated to temperatures varying from ambient temperature (20 ºC) up to 140 ºC.

Considerable bond strength reductions were observed with increasing temperature (see Figure 2.9), resulting in a rapid strength loss when the adhesive reached the temperature range between 50 ºC and 75 ºC (about 25% of bond strength compared to ambient temperature). At this same temperature range, a transition of the failure modes (Figure 2.10) occurred from a combination of bond failure and concrete rupture (up to 50 ºC) to peeling-off adhesive failure (above 60 ºC).

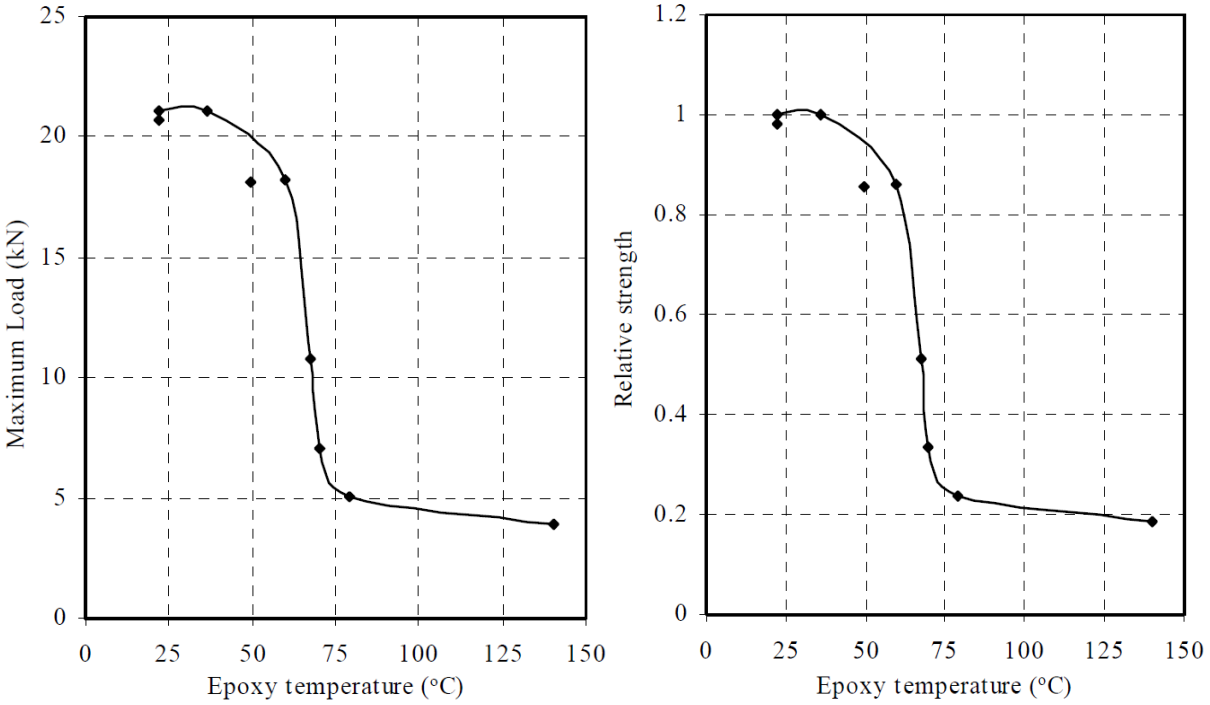

(a) **(b)**

Figure 2.9 – (a) Bond strength and (b) relative strength evolution as a function of temperature for the tested specimens [42]

(a) **(b)**

Figure 2.10 – Typical failure modes observed from shear test under raised temperature: (a) epoxy temperature < 50 ºC; (b) epoxy temperature > 60 ºC [42]

The works of the authors addressed above (Wu et al. [41] and Gamage et al. [42]) presented different tendencies from the previous ones [36–40] concerning the behaviour of the bond between the CFRP and the concrete element at elevated temperatures. These authors reported a consistent decreasing on the bond strength with increasing temperature for temperatures below the T_g while in previous studies an increasing was observed.

Another work was the one of Leone et al. [43] that have performed DST tests (Figure 2.11) on concrete blocks externally strengthened with CFRP laminates. The specimens (two prisms of 150 x 150 x 400 mm) were tested at temperatures of 20 ºC (ambient temperature), 50 ºC and 80 ºC (specimens C_L_20, C_L_50 and C_L_80, respectively). The T_g of the adhesive (55 ºC) was determined by Differential Scanning Calorimetry (DSC) test and the estimation method to obtain it was not specified.

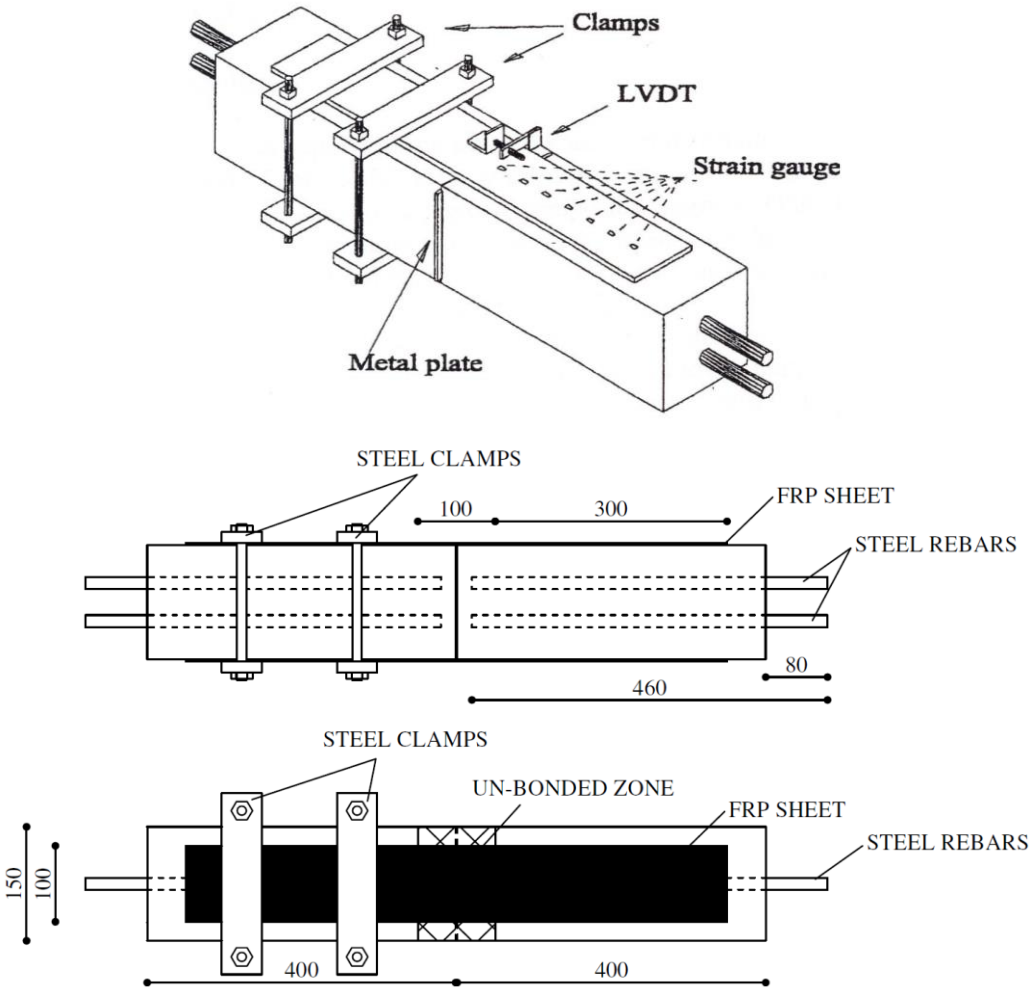

Figure 2.11 – Test set-up [43]

The results of these authors presented some differences to the ones of Blontrock, Klamer et al., Klamer and Ferrier [36–38,40]. Comparing with these authors, Leone et al. [43] found a slight decrease of the bond strength for temperatures lower than T_g (85% of strength retention at 50 ºC) and a surprisingly slight increase for temperatures higher than T_g (109% of strength retention at 80 ºC). The results (Table 2.1) were compared to the behaviour of the tests performed at ambient temperature (reference test specimen C_L_20). This bond behaviour was contradictory to the ones observed by Firmo et al. [39], Wu et al. [41] and Gamage et al. [42]

for temperatures above the T_g, although a similar behaviour has been noted for temperatures below the T_g. Leone et al. [43] related these unexpected and anomalous behaviour to a probable influence of the chemical processes occurring at the T_g temperature range and concluded that this needs further investigation. Concerning the failure modes of the specimens, at ambient temperature and 50 ºC it was in the concrete substrate and at elevated temperatures (80 ºC) in the adhesive, in agreement with the other works.

Table 2.1 – Test results (adapted from [43])

Test specimens	Temperature (ºC)	Failure load (F_u) (kN)	Relative bond strength (F_u / $F_{u,20\ ºC}$)	Failure mode
C_L_20	20	40.47	1.00	Concrete substrate
C_L_50	50	34.33	0.85	Concrete substrate
C_L_80	80	44.02	1.10	Adhesive

$F_{u,20\ ºC}$ – Failure load at ambient temperature

According to the aforementioned authors, at elevated temperatures a significant residual bond strength is still observed, even in cases where the T_g of the adhesive has been significantly exceeded. It is indispensable that the thermal and mechanical response of the CFRP-concrete bond for temperatures higher and much higher than T_g be analysed and, unfortunately, most of the studies described above have evaluated the degradation of the bond for limited temperatures, slightly exceeding the T_g of the adhesive. In addition, the experimental results addressed above are contradictory, presenting opposite tendencies, especially concerning the bond strength evolution for temperatures below or above T_g. Some authors (Wu et al. [41], Gamage et al. [42] and Leone et al. [43]) reported a decreasing on the bond strength with increasing temperature for temperatures below the T_g while in others (Blontrock [36], Klamer et al. [37], Klamer [38] and Ferrier [40]) an increasing was observed. For temperatures above T_g, Leone et al. [43] reported a slight increase of the bond strength, in opposition to the ones observed by Firmo et al. [39], Wu et al. [41] and Gamage et al. [42] that presented a loss of the bond strength. A benchmarking of the current research results with the ones reported by the previous investigations concerning the CFRP-concrete bond behaviour at elevated is addressed and discussed in further detail in Chapter 3.

2.1.2 Analytical and numerical investigations

A few analytical and numerical investigations reported in the literature [38,44–48] have focused on the behaviour of the bond between the CFRP and concrete at elevated temperatures in strengthening systems.

Dai et al. [44] presented a non-linear model for the bond-slip behaviour between the CFRP laminates and concrete element at elevated temperatures considering the EBR technique for bonding. The numerical model is an extension of a previous bond-slip model at ambient temperature by Dai et al. [45], where the parameters of interfacial fracture energy and interfacial brittleness index were considered. They are respectively related to the ultimate pull load and the global load–displacement response of CFRP-concrete interfaces at elevated temperatures (experimentally obtained using existing SST test data). Moreover, the authors took into account the influences of temperature-induced thermal stress and bond degradation. The results showed that initially the interfacial fracture energy was approximately constant and then begins to decrease when the temperature approaches the T_g of the adhesive. A similar tendency was observed for the interfacial brittleness. Despite the large dispersion of the test data, the developed bond-slip model was capable of representing the test data upon which it was based.

Gao et al. [46] developed an analytical solution for the deformation process of CFRP-concrete bond subjected to thermal and mechanical conditions based on a bilinear bond-slip model. The analytical model was validated through comparisons with experimental results and finite-element predictions. Two limitations were assumed in this investigation – the material properties are not affected by temperature variations and the concrete-adhesive interface is linear elastic. These simplifications limited the model to the temperature variation up to the T_g of the adhesive provided by the experimental data. A good agreement with experimental data was obtained (up to temperatures of the T_g), including the temperature-induced interfacial stresses developed during heating.

Similarly, Klamer [38] performed numerical simulations on concrete blocks EBR-strengthened with CFRP laminates to analyse the CFRP-concrete bond behaviour at elevated temperatures. The data from his previous experimental investigation [37] (described in detail in Section 2.1.1) was used for the validation of a two-dimensional FE model. The simulations were carried out according to a bi-linear bond–slip relationships using the commercial software package DIANA [49]. Despite the success of the predictions considered in the FE model for temperatures limited up to the T_g of the adhesive, the bond-slip relationship for temperatures above T_g did not provide good results. This may be due to the simplifications in the bond–slip relationship for higher temperatures (up to 70 ºC). Reductions about 85% on maximum shear stress at temperature of 70 ºC (above T_g of the adhesive) were observed.

A three-dimensional FE model was developed by Gamage et al. [47] to simulate the behaviour of the bond interface on CFRP-strengthened concrete blocks under thermal and mechanical influence. The commercial software package STRAND7 [50] was used for numerical simulations. The relationship between the CFRP-concrete stiffness and temperature of the

adhesive was considered in a simple thermal and structural analysis. However, information about the modelling procedure for the CFRP-concrete bond was not reported. The numerical FE models were validated using experimental results from both non-insulated [51] and insulated [52] specimens, modelled in 3D as shown in Figure 2.12a and Figure 2.12b, respectively.

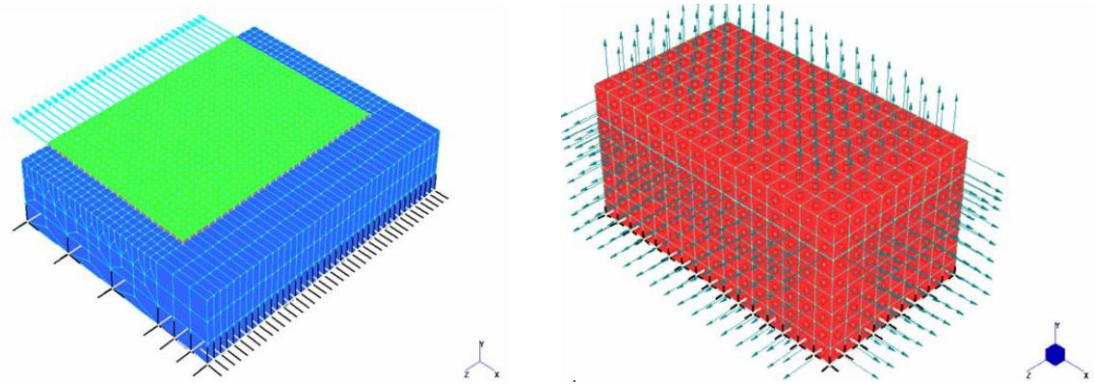

(a) **(b)**

Figure 2.12 – Finite element mesh and details of the (a) non-insulated [51] and (b) insulated [52] models (adapted from [47])

Figure 2.13 shows almost identical bonding failure times for the different tested CFRP bond lengths (BL), ranging from 5 to 6 min. This indicated that the bond strength does not depend on the bond length of CFRP when subjected to elevated temperatures and the need for passive fire protection systems to maintain the CFRP-concrete bond effectiveness for longer periods of exposure.

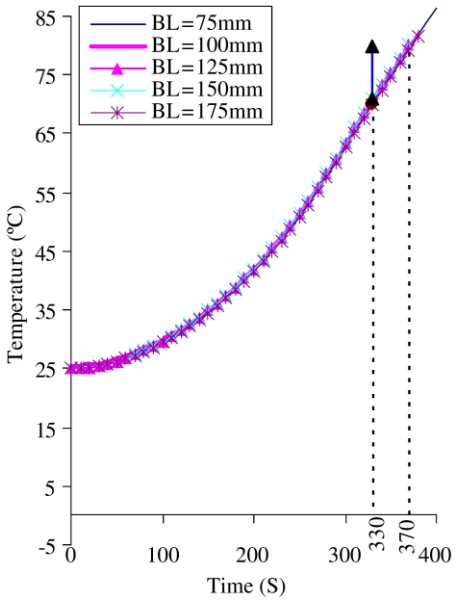

Figure 2.13 – Temperature distributions within the epoxy layer for non-insulated specimens analysed under the AS1530.4 standard fire curve [47,53]

The authors also concluded that the thermal conductivity and the thickness of the fire protection systems significantly affect the temperature evolution at the adhesive of the insulated specimens, consequently their fire resistance (as can be seen in Figure 2.14a and Figure 2.14b, respectively).

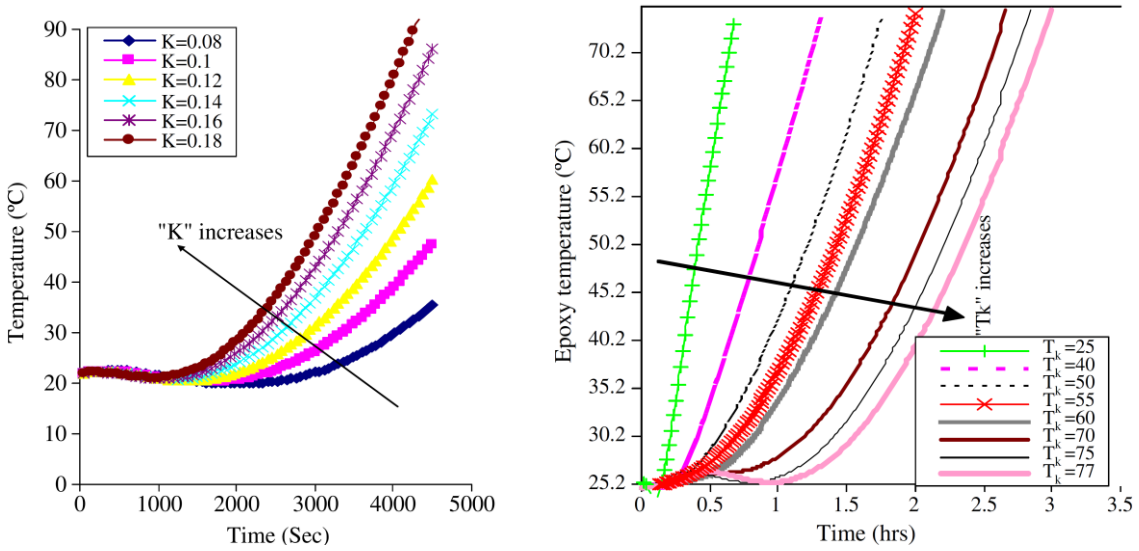

(a) **(b)**

Figure 2.14 – (a) Temperature distributions with in the epoxy layer as a function of time and thermal conductivity of insulation ("K" in W/m/ºC); (b) Epoxy temperature variations with the insulation thickness ("T_k" in mm) (adapted from [47])

Another conclusion was concerning the influence of the heating rate on models, in which a temperature rise in the adhesive and a reduction of the bond strength were observed with the increase of the heating rate (Figure 2.15).

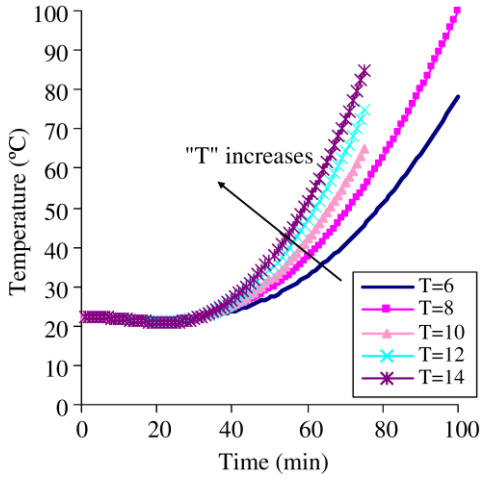

Figure 2.15 – Epoxy temperature variations for different fire conditions ("T" = rate of heat in ºC/min) [47]

Moreover, comparison between experimental and numerical results (Figure 2.16a-e) indicated a good accuracy of the model to predict the behaviour of the CFRP-strengthened concrete members in terms of temperature evolution, fire resistance, failure temperature and time of the bond between CFRP and concrete.

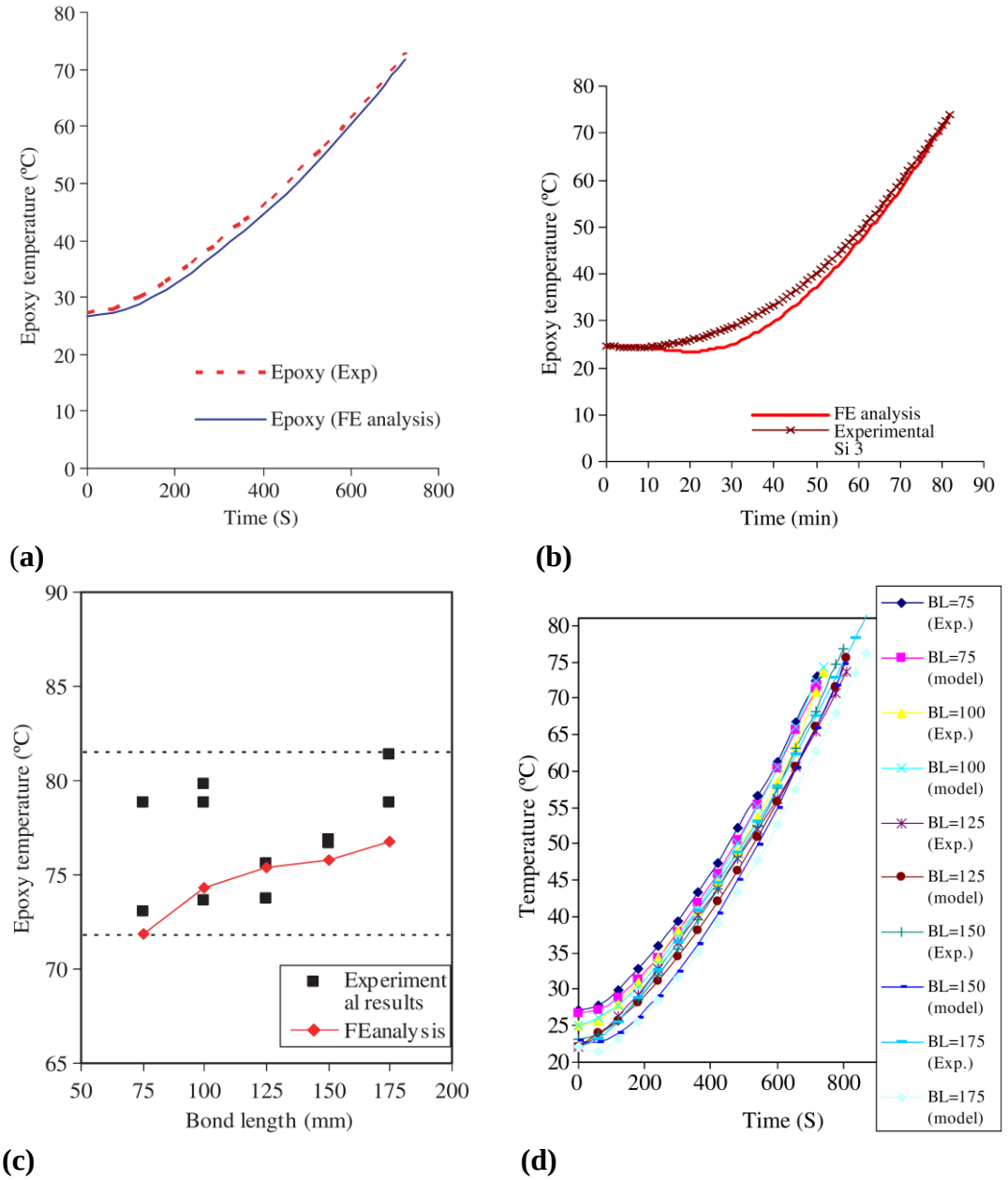

Figure 2.16 – Temperature distributions of (a) non-insulated and (b) insulated CFRP-strengthened specimens; (c) comparison between experimental and model predicted failure points; (d) temperature distributions at the adhesive layer for non-insulated members fire; (e) fire resistance levels for the insulated members under experimental temperature (adapted from [47])

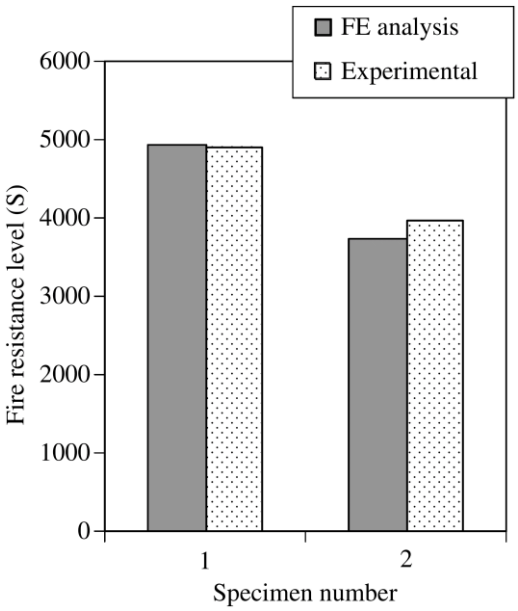

(e)

Figure 2.16 – Temperature distributions of (a) non-insulated and (b) insulated CFRP-strengthened specimens; (c) comparison between experimental and model predicted failure points; (d) temperature distributions at the adhesive layer for non-insulated members fire; (e) fire resistance levels for the insulated members under experimental temperature (adapted from [47]) (Continuation)

Arruda et al. [48] presented more recently a numerical study on bond between concrete and CFRP laminates in strengthening systems at moderate elevated temperatures (20 ºC, 55 ºC, 90 ºC and 120 ºC). Three-dimensional finite element (FE) models were developed based on data from a previous experimental investigation by Firmo et. al [39] (described in detail in previous section) that performed DST tests on concrete blocks strengthened with CFRP laminates bonded using the EBR technique. The mesh geometry of the FE models replicated from that of the DST tests for EBR specimens [39] is illustrated in Figure 2.17. The numerical simulations were conducted using the commercial software package Abaqus [54]. Bi-linear bond–slip laws were proposed to evaluate the CFRP-concrete bond response at elevated temperatures.

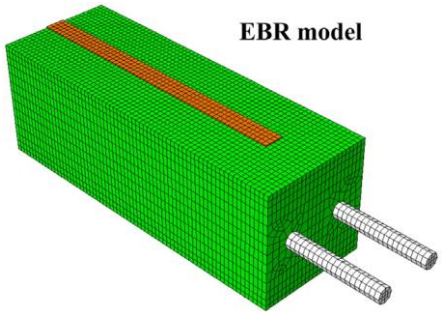

Figure 2.17 – Mesh geometry for the EBR specimens [48]

The results provided by the proposed bond-slip laws presented significant reductions of stiffness and maximum shear stress of the bond with increasing temperature, approaching with faithfulness the experimental data. These results confirmed the stiffness dependency of the CFRP-concrete bond with the adhesive behaviour at elevated temperatures. Moreover, with the exception of the results at 120 ºC, a good agreement between numerical results and experimental data were obtained for the failure loads of the models (Table 2.2) with an error from –0.4% to 5.2%, depending on temperature level. At 120 ºC, the error between the models was more significant, corresponding to 8.3%.

Table 2.2 – Experimental vs. numerical failure loads for the EBR series (adapted from [48])

Temperature (ºC)	Experimental failure load (F_u) - (kN)	Numerical failure load ($F_{u,n}$) - (kN)	Relative error
20	25.9	25.8	–0.4
55	22.1	23.1	4.5
90	11.6	12.2	5.2
120	4.8	5.2	8.3

The inelastic strain results for different numerical failure load and temperature levels (Figure 2.18 and Figure 2.19) indicated a behaviour very similar to each other in terms of failure modes with the specimens from experimental investigation, where a concrete substrate failure was observed at ambient temperature and an adhesive failure at the concrete-adhesive interface at elevated temperatures occurred.

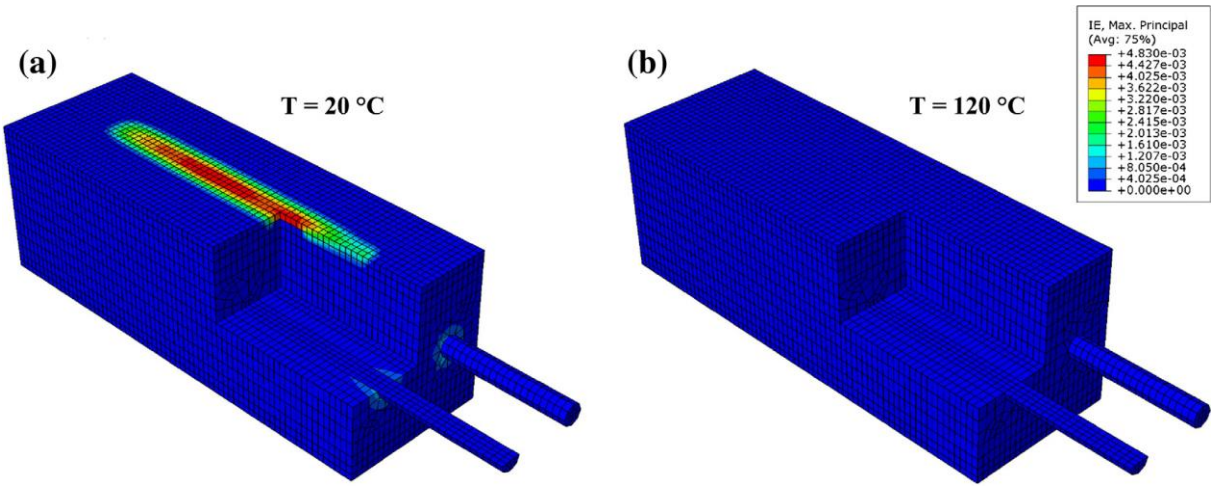

Figure 2.18 – Inelastic maximum principal strains in the concrete at failure for the EBR specimens at (a) 20 ºC and (b) 120 ºC [48]

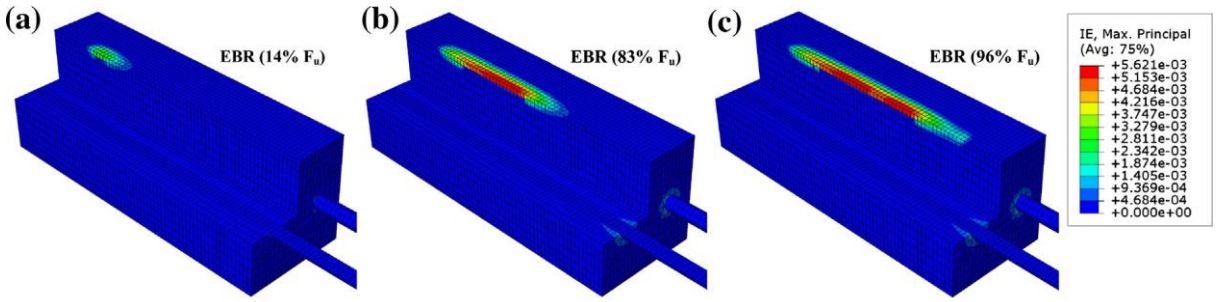

Figure 2.19 – Inelastic maximum principal strain in the concrete for the EBR specimens at 20 ºC for (a) 14%, (b) 83% and (c) 96% of the failure load [48]

As result of the considerable complexity involved in this type of research, a scarce number of analytical and numerical works are available in the literature to simulate the behaviour of CFRP-concrete bond at elevated temperatures. Most of these studies were limited to the T_g of the adhesive. The lack of experimental data (as discussed in the previous section) for the validation of numerical models at temperatures higher and much higher than T_g (or at specific levels of temperature) contributed to this limitation. Moreover, simplifications assumed by the authors on the bond-slip relationships for higher temperatures, such as the consideration that the concrete-adhesive interface is linear elastic, did not provide good results for temperatures above or much higher than T_g (although good accuracy has been observed for temperatures below T_g).

Finally, the development of accurate models to simulate the CFRP-concrete bond behaviour with good predictions for temperatures above T_g and that consider the complexities mentioned above are essential, particularly due to the residual strength phenomena observed in the bond during high thermal exposure and until its failure. These shortcomings, both in the experimental and numerical field, were some of the motivations of the present study.

2.2 Behaviour of CFRP-strengthened RC beams

2.2.1 Experimental investigations

Concerning the behaviour of CFRP-strengthened RC beams under fire conditions a few studies have been reported in the literature over the years [55–62]. The most important works in this regard, investigated experimentally for both ambient and fire conditions, are discussed in this section.

An experimental program conducted by Ahmed and Kodur [55], studied the effectiveness of the insulation systems, anchorage systems, axial restraint effects, and fire exposure on the

behaviour of RC beams strengthened with CFRP laminates. Fire resistance tests in a four-point bending configuration (Figure 2.21) were carried out on four CFRP-strengthened RC beams (specimens B1, B2, B3 and B4) subjected to the ASTM E119 (2002) [63] standard fire or a "design fire" for a "typical" office compartment. The beams were simply supported and loaded up to 50% of their predicted loadbearing capacity. The specimens (Figure 2.20) were insulated with two types of U-shaped vermiculite-gypsum based fire protection systems of 25 mm thickness, sprayed on the bottom and lateral faces of the beams. On the top surface an intumescent coating was applied. Moreover, the presence of cool anchorages (by insultation of supported length of beams) was investigated in two beams (B3 and B4). The resin used to bond the laminates to the concrete had a T_g of 82 ºC determined by Dynamic Mechanical Analysis (DMA) as per ASTM D4065 (2006) [64] specification and was based on the peak value of the Tan δ.

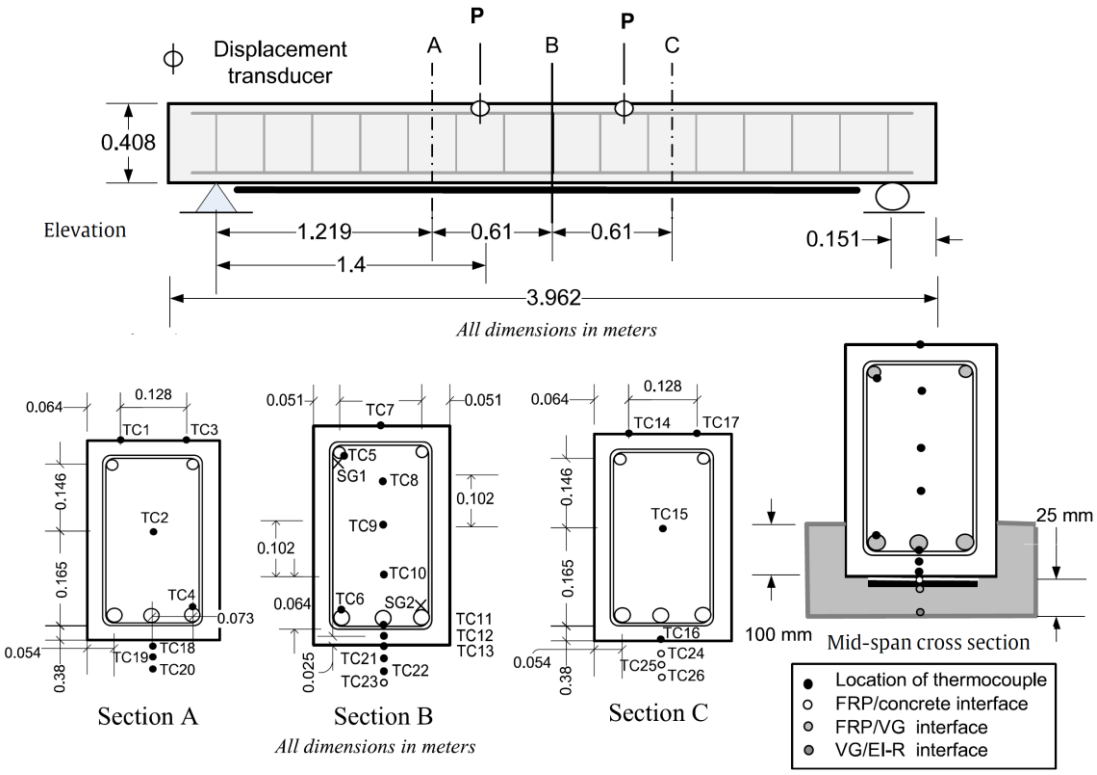

Figure 2.20 – Elevation, cross-sectional details and instrumentation of tested FRP-strengthened RC beam [55]

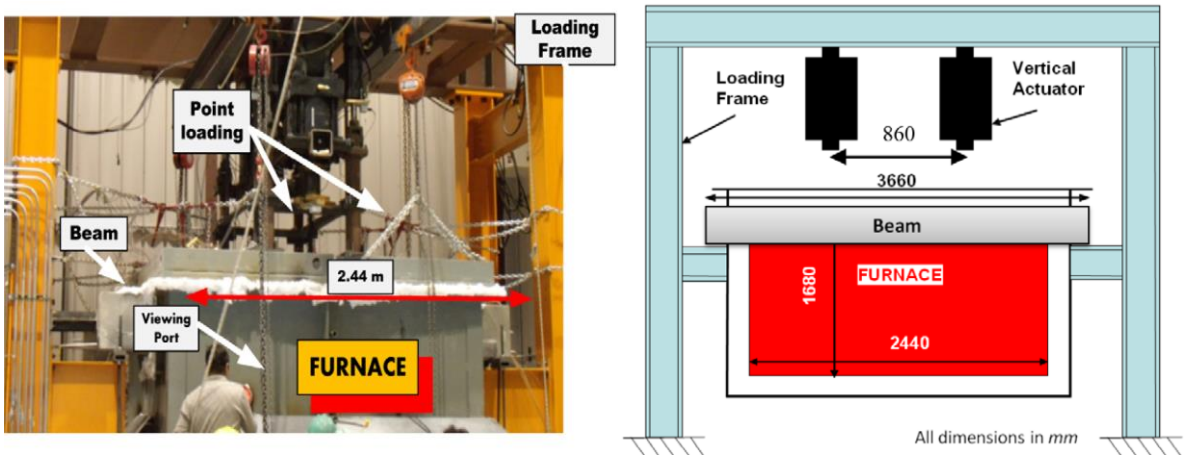

(a) **(b)**

Figure 2.21 – Fire resistance test setup: (a) general view and (b) schematic view [55]

According to the results, the debonding of the CFRP occurred when the temperature in the CFRP-concrete interface reached T_g ±10 ºC, corresponding to a time period between 20 and 25 minutes. Despite the debonding of the CFRP, no structural failure of the beams occurred, where the beam remaining effective to the applied loading for the full duration of fire exposure (Figure 2.22). That was probably due to the presence of cooler anchorages, which plays a critical role in limiting the deflections of the strengthened beam after debonding of the CFRP in its central length, where the unbonded continuous fibres on the beams' soffits continued to contribute to the flexural strength of the beam by catenary action ("cable action" – see Figure 2.23). In addition, the fire passive protection contributed on the increasing of fire resistance of the CFRP-strengthened beams.

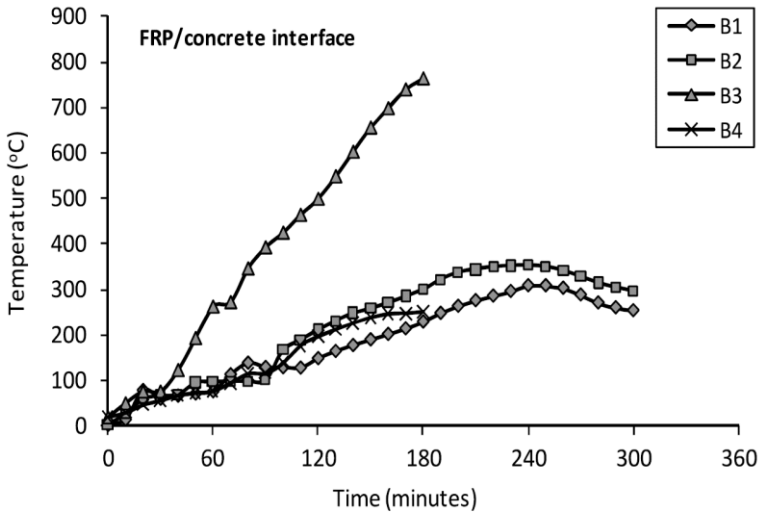

Figure 2.22 – Measured temperatures at the and FRP/concrete interface [55]

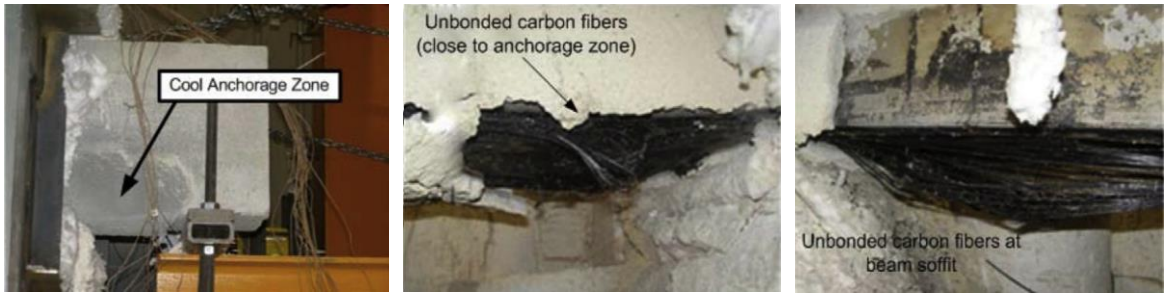

Figure 2.23 – Unbonded continuous carbon fibers at the beam soffit providing cable action [55]

Firmo *et al.* [56] and Firmo and Correia [57] presented two similar experimental researches on the behaviour of RC beams strengthened with CFRP laminates and subjected to the ISO 834 (1999) [34] standard fire. These works investigated the efficiency of the different fire protection systems and the insulation of the anchorage zones of the strengthening system of the beams.

In the first research [56], they performed six fire resistance tests on CFRP-strengthened RC beams, in a four-point bending configuration (Figure 2.25), simply supported and loaded up to about 50% of their predicted ambient temperature loadbearing capacity. The supports of the testing beam were outside the furnace. The specimens (2.10 m long, 0.10 m wide and 0.12 m height – Figure 2.24) were protected on the bottom surface with calcium silicate boards or vermiculite-perlite mortar (25 or 40 mm thick). The ends of the CFRP laminates were not directly exposed to the thermal action (thermally insulated by the furnace walls) in order to simulate anchorage zones (Figure 2.26).

Figure 2.24 – Geometry of the beams flexurally strengthened with a CFRP laminate (before the installation of the fire protection system) [56]

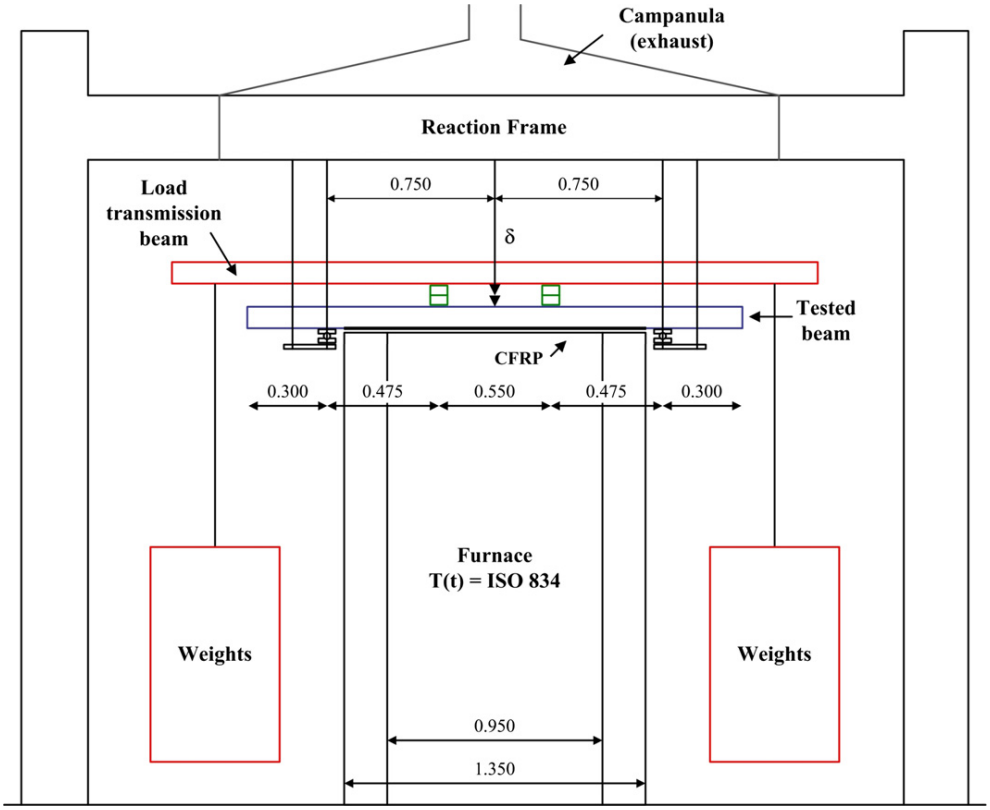

Figure 2.25 – Test setup of fire resistance tests – frontal view (not to scale, dimensions in m) [56]

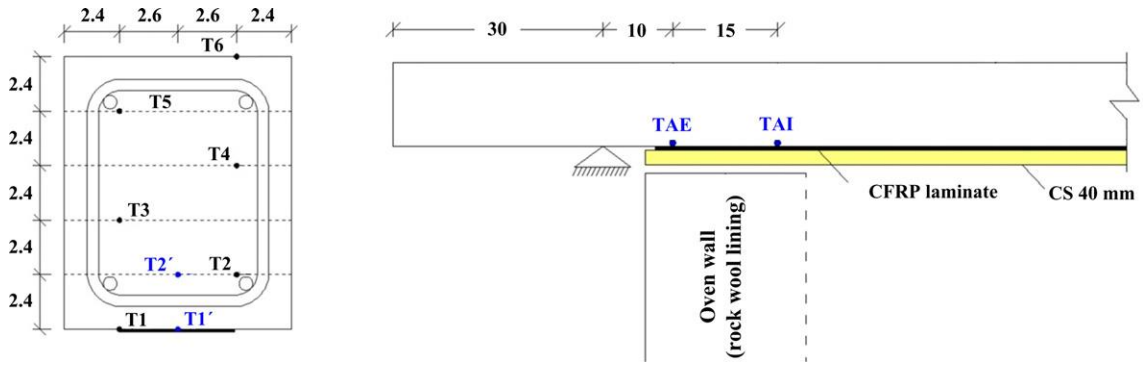

Figure 2.26 – Position of thermocouples: mid-span section of all beams (left) and anchorage zone of beam CS40 (right), dimensions in cm [56]

The results reported that (in the better case, with the insulation of the anchorage zones and 40 mm thick VP mortar at the beam soffit – Beam VP40) the CFRP system failed after 167 min of fire exposure (Figure 2.27b) when one of the anchorage zones reached the glass transition temperature (indicated as 55 ºC and determined by DMA test and based on the peak values of the loss modulus curves), losing its bond strength. The strengthening system resisted only 23

min for the beam without fire passive protection and only insulated at the anchorage zones (Beam CFRP), as shown in Figure 2.27b.

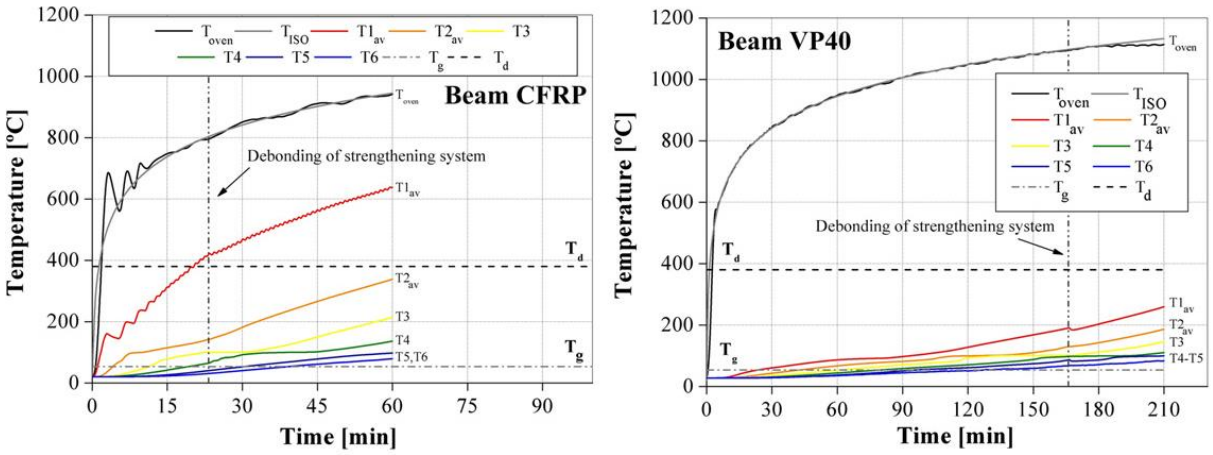

(a) **(b)**

Figure 2.27 – Measured temperatures vs. time for the (a) beam CFRP and (b) beam VP40 [56]

The strengthening system resisted for long periods of exposure due to the insulation of the anchorage zones, which maintained low temperatures in this area and promoted the system to work as a "cable" mechanism, although the bond in the exposed part along the beams had already been lost (Figure 2.28).

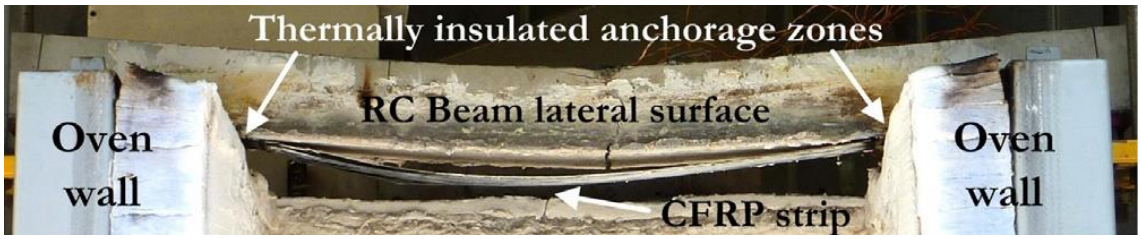

Figure 2.28 – CFRP strip detached from the RC beam only at the central zone and "cable" behaviour (adapted from Firmo et al. [56])

The second research reported by Firmo and Correia [57] is similar to the first [56] with differences on the lengths of the CFRP system exposed to fire and the type and thicknesses of the fire protection used in the anchorage zones (Figure 2.29).

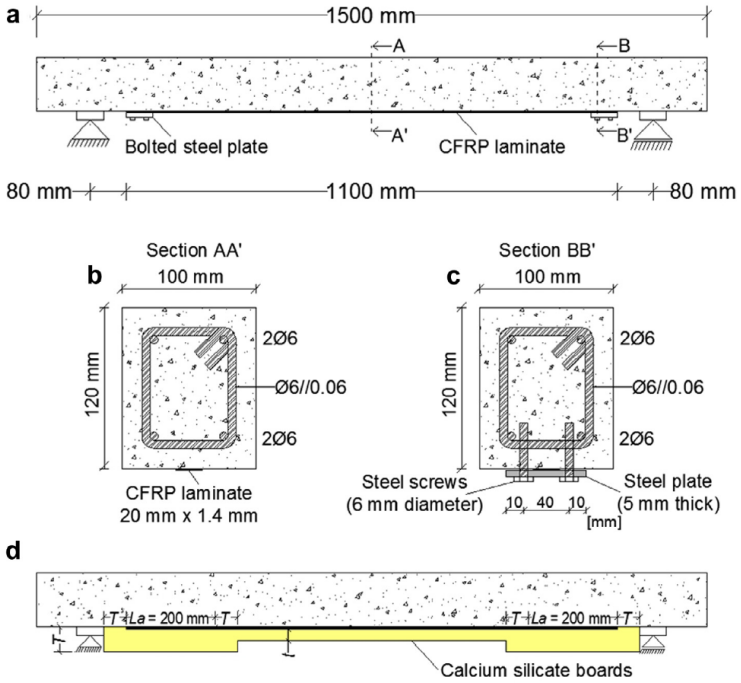

Figure 2.29 – Geometry of the test specimens: (a) longitudinal view of the specimen with mechanical anchorages on the CFRP extremities; (b) current cross-section; (c) cross-section with mechanical anchorage; (d) longitudinal geometry of the fire protection system [57]

Nine fire resistance tests (Figure 2.30) on RC beams strengthened with CFRP laminates were conducted. The T_g of the adhesive (47 ºC) was determined by DMA tests, based on the onset value of the storage modulus curve.

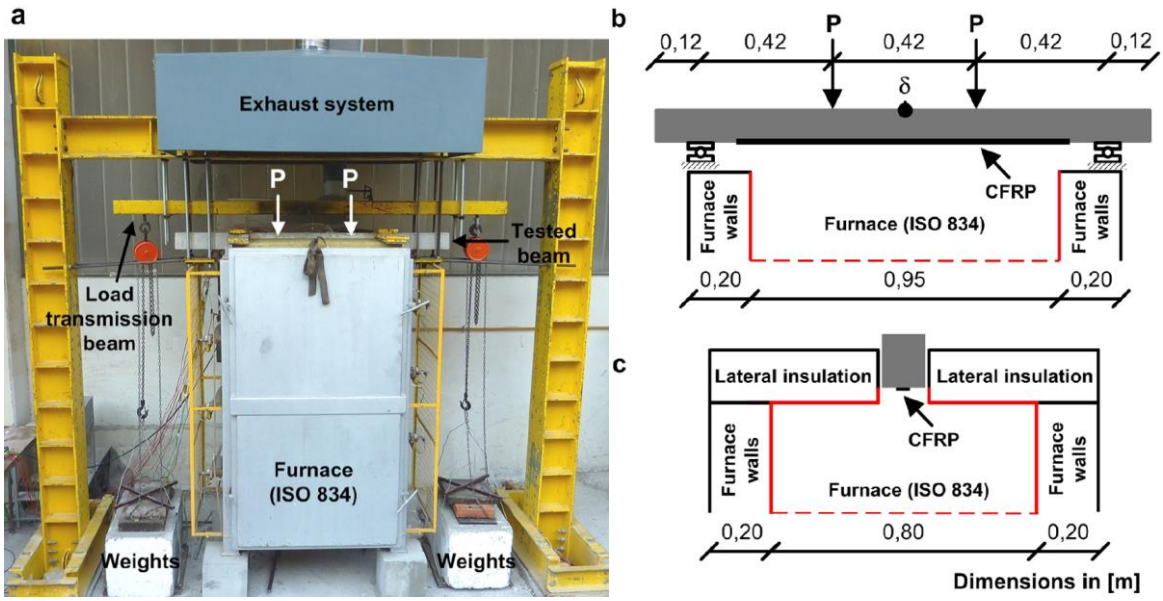

Figure 2.30 – Test setup: (a) general view of the furnace tests; (b) longitudinal and (c) transversal schematic views of the test setup [57]

According to Figure 2.31, the effectiveness of the strengthening system protected by calcium silicate boards was extended beyond 70 min (depending on the insulation system). At that point, the average temperature in the adhesive of the anchorage zones reached values between $1.2T_g$ to $1.5T_g$ (excluding the results of beams A-0-0, A-50-25 and 50-25-T_g) – again by taking advantage of the "cable" mechanism (Figure 2.32b) that usually forms in this type of reinforced beams in case of fire. The tensile failure of the CFRP did not occur, even at temperatures above 400 ºC at the central zone of the interface of the beams.

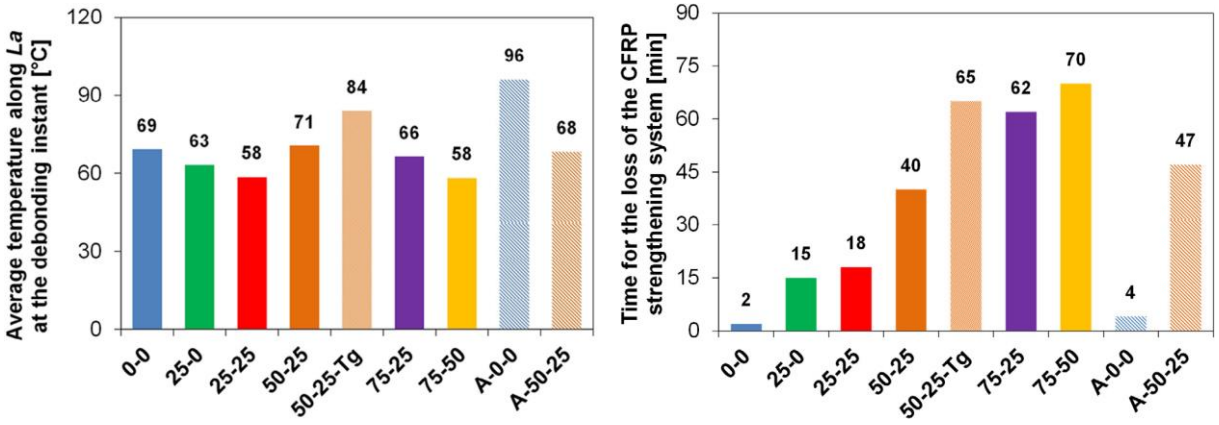

(a) **(b)**

Figure 2.31 – (a) Average temperatures in the adhesive along the anchorage length when the CFRP system debonded; (b) fire resistance of the strengthening system [57]

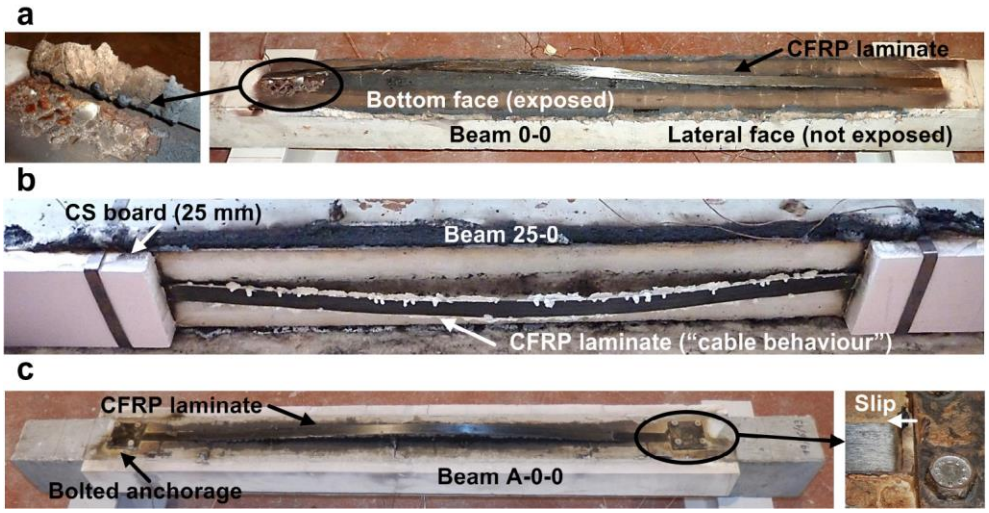

Figure 2.32 – Examples of the failure modes of the CFRP strengthening system: (a) beam 0-0; (b) beam 25-0; (c) beam A-0-0 [57]

Full-scale fire tests under ASTM E119 (2002) [63] standard fire curve on two CFRP-strengthened RC T-beams (span of 3.9 m) were conducted by Williams *et al.* [58] to assess the

fire behaviour of the strengthening system protected by vermiculite-gypsum plaster. This fire protection was applied on the lateral and bottom surfaces of the beams with layers of 25 mm or 38 mm thick. In addition, anchorage zones at the ends of the beams were created to prevent the premature collapse of the strengthening system. The specimens were loaded by 48% of the predicted ambient loadbearing capacity as serviceability load. In this experimental program, it was observed that both protected beams (insulation thickness of 25 or 38 mm) achieved 4 h of fire resistance although the T_g of the adhesive (defined as 93 ºC) had been reached at 54 min of test. The high fire resistance of these beams was surely due to the mechanical resistance performed by the anchorage system and the good performance of the fire protection system during the tests. Unfortunately, they were unable to identify the time and temperature when the bond between the concrete and CFRP lost its strength. More recently, similar results were reported by Adelzadeh et al. [59] in an extension of the study by Williams et al. [58].

Deuring [60] conducted an experimental study on large-scale RC beams EBR-strengthened with CFRP laminates exposed to the ISO 834 standard fire curve [34]. The specimens (cross-section of 30 cm x 40 cm and length of 500 cm) were tested under flexural and loaded to approximately 55% of their theoretical loadbearing capacity. A series of fire resistance tests were performed on four CFRP-strengthened beams in a four-point bending configuration, where two specimens were fire-protected along their bottom surface with a 40 mm thickness of calcium silicate boards. Moreover, two beams without strengthening were tested as reference. According to results, the beams without fire protection obtained a fire resistance of 81 min, although the debonding of the CFRP occurred at 20 min of fire exposure. The fire resistance was longer for fire-protected beams, reaching 146 min of fire exposure while the debonding of the strengthening system occurred at about 60 min of fire exposure. Similar results have recently been reported by Grace and Bebawy [61].

In a similar experimental investigation, Blontrock et al. [62] conducted a series of ten fire resistance tests on RC beams strengthened with CFRP laminates using the EBR technique. The specimens were fire-protected by U-shaped calcium silicate boards varying in thickness, length, location and bonding method. The tests were performed according to the ISO 834 standard fire curve [34] and under a flexural loading (corresponding to 38% of ultimate capacity of the beams at ambient temperature). The test results confirmed a significant reduction of temperature at the CFRP-concrete interface of the specimens due to passive fire protection systems adopted and maintaining the effectiveness of the strengthening system for longer periods. The debonding of the strengthening system occurred when the temperature in the CFRP-concrete bond interface reached between 66 ºC and 80 ºC, corresponding to temperature range of the T_g of the epoxy adhesive. Moreover, for specimens tested with anchorage zones and the ones that the protection was applied only at this area (with the middle length of the laminate directly exposed to fire) it

was observed that the bond was preserved for a similar time of exposure as in the case of specimens protected along its entire length. The behaviour observed in Firmo et al. [56] was also noticed in this case, where the CFRP contributed to the flexural strength of the beams with mechanical anchorage as a "cable" during the test (even after the debonding of the strengthening system at unprotected length).

The above experimental review clearly demonstrated the vulnerability of CFRP strengthening systems when directly exposed to high temperatures and confirmed the effectiveness of using some specific materials for passive fire protection in strengthened RC beams. However, it is still important to develop new and more effective fire protection systems for different building typologies (according to their intended use) in order to extend the lifetime of this type of structure in an eventual fire occurrence, consequently providing the respective minimum time necessary for the safe evacuation of the users. Furthermore, the authors did not consider the interaction between a CFRP-strengthened element and the typical surrounding structures. That interaction plays a significant influence on thermal-mechanical behaviour of the beam due to shading phenomena and the different ways of heat transfer with the primary element, as it happens in real situations. These limitations found in the recent literature were one of the most important motivations of this work and they are contemplated in the current PhD thesis.

Concerning the failure of the CFRP strengthening systems, some authors associate the loss of strengthening effectiveness with the achievement of CFRP-concrete interface temperatures to the T_g of the adhesive whereas for others the loss of strengthening was observed at temperatures above T_g. According to these results, it may be noted that it is still difficult to define a critical temperature in EBR-CFRP strengthening systems and it can be conservative to assume the T_g as an upper limit of fire resistance of in the CFRP-strengthened beams. Further investigation is needed to rationally define fire limit states in this type of system and this thesis therefore intends to fill this gap bringing a better understanding about these issues in Chapters 3 and 4.

2.2.2 Analytical and numerical investigations

Recent concerns about the fire influence on CFRP-strengthened RC beams structures have generated some analytical and numerical investigations in this area, in order to better understand their behaviour at elevated temperatures. Relevant analytical and numerical studies on this issue are presented in detail in the current section [65–69].

Hawileh et al. [65] numerically investigated the fire behaviour of thermally insulated EBR-CFRP-strengthened T-section RC beams (Figure 2.33a) previously fire-tested by Williams et al. [58] which was described in the previous section. For this purpose, detailed 3D FE models

(Figure 2.33b) were developed using the commercial software ANSYS [70] to perform a nonlinear transient thermal-stress analysis under fire conditions. The FE models were composed by thermal and structural elements, in order to enable independent thermal and structural analysis. The temperature-dependency of thermal and mechanical properties of the constituent materials of the specimens were considered, including CFRP and passive fire protection materials.

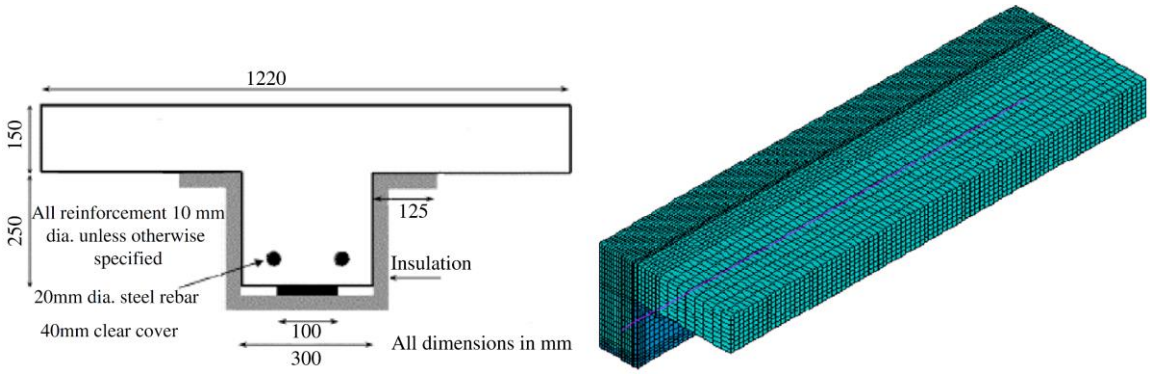

(a) **(b)**

Figure 2.33 – (a) Dimensions of the test specimen [58] and (b) Finite Element model and mesh [65]

Numerical results were compared with experimental data [58] in terms of temperature evolution in the beam, in the CFRP, in the reinforcements, along the CFRP-concrete interface as well as the deflections of the beams when subjected to fire. The heating was applied only at the bottom surface of the specimens in a transient state according to ASTM E119 [63]. In addition, a sustained uniformly distributed load at the top surface of the T-beam was applied to simulate the serviceability loads during heating. The temperature distribution in the cross-section of the T-beam obtained after 240 min of fire exposure is shown in Figure 2.34.

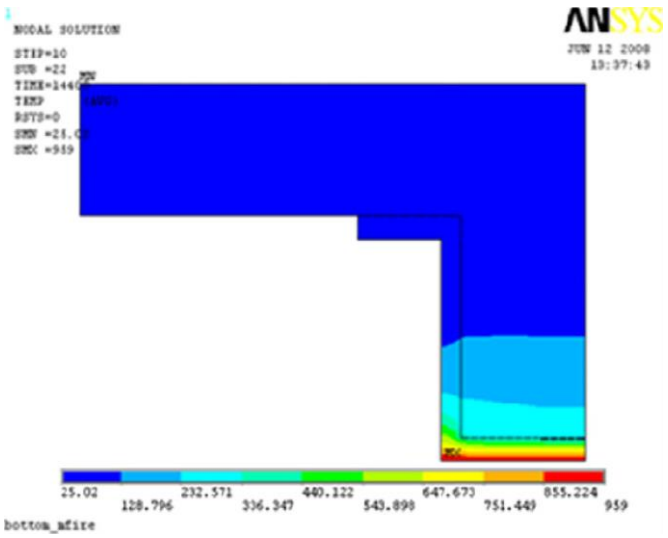

Figure 2.34 – Cross-section temperature distribution [65]

The numerical models presented a good predictability with the experimental results in terms of temperatures, as can be seen in Figure 2.35a and Figure 2.35b. Regarding the predicted mid-span vertical deflections as a function of fire exposure time (Figure 2.36), the results also showed a good agreement with the ones experimentally measured in the first 33 minutes of test (until the hydraulic pressure was lost accidentally in the experiment). However, the authors were unable to validate the numerical procedure in terms of mechanical response (such as the CFRP debonding phenomenon) due to limited experimental data.

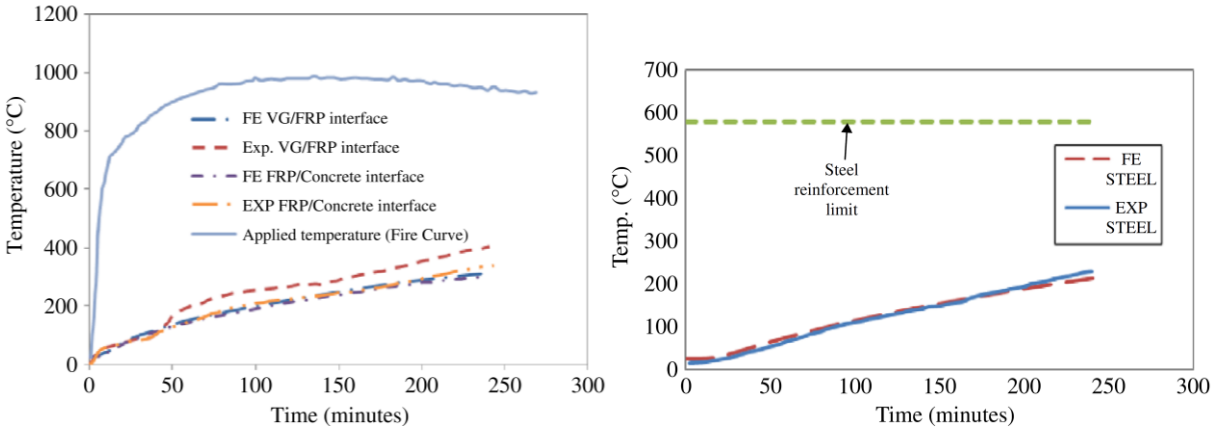

(a) **(b)**

Figure 2.35 – (a) FE and measured temperature as a function of time; (b) predicted and measured steel temperature as a function of exposure time [65]

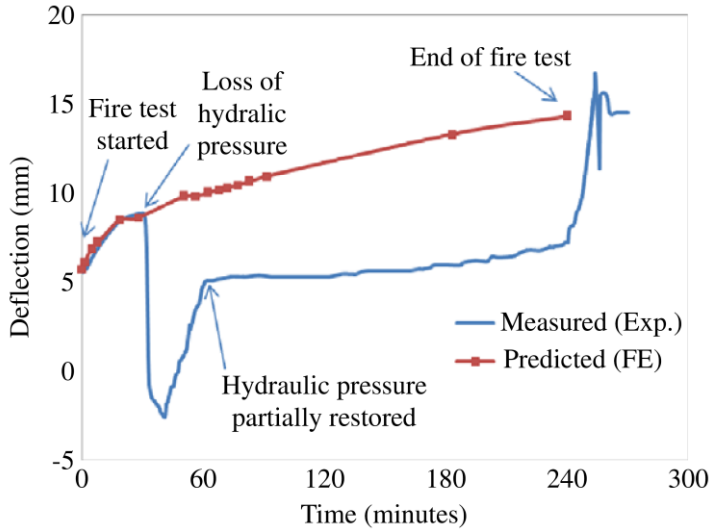

Figure 2.36 – Predicted and measured mid-span deflection as a function of exposure time [65]

Ahmed and Kodur [66] improved a numerical approach previously developed by Kodur and Ahmed [71] regarding the modelling of the degradation of connections of reinforced RC beams

with EBR-CFRP laminates exposed to fire. The main innovation presented by [66] was the simulation of the bond degradation at the CFRP-concrete interface by means of an explicit model by means the bond-slip laws, which was not considered in the previous study [71]. The numerical procedure was implemented into a macroscopic FE model which is capable of predict the temperature-dependency of material properties, different fire scenarios, and failure limit states in evaluating fire response of CFRP-strengthened RC beams. Figure 2.37a and Figure 2.37b shows the schematic view of longitudinal section of the beams and the element mesh discretization, respectively.

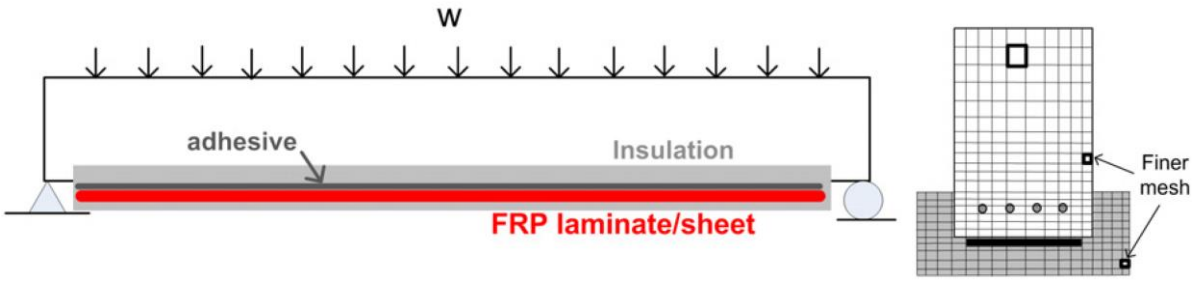

(a) **(b)**

Figure 2.37 – (a) schematic view of beams' longitudinal section; (b) element mesh discretization (adapted from Ahmed and Kodur [66])

The numerical model validity and accuracy was based on the experimental data from fire resistance tests on CFRP-strengthened RC beams (designed as Beam I and II) performed by Blontrock et al. [62] and Ahmed and Kodur [55], both described in detail in previous section. Moreover, a parametric study has been carried out on another CFRP-strengthened RC beam [72], designated as Beam III to simulate the effect of bond degradation and insultation schemes at CFRP–concrete interface response under fire situation. The characteristics and properties of the beams used in the fire resistance analysis as well as the materials composing them are presented in Table 2.3.

Table 2.3 – Summary of properties for CFRP-strengthened RC beam I [62] and II [55] used in the fire resistance analysis (adapted from Ahmed and Kodur [66])

Property		Beam I	Beam II	Beam III
Description		Tested by Blontrock et al.	Tested by Ahmed and Kodur	Typical FRP-strengthened RC beam
Cross Section (mm)		200 × 300	254 × 406	380 × 610
Length (m)		3.15	3.96	6.7
Reinforcement	Top bars	2 ϕ 10 mm	2 ϕ 13 mm	2 ϕ 15.8 mm
	Bottom bars	2 ϕ 16 mm	3 ϕ 19 mm	4 ϕ 25 mm
$f'c$ (N/mm^2)		57.5	52	38
f_y (N/mm^2)		591	450	414
Applied total load		2 × 40.6 (kN)	2 × 70 (kN)	60 (kN/m)
Concrete cover thickness (mm)		25	54	40
Aggregate type		Siliceous	Carbonate	Carbonate
FRP type		Sika carbodur S1012	CFRP (Tyfo® SCH-41)	CFRP
FRP thickness (mm)		1.2	2	3
FRP ultimate tensile strength (kN/mm^2)		2.8	986	2450
Modulus of elasticity FRP (kN/mm^2)		165	95.8	176
Rupture strain of FRP (mm/mm)		1.7%	1.0%	1.41%
Insulation thickness (mm)		25	25	20
Insulation type		Promatect – H	Tyfo® WR AFP system	Vermiculite–gypsum (VG)

Overall, according to the results a good agreement between the experimental and numerical FE models was obtained in terms of temperatures (Figure 2.38), as well as the deflections and the instant to CFRP debonding (Figure 2.39).

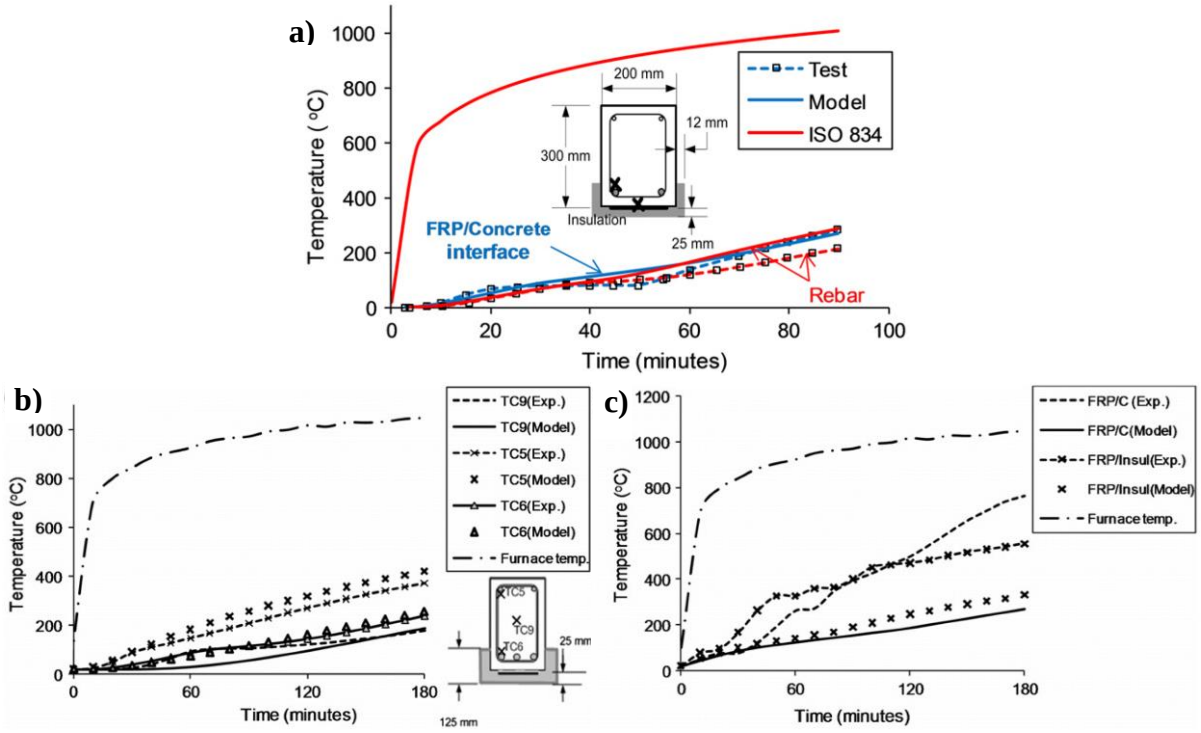

Figure 2.38 – Measured and predicted temperatures (a) at the interface of FRP–concrete and corner rebar for Beam I, (b) at corner rebars and mid-depth of the beam cross-section for FRP-RC Beam II and (c) at FRP/insulation and FRP/concrete interfaces for FRP-RC Beam II [66]

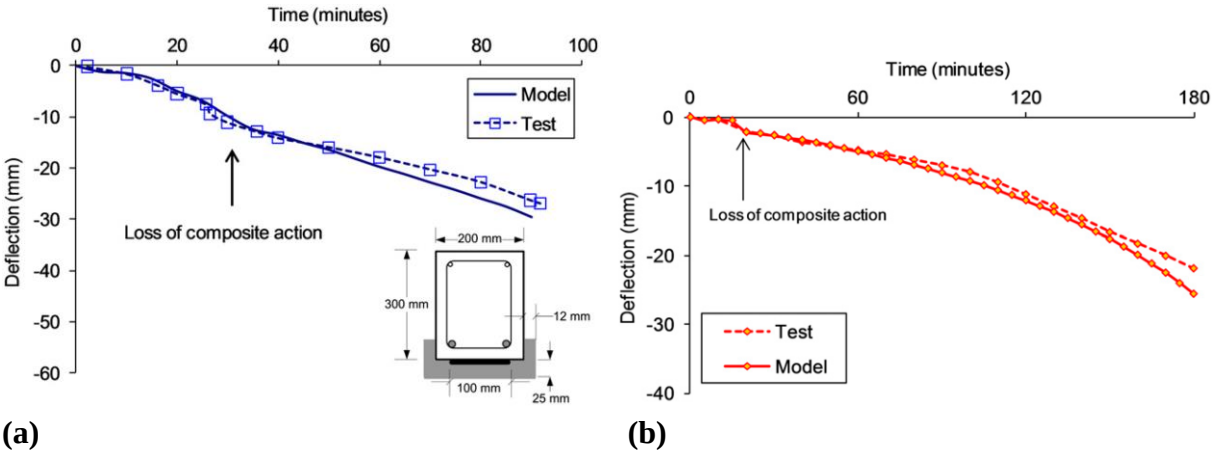

Figure 2.39 – Measured and predicted deflection as a function of fire exposure time for (a) Beam I and (b) Beam II [66]

Regarding to parametric analysis, the Figure 2.40 shows a significant bond degradation in moment capacity and stiffness when the temperature at CFRP–concrete interface slightly exceeds T_g of the adhesive (81 ºC), leading to the initiation of CFRP laminate debonding (around 40 min of fire exposure).

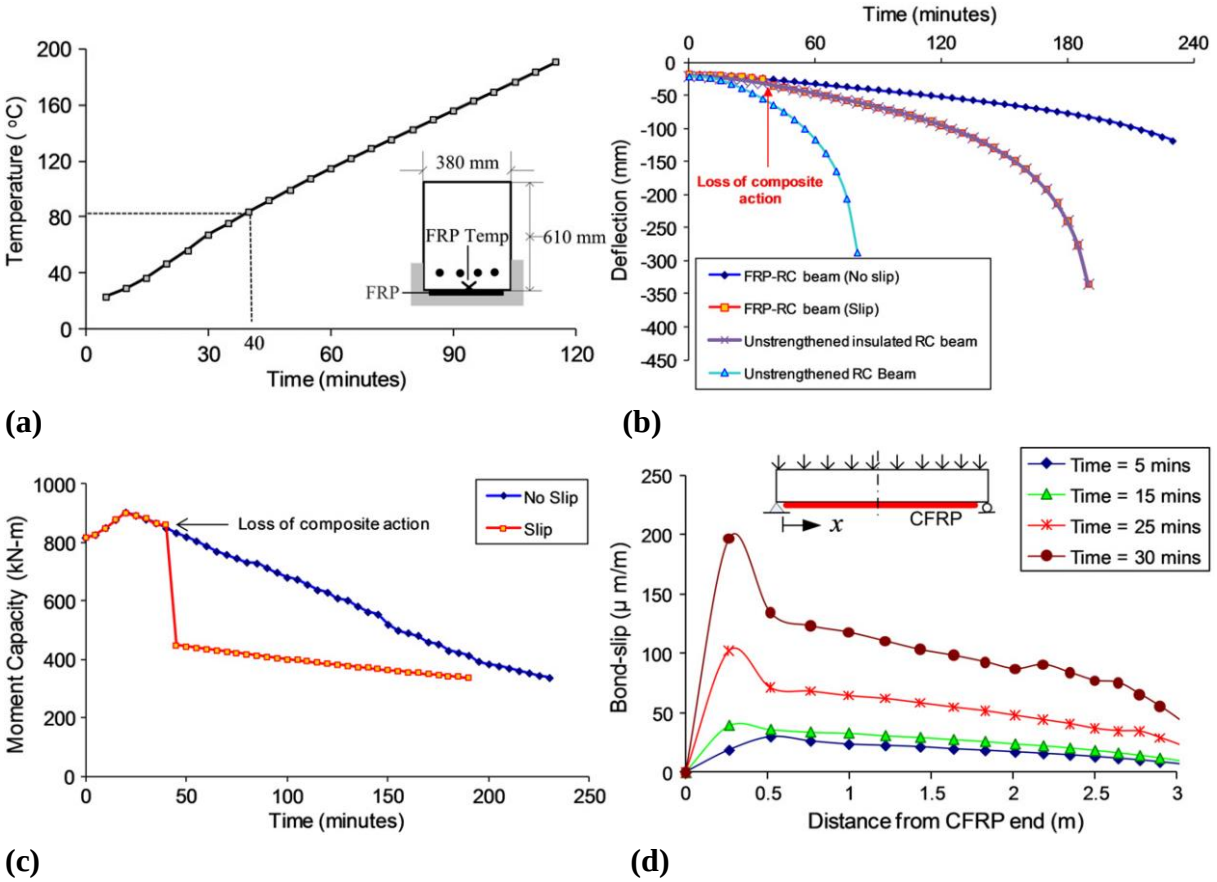

Figure 2.40 – (a) Temperature variation at the interface of FRP–concrete interface as a function of fire exposure time; (b) deflection of beams as function of fire exposure time; (c) moment capacity of FRP-strengthened and RC beam as function of fire exposure time; (d) slip distribution for mid-span of the beam as a function of fire exposure time [66]

In addition, the authors concluded that the time the bond degradation in CFRP-strengthened concrete members occurs depends on the fire protection thickness and T_g of the adhesive (see Figure 2.41).

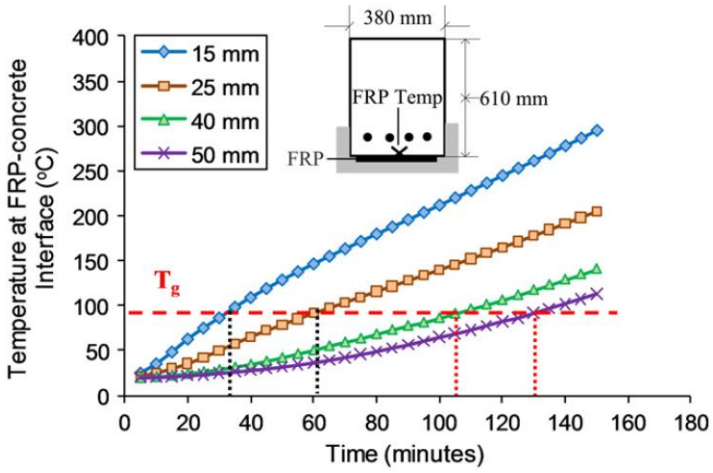

Figure 2.41 – Effect of insulation thickness on time to reach T_g [66]

Dai et al. [67] developed the first 3D FE model for the simulation of the thermomechanical behaviour of insulated EBR-CFRP-strengthened RC beams under fire conditions. The 3D FE models were developed and validated based on the experimental data and results from fire resistance tests performed by Blontrock et al. [62] and Williams et al. [58], both described in the previous section through the commercial software package Abaqus [73]. The bond degradation with temperature evolution for the internal steel reinforcement, the external CFRP, the temperature-dependency of thermo-physical and mechanical properties of all materials were considered in the simulations. The properties of concrete and steel were defined according to Eurocode 2 - Part 1-2 [1] standard. Regarding the properties of CFRP and fire protection materials, the propositions suggested by Griffis et al. [74] and the ones reported in the fire resistance tests [58,62] were both adopted. In addition, the bond-slip laws recommended in Model Code [75] for ambient temperature was used to represent the interaction between the concrete surface and steel reinforcements. The proposed numerical approach achieved a good accuracy of thermal and structural response of thermally protected EBR-CFRP strengthened RC beams under fire conditions in comparison to the ones obtained in experimental studies (Blontrock et al. [62] and Williams et al. [58]). Numerical results show that the consideration of a perfect bonding between CFRP and concrete leads to underestimations of fire resistance in CFRP-strengthened RC beams, as adopted in most of previous numerical investigations.

Another relevant numerical investigation on the fire behaviour of RC beams strengthened with CFRP laminates bonded according the EBR technique was performed by Firmo et al. [68]. Two-dimensional FE models were developed to simulate fire resistance tests of simply supported RC beams strengthened with EBR-CFRP laminates previously studied by Firmo and Correia [57] (described in detail in previous section) and Firmo et al. [76]. The thermomechanical response of models was numerically simulated taking into account the

influence of CFRP anchorage systems and different passive fire protection schemes applied along the bottom surface of the beams and in the anchorage zones. The commercial software package Abaqus [54] was used in the numerical simulations where the temperature variation of the thermomechanical properties of the materials was considered and the CFRP-concrete bond interaction was modelled based on bi-linear bond-slip laws previously calibrated for different temperatures (up to 120 ºC). The geometry of the specimens and FE mesh adopted for the models of the insulated CFRP-strengthened beams is illustrated in Figure 2.42.

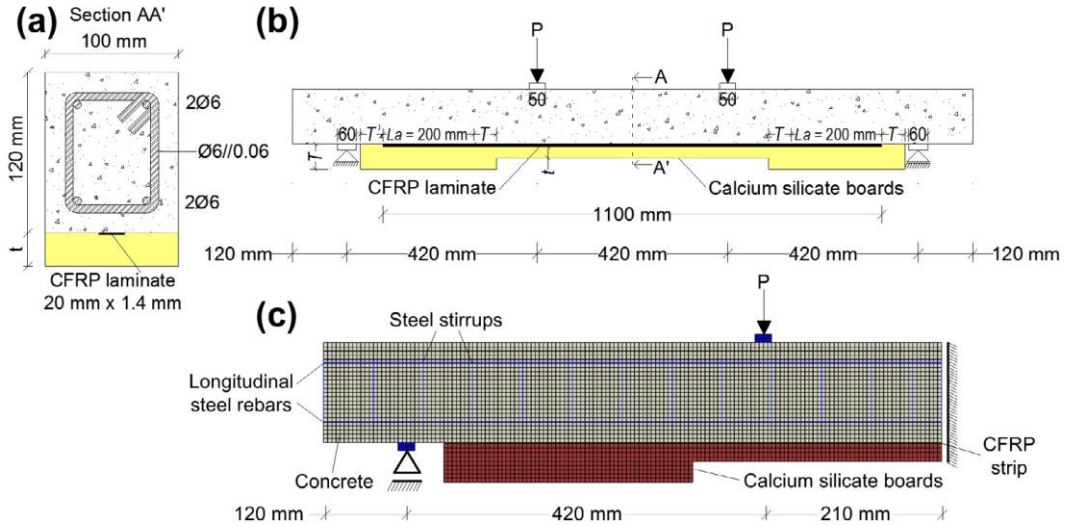

Figure 2.42 – Geometry of the beams: (a) mid-span cross-section; (b) longitudinal view of the tested beams; (c) FE mesh of the beams' models (example of the model 50-25) ([68])

As it can be seen in Figure 2.43 and Figure 2.44, the numerical results showed a good accuracy in terms of fire behaviour of CFRP-strengthened RC beams, including the "cable mechanism" phenomena, the time and temperature at debonding of the strengthening system as observed in the reported experimental results [57,76].

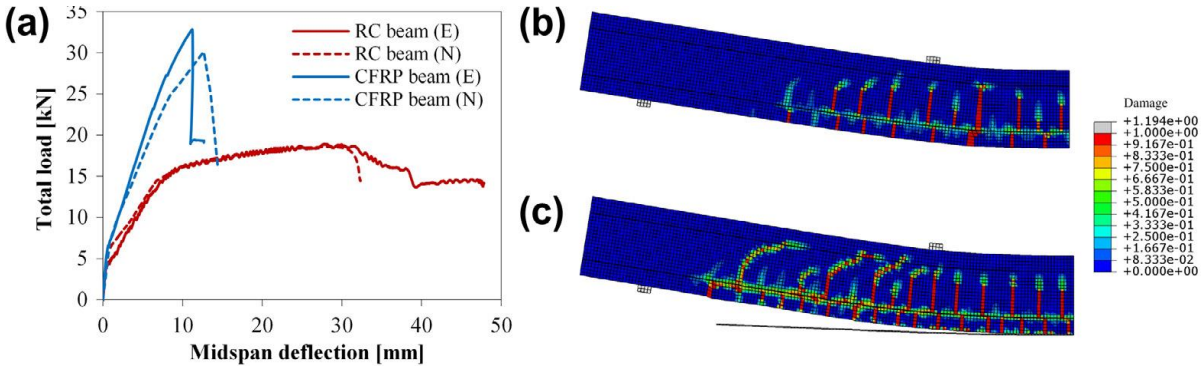

Figure 2.43 – (a) Experimental (E) and numerical (N) load vs. mid-span deflection curves of unstrengthened (RC) and CFRP-strengthened (CFRP) beams tested by Firmo et al. [76] at ambient temperature; damage at failure of (b) RC beam, and (c) CFRP beam ([68])

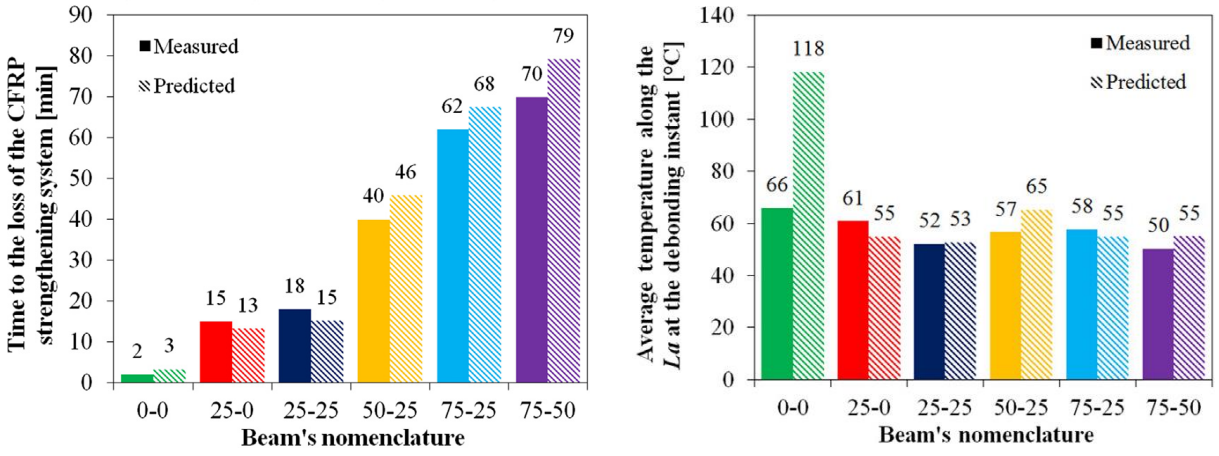

Figure 2.44 – Measured [57] and predicted (a) time to complete debonding of the strengthening system and (b) average temperature (in the adhesive) along the anchorage length (La) when the strengthening system lost its structural effectiveness (adapted from [68])

Furthermore, this numerical study allowed the validation of the proposed bond-slip laws for the CFRP-concrete bond interaction, showing their suitability for simulating the behaviour of EBR-CFRP-strengthened RC beams subjected to fire.

A more recent and detailed numerical investigation carried out by Firmo et al. [69] (improving their initial study mentioned above [68]) proposed 3D FE models to simulate the fire response of the RC beams strengthened with CFRP laminates bonded according to the EBR technique. The CFRP-concrete bond interaction was modelled by bi-linear bond-slip laws as well as the one previously validated by Firmo et al. [68] with Abaqus [54] software. The geometry, position of the thermocouples and the FE mesh of the models of the beams are illustrated in Figure 2.45.

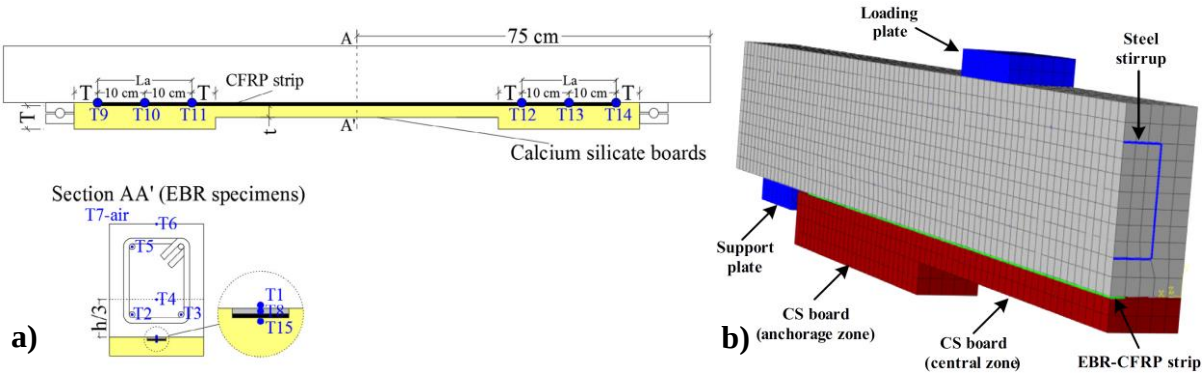

Figure 2.45 – (a) Geometry and position of the thermocouples and (b) FE mesh of the EBR-strengthened beams' models (example of insulation scheme 50–25) (adapted from Firmo et al. [69])

According to results (Figure 2.46 and Figure 2.47), the structural response of the CFRP-strengthened RC beams was achieved with reasonable accuracy when compared with experimental results obtained in fire resistance tests [57], despite some deviations observed.

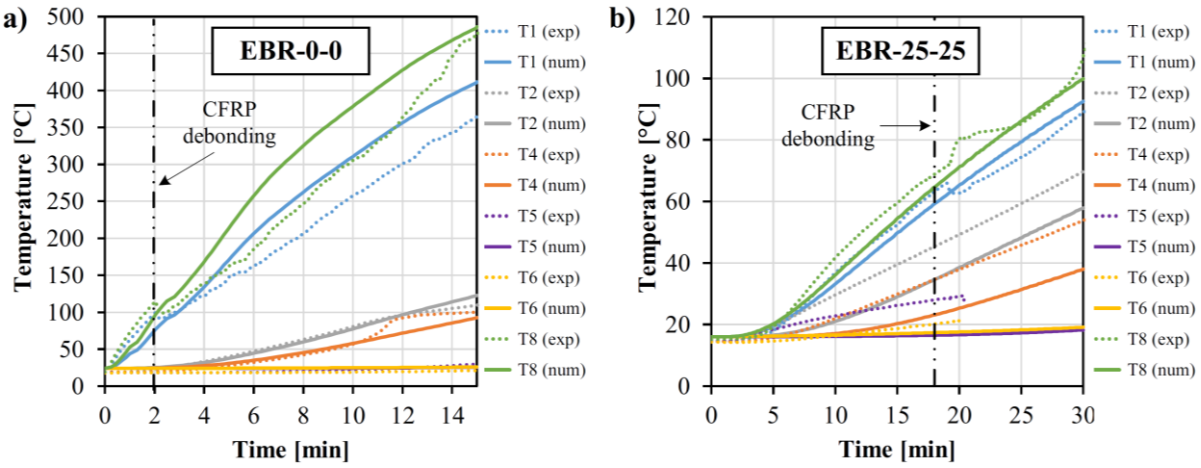

Figure 2.46 – Measured (exp) and predicted (num) temperatures as a function of the time of fire exposure at different locations in beams (a) EBR-0-0 and (b) EBR-25-25 (adapted from [69]).

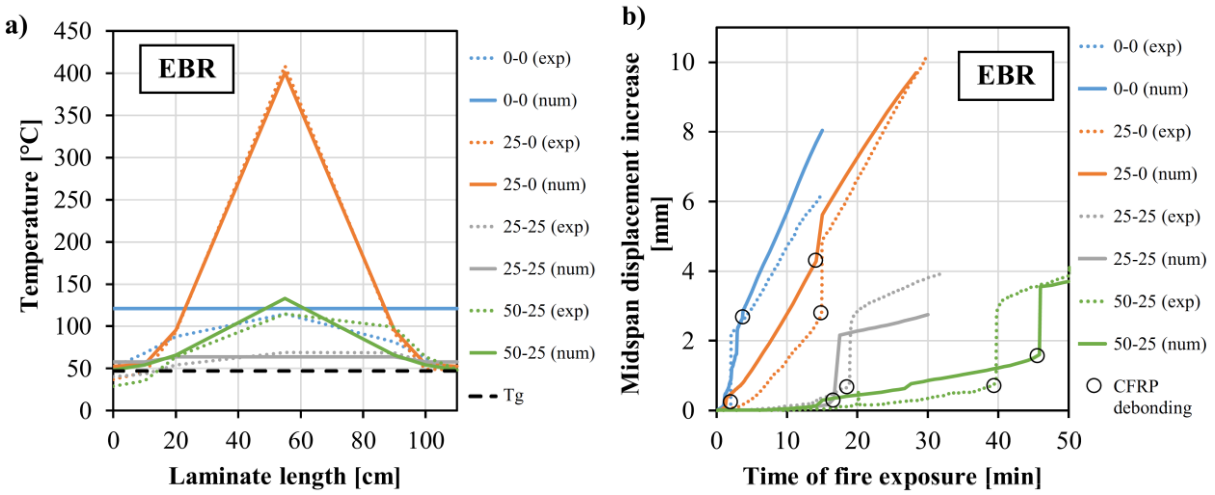

Figure 2.47 – (a) Measured (exp) and predicted (num) temperatures in the adhesive along bonded interface when the CFRP system debonded for EBR beams; (b) measured (exp) and predicted (num) mid-span displacement vs. time of fire exposure for EBR beams and (adapted from [69])

These satisfactory results confirmed that the bond-slip laws for the CFRP-concrete interaction, previously used in the 2D FE model by Firmo et al. [68], can be used for the 3D simulation of EBR-CFRP strengthening systems subjected to fire conditions and allow more complex

analyses. Moreover, the possibility of exploring the mechanical contribution of the CFRP in a fire situation by a “cable” behaviour with the application of a thicker insulation in the CFRP anchorage zones is highlighted.

The literature review described above shows that the numerical efforts to simulate the fire behaviour of CFRP-strengthened concrete beams are very limited. Few numerical studies have been carried so far, especially using 3D models that are theoretically more realistic. Moreover, numerical results have shown that accurate predictions of the fire response of CFRP-strengthened beams require the inclusion of explicit temperature-dependent bond-slip models for the CFRP-concrete interface, which has been neglected in most of the above-cited studies. The reason for that is the lack of experimental data available in this respect (that are sometimes contradictory), as discussed in Section 2.1, making it difficult to validate more accurate models to better simulate the behaviour of CFRP-strengthened RC beams subjected to fire. In this regard, the present research intends to be an important contribution to provide valuable experimental data and to allow the validation of a more realistic model, as well as to develop a large parametric study in order to simulate different parameters not experimentally tested yet.

3 EXPERIMENTAL INVESTIGATION ON BOND BEHAVIOUR BETWEEN CFRP AND CONCRETE AT ELEVATED TEMPERATURES

The current chapter addresses and discusses the results of an experimental investigation to assess the bond behaviour between the concrete and the CFRP strengthening system at elevated temperatures. The mechanical response of this bond, used in EBR-strengthened concrete structures, was studied in terms of the temperature evolution, the load-displacement behaviour, the bond strength, the axial strains and the failure modes when exposed to elevated temperatures.

A series of Single lap Shear Tests on strengthened concrete blocks under different temperature series (including ambient temperature) were performed, fulfilling the experimental phase predicted in this thesis. The experimental program, the testing procedures, the test specimens and the test set-up designed for SST tests were also presented in detail. These experiments were carried out at the Laboratory of Testing Materials and Structures of UC.

Furthermore, tests at ambient temperature were carried out to provide a reference for the elevated temperature tests. Other important goal of this research was to provide experimental data for numerical studies (Chapter 5).

3.1 Test Set-up

A general and schematic view with details of the experimental system to perform SST tests at ambient and elevated temperature are illustrated in Figure 3.1a-d, respectively. The numbers in the figures are referenced to the parts of the experimental system described in the text.

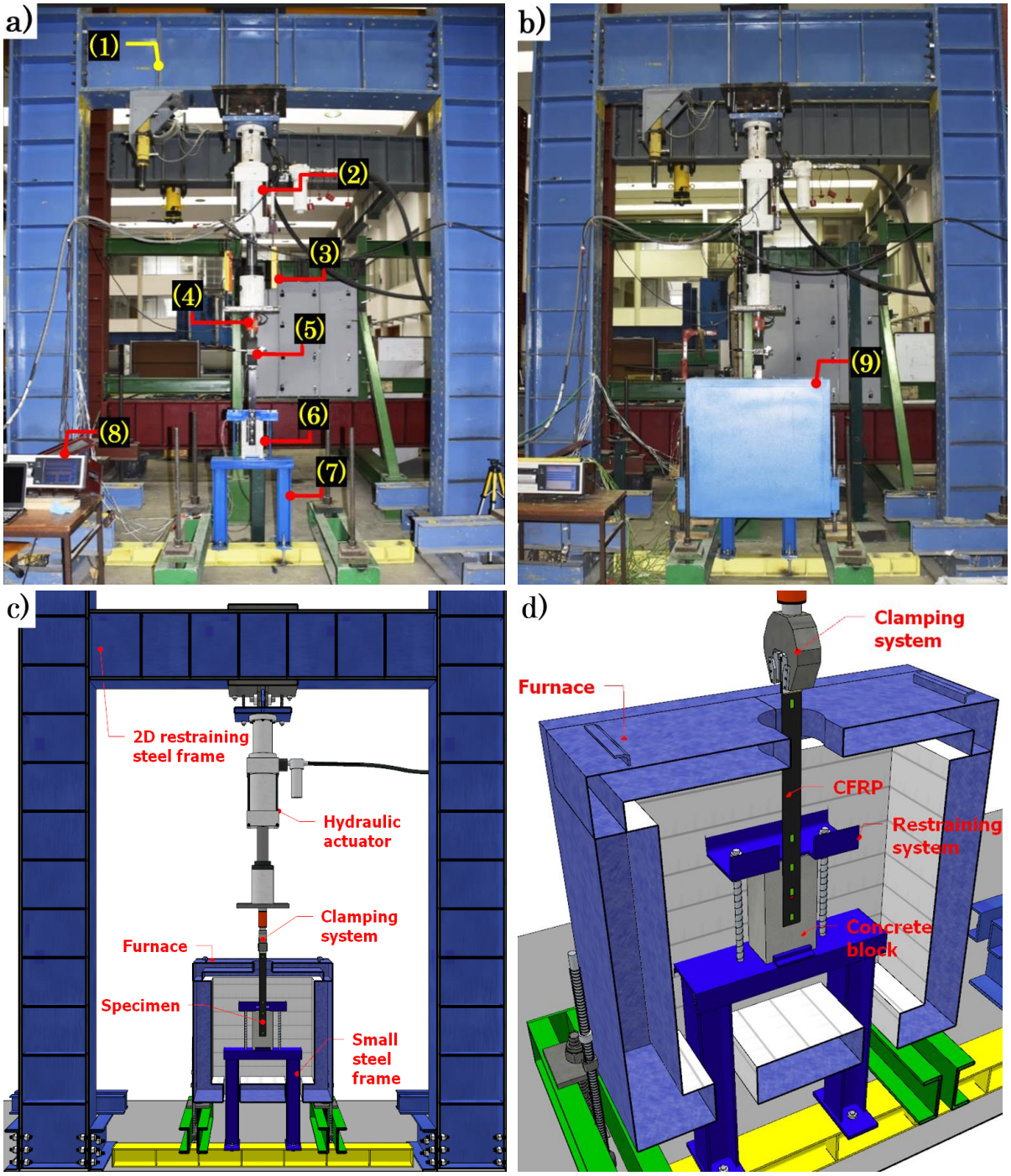

Figure 3.1 – Test set-up for the SST tests at (a) ambient temperature and (b-d) elevated temperatures (general and schematic views)

The test set-up consisted of a 2D restraining steel frame (No. 1 in Figure 3.1a) composed of two HEB500 columns and one HEB500 beam. The load was applied in the specimens by tension with a servo-controlled hydraulic actuator (No. 2 in Figure 3.1a) connected to the top

beam of the 2D restraining steel frame. The hydraulic actuator had a maximum load capacity of 200 kN and a maximum stroke of 200 mm and was servo-controlled by a Dartec (Instron) central unit. In addition, the load applied during the tests was monitored by a TML load cell (No. 4 in Figure 3.1a) with a load capacity of 250 kN.

A clamping system (No. 5 in Figure 3.1a) was used to grip and pull the CFRP laminates, providing a rigid and non-deformable connection between the loading application point and the specimens during the tests.

A small steel frame (No. 7 in Figure 3.1a) was installed on the experimental system to restrain the vertical, horizontal and rotational displacements of the specimens during the load application. The positioning of the specimens in this restraining system can be seen in Figure 3.1d.

In the tests at elevated temperatures, the thermal action was applied by an electric furnace (No. 9 in Figure 3.1b). This furnace had 750 x 250 x 750 mm of internal dimensions, capable of reaching temperatures up to 1200 ºC with different heating curves. In these tests the specimens (No. 6 in Figure 3.1a) were completely exposed to the heating and only the loading application point was outside the furnace.

Type K probe and cable thermocouples were used for temperature measurements inside the furnace and at different locations of the specimens, respectively. Figure 3.2 shows the nomenclature and location of the thermocouples at different points of the CFRP-strengthened concrete blocks. This distribution of thermocouples allowed the assessment of temperatures along the cross-section of the concrete blocks (by T4, T5 and T6), in the CFRP laminate exposed surface (by T7) and at three different locations of the interface between the laminate and the concrete block (by T1, T2 and T3).

TML strain gauges (model ZFLA-6-11) were placed along the bonded and free lengths of the CFRP laminate surface (respectively designated as S1, S2, S3 and S4, S5) for axial strain measurements. Moreover, another strain gauge was mounted on the laminate not exposed to the thermal action (outside the furnace near the load application point). This type of strain gauges is designed for measurement at low and elevated temperatures (from –20 ºC to 300ºC) with a resistance of 120Ω and it was applied on the CFRP surface using a suitable adhesive (type NP-50B). The NP-50B is a two-component polyester adhesive (consisting of a main agent and a hardener) and operates in a temperature range from –30 ºC to 300 ºC. More information can be found in [77,78]. The location of the strain gauges is presented in Figure 3.2.

The vertical displacements of the specimens were measured by cable linear variable displacement transducers (LVDTs) positioned in the cross-head of the system, indicated as No. 3 in Figure 3.1a., and by the internal transducer of the hydraulic actuator. For the tests at ambient temperature, additional LVDTs were mounted on the lower 2D restraining frame (No. 7 in Figure 3.1a) to detect possible set-up displacements.

A TML data logger TDS-602 (No. 8 in Figure 3.1a) was used for data acquisition.

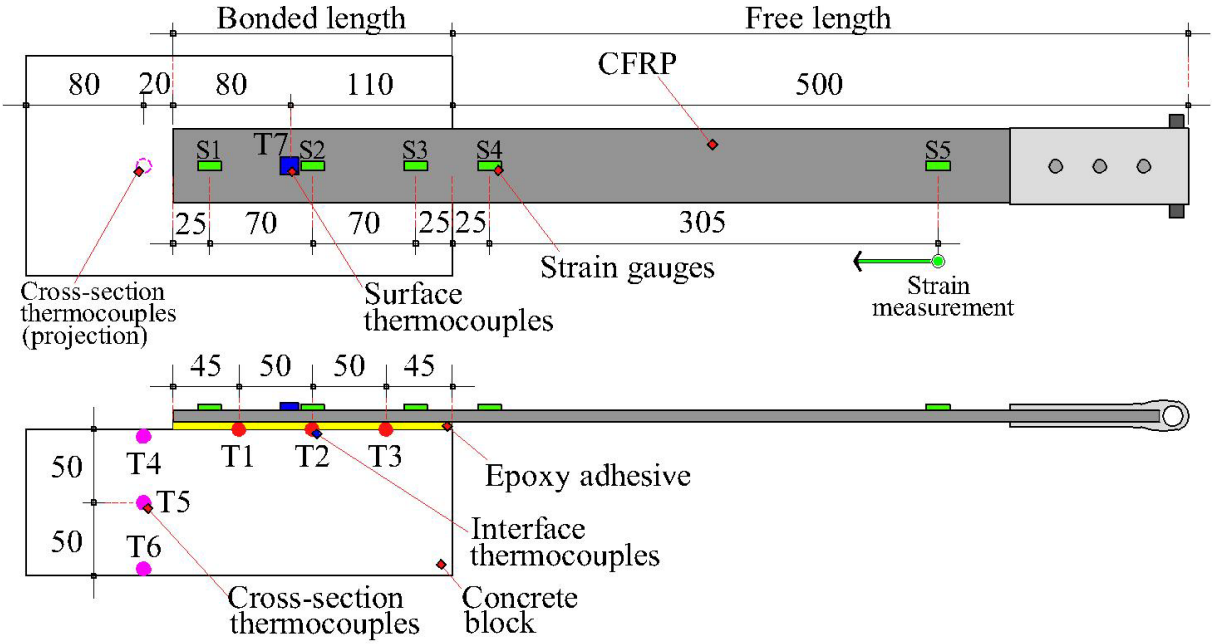

Figure 3.2 – Location of the strain gauges and thermocouples on the specimens (dimensions in mm)

3.2 Specimens

The specimens consisted of concrete blocks externally bonded with CFRP laminates. The concrete blocks were prismatic with dimensions of 150 mm wide, 100 mm high and 290 mm long.

The mean cube compressive strength (f_{cm}) of the concrete used in all specimens (at 28 days) was f_{cm}=30.1 MPa, that means a class C25/30, according to EN 206-1 (2000) [79]. A Portland cement type CEM II/A-L 42,5R [80] and a plasticizing additive MasterPozzolith 7002 [81] were used in the concrete composition. Two different aggregates, a fine and medium sand aggregate of 0.2 mm and 0.4 mm, respectively, were used. The crushed stone was formed by

aggregates of calcareous with a granulometry of 16mm. The composition of the concrete is presented in Table 3.1.

Table 3.1 – Concrete composition (kg/m^3)

Portland cement	Fly ash	Crushed stone	Fine sand	Medium sand	Water	Plasticizing additive
195	105	1000	300	550	165	3

The CFRP laminate was bonded along 190 mm of the surface of the concrete block using the EBR technique. These strips have a cross-section of 50 mm x 1.2 mm and is commercially designated as *S&P Laminates 150/2000*. This type of laminate has an average tensile strength of 2800 MPa, modulus of elasticity of 170 GPa and ultimate strain of 16.0‰ (at ambient temperature), according to the manufacturer's report [20]. The geometric configuration and other details of the test specimens are illustrated in Figure 3.3.

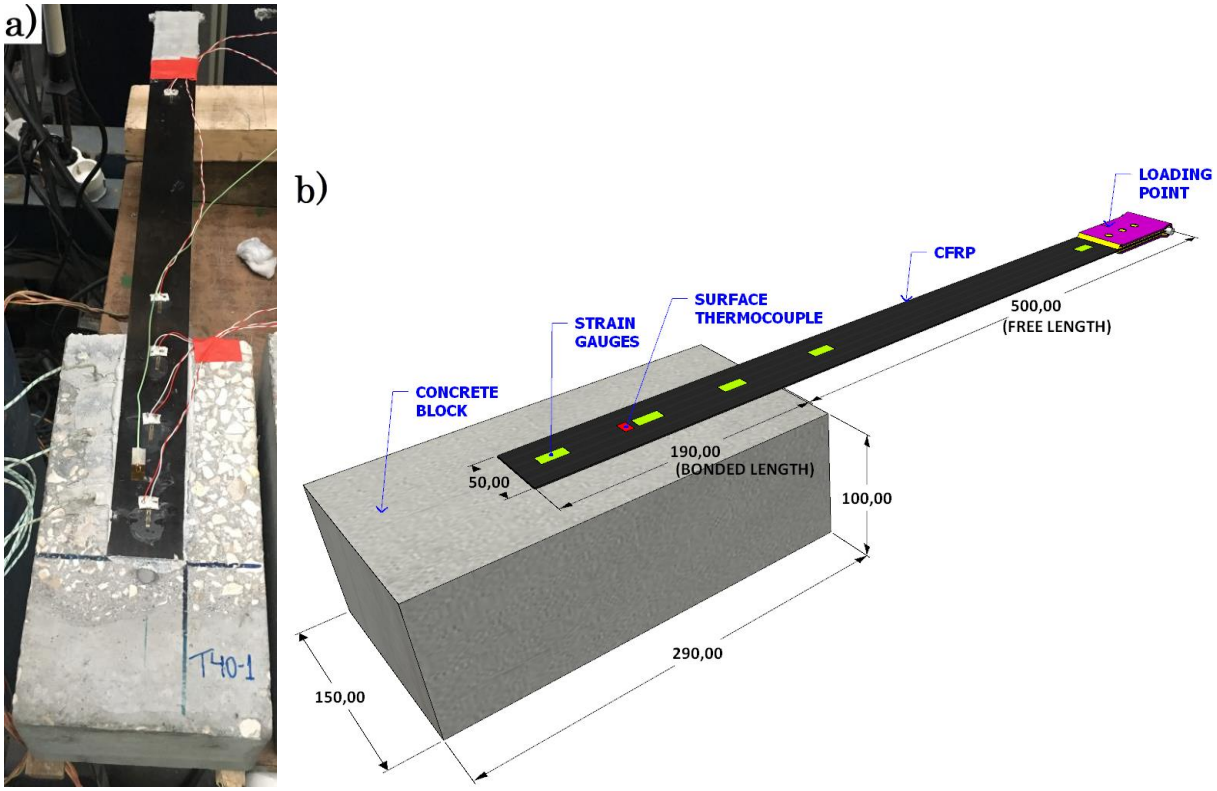

Figure 3.3 – Geometry and details of the specimens: (a) general and (b) schematic view (dimensions in mm)

A two-component epoxy resin (commercially designated as *S&P Resin 220* [82]) was used to bond the CFRP laminate to the surface of the concrete blocks. The T_g of the adhesive was quoted

as 75 ºC and was determined by DMA tests [83] according to ASTM E1640 (2013) standard [84] and defined based on the peak value of the Tan δ curve (loss factor). Moreover, according to tensile tests presented in [14], the resin has a modulus of elasticity of 8.8 GPa and a tensile strength of 17.3 MPa (at ambient temperature). Table 3.2 shows some physical properties of the CFRP laminate and the epoxy adhesive.

Table 3.2 – Physical properties of the CFRP laminate and epoxy adhesive

		CFRP	Adhesive
Tensile strength	MPa	2800	17.3
Modulus of elasticity	GPa	170	8.8
Ultimate strain	‰	16	-
Glass transition temperature (T_g)	ºC	-	75
Cross-section	mm^2	50x1.2	50x1.5*

* Average adhesive thickness

3.3 Test Program

The experimental program included 21 SST tests on CFRP-strengthened concrete blocks at elevated temperatures. Eighteen tests were performed at heat conditions and three others at ambient temperature (reference tests). The test specimens were divided into seven batches according to the respective series of temperature. Thus, 3 tests were carried out for each series of temperature, in order to obtain a better correlation of the results.

Therefore, the test specimens subjected to temperatures of 40 ºC, 65 ºC, 90 ºC, 115 ºC, 140 ºC and 165 ºC were respectively designated as T40, T65, T90, T115, T140 and T165. Specimens tested at ambient temperature (15 ºC) were designated in the experimental plan as TA. The test program is summarised in Table 3.3.

Table 3.3 – Test program for SST tests

Test reference	Temperature series*	Heating rate	Loading regime
TA-1, TA-2, TA-3	Ambient (15ºC)	-	Under displacement control at 0.03mm/min until specimen's rupture
T40-1, T40-2, T40-3	40 ºC	1 ºC/min	
T65-1, T65-2, T65-3	65 ºC		
T90-1, T90-2, T90-3	90 ºC		
T115-1, T115-2, T115-3	115 ºC		
T140-1, T140-2, T140-3	140 ºC		
T165-1, T165-2, T165-3	165 ºC		

* at the CFRP-concrete bond interface

3.4 Test Procedure

The specimens were first heated to the desired temperature level and, in a second stage (after the temperature stabilization) loaded in tension all the way up to failure. The specimens were positioned completely inside the furnace and heated up to the desired temperature level at a heating rate of 1 ºC/min. Therefore, the time to reach at the setpoint temperature by the furnace (heating period) was between 25 min and 150 min, considering the temperature series between 40 ºC and 165 ºC and an ambient temperature of 15 ºC. However, the time to uniformly achieve the setpoint temperatures at the CFRP-concrete bond interface of the specimens (temperature stabilization period) was 120 min for the specimens heated to 40 ºC, 160 min for the specimens heated from 65 ºC to 115 ºC, 180 min for the specimens heated to 140 ºC and 300 min for the specimens heated to 165 ºC. After the heating stage, the loading was applied under displacement control at a rate of 0.3 mm/min until the failure of the CFRP-concrete bond system. The selected loading rate was based on researches of other authors [39,43,47,85] which used similar values (between 0.1 and 0.5 mm/min). In addition, reference tests were performed at ambient temperature.

The defined series of temperature allowed to test the specimens for temperatures lower, near, higher and much higher than the T_g of the adhesive. The specimens were tested for temperature levels distant 25 ºC among them. Moreover, the adopted heating rates, controlled by the specimen's thermocouples, allowed a uniform temperature distribution at the CFRP–concrete interface, avoiding excessive temperature gradients and minimizing post-curing phenomena in the adhesive and in the concrete (spalling).

The failure in the SST tests was considered when the CFRP-concrete bond suffered an abrupt loss of load and the stiffness reduced to null values.

During the tests, the applied load, the axial strains along the bonded length, the global and displacement of the specimens, the specimen temperatures (essentially at the CFRP-concrete interface) and the gas temperatures in the interior of the furnace, were monitored.

3.5 Results and Discussion

3.5.1 Temperatures

The results of the evolution of temperatures for each tested temperature level (40º to 165 ºC) in the SST tests are presented in this section. Figure 3.4a-f show the evolution of temperatures in relation to the time at different points of the bond interface between the CFRP and concrete (T1, T2 and T3), along the cross-section of the concrete blocks (T4, T5 and T6) and at the

surface of CFRP in the bonded area (T7). Moreover, the furnace and the setpoint temperature curves, as well as the periods of temperature stabilization and loading regime are also indicated in these figures. The origin of the time scale (time = 0 min) in Figure 3.4a-f corresponds to the beginning of the heating. The end of the test was defined when an abrupt strength loss was observed in the CFRP-concrete bond, according to the observations discussed in Section 0. In the SST tests all thermocouples worked properly.

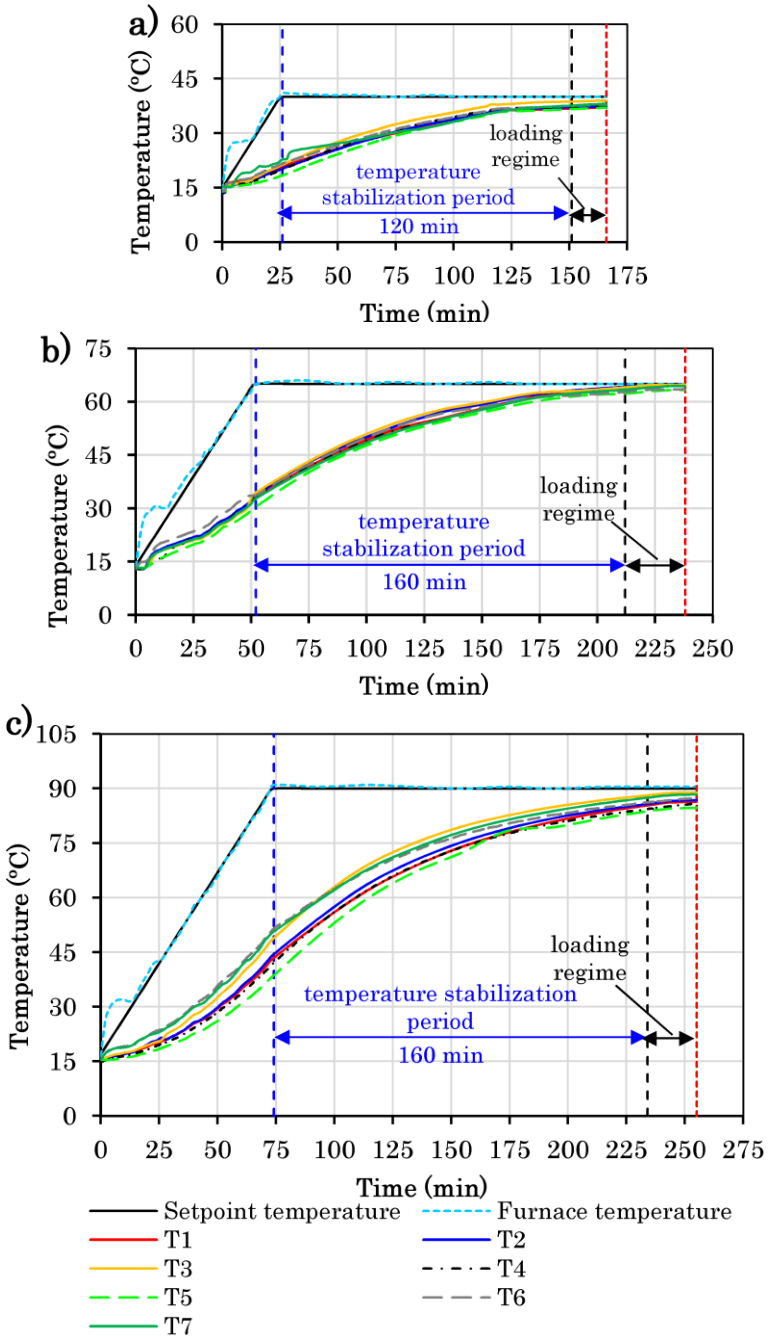

Figure 3.4 – Evolution of temperatures recorded at different points of the specimen (a) T40, (b) T65, (c) T90, (d) T115, (e) T140 and (f) T165

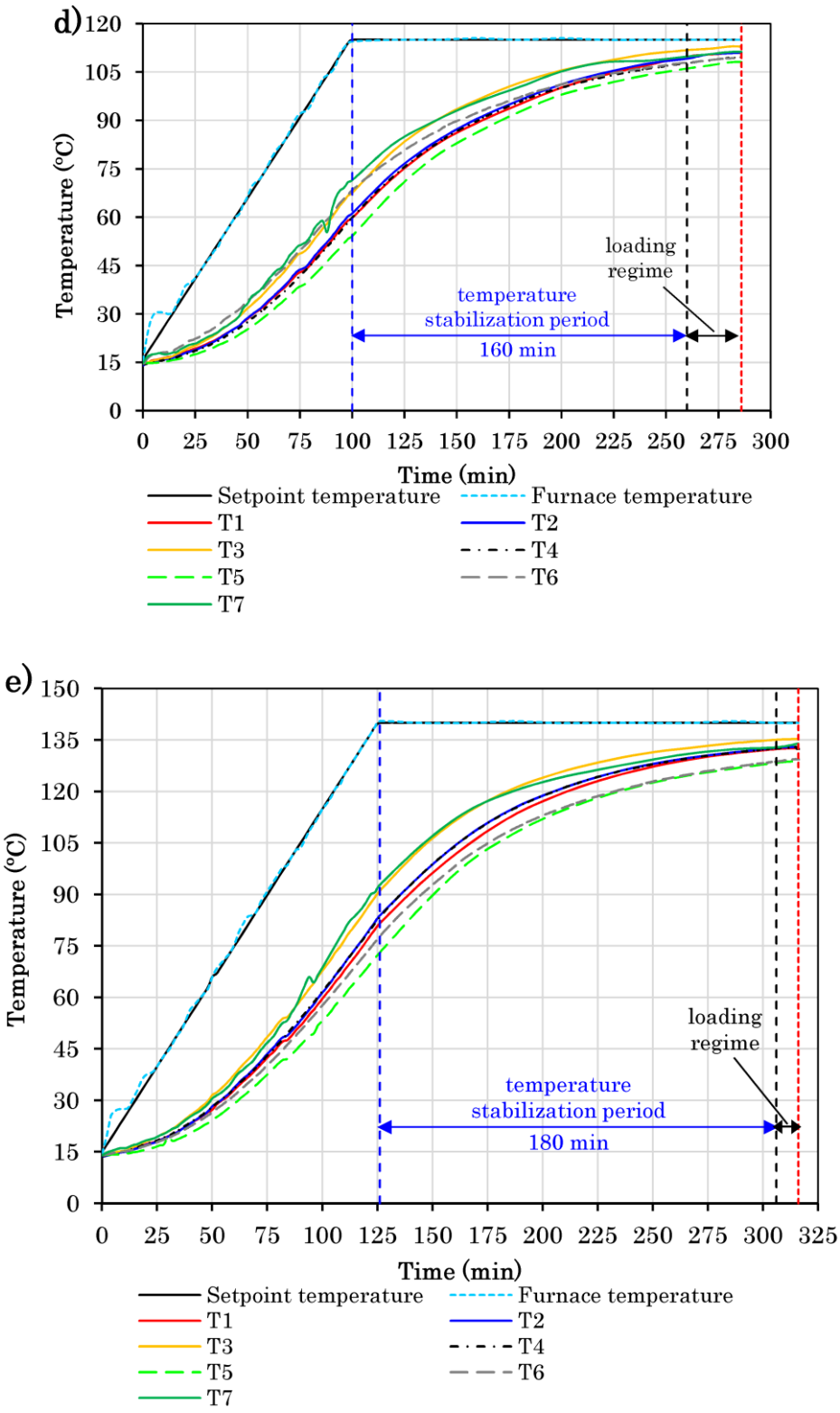

Figure 3.4 – Evolution of temperatures recorded at different points of the specimen (a) T40, (b) T65, (c) T90, (d) T115, (e) T140 and (f) T165 (Continuation)

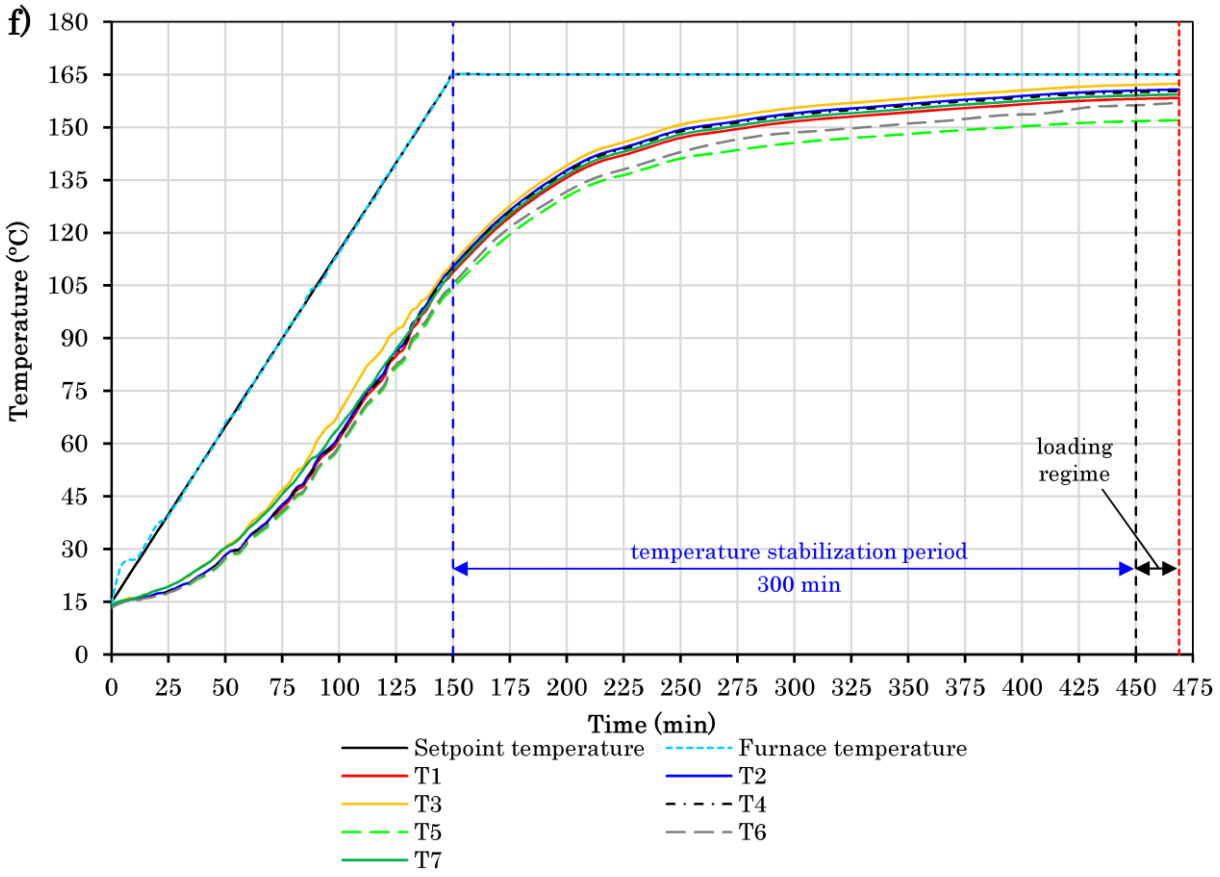

Figure 3.4 – Evolution of temperatures recorded at different points of the specimen (a) T40, (b) T65, (c) T90, (d) T115, (e) T140 and (f) T165 (Continuation)

A non-linear evolution of the temperature-time curve with a roughly linear final domain (starting near the end of the temperature stabilization period) represents the temperature profiles for all specimens.

The furnace temperatures generally approach very close to the setpoint temperature curve a few minutes after the test starts following the defined heating rate (1 ºC/min).

Regarding the temperatures at the CFRP-concrete interface (T1, T2 and T3), a good approximation to the setpoint temperature was achieved after the stabilization period, where a negligible difference (on average 2 ºC) was registered, complying to the desired temperature level for the subsequent period of loading in all specimens. A similar tendency was observed in the temperatures recorded at the surface of the CFRP in the bonded length (T7). For some specimens the temperatures at this area were slightly higher and in others quite close to the interface temperature. The temperatures along the cross-section of the concrete block were generally lower than the ones recorded at the interface, as expected. Particularly at the middle

of the cross-section (T5), the temperatures were consistently lower than the target temperatures, on average 7 ºC lower in the loading period. However, this difference did not affect the performance of the tests since the required homogeneity and level of temperature at the bonded region were achieved.

3.5.2 Load-displacement curves

Figure 3.5 shows the load-displacement curves for the different temperature series of the tested specimens. Each curve plotted in Figure 3.5 represents the results of the first specimen among the three testes carried out in each series of temperature, for example TA-1, T40-1 and so on. The instant of the failure is also indicated in this figure.

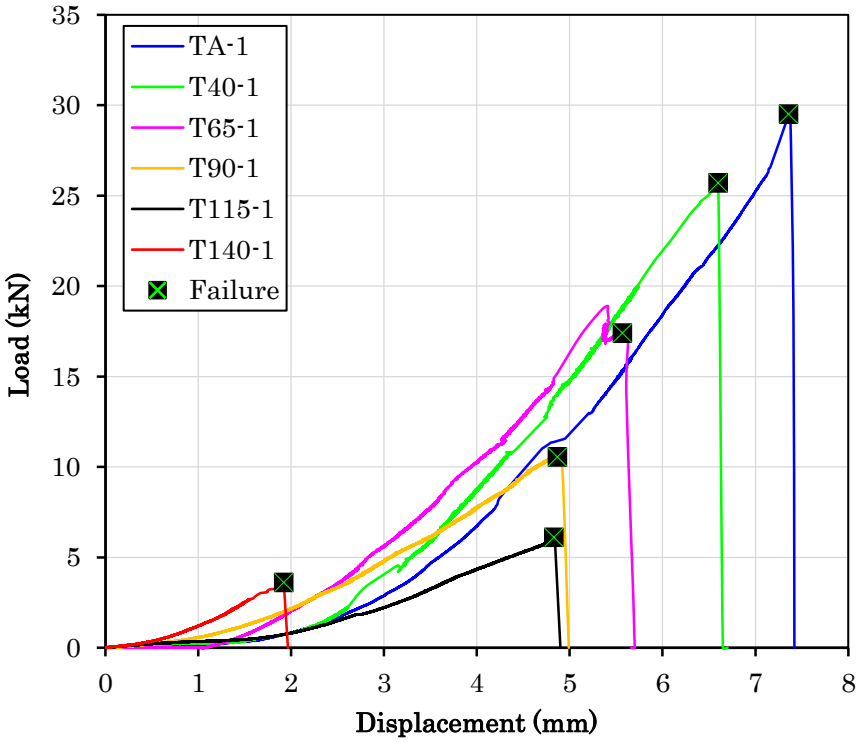

Figure 3.5 – Load-displacement curves for the different temperature series of the tested specimens

According to the obtained curves, a load-deflection evolution approximately linear with an initial non-linear elastic domain characterizes the shear behaviour for all specimens. Moreover, the bond presented a brittle behaviour, losing completely and immediately their stiffness at the moment of failure (after the elastic phase). For the specimens tested at ambient temperature only, it was noticed an increase of stiffness before the failure. Comparing the results among the

different temperature series, it was possible to observe a continuous reduction of the ultimate load and the maximum deflection with the temperature increase. This can be attributed mainly to the loss of strength of the interface, which is severely affected by the temperature. At 165 °C, the specimens did not show any loadbearing capacity. The maximum displacements for the tested specimens are also presented in Table 3.4 in Section 3.5.4.

3.5.3 Strain profiles

The axial strains along the bonded and free lengths of the CFRP laminate for the different series of temperature and considering four different fractions of the failure load (30%, 50%, 70% and 90%) are indicated in Figure 3.6a-d. These values were measured by the sets of strain gauges S1, S2, S3 and S4, S5, respectively mounted along the bonded and free lengths of the CFRP laminate surface. The strain profiles evaluation allowed to verify the bond length capable of transferring the axial stresses (transfer stress length) from CFRP laminate to the concrete member for the different temperature levels.

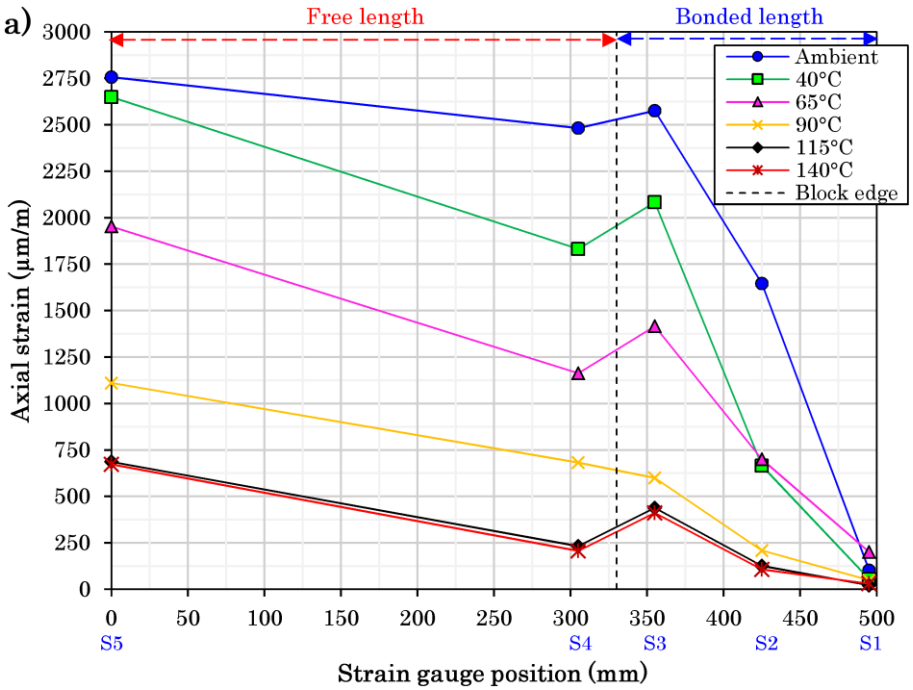

Figure 3.6 – Axial strains along the bonded and free lengths of the CFRP laminate for the different temperatures and fractions of (a) 90%, (b) 70%, (c) 50% and (d) 30% of the failure load

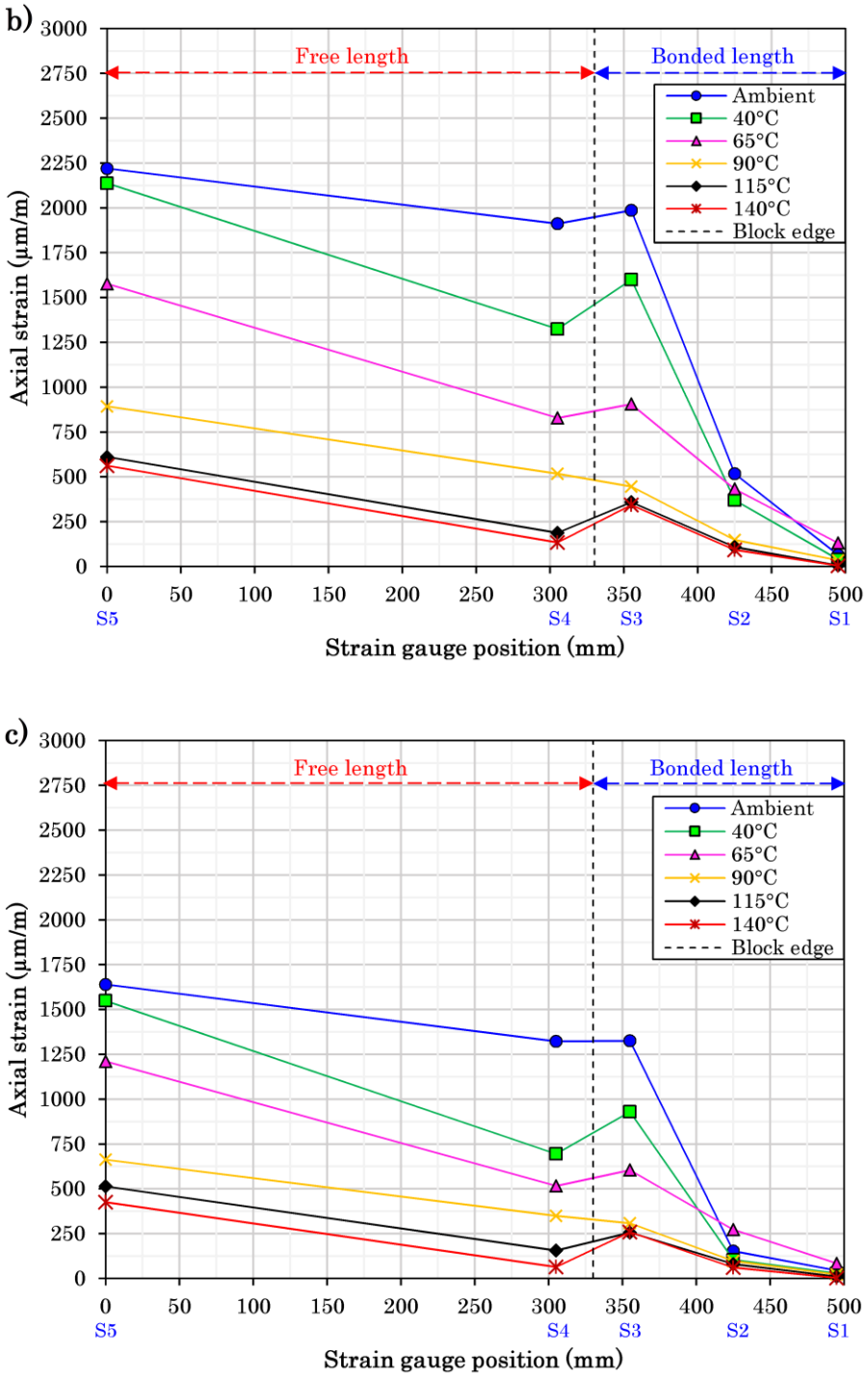

Figure 3.6 – Axial strains along the bonded and free lengths of the CFRP laminate for the different temperatures and fractions of (a) 90%, (b) 70%, (c) 50% and (d) 30% of the failure load (Continuation)

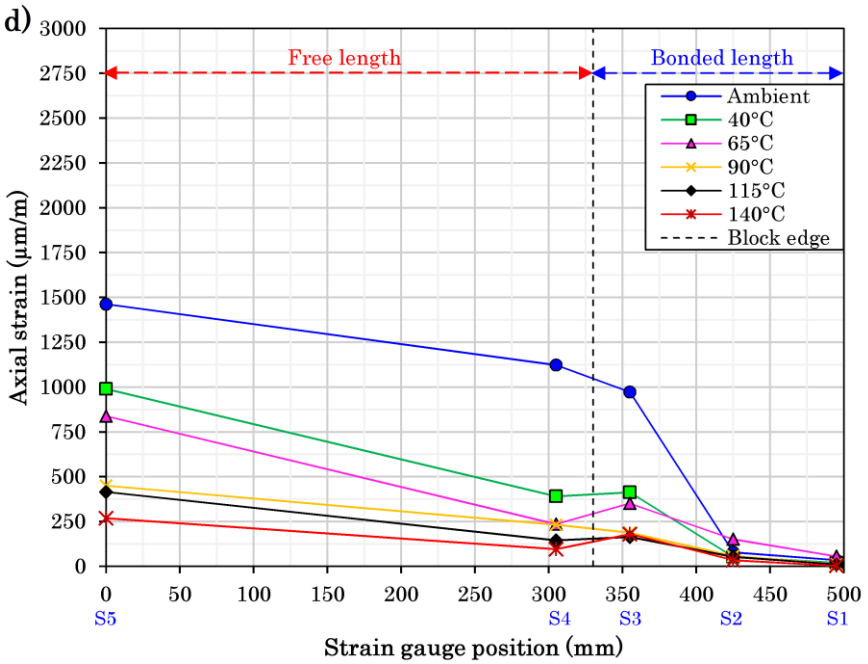

Figure 3.6 – Axial strains along the bonded and free lengths of the CFRP laminate for the different temperatures and fractions of (a) 90%, (b) 70%, (c) 50% and (d) 30% of the failure load (Continuation)

According to Figure 3.6, at low and moderate temperatures (ambient to 40 °C), the strain profiles reveal a non-linear behaviour along the bonded length of the CFRP, while for the highest temperatures (from 65 °C to 140 °C) show a smoother and more uniform evolution (close to linear). Furthermore, the lack of a secondary surface to dissipate the axial stresses resulted in high and smooth profiles along the free length of the laminate. However, axial strains profiles along the free length were expected to be uniform, since this is known as a stress equilibrium zone. The limited number of strain gauges in this region (only two) or the proximity of the strain gauge S4 to the bonded plane may have caused this broadcast. Cross curvatures in the laminate along the free length can also justify this difference between S4 and S5.

Considering the same load fraction, the overall magnitude of the axial strain profiles decreases with the evolution of the temperature. Concerning the maximum values of the strain profiles, they are significantly lower at elevated temperatures than at ambient temperature. At ambient temperature, the strain value was near zero at close to the end of the CFRP laminate with a peak value at the opposite extremity. At moderate and elevated temperatures (varying from 40 °C to 140 °C) the strain distribution was more attenuated and uniform along the bonded length, with stresses very low at the end of the laminate (strain gauge S1), but not negligible. These results indicated that the transfer stress length (length needed to transfer the axial strains from the CFRP laminate to the concrete member) at ambient temperature corresponded to the bonded length, while at temperatures ranging from 40 °C to 140 °C the length needed to transfer the

axial strains from CFRP to concrete should be higher than the bonded length adopted due to a degradation of the adhesive properties. Moreover, the changes observed in the strain profiles along the bonded length of the CFRP with increasing temperature (axial stress more uniform) is attributed to the reduction of stiffness and strength of the adhesive, which in turn is affected by the heating exposure. The axial strains measured along the bonded length were null at 165 °C since the bond strength was completely lost at that temperature (as noticed in Section 3.5.2).

3.5.4 Bond strength

The ultimate loads of the CFRP-concrete bond (bond failure load) as function of the interface temperature are presented in Table 3.4. The normalized bond strength determined by the ratio between the ultimate load for the different temperatures and the one at ambient temperature as well as the maximum displacement and failure modes of the specimens are also listed in Table 3.4.

Table 3.4 – Bond strength of the specimens as function of temperature

		Test reference	Bond failure load (kN)	Bond failure load – average (kN)	Normalized bond strength	Maximum displacement (mm)	Failure mode
Temperature	Ambient	TA-1	29.5	29.3	1.00	7.4	Concrete substrate
		TA-2	29.0			7.6	
		TA-3	29.4			7.1	
	40 °C	T40-1	25.7	27.9	0.95	6.6	Concrete substrate
		T40-2	28.3			6.7	
		T40-3	29.7			6.9	
	65 °C	T65-1	17.4	17.4	0.59	5.5	Adhesive
		T65-2	17.2			5.6	
		T65-3	17.5			5.8	
	90 °C	T90-1	10.5	10.0	0.34	4.9	Adhesive
		T90-2	10.1			4.8	
		T90-3	9.4			5.2	
	115 °C	T115-1	6.1	6.2	0.21	4.8	Adhesive
		T115-2	6.2			4.9	
		T115-3	6.4			4.9	
	140 °C	T140-1	3.5	3.5	0.11	2.1	Adhesive
		T140-2	3.2			1.7	
		T140-3	3.8			1.9	
	165 °C	T165-1	0.7	0.5	~ 0	0	Adhesive
		T165-2	0.3				
		T165-3	0.4				

Figure 3.7 shows the normalized bond strength obtained for each testing temperatures at the CFRP-concrete interface. The bond strength results from previous experimental investigations [36,37,39–43] carried out bond between CFRP and concrete of EBR-strengthened concrete blocks at elevated temperatures are also presented in the graph of Figure 3.7. The study by Palmieri et al. [86] was also included in this benchmarking, although this investigation had been performed on specimens strengthened by the NSM technique. In addition, Table 3.5 summarizes the main characteristics of the different experimental campaigns performed, including the current study.

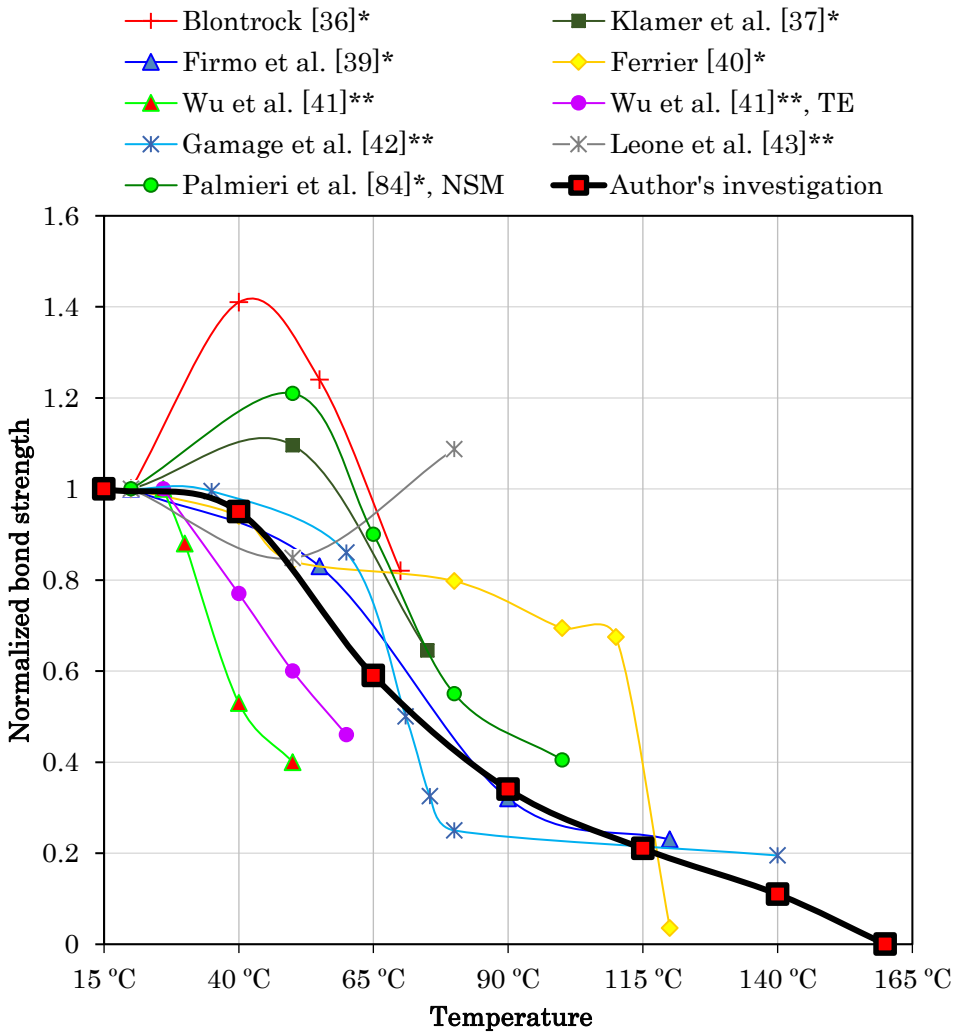

Figure 3.7 – Normalized bond strength as function of temperatures at the CFRP-concrete interface in benchmarking with previous studies (*CFRP laminates; **CFRP sheets; TE – Thermo-resistant Adhesive Epoxy; NSM – Strengthened by the near surface mounted technique)

Table 3.5 – Experimental investigations carried out on bond between CFRP and concrete at elevated temperatures

Investigations	Type of test	CFRP format	Adhesive T_g (ºC) (test – method)	Temp. range (ºC)	Heating period
Author's study	SST	Laminate	75 (DMA – Tan δ)	15 to 165	0.4 to 2.5 h
Blontrock [36]	DST	Laminate	62 (*N.R.*)	20 to 70	*N.R.*
Klamer et al. [37]	DST	Laminate	62 (*N.R.*)	20 to 75	12 h
Firmo et al. [39]	DST	Laminate	47 (DMA – E')	20 to 120	1.5 to 2 h
Ferrier [40]	DST	Laminate	58 (*N.R.*)	– 20 to 80	3 h
Wu et al. [41]	DST	Sheets	34 (*N.R.*)	26 to 50	*N.R.*
Wu et al. [41] (TE)			40 (*N.R.*)	26 to 60	*N.R.*
Gamage et al. [42]	SST	Sheets	x	20 to 140	> 0.75 h
Leone et al. [43]	DST	Laminate	55 (DSC – *N.R.*)	20 to 80	*N.R.*
Palmieri et al. [86] (NSM)	DST	Laminate	65 (*N.R.*)	20 to 100	> 12 h

(TE) – Thermo-resistant Adhesive Epoxy;
(NSM) – Strengthened by the near surface mounted technique.
N.R. – Not reported

The results observed in the current investigation (Figure 3.7) reveal a reduction of the bond strength of the CFRP-concrete interface with the increasing temperatures. For moderate temperature (40 °C), a low decrease (5%) in the bond strength is observed, considering the results at ambient temperature as reference. The bond strength is most affected when the temperatures approach the T_g of the adhesive (quoted as 75°C). In this case, about 40% reduction at 65 °C is noticed compared to the ambient temperature. For higher temperatures (90°C, 115 °C and 140 °C), this reduction is more significant, reaching values greater than 66%. However, a significative residual bond strength was observed for temperatures substantially higher than the T_g. For the series of temperature of 90 °C, 115 °C and 140 °C a bond strength retention of 34%, 21% and 11% (compared to the reference) were registered, respectively. The bond strength was completely lost only at temperatures of around 165 °C, corresponding to a temperature level of +90 °C higher than the T_g of the adhesive.

Finally, it is important to note that the CFRP-concrete bond presented a similar behaviour in terms of strength compared to the cases previously investigated by Firmo et al. [39], Ferrier [40], Wu et al. [41] and Gamage et al. [42], as illustrated in Figure 3.7. A regular and continuous decrease of the bond strength was observed with increasing temperature. Moreover, a significant strength retention for temperatures above the T_g was reported by these authors similar to what was noticed in the current research. In contrast, Leone et al. [43] surprisingly reported a slight increase of the bond strength for temperatures higher than T_g while in the

current study a decrease was observed. At temperatures below T_g, a similar tendency was noticed, with a slight decrease of the strength. Results from Blontrock and Klamer et al. and Palmieri et al. [36,37,86] also showed a loss of strength at temperatures above T_g. Nevertheless, an opposite tendency in the bond behaviour even at temperatures lower than the T_g was noticed [36,37,86] in contrast to the current study where there was an increase in the strength. According to literature [87], the reason for the different tendencies noticed among the authors on CFRP-concrete bond behaviour, in cases where the bond strength increase at interface temperatures below T_g, can be attributed to two issues: due to the effects of thermally induced stresses arising from differential thermal expansion of the constituent materials or due to the more uniform shear stresses at the bonded interfaces with increasing temperature due to adhesive softening. In addition, it is important to highlight a common condition observed in experimental campaigns that presented increases in the bond strength at temperatures below T_g [37,86]: the heating period applied on specimens (time to achieve the target temperature at the CFRP-concrete interface before loading application) was done in overly long durations, at least 12 h. The assumption of these condition by the authors [37,84] may have provided scattered results from the other authors. The current investigation suggest that this bond behaviour should not occur in the reality, since the current adopted heating period is closer to the ones developed in a fire situation than those adopted in the addressed studies [37,86]. Concerning the significant bond retention for temperatures above T_g, as noticed in the current research and in the most of prior investigations, this behaviour may be due to the frictional forces at the bonded interface and the chemical adhesion provided by the concrete–adhesive interface at elevated temperatures, according to suggestions by Firmo et al. [39,88].

3.5.5 Failure modes

The failure modes observed in the specimens after the SST tests occurred in two ways: (i) failure of the concrete substrate in the bonded length region; (ii) failure of the adhesive at the CFRP-concrete interface (Table 3.4). The concrete cohesive failure mode was observed in the specimens tested at ambient temperature and 40 °C, while the adhesive failure mode happened for temperatures higher than 65 °C. It was noticed that in the failure by concrete substrate a thin layer (a few millimetres) of concrete was detached from it and it came attached to the adhesive after test, as shown in the Figure 3.8a and b. Failure in the adhesive was observed in specimens exposed to temperatures of 65 ºC, 90 ºC, 115 ºC, 140 ºC and 165 ºC (Figure 3.8c-g).

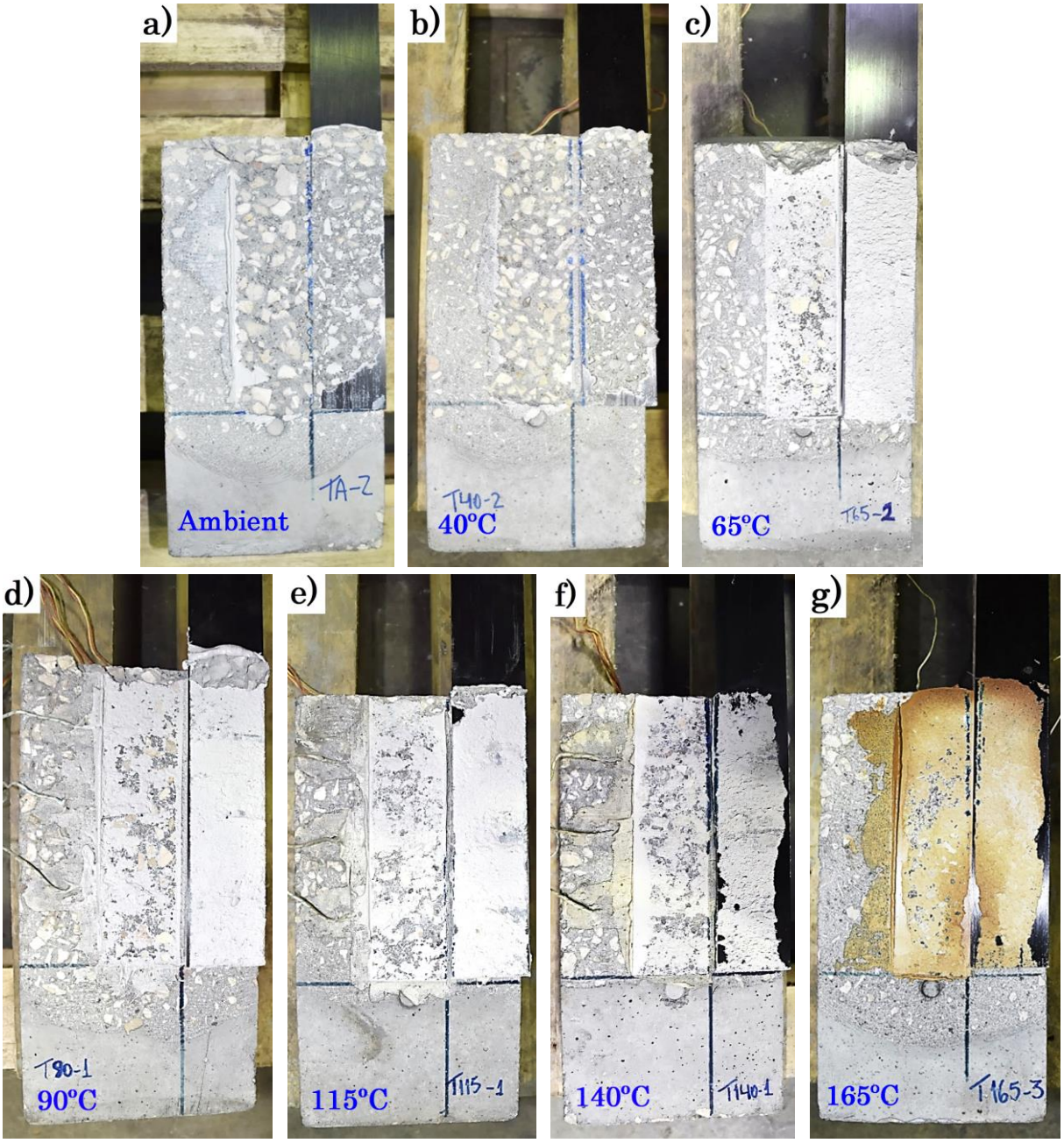

Figure 3.8 – Failure modes in the concrete substrate at (a) ambient temperature and (b) 40 ºC and failure modes in adhesive at the CFRP-concrete interface at (c) 65 ºC (close T_g), (d) 90 ºC (slightly above T_g), (e) 115 ºC (higher than T_g), 140 ºC and (g) 165 ºC (much higher than T_g)

As can be seen in Figure 3.8g, a physical decomposition of the adhesive when the CFRP-concrete interface was exposed to temperatures of 165 ºC was noticed. Finally, it was observed (Figure 3.8a-g) that the concrete block and CFRP laminate directly exposed to the thermal action remained relatively non-degraded after tests. Figures of identical failure modes of the other tested specimens described in the current test plan are presented in APPENDIX A.

3.6 Final Remarks

The results of an experimental investigation on the CFRP-concrete bond behaviour by subjecting strengthened concrete blocks to SST tests at ambient and elevated temperatures were addressed in this chapter. The main purpose of this investigation was to assess the mechanical response of the bond between the laminate and the concrete in CFRP-strengthened concrete structures when exposed to different temperatures and under steady state conditions in terms of load-displacement behaviour, bond strength, axial strains and failure modes in relation to the temperature evolution.

The results showed a continuous reduction of the bond strength with the increasing temperature in the specimens. On the other hand, an important behaviour was noticed at interface temperatures higher than 90 ºC (above T_g), which a significant retention of CFRP-concrete bond strength (up to 34%) was verified.

The failure load, the axial strains, and the maximum displacements were also severally affected by the increasing of the temperature, confirming the induced thermal damage to the stiffness of the adhesive, which in turn is very sensitive to fire exposure.

In the post-fire assessment, failure mode in the concrete substrate along bonded length area was observed on the specimens tested at ambient temperature and at 40 °C, while a failure mode developed in the interface epoxy adhesive was obtained for the specimens exposed at temperatures between 65 °C and 165 °C. In addition, the specimens presented a brittle rupture, when their stiffness was lost abruptly.

In benchmarking with previous investigations, the experimental results were broadly similar with the available data. The similarity was observed in the axial strain-temperature evolution along the CFRP bonded length region of the specimens (the strains become more linear due to the adhesive softening), in the transfer stress length needed to transfer the axial strains from the CFRP laminate to the concrete member (where an increase of the effective bond length with increasing temperature was noticed) and in the change of failure modes by temperature influence (from cohesive concrete substrate to adhesive failure). However, comparing current research with the previous studies addressed, the results were divergent in terms of CFRP-concrete bond strength variation with temperature. The contradictions were noticed specially for temperatures below T_g, where the bond presented a strength decreases for some authors and increases for others. Nevertheless, surprising behaviour was reported by the authors Leone et al. [43], which an increase of the bond strength for temperatures higher than T_g was achieved. The authors [43] considered that these unexpected and anomalous results were probably due to

the chemical processes occurring at the T_g temperature range and concluded that this needs further investigation. However, as observed in the current research and in other investigations addressed above, despite the chemical processes provided a strength retention, this did not cause the increase in the bond strength at the T_g temperature range. In addition, it is important to highlight a common condition observed in experimental campaigns that presented increases in the bond strength at temperatures below T_g [37,86]: the heating period applied on specimens (time to achieve the target temperature at the CFRP-concrete interface before loading application) was done in overly long durations, at least 12 h. The assumption of these condition by the authors [37,84] may have provided scattered results from the other authors. The current investigation suggest that this bond behaviour should not occur in the reality, since the current adopted heating period is closer to the ones developed in a fire situation than those adopted in the addressed studies [37,86]. Other important achievement of this investigation is related to an expressive bond retention noticed for temperatures much higher than the T_g, since it is a very relevant phenomenon in the effectiveness of the CFRP-strengthened concrete structures which needs to be taken into account for their fire design and a limited number of studies have been performed under these test and temperature conditions. Therefore, the current research contributes to evidence and proof this important phenomenon developed in the CFRP-concrete bond, which is neglected by the standards that guide the fire design of concrete structures, such as EN 1992-1-2 (2004), ACI 440.2R-17 (2017) and Fib bulletin (2001) [1–3]. The results achieved in this thesis are fundamental to a better understanding of the CFRP-concrete bond behaviour at elevated temperatures, particularly concerning to its behaviour at temperatures above T_g of the adhesive. Moreover, it can be concluded that this phenomenon must be considered in the fire design of the CFRP strengthening systems and that the standards are quite conservative in this regard, where they merely define the critical temperature of the system by the T_g of the adhesive or, in an oversimply way, recommend not consider the effectiveness of the strengthening system in a fire situation. Finally, these reported data are valuable and can be useful for the review and improvement of the mentioned standards or still for creating new rules, documents or calculation methods for guiding the fire design of these structures.

4 EXPERIMENTAL INVESTIGATION ON RC BEAMS FLEXURALLY STRENGTHENED WITH EBR-CFRP LAMINATES UNDER FIRE CONDITIONS

This chapter introduces a series of flexural tests at ambient temperature and under fire conditions (Fire Resistance tests) focused on simply supported RC beams and CFRP-strengthened RC beams protected by different fire protection materials. It describes in detail the experimental program, the testing procedures, the test specimens and the test set-up for flexural tests that were carried out at the Laboratory of Testing Materials and Structures of the University of Coimbra (UC). Furthermore, the results of this experimental approach are duly presented and discussed on it.

The main purpose of this investigation was to access the influence of externally bonded strengthening system with CFRP laminates, along with fire protection materials and surrounding boundary conditions on the fire performance of simply supported beams under flexural conditions. The failure modes and aspects responsible for the collapse of the beams and the interaction systems were also investigated. Similarly to the Single lap Shear tests, this experimental campaign also provides valuable experimental data for the development of a relevant numerical study which was described in detail in Chapter 5.

4.1 Test Set-up

The configuration and details of the experimental system used in the ambient temperature and fire resistance (FR) tests, designed for these loadbearing capacity tests, are shown in Figure 4.1 and Figure 4.2, respectively.

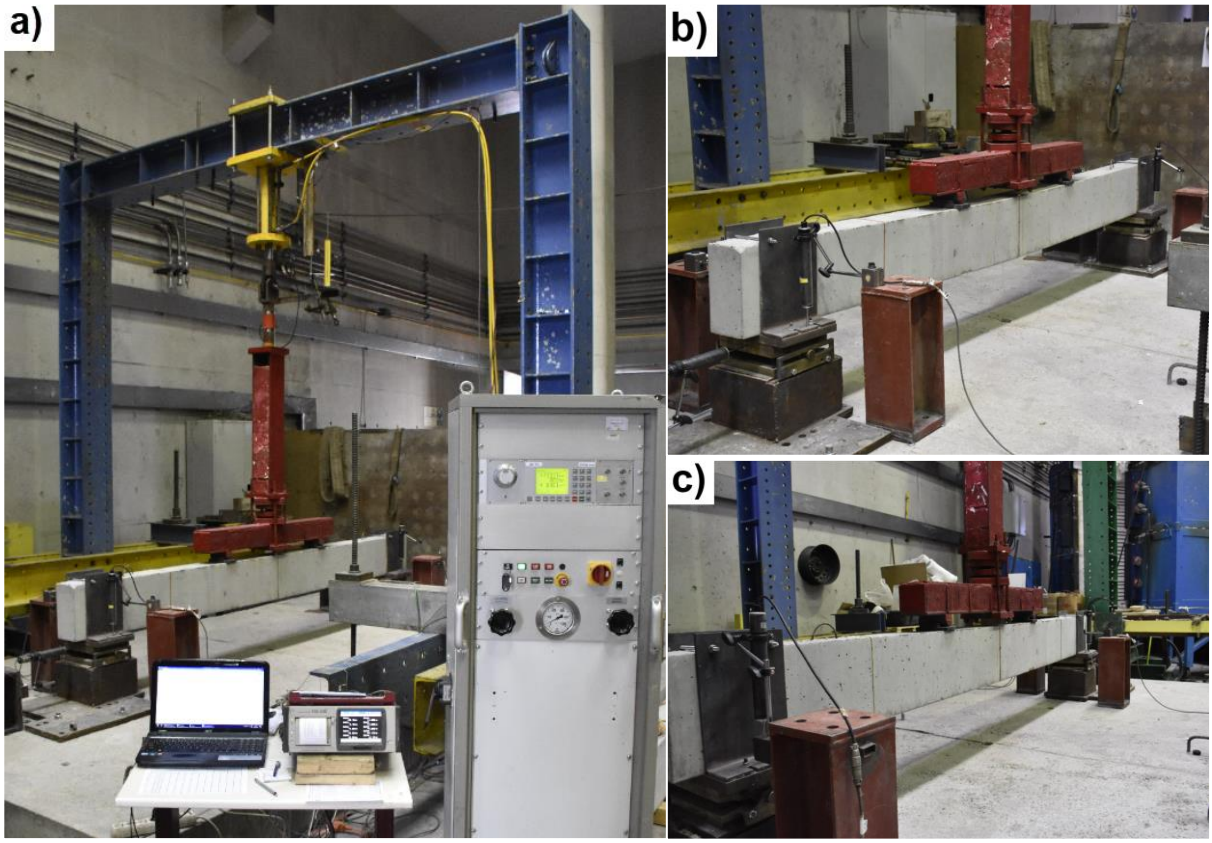

Figure 4.1 – Test set-up for ambient temperature tests: (a) general view and (b, c) detail views

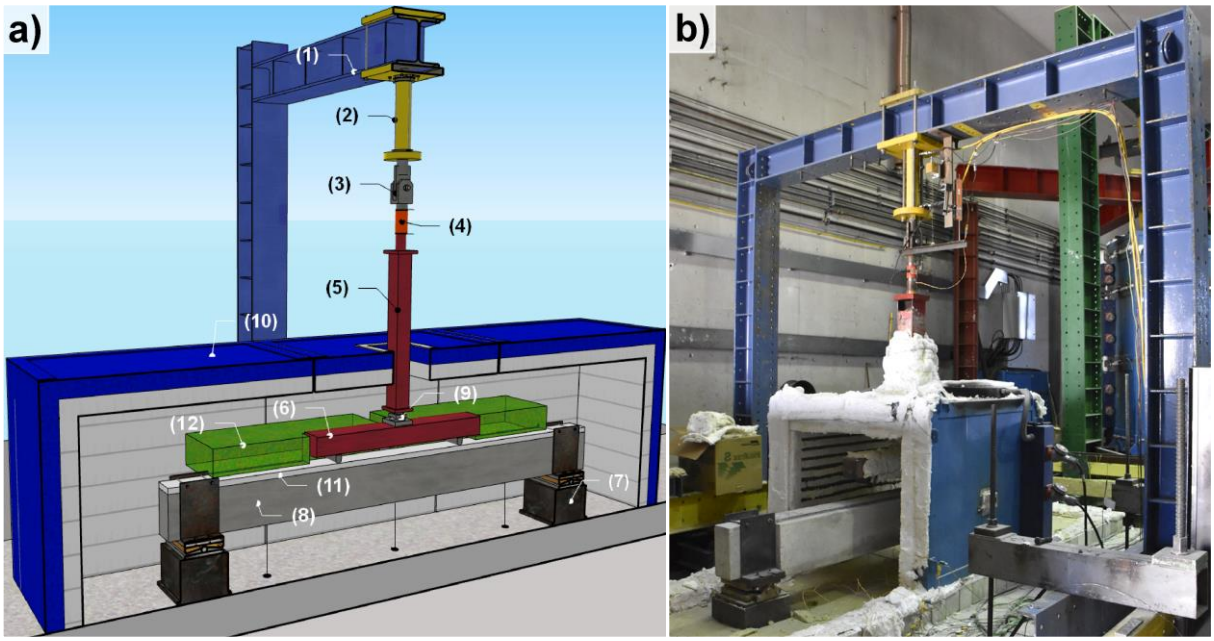

Figure 4.2 – Test set-up for fire resistance tests: (a) schematic, (b) general view with only central furnace module, c) general view with complete furnace system and (d) detail view

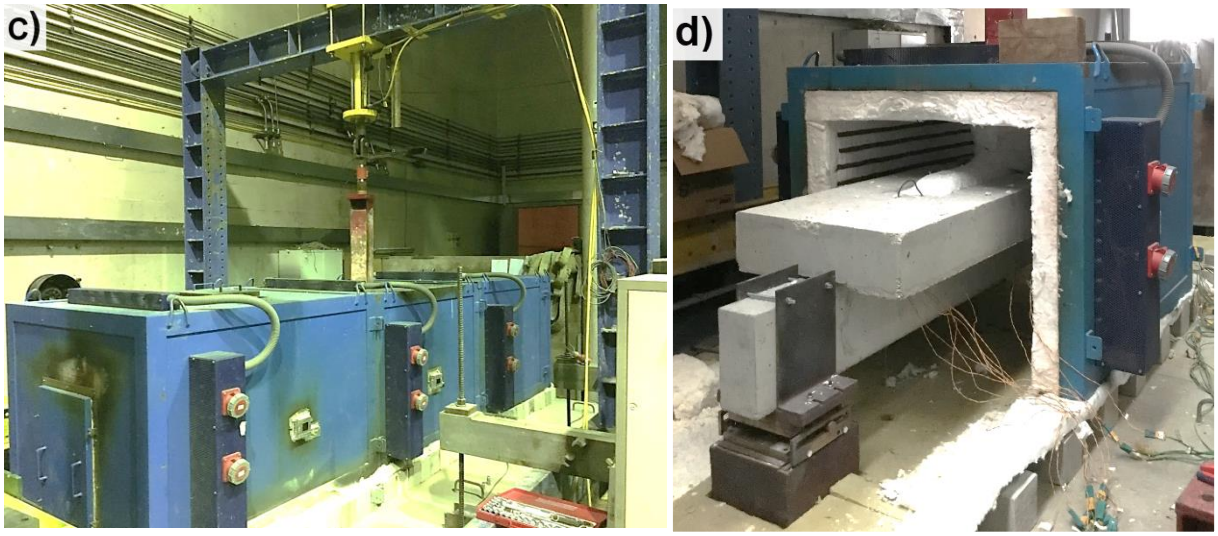

Figure 4.2 – Test set-up for fire resistance tests: (a) schematic, (b) general view with only central furnace module, c) general view with complete furnace system and (d) detail view (Continuation)

The mechanical loads have been applied on the specimen by the loading system in four points (four-point bending) for both ambient temperature and fire resistance tests. The test set-up consisted essentially of a two-dimensional (2D) reaction steel frame (No. 1 in Figure 4.2a), composed by two HEB300 columns and one HEB 300 beam, steel class S355. The loading was applied by a hydraulic jack (No. 2 in Figure 4.2a) with a load capacity in compression of 295 kN and a maximum stroke of 360 mm, controlled by a servo-hydraulic power unit, and hanged on the plane reaction frame. The test specimen (No. 8 in Figure 4.2a) was loaded at two points 1.0m apart from each other. The points of application of the load divided the specimen in three equal lengths, resulting into a four-point bending test, in order to have pure bending in the central third length (Figure 4.4). This load was applied to the specimen by and hydraulic jack acting on a load application system composed by a HEA160 stub column (No. 5 in Figure 4.2a) connected to a HEB140 distribution beam (No. 6 in Figure 4.2a). The steel profiles of this load application system were fire-protected to prevent their destruction by high temperatures during the fire resistance tests.

As shown in Figure 4.2a (No. 7), the tested beams were simply supported simulating a statically determinate beam. A pinned and a roller support have materialised the boundary conditions for the testing beams. The pinned support allowed the rotation and prevented the displacements in the direction of the longitudinal axis of the beam and the roller support allowed both types of movements. The span of the testing beams between axis of the supports was 3000 mm and the support regions were 250 mm long (see Figure 4.7). The testing beams with the supports and the surrounding adjacent part of slab, were completely inside the furnace during the fire test.

The supports were made of refractory steel in order to prevent major fire damages among the different tests (see Figure 4.2a and Figure 4.2b).

Other important components essential for the correct operation of the experimental system, such as a spherical plain bearing and a spherical hinge (respectively No. 3 and 9 in Figure 4.2a) were also assembled in the experimental system. The purpose of these elements was to ensure that the load applied could easily follow the deformations of the testing beam during the fire tests.

A horizontal modular electric furnace (No. 10 in Figure 4.2a) exclusively for fire resistance tests with internal dimensions of 4500×1000×1000 mm, capable to heat up to 1200 ºC and follow fire curves with different heating rates, was used to apply the thermal action in specimens.

In fire tests three faces of the beams were exposed to fire. The bottom and lateral faces were exposed to fire, whereas the upper face was not subjected to heating. The unexposed face of the specimens was protected by ceramic wool (No. 11 in Figure 4.2a) and a concrete slab (No. 12 in Figure 4.2a). This system (illustrated in Figure 4.3) is intended to reproduce an RC beam as faithfully as possible in contact with a slab as if it were a real building structure resulting in an approximate thermal adiabatic surface on these tests. The use of the concrete slab along the upper face of the specimens makes it possible to create a thermal influence zone on the beams when subjected to fire, reproducing the effects arising from a real surrounding slab, such as the heat transfer reactions and the shading effect. The concrete slab was supported on the beams by means of a docking system and designed to accompany the deformation of the beam and to prevent voids between its interactive interfaces, maintaining contact between both elements throughout the test. This kind of testing considers the influence of the surrounding slab on the beam under fire conditions, has not been considered before on other experimental works carried out by other authors and this is an important issue addressed in the present research.

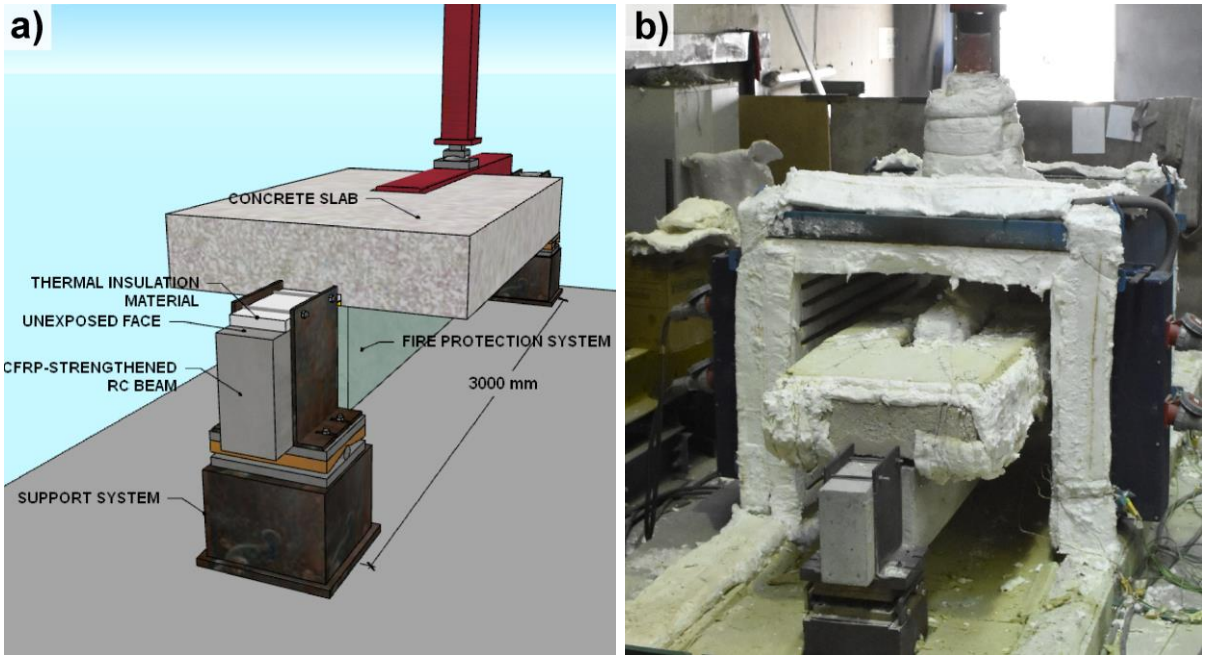

Figure 4.3 – Experimental system for fire resistance tests: (a) details of the beam's supports and protecting slab (without furnace); (b) general view of the beam inside furnace

The displacements of the beams at Sections S1 (mid-span), S2 and S3 (Figure 4.4) were measured by cable linear variable displacement transducers (LVDTs). Figure 4.4 and Figure 4.5 shows that these cable LVDTs were placed in the Laboratory's basement floor (below the testing floor) in such a way to prevent its damage during the tests. The LVDT cables from the specimens up to the measurement points was made of chromel-alumel wires (material with low thermal elongation coefficient) that passed through existing holes in the Laboratory slab. Additional LVDTs were installed at different points of the fire protection materials to provide means for detecting their collapse during the fire tests (these LVDTs were not represented in Figure 4.4).

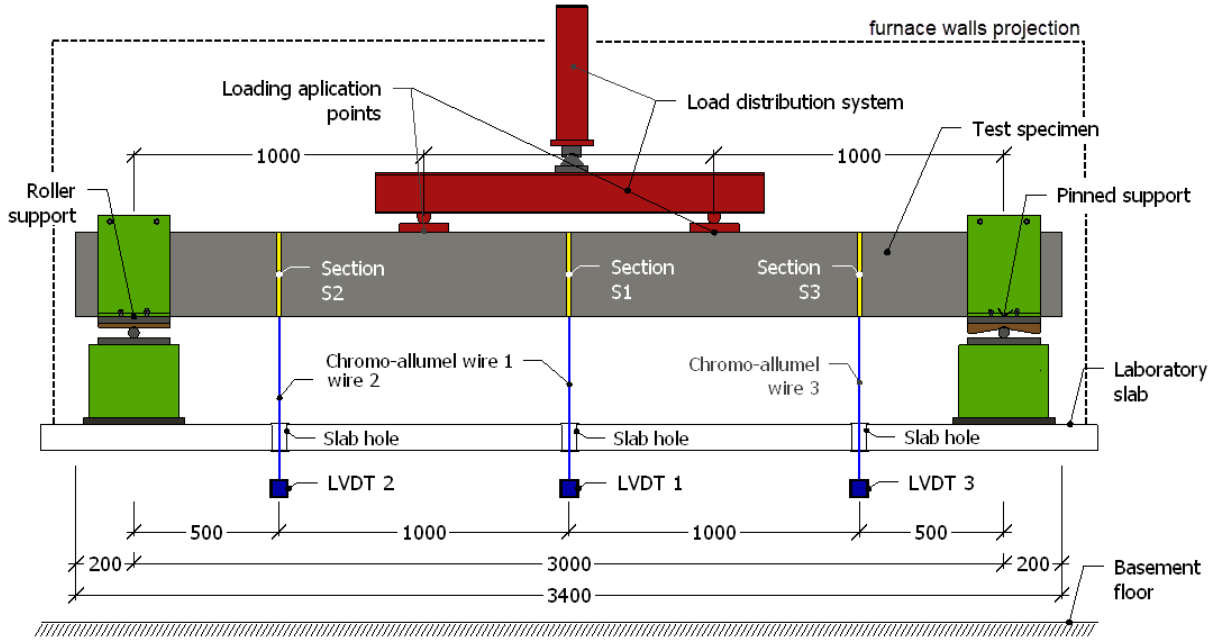

Figure 4.4 – Schematic view of test set-up with location of measuring points and other details

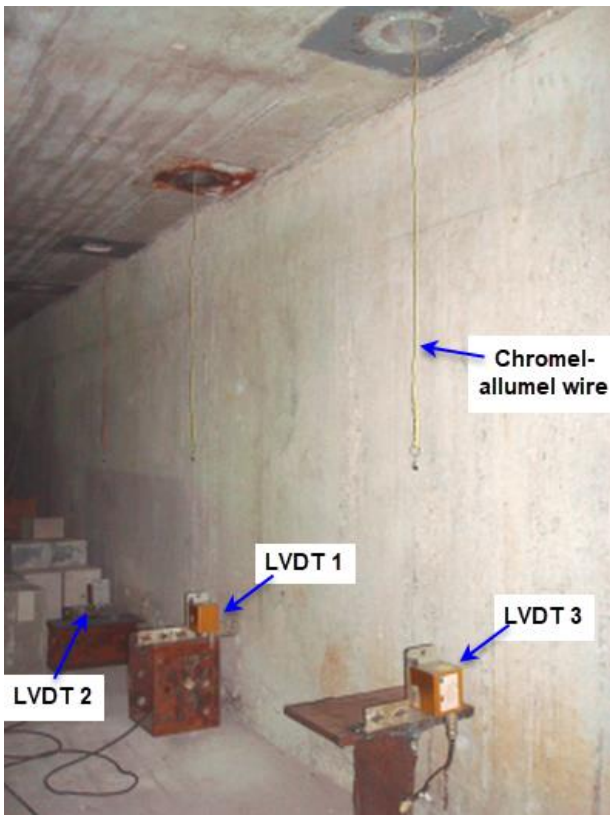

Figure 4.5 – LVDTs placed in the Laboratory's basement floor (below the testing floor) to displacements measurements of the beams

Finally, type K thermocouples were used for temperature measurements inside the furnace and at different points of the specimen's cross-section (Figure 4.6), at mid-span (Section S1). Exclusively at the regions of CFRP-concrete interface, CFRP laminate and fire protection material surfaces of the strengthened beams, the measurements were made on the four sections by additional thermocouples that corresponded to Sections S1, S2 and S3 and an intermediate region measurement referred as $SM_{1\text{-}3}$ located between the Sections S1 and S3 (this section was not represented in Figure 4.4). These additional measurement points were installed with the purpose of capturing a broad temperature profile along the length of the CFRP-concrete interface, allowing to assess possible cold zones and the effective temperature of the bond, since this region is very sensitive and relevant in estimating the failure temperature of these member. Moreover, these points are essential to provide data to the failure detection procedure of the strengthening and fire protection systems during the fire tests, since the visualization of the structure in test is not possible by the available furnaces. The data recording was done by a TML data logger (model TDS-530). The thermocouple distribution and nomenclature are presented in Figure 4.6a and Figure 4.6b, respectively for the simple and CFRP-strengthened RC beams. Such distribution allowed the assessment of the evolution of temperatures along the height and width of the beam's cross-section at different points, especially in the interface between the CFRP laminate and the concrete. In the protected beams two additional thermocouples were installed at the CFRP laminate and fire protection material surfaces (T6 and T7, respectively).

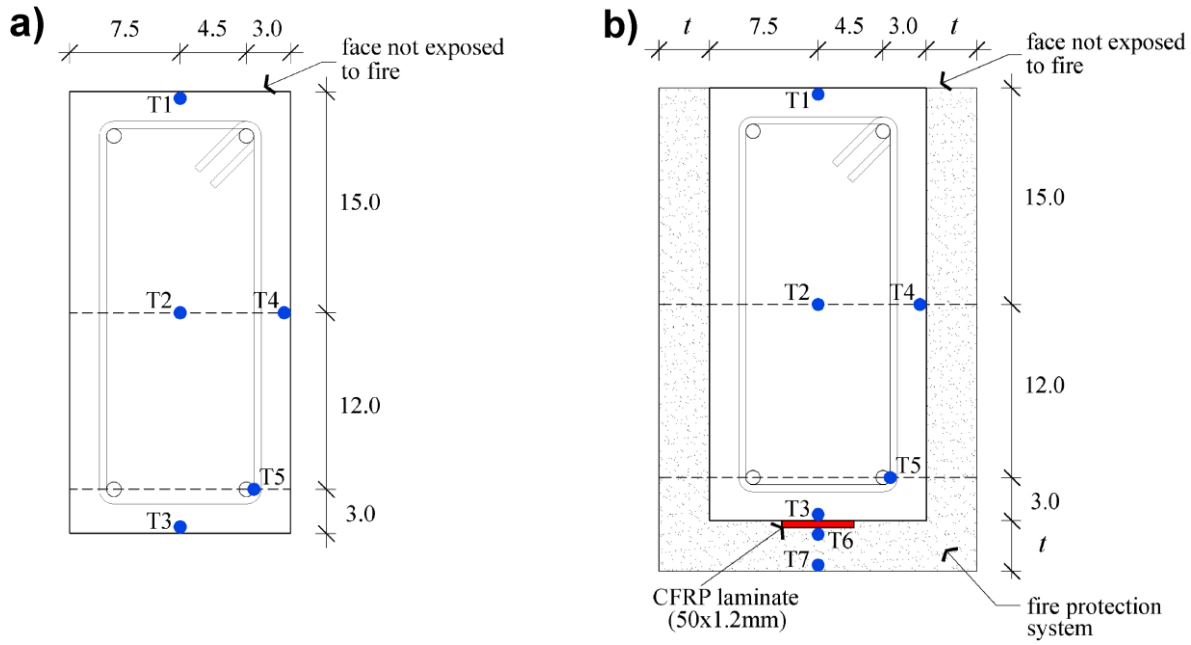

Figure 4.6 – Location of thermocouples for the (a) simple and (b) CFRP-strengthened RC beams (not declared units in cm)

4.2 Specimens

The specimens consisted of CFRP-strengthened RC beams of rectangular cross-section with 150 mm of width and 300 mm of height and 3400 mm of length (3000 mm between support's axis), as illustrated in Figure 4.7a. These beams were casted with normal reinforced concrete (RC). Moreover, an additional type of specimen was designed to perform reference tests, which consists of an unstrengthened and unprotected RC beam, as it can be seen in Figure 4.7b.

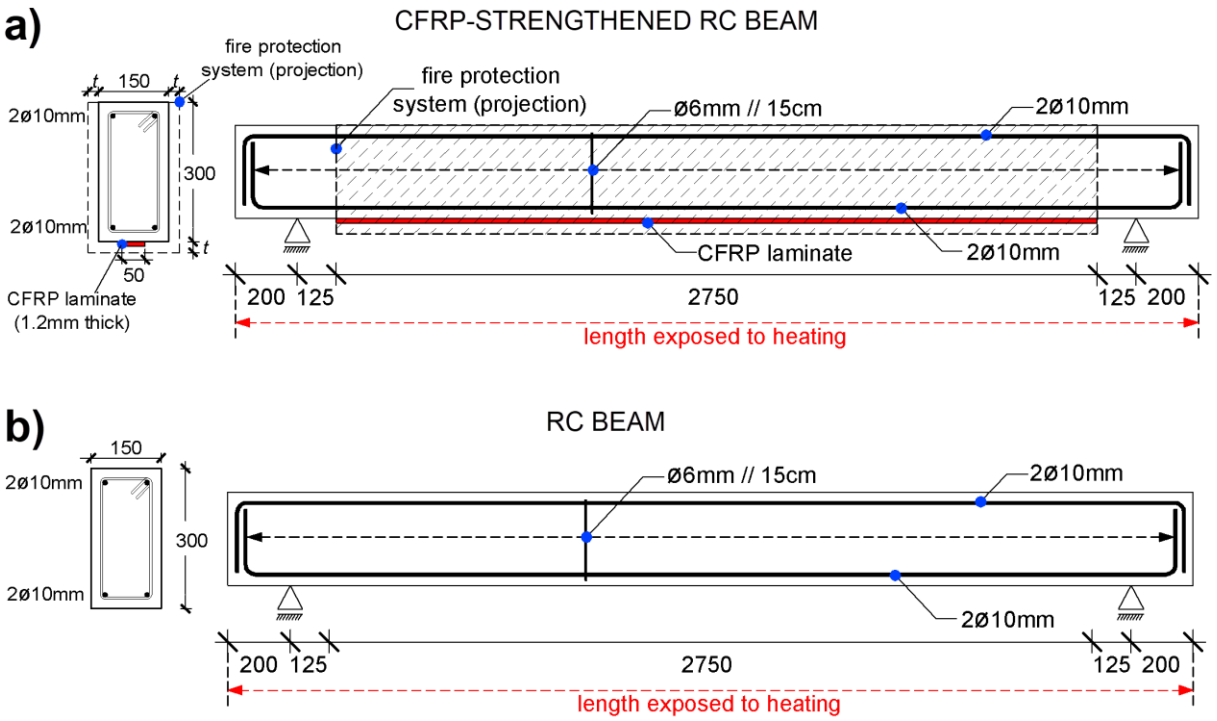

Figure 4.7 – Geometry of the tested (a) CFRP-strengthened and (b) RC beams (not to scale, dimensions in mm)

The concrete used in all tested specimens had the same characteristics as the one used in the fabrication process of concrete blocks beams for the Single lap Shear tests (see Table 3.1 in Section 3.2). Thus, at 28 days the f_{cm} corresponded to 30.1 MPa (C25/30 class [79]). Other parameters of the concrete composition, such as cement type, plastizer additive, aggregates with their respective granulometry, is summarised in Table 3.1 in Section 3.2.

The longitudinal reinforcement of the beams was 2Ø10mm rebars on the upper region and 2Ø10mm bars on the lower region, B500 steel class. Transversal reinforcement consisted of

Ø6mm stirrups spaced apart of 15 cm. The mechanical properties of the rebars used in the concrete beams were as follows: yield stress of 500 MPa, modulus of elasticity of 210 GPa and ultimate tensile strength of 550 MPa. The concrete cover was 25 mm in all beams.

For the strengthened specimens, the CFRP laminate was bonded along the bottom surface of the RC beams and was not mechanically anchored at its ends (Figure 4.7). For this purpose, the externally bonded reinforcement (EBR) technique was used. These laminates (commercially designated as *S&P Laminates 150/2000*) have a cross-section of 50 mm x 1.2 mm. According to the manufacturer [20], these CFRP laminates have an average tensile strength of 2800 MPa, modulus of elasticity of 170 GPa and ultimate strain of 16.0‰, at ambient temperature.

The adhesive used to bond the CFRP laminate strips to the bottom surface of the beams (commercially designated as *S&P Resin 220* [82]) was a two-component epoxy material with a T_g of 75 ºC. The T_g was determined by DMA tests [83] (heating rate of 5 ºC/min from 0 to 300 ºC and a frequency of 1 Hz) according to ASTM E1640 (2013) standard [84]. The T_g was defined based on the peak value of the Tan δ curve. This adhesive is the same of the one used in the Single lap Shear tests. More information concerning the physical properties of the CFRP laminate and the epoxy adhesive used in strengthening the concrete blocks can be seen in Table 3.2 in Section 3.2.

The CFRP-strengthened RC beams were protected by three types of fire protection systems composed by the following sprayed materials: Vermiculite-Perlite (VP), ordinary Portland cement with Expanded Clay aggregates (EC) and Ordinary Portland (OP) cement-based mortars. Moreover, for each fire protection system three thickness (*t*) levels were tested: 20 mm, 35 mm and 50 mm. The fire protection material was applied to the bottom and lateral surface of the beams by dry spraying method. RC beams strengthened with CFRP and protected by fire protection systems composed by EC, OP or VP mortar, before testing, are shown in Figure 4.8a, Figure 4.8b and Figure 4.8c, respectively.

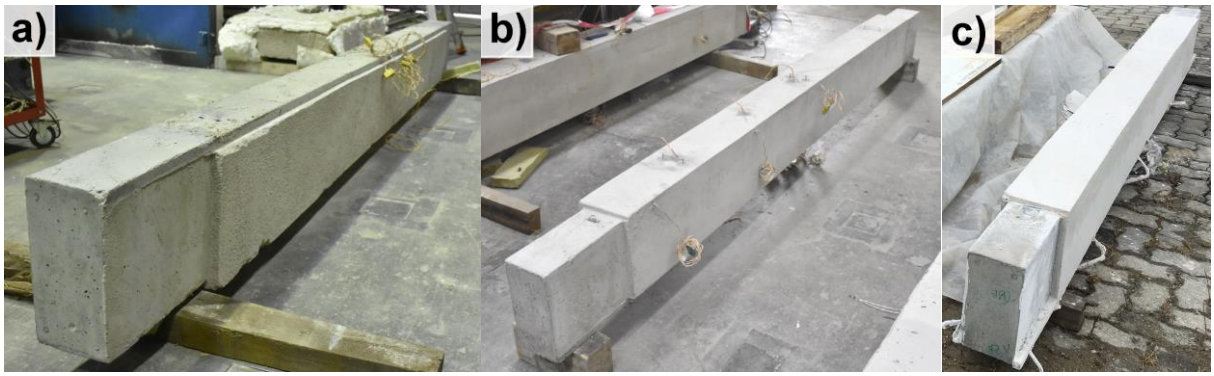

Figure 4.8 – RC beams strengthened with CFRP and protected by (a) EC, (b) OP and (c) VP mortars

Additionally, Figure 4.9 shows a schematic of the strengthened specimens with each fire protection system and its different applied thickness.

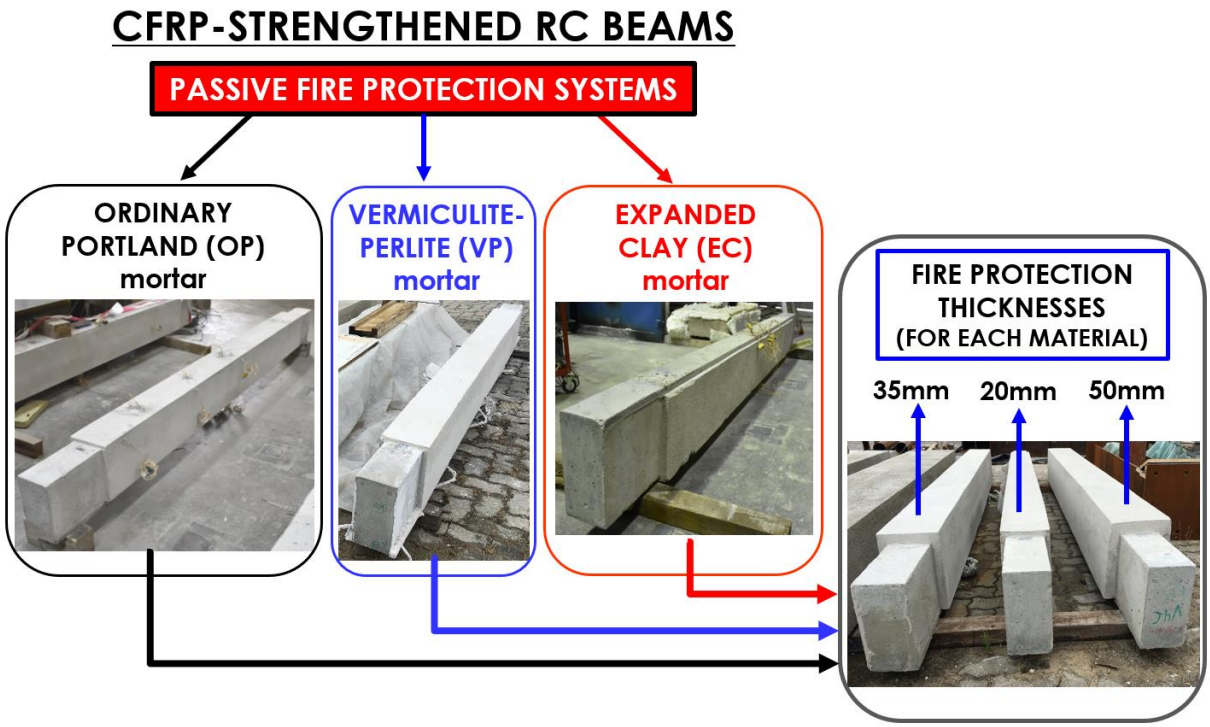

Figure 4.9 – Schematic view of the strengthened specimens with each fire protection system and its different applied thickness

The VP mortar was a commercial mortar made with lightweight expanded perlite and vermiculate aggregates, refractory compounds, cementitious binders and a ratio water/compounds of 0.67–0.80 l/kg. Also, this fire protection material presents a dry density of 450–500 kg/m^3 and a thermal conductivity of 0.0581 W/m.K [89]. The OP mortar, also commercial, was formulated from hydraulic binders, calcareous, siliceous aggregates and some other non-specified additions, with dry density of 1500–1800 kg/m^3, thermal conductivity 0.67 W/m.K and a ratio water/compounds of 0.13–0.15 l/kg [90]. The EC mortar differed from the OP mortar by replacing the calcareous aggregates by expanded clay aggregates. A ratio water/compounds of 0.35–0.40 l/kg was used. The expanded clay is a lightweight aggregate with a granulometry distribution of 0.25–2.0 mm, a dry density of 468–633 kg/m^3 and a thermal conductivity of 0.13 W/m.K [91]. This material was incorporated into the mortar mixture in a ratio of 2.6:1 (cement:aggregate). The aforementioned thermal property values are for ambient temperature.

4.3 Test Program

4.3.1 Loadbearing capacity tests at ambient temperature

The experimental program, summarized in Table 4.1 and Table 4.2, included a total of twelve four-point bending tests on simply supported beams under ambient and fire conditions. Among them, two tests were performed on an unstrengthened and a CFRP-strengthened RC beam at ambient temperature conditions. These specimens were respectively referenced in the ambient temperature test program (Table 4.1) as RC_AT and CFRP_AT.

Other parameters experimentally and analytically obtained, such as the design value of the loadbearing capacity of the reference unstrengthened RC beam at ambient temperature (P_{calc}), ultimate capacity of the different beams at ambient temperature (P_{ult}) and the enhancing of flexural strength capacity at ambient temperature for CFRP-strengthened beams compared to the unstrengthened beams, are also reported in Table 4.1. P_{calc} was calculated according to the standard EN 1992-1-1 (2004) [33].

Table 4.1 – Test program for ambient temperature tests

Test reference	P_{calc} (kN)	P_{ult} (kN)	Flexural strength capacity (%)	Temperature	Loading	Type of test
RC_AT	34.4	48.0	100	Ambient	Load increase under displacement control (0.01mm/s) until specimen's rupture	Ultimate capacity in a four-point bending configuration
CFRP_AT	-	79.5	160			

The experimental program for the FR tests is detailed and presented in the next section (Table 4.2).

4.3.2 Fire resistance tests

As mentioned in the previous section, the experimental program also included ten fire resistance tests, nine of which were performed on CFRP-strengthened beams protected by three different passive fire protection materials and three possible thicknesses (t), and one on an unstrengthened and unprotected RC beam.

In the test plan (Table 4.2), the specimens strengthened with CFRP laminates were divided in three batches, according to the type of passive fire protection system. Three tests were carried out per each batch, one for each thickness of the fire protection material. Therefore, according to the thickness applied, the specimens protected by EC mortar were designated by EC-20, EC-35 and EC-50 (20, 35 and 50 mm thick, respectively). The same type of referencing was used for the specimens protected by OP and VP mortars. The un-strengthened and un-protected reinforced concrete beam was designated in the experimental program as RC. The experimental program for the fire resistance tests is summarised in Table 4.2.

Table 4.2 – Test program for fire resistance tests

	Test reference	Insulation material	t (mm)	P (kN)	P_{ult} (kN)	Load ratio (P/P_{ult})	Temperature	Loading	Type of test
unstrengthened	RC	unprotected	-	24.0	48.0	0.5	Standard fire curve ISO 834 (fire resistance tests)	Subjected to a fixed service load of 70% of the P_{calc}	Fire resistance in a four-point bending configuration
CFRP-strengthened	EC-20	EC mortar	20		79.5	0.3			
	EC-35		35						
	EC-50		50						
	OP-20	OP mortar	20						
	OP-35		35						
	OP-50		50						
	VP-20	VP mortar	20						
	VP-35		35						
	VP-50		50						

Both ambient temperature and fire resistance tests were carried out in the Laboratory of Testing Materials and Structures of the University of Coimbra (UC), in Portugal.

4.4 Test Procedure

4.4.1 Loadbearing capacity tests at ambient temperature

Four-point bending tests at ambient temperature were used to measure the ultimate flexural strength (failure load) of specimens RC_AT and CFRP_AT at ambient temperature, as well as to check their critical deflection, final deformed shape, failure modes and aspects responsible for collapses and their interactions.

The beams were loaded under displacement control at a rate of 0.01 mm/s until the failure of the specimen. The tests were conducted until the bars of the lower longitudinal reinforcement ruptured and the specimen completely collapsed abruptly, allowing the desired measurements and limit verifications to be effectively carried out.

The failure load of the specimen was assumed to be the maximum value reached in the loading regime when the critical deflection was verified at this time instant.

During these tests, the load applied and the vertical displacements at the different sections of the beams were measured.

4.4.2 Fire resistance tests

The fire resistance tests were performed in two stages. In the first stage, the specimens were loaded under load control up to the desired level of load at a rate of 0.05 kN/s (a rate of 0.03 kN/s was used in a second step closer of target load). The load applied to the beams during the tests, fixed in P=24.0 kN, corresponded to 70% of the design value of the loadbearing capacity of the reference RC beam at ambient temperature (P_{calc} – see Table 4.2) calculated according to the EN 1992-1-1 (2004) [33] provisions. This load tried to simulate the serviceability load of the beam when inserted in a real building structure and was kept constant during the tests. After the stabilization of the desired loading, in a second stage, the heating was started by the furnace. The heating of the specimens was programmed to reproduce the standard fire curve ISO 834 (1999) [34].

The RC beams strengthened with CFRP laminates had their flexural strength capacity at ambient temperature increased by 60% in relation to the unstrengthened beams, as it can be seen in Table 4.2. These reported results were obtained by experimental tests performed at ambient temperature. The ratio between the applied load and the ultimate capacity of the different beams (P_{ult}) at ambient temperature are presented in Table 4.2.

The failure criteria adopted for beams in the fire tests was the one of EN 1363-1 (1999) [92]. According to this standard, the failure of the tested beams occurred when the deflection reached the limit of $L^2/(400\ h)$ mm or the deflection rate reached $L^2/(9000\ h)$ mm/min for a maximum deflection higher than $L/30$ mm (L and h in mm), considering a fixed load.

The detection of the strengthening system debonding was assumed when the following criteria occurred simultaneously: (i) when the beam suffered an abrupt deflection increase at mid-span along with a quick load loss and (ii) when the temperatures at the CFRP-concrete interface

started to increase at a heating rate significantly higher than the ones developed before CFRP debonding.

Two criteria were adopted for the failure detection of the fire protection systems. The failure was defined when the following conditions occurred simultaneously: (i) when the fire protection material suffered an abrupt deflection at the measurement points of the additional LVDTs (discussed in Section 4.1), reaching values close to zero and (ii) when the temperatures at the beam's lateral and bottom surface or at the CFRP laminate's bottom surface started to increase at a heating rate excessive higher than the ones exhibited before fire protection collapse.

During the tests, the following measurements were performed: the load applied, the vertical displacements, the cross-section temperatures of the beams and the gas temperatures in the interior of the furnace.

4.5 Results and Discussion

4.5.1 Loadbearing capacity tests at ambient temperature

4.5.1.1 Load-displacement evolution

The experimental tests in a four-point bending configuration allowed the assessment of the failure load of unstrengthened and CFRP-strengthened RC beams at ambient temperature, as well as to check their critical deflection, final deformed shape, failure modes and aspects responsible for collapse and their interactions.

The load evolution as a function of the vertical displacement at Section S1 (mid-span) of the ambient temperature tested unstrengthened (specimen RC_AT) and CFRP-strengthened beams (specimen CFRP_AT), is shown in Figure 4.10. The results are presented until 100 mm displacement for both specimens.

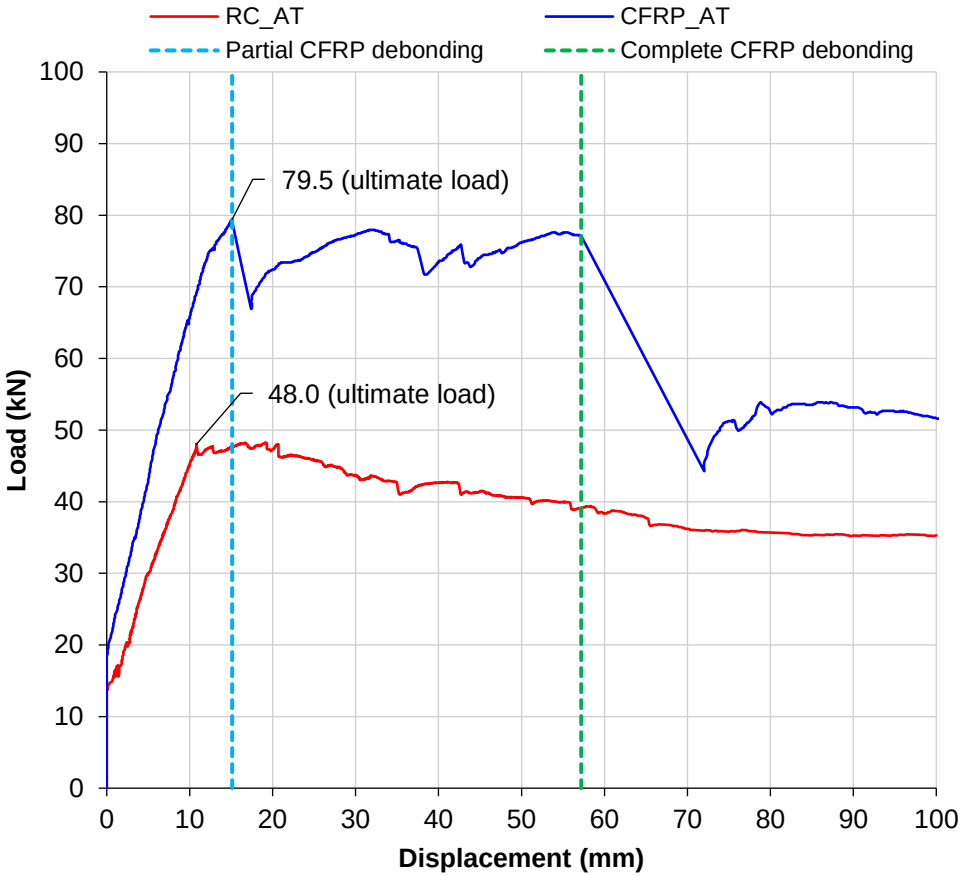

Figure 4.10 – Load-displacement evolution at Section S1 for the RC_AT and CFRP_AT beams

The experimental results of the ambient temperature tests showed a quasi-static structural behaviour (i.e., loading stage, failure load and unloading stage) for two types of beam. However, two failure peaks were observed in strengthened beam, that corresponded to a partial and complete CFRP debonding.

The partial failure of strengthening was assumed as the ultimate flexural strength of the beam, which the maximum load value was verified. The reason for that may be essentially due to eccentricities of testing, of the applied load or non-linearity and imperfections of the materials in the specimen. This failure aspect is discussed in further detail in the next section.

The failure load obtained for the CFRP_AT specimen was significantly higher than the one obtained for the RC_AT due to an increasing of the additional flexural strength provided by the strengthening system. While the failure load for the RC_AT beam was 48.0 for the CFRP_AT beam, the failure load measured was 79.5 kN.

After complete debonding of the laminate, the specimen CFRP_AT continued to resist similarly to an RC beam until its total collapse. Although the load-displacement results had been exhibited up to 100 mm deflection, the total collapse of the specimens was registered at much higher values when the final deformed shape was verified.

Concerning the measured displacements, the CFRP-strengthened beam (CFRP_AT) achieved 15.9 mm of critical deflection, while for the unstrengthened beam (RC_AT) 10.8 mm was obtained (see Figure 4.10). Moreover, for an identical load level, lower deflection values are obtained by the CFRP-strengthened beam compared to the unstrengthened beam, providing deflection at least 50% lower at the ultimate load instant. For example, at a loading of 48.0 kN (failure load of the RC_AT specimens) the unstrengthened beam had a displacement of 10.8 mm, while, in contrast, the displacement of the strengthened specimen was only 5.9 mm (approximately 83% lower).

As clarified in Section 4.3.1, the ultimate design load value of the unstrengthened RC beam at ambient temperature, calculated in accordance with EN 1992-1-1 (2004) [33], was equal to 34.4 kN. However, the characteristic value, that is compared with the tests, was defined as 40.4 kN. Based on the experimental result (realistic value), the predicted value presented a reasonable approximation with a variation of around 15% lower. This result indicates a conservatism of the adopted analytical method.

As mentioned before, an increase of about 60% in load-bearing capacity of the beam was achieved by using the CFRP strengthening system, where an ultimate flexural capacity of 48.0 kN and 79.5 kN was experimentally obtained at ambient temperature for the unstrengthened and strengthened beams, respectively. The flexural strength capacity relationship for the different specimens tested at ambient temperature is presented in Figure 4.11.

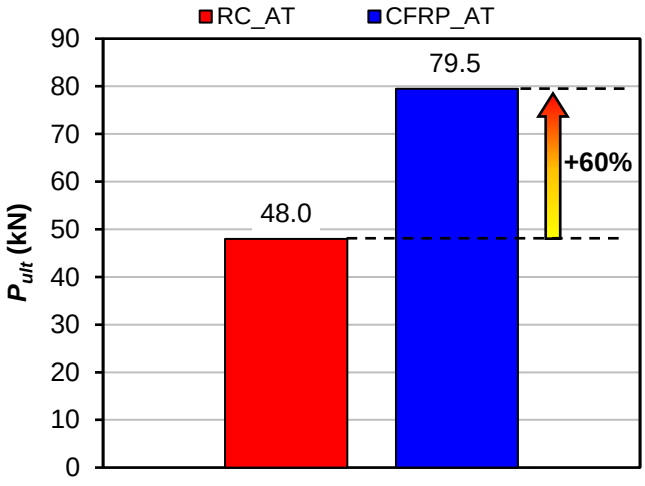

Figure 4.11 – Flexural strength capacity for the RC_AT and CFRP_AT specimens

4.5.1.2 Failure modes

The experimental failure modes and final aspects of the simply supported RC beam tested under flexural loading conditions and at ambient temperature are illustrate in Figure 4.12.

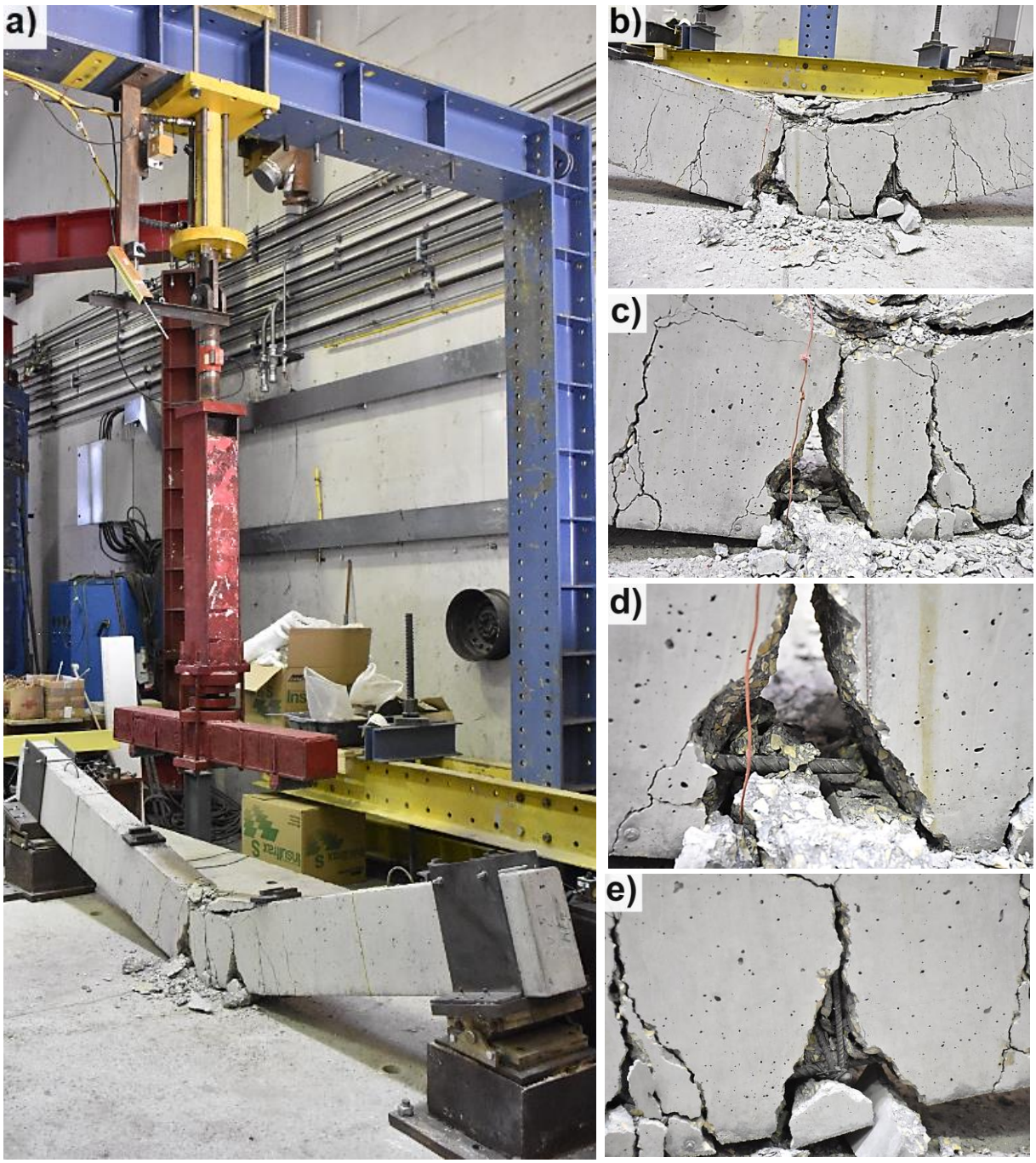

Figure 4.12 – Failure modes of the RC beam tested at ambient temperature: (a) general view, (b) failure zone detail with excessive cracking and loss of concrete cover, (c) longitudinal rebars rupture zone, (d) approximate detail of longitudinal rebars collapsed and (e) detail of stirrups exposed after concrete cover detachment

The final deformed shape of the RC beam was by snapping at mid-span with excessive deflections and flexural cracks, without lateral displacements (Figure 4.12a and Figure 4.12b). Tensile rupture and excessive elongation of the bottom longitudinal rebars that were responsible for collapse of the beams are clearly identified in Figure 4.12c and Figure 4.12d. In addition, it is possible to note the stirrups exposed after the concrete cover detachment in the end of test (Figure 4.12e). The cracking along the cross-section and other failure aspects of the RC beam, visible during the flexural tests and a few instants before the collapse of the beam, can be seen in Figure 4.13.

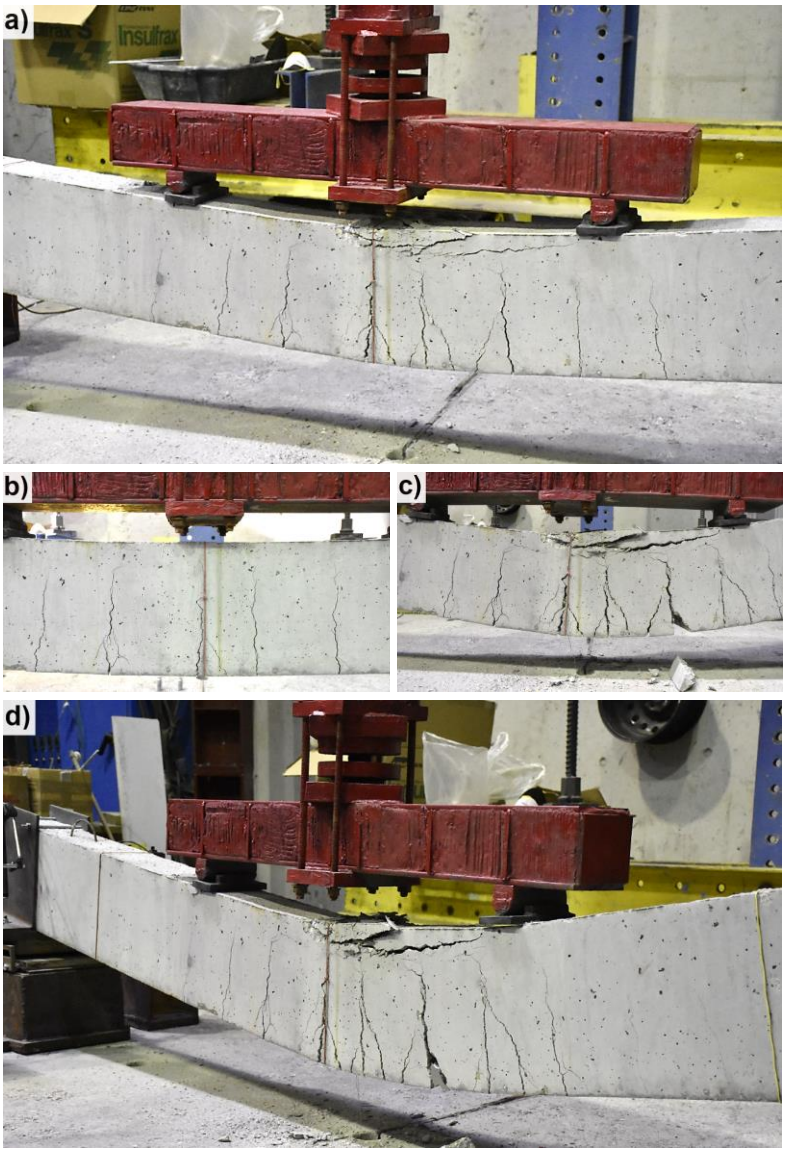

Figure 4.13 – Failure aspects of the RC beam a few instants before collapse: (a, b) deformed shape with initial cracking signals and deflection; (c, d) deformed shape with excessive deflection and cracking, partial loss of concrete cover and concrete crushing in the compressed zone of the beam

A few instants before collapsing, the deformed shape of the RC beam already presented significant values of deflection and initial cracking signs, as illustrated in Figure 4.13a and Figure 4.13b. In the instants immediately preceding the collapse (Figure 4.13c and Figure 4.13d), more excessive deflection and cracking, partial loss of concrete cover in the tensile zone and concrete crushing in the compressed zone of the beam were observed.

Concerning the failure mode of CFRP-strengthened beam tested at ambient temperature, as shown in Figure 4.15 and Figure 4.16, it was due to the collapse of CFRP system by a cohesive concrete substrate rupture in the CFRP-concrete interface. Initially, a partial debonding of the CFRP system was verified (Figure 4.15) when the specimen had not shown any excessive displacements and cracks yet – in the CFRP-debonded region the displacements and cracks were more significant than the ones registered in region where the bonding contact was still preserved (see Figure 4.15a). A few instants before collapse of the beam, a complete CFRP debonding with delamination of laminate was verified, as illustrated in Figure 4.16. It is important to mention that, before the strengthening system failure, the specimen had not presented any significant displacements and cracks yet (Figure 4.14). Therefore, it can be concluded that an important contribution in the flexural stiffness and load capacity of the beam can be attributed to this system.

Figure 4.14 – Failure aspects of the CFRP-strengthened beam a few instants before strengthening collapse: (a) general view; (b, c) section with low displacements and initial cracking signals

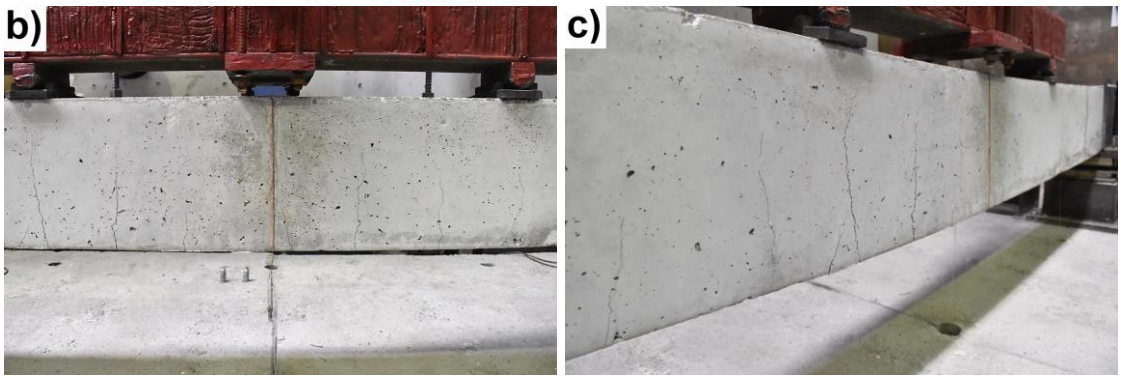

Figure 4.14 – Failure aspects of the CFRP-strengthened beam a few instants before strengthening collapse: (a) general view; (b, c) section with low displacements and initial cracking signals (Continuation)

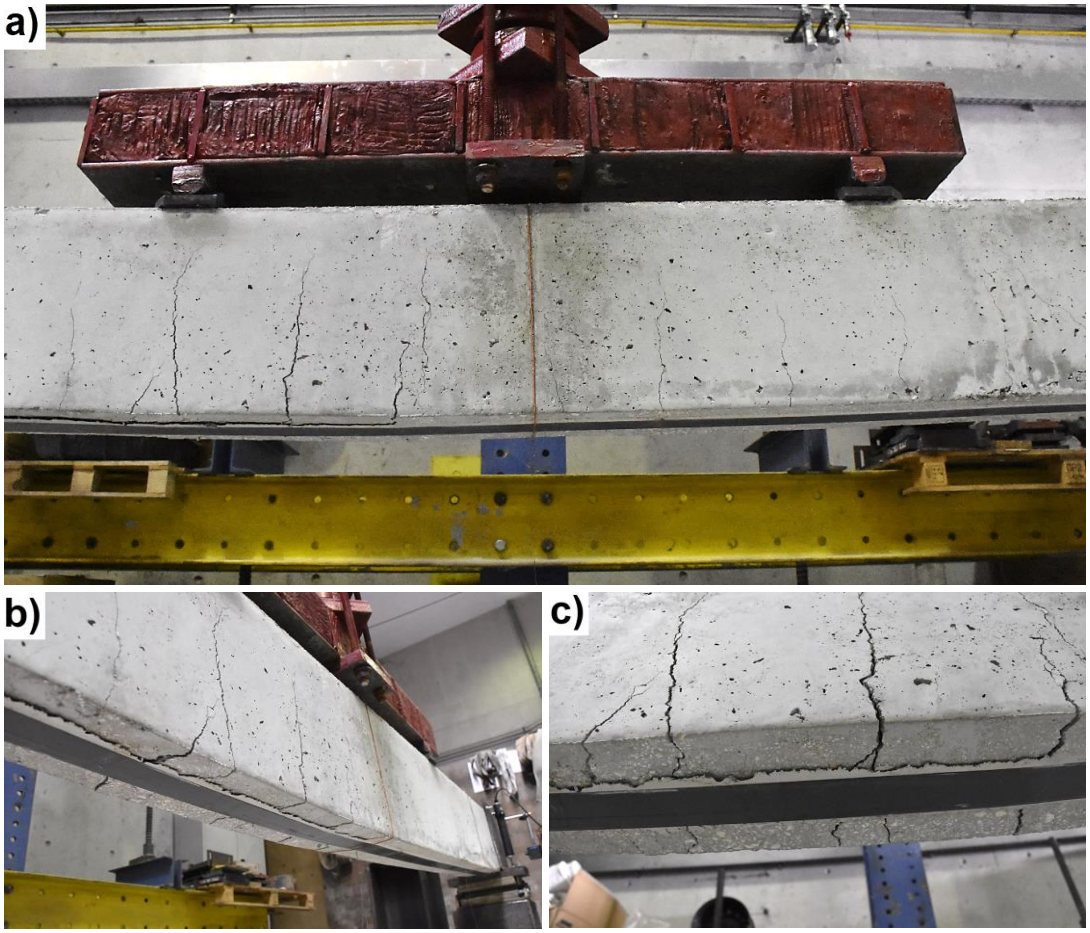

Figure 4.15 – Failure aspects of the CFRP-strengthened beam a few instants after strengthening collapse: (a, b) deformed shape with partial CFRP debonding and signals of cracking, deflection (more significant in the CFRP-debonded region) and concrete crushing in the compressed zone; (c) laminate debonded by a cohesive concrete substrate rupture at the CFRP-concrete interface

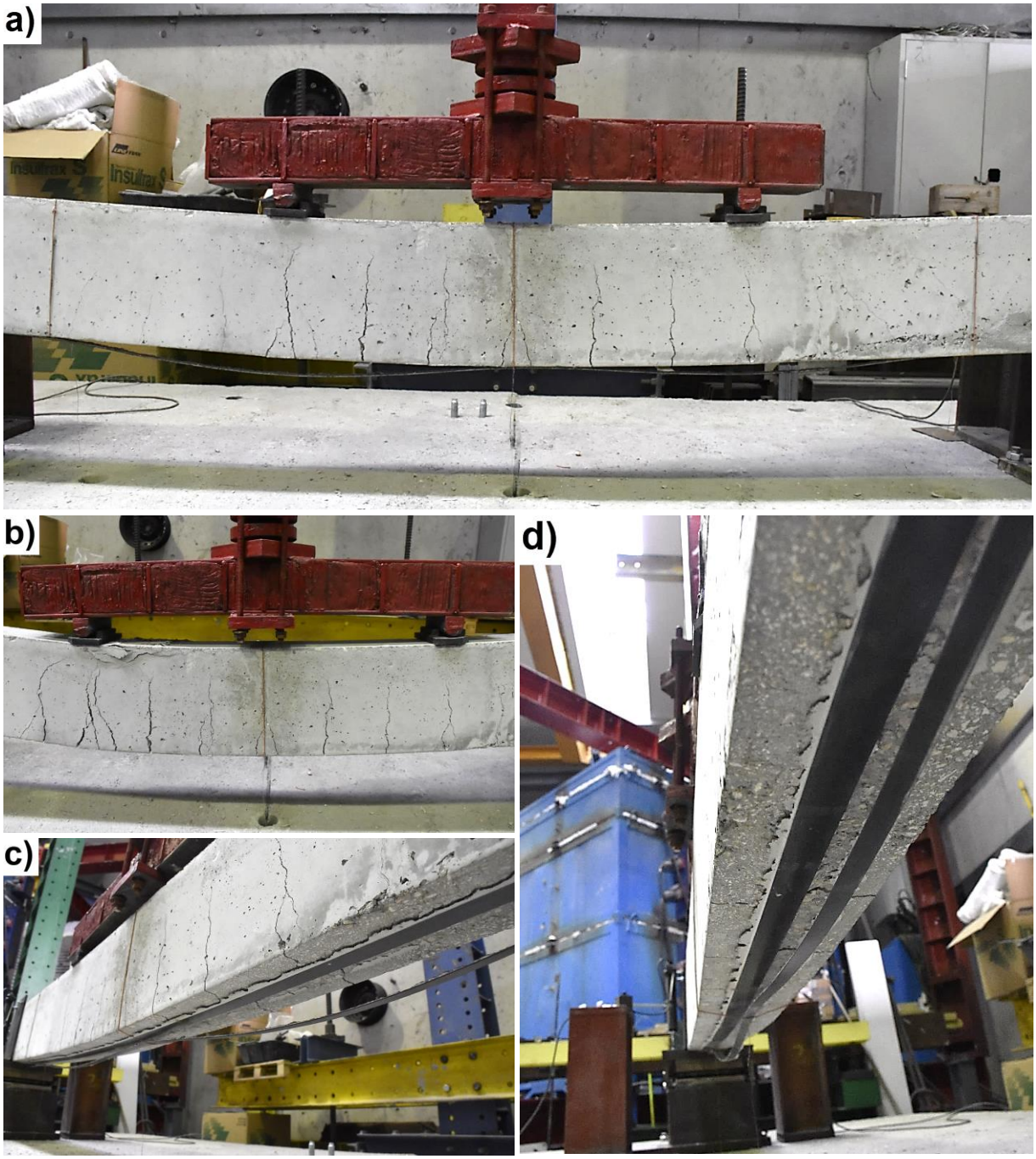

Figure 4.16 – (a-d) Deformed shape of strengthened beam after complete debonding and delamination of laminate with excessive deflection and cracking

The excessive elongation and consequent achievement of ultimate tensile strength of the bottom longitudinal rebars, caused the rupture of the beam that remained without the CFRP strength contribution until the end of tests (see Figure 4.17d). The final deformed shape of these specimens, similar to the RC beam, was characterized by excessive vertical displacements and

flexural cracks, without lateral displacements, as presented in Figure 4.17. The rupture point was displaced from the mid-span and occurred between sections S1 and S2 of the strengthened beam, precisely at the load application point, as shown in Figure 4.17b and Figure 4.17c. The eccentricities of testing, of the applied load, the non-linearity of the RC material as well as those caused by the observed initial partial debonding of the CFRP laminates along the Section S2 of the beam (Figure 4.15) can justify this failure mode.

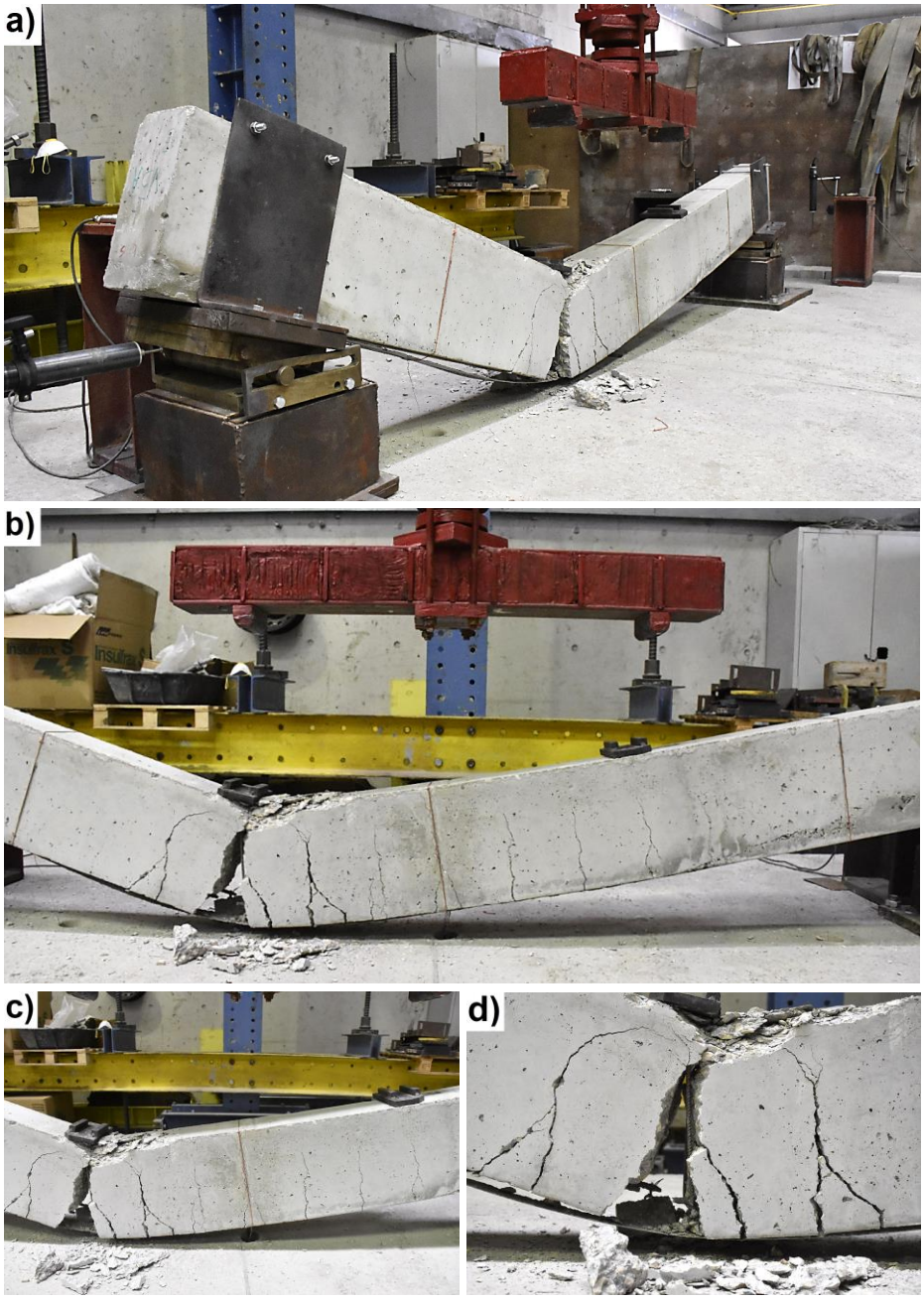

Figure 4.17 – Failure aspects of the CFRP-strengthened beam observed at the end of the flexural tests.

Both tests at ambient temperature were performed according to the criteria defined in test procedures (Section 4.4.1) and in accordance to the standard EN 1363-1 (1999) [92] recommendations.

4.5.2 Fire resistance tests

4.5.2.1 Temperature evolution

Figure 4.18, Figure 4.19, Figure 4.20 and Figure 4.21 show the evolution of temperatures at different points of cross-section S1, mid-span of the RC and CFRP beams, the furnace gas and the standard fire curve ISO 834 temperatures [34], as a function of time. It can be observed a delay on the evolution of the furnace temperatures when comparing with ISO 834 fire curve [34]. This delay is significant during the first 30 minutes of fire test. This fact can be explained due to the high initial thermal inertia of the electric furnace and heat absorbed by the materials of the tested specimen. However, the furnace temperatures generally approached quite closely to the ISO 834 fire curve [34] a few minutes after the test started. Also, in all fire resistance tests the temperatures inside the furnace were very similar, so they are comparable. The origin of the time scale (time = 0 min) in Figure 4.18, Figure 4.19, Figure 4.20 and Figure 4.21 corresponds to the beginning of the heating.

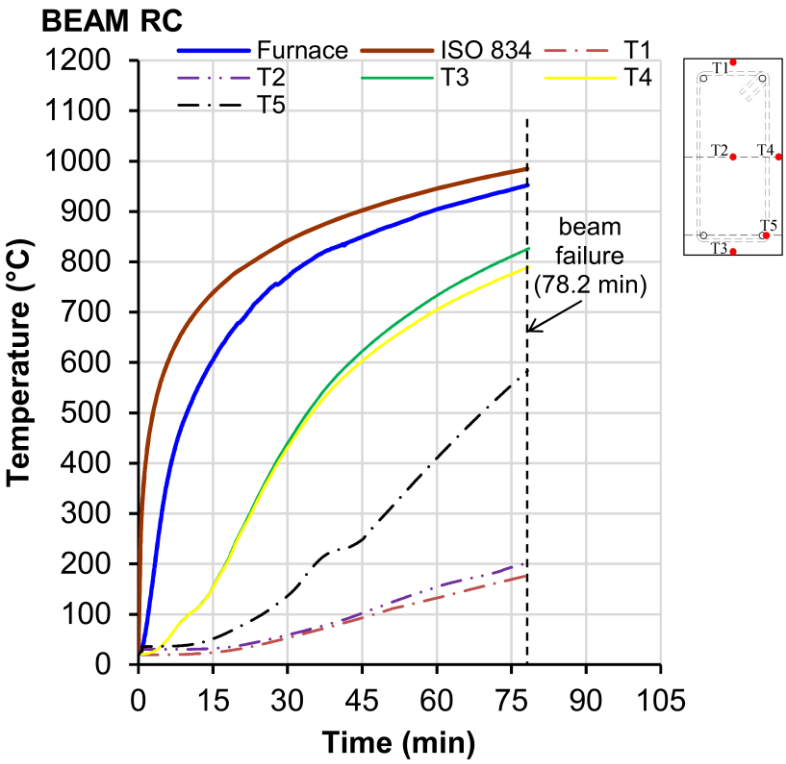

Figure 4.18 – Temperatures at cross-section S1 of the RC beam

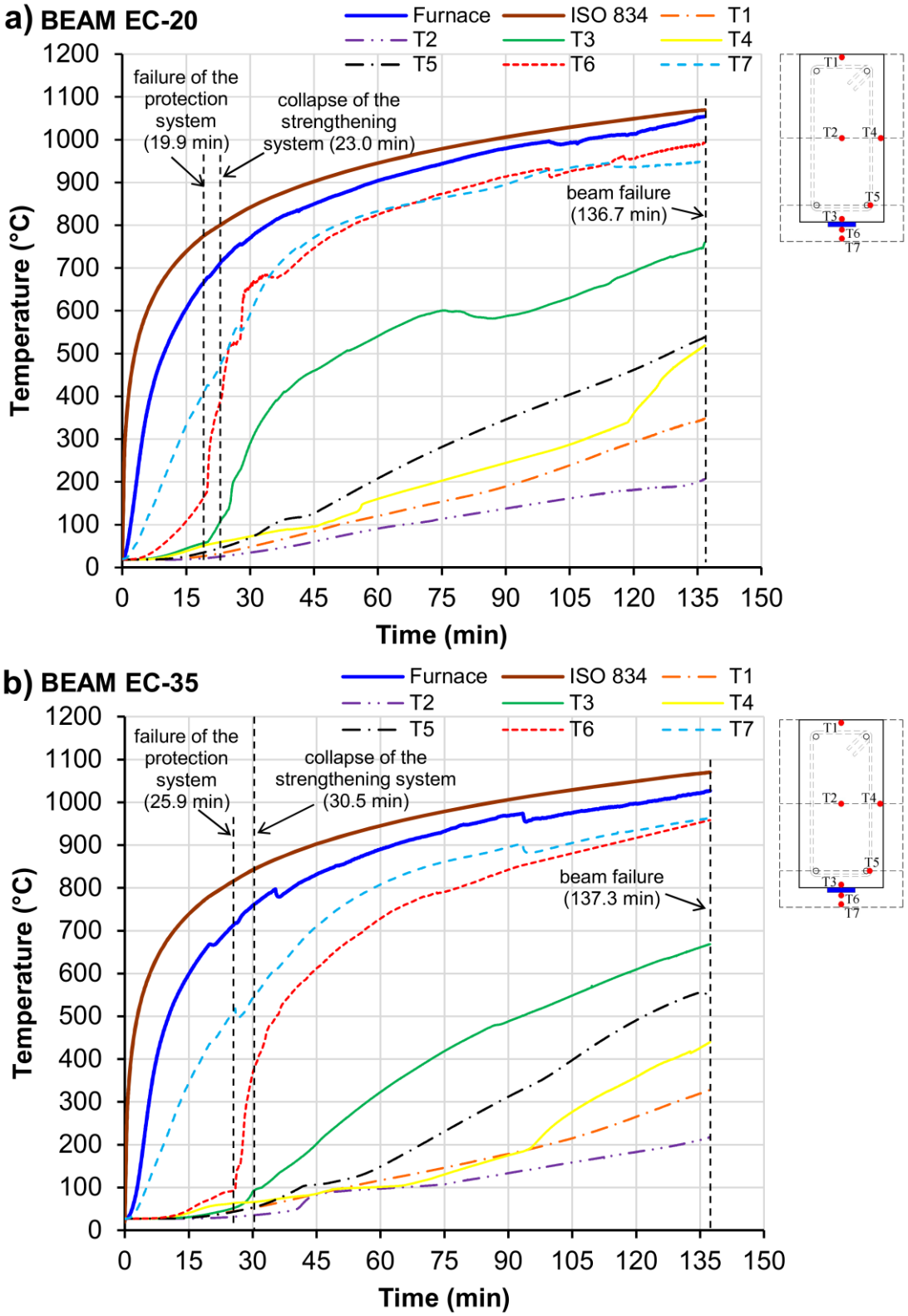

Figure 4.19 – Temperatures at cross-section S1 of the EC beams: (a) EC-20; (b) EC-35 and (c) EC-50

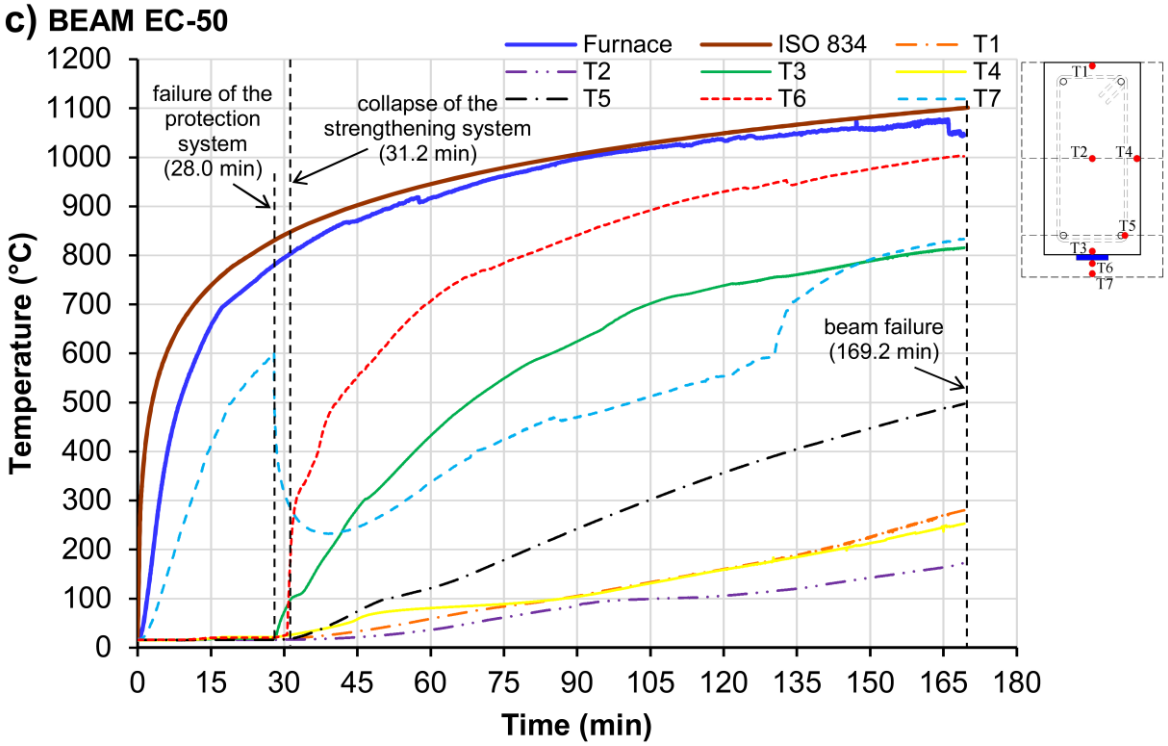

Figure 4.19 – Temperatures at cross-section S1 of the EC beams: (a) EC-20; (b) EC-35 and (c) EC-50 (Continuation)

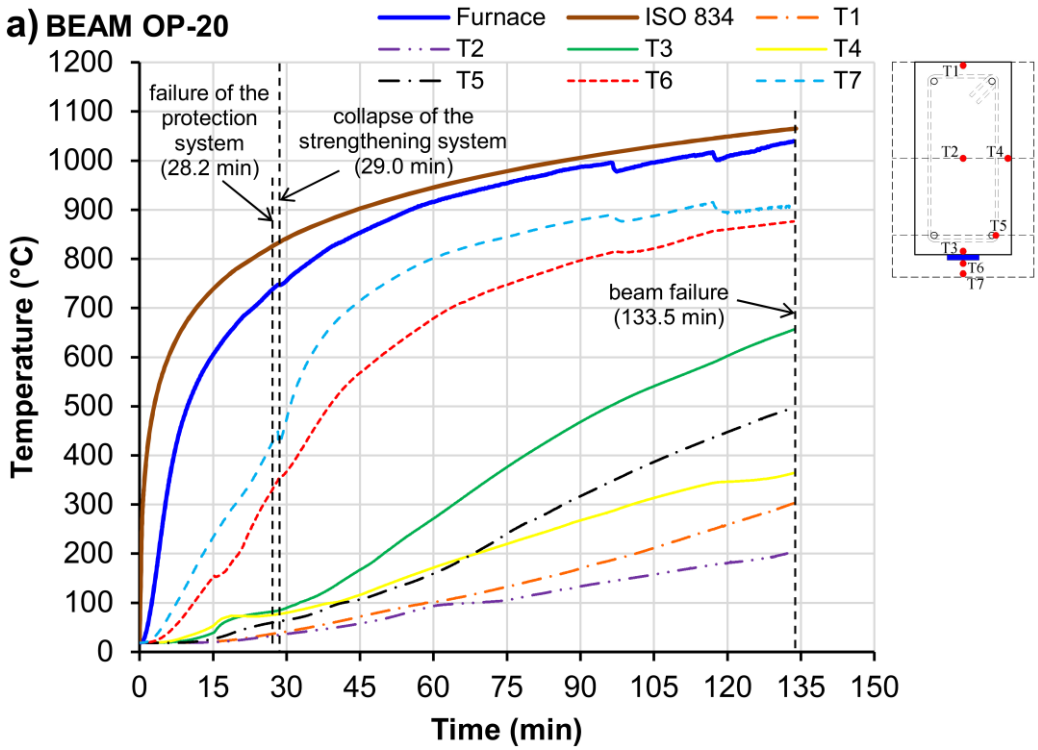

Figure 4.20 – Temperatures at cross-section S1 of the OP beams: (a) OP-20; (b) OP-35 and (c) OP-50

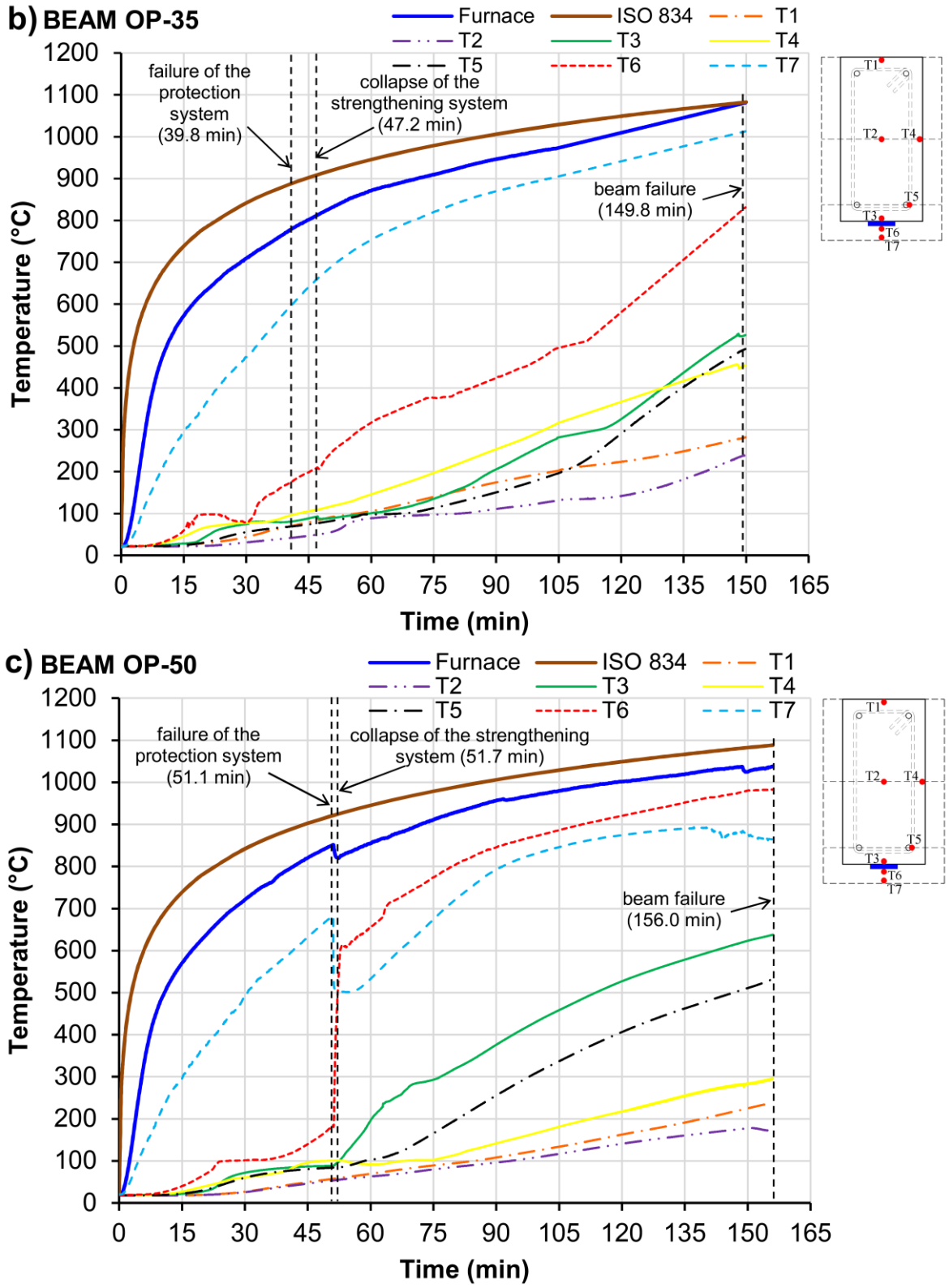

Figure 4.20 – Temperatures at cross-section S1 of the OP beams: (a) OP-20; (b) OP-35 and (c) OP-50 (Continuation)

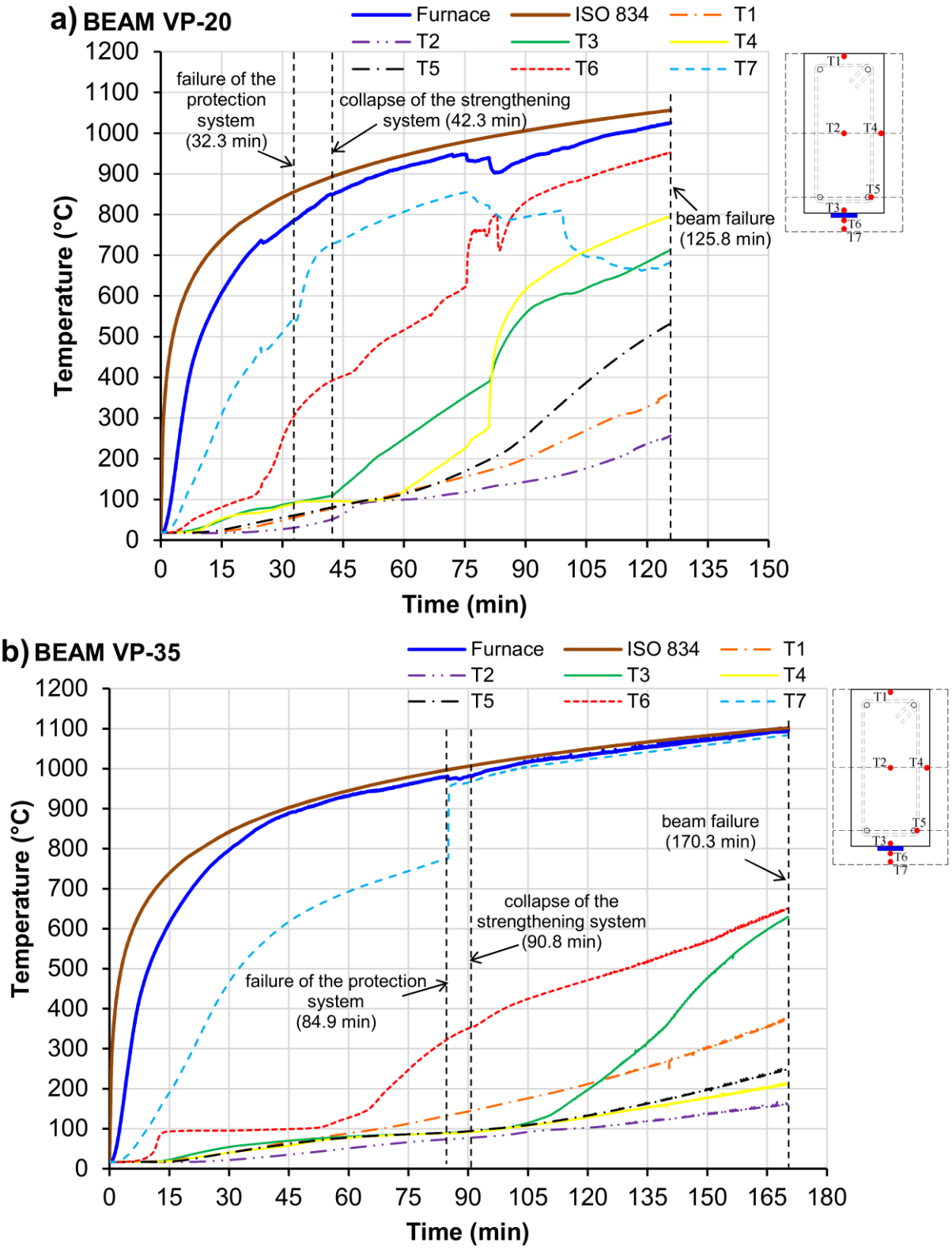

Figure 4.21 – Temperatures at cross-section S1 of the VP beams: (a) VP-20; (b) VP-35 and (c) VP-50

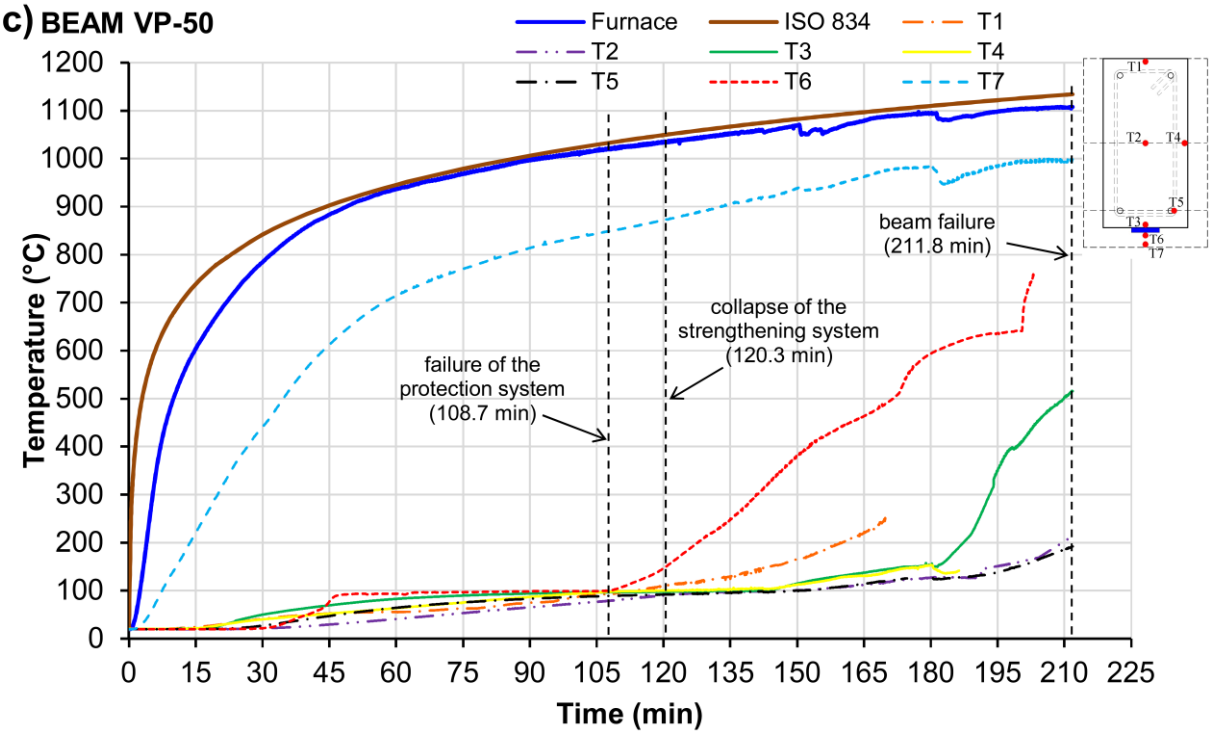

Figure 4.21 – Temperatures at cross-section S1 of the VP beams: (a) VP-20; (b) VP-35 and (c) VP-50 (Continuation)

The instants of the failure of the fire protection system, the debonding of the CFRP strengthening system and the failure of the beam are indicated in Figure 4.18, Figure 4.19, Figure 4.20 and Figure 4.21. The adopted criteria to detect the debonding of the strengthening system and the failure of the fire protection systems was addressed and discussed in the *Test Procedure* (Section 4.4.2).

During the fire tests, the temperature measurements were successful for most of thermocouples, with the exception of a few thermocouples of the VP-50 beam (T1, T4 and T6) that were damaged and stopped recording a few minutes before the end of the test. This occurred especially in the beam VP-50 due to the excessive duration of this test.

According to Figure 4.18, the temperatures recorded along the cross-section of the unprotected and unstrengthened beam (RC beam) increased at a much higher pace than the ones on the protected CFRP beams (Figure 4.19, Figure 4.20 and Figure 4.21). For the same time of exposure, the temperatures measured in the cross-section of all strengthened beams with passive fire protection (series EC, OP and VP) were significantly lower than those reached in the RC beam, especially at the interface between CFRP laminate and concrete or, in the case of the RC

beam, at the bottom surface of concrete (both measured with thermocouple T3). This difference was due to the thermal insulation provided by the materials used in passive fire protection.

The evolution of temperatures along the cross-section of the beams was considerably influenced by the type and thickness of the fire protection material. For all fire protection materials tested, thicker insulations were more effective in reducing temperature profiles in the specimens. As a result, the fire resistance of the CFRP strengthening system was extended. Considering the same insulation thickness, the fire resistance reached in specimens protected by VP mortar (Figure 4.21) was significantly greater than the one in the beams with fire protection of EC and OP mortar (Figure 4.19 and Figure 4.20, respectively), maintaining the integrity of the CFRP strengthening system for longer periods of time. This higher fire insulation provided by VP mortar was due to its quite low thermal conductivity.

The EC mortar caused a premature loss of effectiveness in the fire protection of the strengthening system (Figure 4.18Figure 4.19). This fact can be explained due to the low capacity of surface adherence and low mechanical resistance to thermal stresses of this material. On the other hand, despite the premature collapse of the CFRP, the temperature profiles and the heating rate remained low along the serviceability period of this fire protection system as noticed in an early stage of the EC tests series. This fact confirms the excellent thermal properties of this material. Further investigations which consider the use of reinforcement systems would be important to improve the fire behaviour of EC mortar in such a way that increases the potential use of this material. New techniques to improve the bond of this mortar to the existing concrete and reinforcement materials should also be studied. Further development of an EC mortar combined with the use of steel wire netting and / or the incorporation of steel or polymeric fibres into the mortar composition as a mechanical enhancement could validate this material as a good passive fire protection solution, since it has an excellent fire performance and low mechanical capacity as noticed in fire resistance tests.

Failure times and temperatures of the fire protection system, CFRP system and beams recorded during fire tests are described in detail in Section 4.5.2.2.

4.5.2.2 Failure temperatures and times

Table 4.3 presents for all tested beams: (i) failure times (tf_{CFRP}) and temperatures (Tf_{CFRP}) at debonding of the CFRP strengthening system; (ii) failure times of the fire protection system (tf_{ps}); (iii) final collapse time (tf_{beam}) of the beam. The criteria used to define the instant and temperature to debonding of the strengthening system and to failure of the fire protection systems was addressed and discussed in the Section 4.4.2 of this thesis.

Table 4.3 – Failure times and temperatures

Test reference	tf_{ps} (min)	tf_{CFRP} (min)	Tf_{CFRP} (ºC)	tf_{beam} (min)
RC	-	-	-	78.2
EC-20	19.9	23.0	108.0	136.7
EC-35	25.9	30.5	93.9	137.3
EC-50	28.0	31.2	96.2	169.2
OP-20	28.2	29.0	86.1	133.5
OP-35	39.8	47.2	93.3	149.8
OP-50	51.1	51.7	93.1	156.0
VP-20	32.3	42.3	109.4	125.8
VP-35	84.9	90.8	92.7	170.3
VP-50	108.7	120.3	97.7	211.8

The temperatures at CFRP-concrete interface when the CFRP strengthening system collapsed (Tf_{CFRP}), shown in Table 4.3, were the lowest recorded among the cross-sections S1, S2, S3 and $SM_{1\text{-}3}$ of the beams. This kind of test instrumentation allowing a broad temperature measurement along the CFRP-concrete interface length including possible colder zones, especially the ones at the ends of the beam (extremities of the CFRP-concrete bond). The temperature measurement at these zones are relevant to define the effective temperature of the strengthening system, since they are the ones that generally present the lowest temperatures of the bond as has been observed in the literature. These colder zones have suffered thermal influence from the support's elements and the surrounding structure. In addition, the collapse of the fire protection system in different parts contributed for this phenomenon. Consequently, non-uniform temperature profiles might have been developed along the length of the beams.

Regarding the strengthened beams, the results observed in Table 4.3 reveal that the temperature at CFRP-concrete interface when the strengthening system collapsed (Tf_{CFRP}) was in the range of about 85–110 ºC. Therefore, the debonding of the strengthening system occurred for temperatures above T_g of the adhesive, which in turn was 75 ºC. The relationship diagram of the Tf_{CFRP} vs. fire-protected beams in correlation with T_g of the adhesive is presented in Figure 4.22.

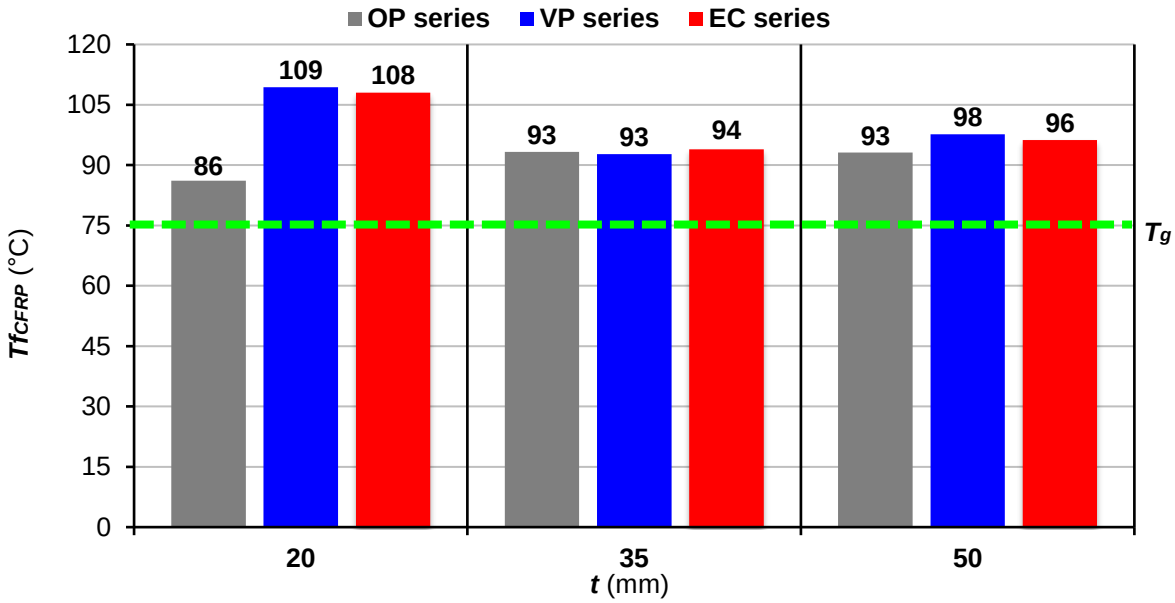

Figure 4.22 – Temperatures at CFRP-concrete interface when the CFRP system collapses for the fire-protected beams

As already mentioned, the higher thickness of the fire protection showed better performance in the fire resistance tests. This fact can be observed in the OP test series results, in which the beam OP-20 (20 mm thick) provided a fire resistance up to the debonding of the CFRP strengthening system of 29.0 min, while in the beams OP-35 (35 mm) and OP-50 (50 mm) the times were 47.2 min and 51.7 min, respectively. Similar characteristic occurred in EC and VP mortars, as shown in Figure 4.23.

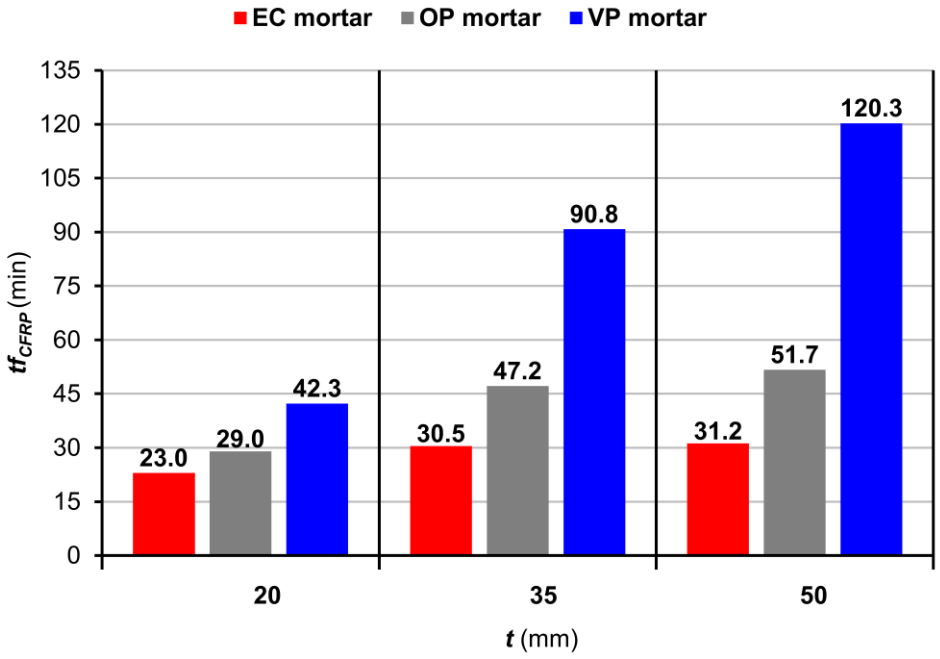

Figure 4.23 – Failure times of the CFRP system for the fire-protected beams

In addition, the failure times (described in Table 4.3) reveal that the debonding of the strengthening system (tf_{CFRP}) occurs almost immediately after the failure of the fire protection system (tf_{ps}). As shown in Figure 4.19, Figure 4.20 and Figure 4.21, the temperatures at the interface between the CFRP laminate and concrete started to rise significantly at a higher rate after the failure of the fire protection, suggesting the imminent failure of the CFRP system. Although the failure of the fire protection system has been registered, it did not mean a global failure since the system presented several partial macro failures. This probably resulted from some heterogeneities on the mechanical behaviour of the fire protection materials that led to partial detachments resulting on nonuniform temperature profiles in the specimens.

The beams protected by VP mortar were significantly more effective than the ones protected by EC and OP mortar, maintaining the integrity of the mechanical properties of the CFRP strengthening system for longer periods of fire exposure: 42.3 min, 90.8 min and 120.3 min in the beams VP-20, VP-35 and VP-50, respectively.

Although the EC mortar has a very low thermal conductivity, it was the material that presented the lower performance in fire protection of the specimens. Table 4.3 shows that the strengthening system debonded only after 31.2 min of fire exposure for the beam EC-50. For the beams EC-20 and EC-35, these results were even lower, 23.0 min and 30.5 min, respectively. This premature loss of effectiveness can be explained due to the low mechanical resistance of the material and its low capacity to surface adherence.

As it can be seen in times registered at the instant of the failure of the beam (tf_{beam}), the periods of exposure were higher in the strengthened beams than in the RC beam. Essentially for the RC beam, the failure (established according to the EN 1363-1 (1999) [92] and limited to a deflection rate of 3.7 mm/min) occurred at 78.2 min of fire exposure due to tensile rupture of the bottom rebars. The collapse of the strengthening system does not mean a collapse of the RC beam since it generally resisted the applied loading for approximately more than 100 min.

4.5.2.3 Vertical displacements

Figure 4.24, Figure 4.25, Figure 4.26 and Figure 4.27 show the vertical displacements of the tested beams at cross-section S1 (mid-span) as a function of time. The origin of the time scale (time = 0 min) matches the beginning of the heating. Moreover, at beginning of tests, the specimens had an initial deflection due to the preloading stage.

For the RC beam (Figure 4.24), the deflection increased at a high rate throughout the fire exposure duration, indicating a progressive stiffness loss.

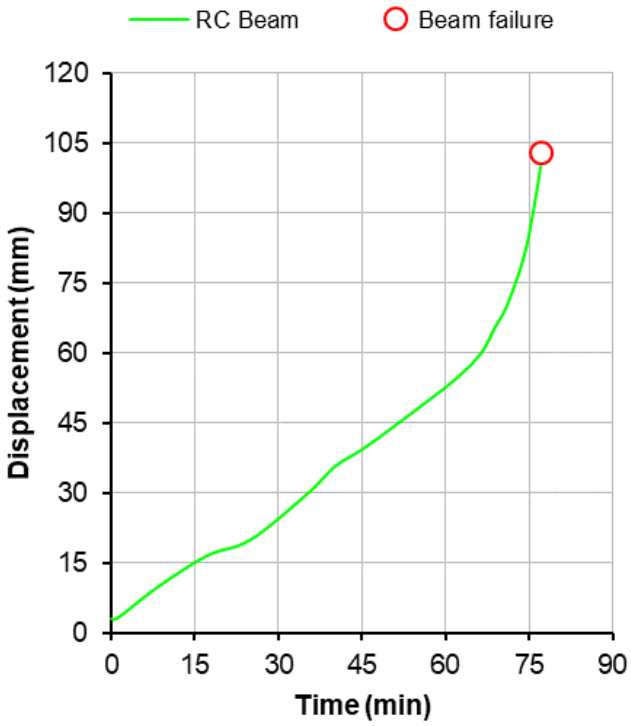

Figure 4.24 – Mid-span displacements for RC beam

The increase of the deflection rate was lower in CFRP-strengthened beams in comparison to the RC beam, as expected (Figure 4.25, Figure 4.26 and Figure 4.27). This fact can be explained by the maintenance of the stiffness properties of the specimen provided by the passive fire protection materials which kept the temperatures significantly lower in those beams for longer periods of time.

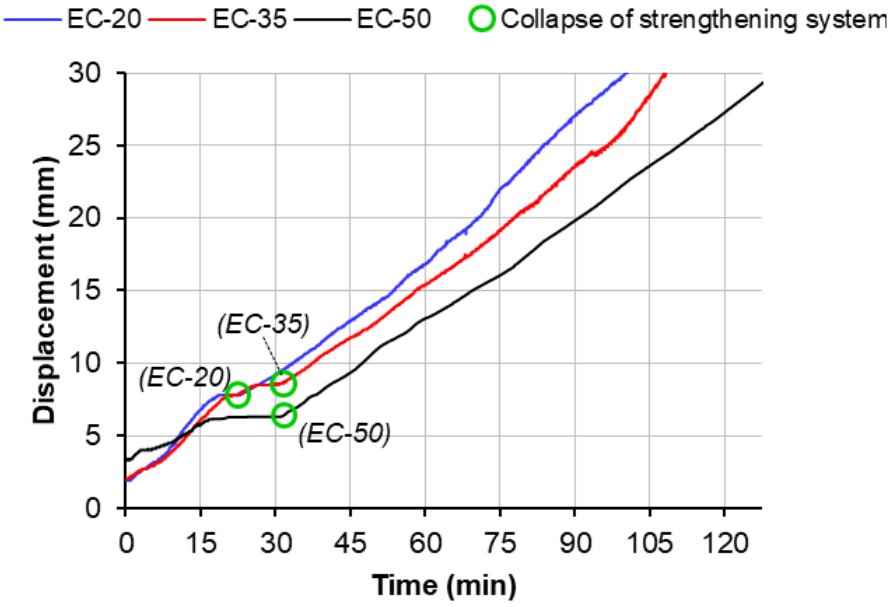

Figure 4.25 – Mid-span displacements for CFRP-strengthened beams protected by EC mortar

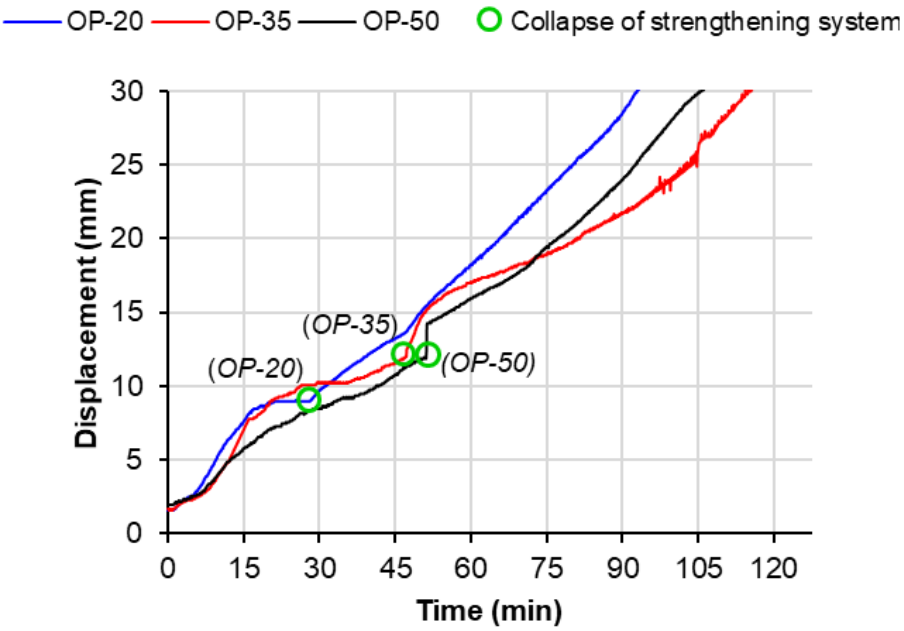

Figure 4.26 – Mid-span displacements for CFRP-strengthened beams protected by OP mortar

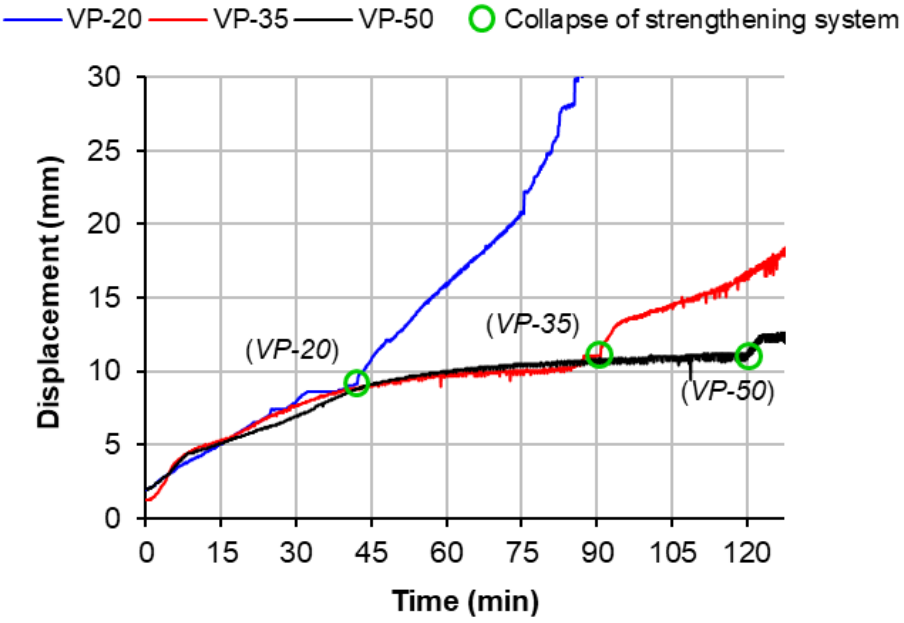

Figure 4.27 – Mid-span displacements for CFRP-strengthened beams protected by VP mortar

For the CFRP-strengthened beams it was noticed a considerable increase on the vertical displacement as well as its rate of deflection at the time of the collapse of the strengthening system (Figure 4.25-Figure 4.27). This was due to the degradation of the bonding properties between the CFRP laminate and the concrete (loss of stiffness) caused by the load that was resisted by the CFRP system and that was transferred to the beam. After the failure of the

strengthening system, the mechanical behaviour of the beams became similar to that of the RC beam.

4.5.2.4 Failure modes

In all fire-tested strengthened beams the failure mode occurred due to debonding of the CFRP laminate from the bottom surface of the beam by adhesive failure at the CFRP-concrete interface, as illustrated in Figure 4.28a. In all cases, the failure was confirmed when the vertical displacement and the rate of deflection reached the prescribed limits.

Although the failure of the strengthening system was imminent in these tests, as shown in Table 4.3, the effectiveness of the passive fire protection systems delayed the increase of temperature in the interface between the concrete and CFRP laminate for longer periods, especially the system composed by vermiculite-perlite mortar. Consequently, the mechanical resistance of the CFRP system and the assembly had their capacity extended.

Concerning the fire protection systems during the tests, a visual inspection was not possible since the used furnace did not allow any observation on its interior. Therefore, these systems were inspected only after the end of the tests.

In the periods following the failure of the CFRP system, the EC, OP and VP beams continued to resist the applied load for significative periods of exposure. At this stage of the tests, the specimens presented a mechanical behaviour similar to that of a RC beam. These tests were conducted up to failure of the specimen (Figure 4.28) as defined in the test procedures (Section 4.4) and in accordance to the methods presented in the standard EN 1363-1 (1999) [92].

Concerning the failure instant of the specimens (beam's failure in Table 4.3), the strengthened beams collapsed with a significantly longer fire exposure time when compared to the RC beam, since the cross-section of such beams was thermally protected by fire protection systems during the tests.

It is important to note that the results shown in the post-fire assessment (discussed below) were from specimens that remained exposed to a period of heating longer than 100 min (see Figure 4.23), which justifies the excessive damage of the beams, as illustrated in Figure 4.28a–e.

In the post-fire assessment, the final deformed shape of the tested beams was predominantly at mid-span without lateral displacements (Figure 4.28e). This failure mode was attributed to tensile rupture and excessive elongation of the bottom rebars. Moreover, in the end of the tests some beams showed excessive cracking along the cross-section (Figure 4.28c). For example,

Figure 4.28e and Figure 4.28f illustrate the failure modes of the tested beams OP-35 and EC-35, respectively. Figures of identical failure modes of the other tested beams are presented in APPENDIX B.

Furthermore, after the fire resistance tests, it was observed in Figure 4.28b that the fire protection system was cracked and detached from the bottom and lateral surface of the beams (this occurred during the test according the detection procedure). As a result, the CFRP strengthening system was directly exposed to the thermal action, showing visible signs of deterioration (Figure 4.28a). Cracking and detachment of the fire protection system occurred due to the material shrinkage, the deflection of the beam and the possible debonding of the CRFP, which in turn resulted from the high thermal action.

In addition to the thermal properties, the surface adhesion and mechanical resistance of the fire protection material are very important for the insulation effectiveness of the assembly. In this case, the failure of the protection system occurred before the end of the tests (tf_{ps} in Table 4.3). Perhaps, the use of a steel wire netting could delay this phenomenon. Further investigations are necessary to confirm this assumption.

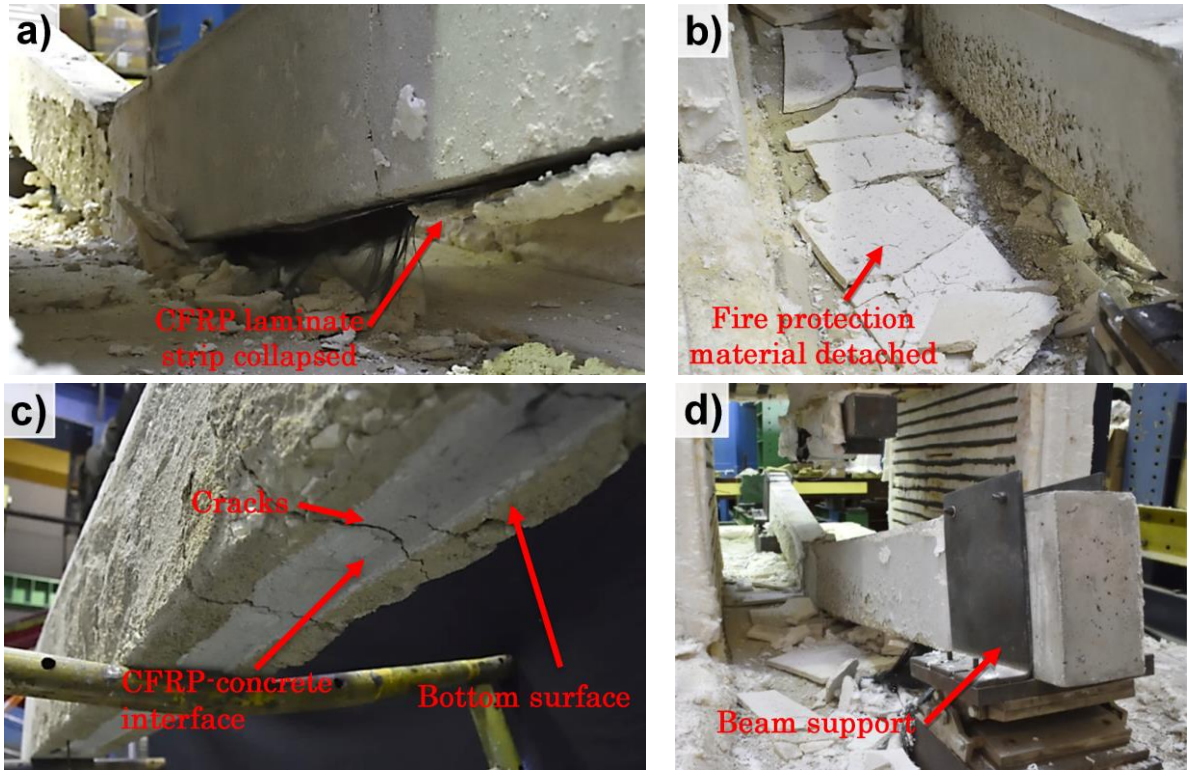

Figure 4.28 – Beams after fire resistance test: (a) CFRP laminate strip collapsed along the heated length; (b) fire protection material detached; (c) cross-section with thermal degradation and cracks; (d) specimen after test in the supports; (e-f) final deformed shape of the specimens

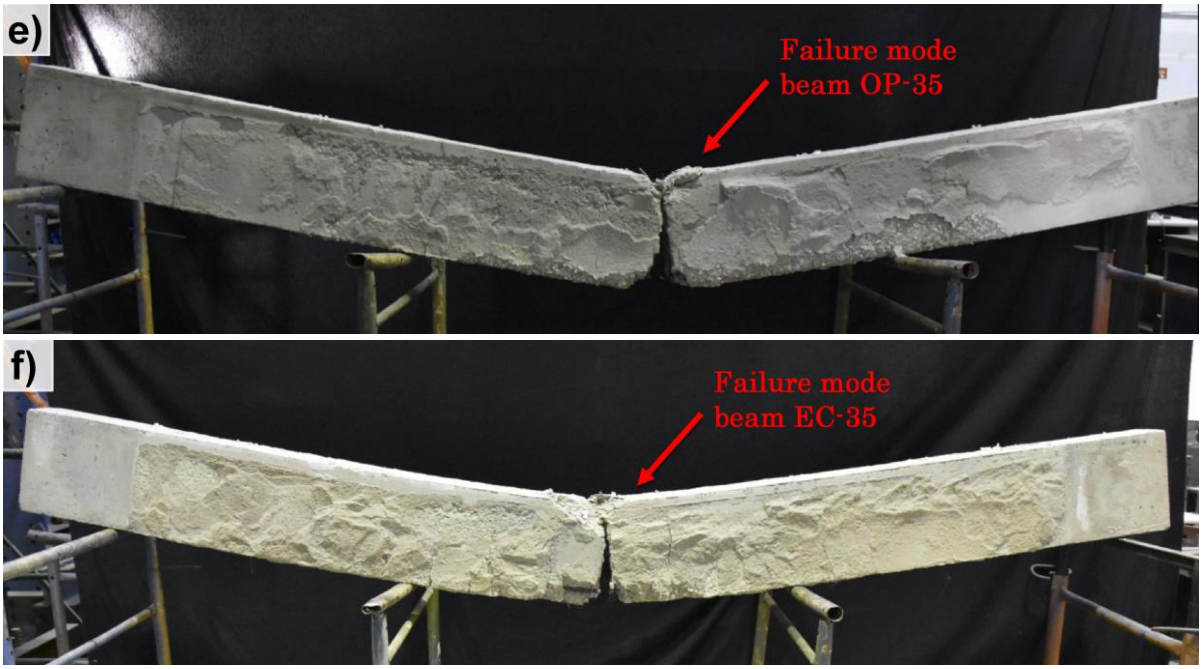

Figure 4.28 – Beams after fire resistance test: (a) CFRP laminate strip collapsed along the heated length; (b) fire protection material detached; (c) cross-section with thermal degradation and cracks; (d) specimen after test in the supports; (e-f) final deformed shape of the specimens (Continuation)

4.6 Final Remarks

This chapter dealt with the experimental analysis of RC beams strengthened with CFRP laminates and unstrengthened RC beams (as reference) at ambient and high temperatures. This experimental phase was performed with the main goal of studying the influence of CFRP strengthening system, along with the fire protection materials and building surrounding elements on the fire behaviour of the beams. The failure modes and aspects responsible for the collapse of the beams and the interaction systems were also investigated.

The main conclusion of this investigation was that the CFRP-strengthened beams is severely affected at CFRP-concrete interface temperatures between 85 ºC and 110 ºC (depending on the configuration of the specimen) – it was the temperature range that the strengthening system debonding occurred. This temperature range corresponded to temperature level between + 10 ºC and + 35 ºC above the T_g of the epoxy adhesive, in this case quoted as 75 ºC. Similar tendency was noticed on the SST tests, where the results showed substantial bond strength retention to temperatures higher or much higher than the glass transition temperature (T_g) of the adhesive, wherein at 90 ºC and 115 ºC (about + 15 ºC and + 40 ºC above T_g, respectively) the CFRP-concrete bond still had about 34% and 21% of its mechanical capacity, respectively. As

previously mentioned, this bond behaviour at temperatures significantly higher than the T_g, noticed in both type of experimental investigations, is an important achievement of the current study, since it is a very relevant phenomenon in the effectiveness of the CFRP-strengthened concrete structures. It is essential to consider the residual bond strength in the fire behaviour of the CFRP-strengthening system and to date a limited number of investigations have been performed considering these temperature conditions at the bond. The current experimental investigation evidenced and proofed this important phenomenon developed in the CFRP-concrete bond at elevated temperatures, which is neglected or simplified by the standards that guide the fire design of concrete structures [1–3]. The extensive data provided by the Single lap Shear tests at elevated temperatures and by the fire resistance tests carried out is valuable and can be useful for the review and improvement of the mentioned standards or still for creating new rules, documents or calculation methods for guiding the fire design of the CFRP-strengthened structures.

The experiments confirmed the need for the fire protection of the strengthening system due the limited fire behaviour of the CFRP-concrete bond under fire conditions. In this regard, new fire protection systems with different thickness levels were investigated. Long serviceability periods of fire exposure were achieved for the strengthening system in the beams fire-protected by the EC, OP and VP mortars. The most effective fire protection system was the one composed by VP mortar, but it is important to highlight that the EC mortar presented an excellent fire performance during its serviceability period. The satisfactory fire behaviour of this material was due to their good thermal capacity. Therefore, the problem in the EC mortar is related to its mechanical behaviour that shown low capacity during the fire tests. Despite the premature failure of the fire protection system composed by EC mortar (due to its low mechanical capacity) was noticed, their excellent thermal properties kept the temperatures practically constant at the CFRP-concrete interface and at the cross-section of the beam at a heating rate almost null while it still had integrity, especially for a thickness level of 50 mm. This is a great achievement of this investigation since these new materials, if improved mechanically, have potential to be a good and alternative solution to fire protection of the CFRP strengthening systems, contributing to the advance of technology and fire performance of buildings and to promote increased fire safety of these structures. The use of steel wire netting or the incorporation of steel or polymeric fibres into the mortar composition as a mechanical enhancement could validate this material as a high-performance fire protection solution in the civil construction industry. Additional investigations to confirm this assumption are suggested in Section 6.4.

It was also observed that the CFRP debonding was the main failure mode responsible for the collapse of the strengthened beams. A cohesive concrete surface failure in CFRP-concrete bond

at ambient temperature and a failure due to the severely deterioration of adhesive and strengthening system at elevated temperatures were observed. Excessive bottom rebars elongation and rupture with significant cracks and deflection at mid-span were the key failure mode responsible for the collapse of the unstrengthened beams for both ambient and high temperatures.

Finally, the results achieved in this thesis are fundamental to a better understanding of the CFRP-concrete bond behaviour at elevated temperatures, particularly concerning to its mechanical behaviour at temperatures above T_g of the adhesive.

5 NUMERICAL INVESTIGATION

A numerical investigation to develop FE models capable of simulating the thermal and mechanical response of the simply supported RC beams flexurally strengthened with EBR-CFRP laminates under fire conditions is addressed in this chapter. The presence of three different passive fire protection materials, the ones previously fire tested in the CFRP-strengthened beams, were also numerically investigated in terms of thermal response.

A large number of mechanical simulations at ambient and fire conditions on 3D FE models were performed using the commercial software package Abaqus. A 2D heat transfer analysis was also carried out to estimate the temperature evolution on the cross-section of the specimens under fire exposure.

The model geometry, the finite element characteristics, the material modelling, the boundary and loading conditions, the criteria analysis, the methods and procedures are duly presented and discussed in the next sections, as well as the validation of FE models and the final remarks of this numerical investigation.

5.1 Model Geometry

Three-dimensional FE models of simply supported RC beams flexurally strengthened with EBR-CFRP laminates (Figure 5.1) were modelled using the commercial software package Abaqus to simulate the mechanical response at ambient and elevated temperatures. In addition, 3D models of unstrengthened beams were also developed for the mechanical analysis (Figure 5.2). Two-dimensional FE models for both type of beams were also developed exclusively for the heat transfer analysis (as described in detail in Section 5.8.4) since this is a type of uncoupled analysis.

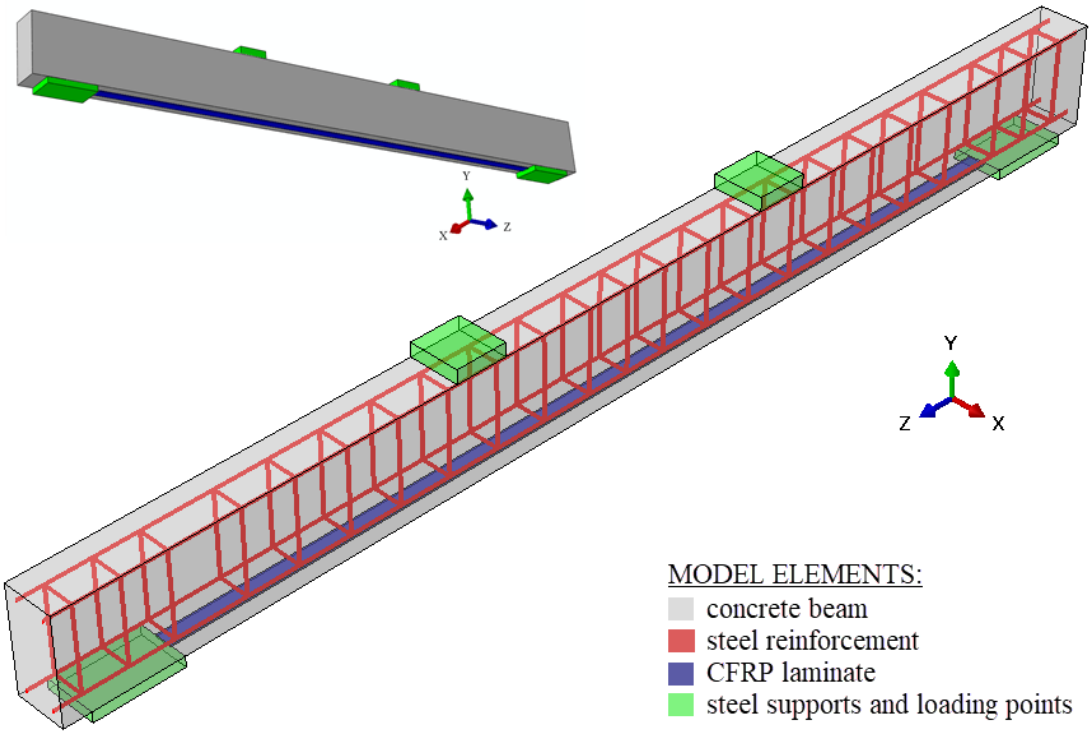

Figure 5.1 – 3D numerical model of the CFRP-strengthened beam for mechanical analysis at ambient and elevated temperatures

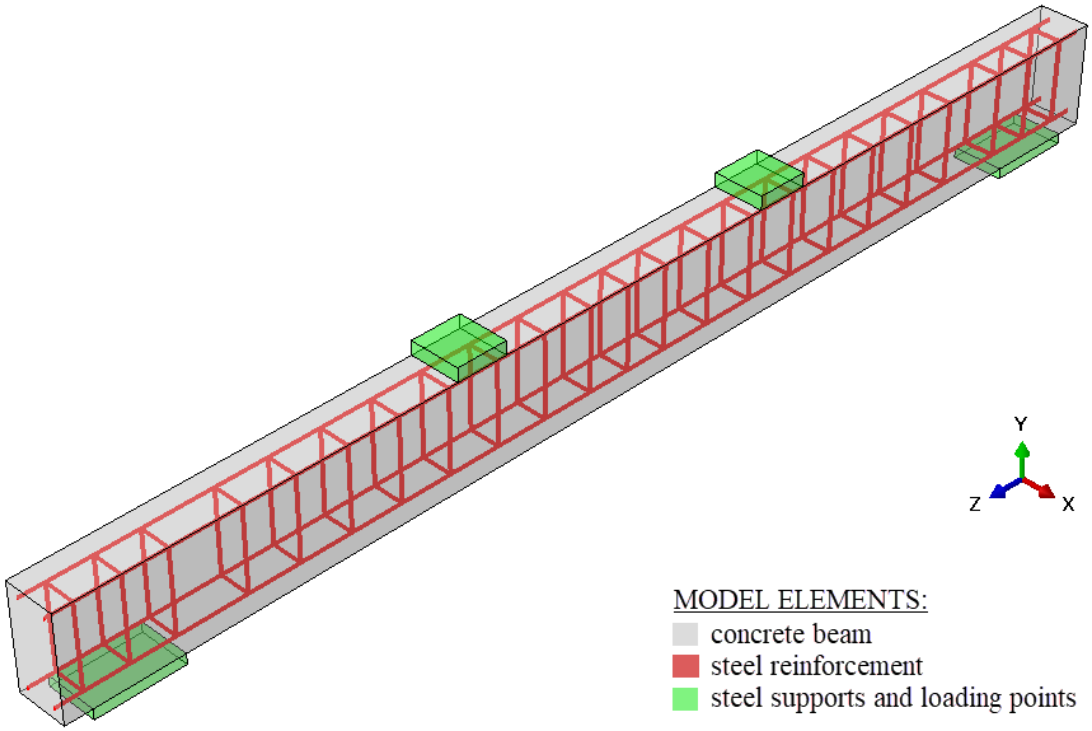

Figure 5.2 – 3D numerical model of the unstrengthened beam for mechanical analysis at ambient and elevated temperatures

The FE models' geometry consisted of a replication of the ones that constitutes the beams tested in the experimental phase of this research, as well as for the other elements and materials involved (cf. Section 4.2 and Figure 4.7).

The nomenclature adopted for the FE models of the beams is analogous to the ones from the experimental campaign and it is related to the presence of the strengthening system (CFRP-strengthened or unstrengthened) and to the type and thicknesses of the fire protection system (cf. Table 4.1, Table 4.2 and Figure 4.8).

Further information concerning the specimens used for this numerical study and other relevant characteristics is provided in Chapter 4.

5.2 Finite Element Software

The 3D finite element program Abaqus/CAE (version 6.14-5) [35] is a powerful computational tool with a strong ability for modelling and simulating structures with material and geometric nonlinear behaviour. For this reason, Abaqus [35] was extensively used by the author to simulate the behaviour and strength of CFRP-strengthened beams under flexural loading conditions and under combined bending and fire conditions. The numerical results were thereby compared with those given by the experimental tests in order to validate the developed finite element model and to allow its use for a future parametric study outside the bounds of the original experimental tests. All the parameters, considerations and assumptions adopted in the developed three-dimensional nonlinear finite element model to predict the behaviour of CFRP-strengthened RC beams at ambient temperature and in fire conditions are also described in the next sections.

5.3 Finite Element Type

The RC beams were modelled by using solid elements (C3D8R) for the concrete material geometry, steel supports and loading points. The C3D8R finite element was also chosen for modelling the CFRP laminate in the case of strengthened RC beams. The longitudinal steel reinforcement and stirrups were modelled by using truss elements (T3D2).

The C3D8R element (Figure 5.3) is defined as a three-dimensional, continuum (C), hexahedral and an eight-node brick element with reduced integration (R), hourglass control and first-order (linear) interpolation. These finite elements have three degrees of freedom per node, referring to translations in the three directions X, Y and Z (global coordinates). One of the reasons for using the C3D8R in the current research is because it can be applied in Abaqus for linear

analysis and complex nonlinear analyses involving contact, plasticity, and large deformations. Moreover, they are available for stress, heat transfer, acoustic, coupled thermal-stress, coupled pore fluid-stress, piezoelectric, and coupled thermal-electrical analyses [93].

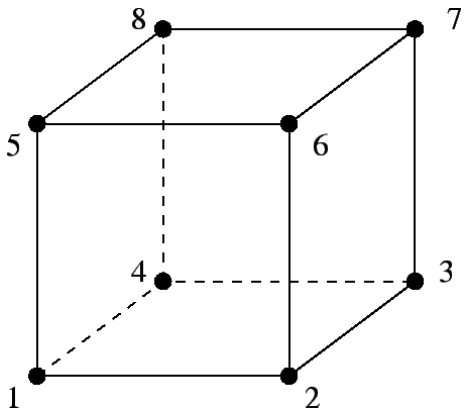

Figure 5.3 – Scheme of the C3D8R element [93]

The selected C3D8R element type uses a reduced (lower-order) integration to form the element stiffness with only one integration location per element. The reduced integration method was chosen because it reduces the amount of CPU time necessary for analysis of the model and avoids shear locking without losing the accuracy of the analysis. Shear locking may occur in elements under pure bending and without reduced integration, because the element edges must remain straight and the angle between the deformed isoparametric lines is not equal to 90º which means that the strain in the thickness direction is not zero (Figure 5.4). So, this can lead to overestimation of the load capacity in bending dominated problems [94].

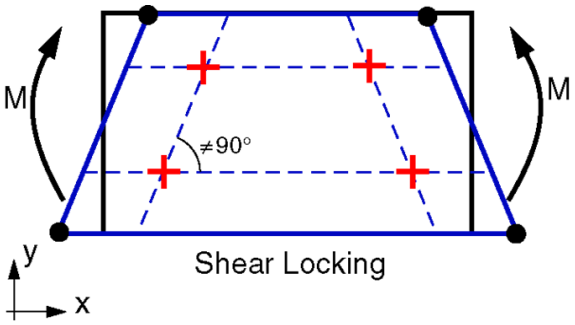

Figure 5.4 – Shear locking in elements without reduced integration points [93]

T3D2 is a three-dimensional and two-node element used to model slender, line-like structures that support loading along the axis only or the centreline of the element (Figure 5.5). No moments or forces which are perpendicular to the centreline are supported. This element allows to define the cross-sectional area associated with the truss element as part of the section definition. When truss elements are used in large-displacement analysis, the updated cross-

sectional area is calculated by assuming that the truss is made of an incompressible material, regardless of the definition of the material being analysed. This assumption is adopted because the most common applications of trusses at large strains involve yielding metal behaviour or rubber elasticity, in which cases the material is effectively incompressible [93].

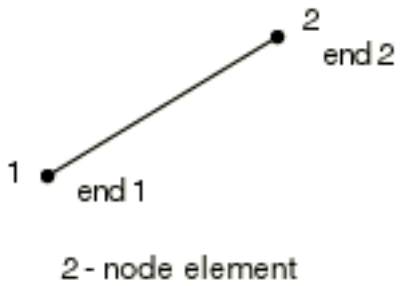

Figure 5.5 – Scheme of the T3D2 element [93]

For the 2D heat transfer analysis, the DC2D4 element was selected. This element type consists of a 4-node linear heat transfer quadrilateral element and was chosen because it presents excellent accuracy to estimate the temperature evolution of different materials in a thermal analysis.

Additional information about the aforementioned finite elements can be seen in detail in [95].

5.4 Material Modelling and Analysis Criteria

The specimens were modelled using the material non-linearity according to the isotropic hardening method and, especially for the concrete material, based on the fracture energy cracking criteria. The properties of the materials used in the FE models were represented in the Abaqus program based on the literature and standardization. So, it was intended to reproduce the thermophysical and mechanical behaviour of the tested beams as faithfully as possible, as described in detail in the following sections.

5.4.1 Thermophysical material properties

The correct modelling of thermophysical properties of the materials that constitute RC beams strengthened with CFRP laminates as function of temperature variation is essential for the development of an accurate numerical model that intends to simulate the thermal response of these structural elements when subjected to fire conditions. The temperature-dependent properties of these constituent materials (concrete, steel reinforcement, CFRP, fire protection

materials) such as specific heat, thermal conductivity, density, emissivity and convection, are presented in this section.

5.4.1.1 Concrete

The increasing of the temperature by the fire action promotes several reactions in the concrete material, causing changes of its thermal and physical properties. In this numerical investigation, the variation of the thermophysical properties of the concrete with temperature were defined according to the relationships recommended in part 1-2 of Eurocode 2 [1] and National French Annex to NF EN 1992-1-2 [96], as presented in the sections ahead.

5.4.1.1.1 Specific heat

The Eurocode recommends that the specific heat (c_p) of dry concrete (moisture content = 0%) when using siliceous and calcareous aggregates may be determined from the following equations:

$c_p(\theta) = 900$ (J/kgºC) for $20\ ºC \leq \theta \leq 100\ ºC$ (5.1)

$c_p(\theta) = 900 + (\theta - 1\ 00)$ (J/kgºC) for $100\ ºC < \theta \leq 200\ °C$ (5.2)

$c_p(\theta) = 1000 + (\theta - 200)/2$ (J/kgºC) for $200\ °C < \theta \leq 400\ °C$ (5.3)

$c_p(\theta) = 1100$ (J/kgºC) for $400\ °C < \theta \leq 1200\ °C$ (5.4)

were,

θ = concrete temperature (ºC)

When the moisture content of the concrete (u) is greater than 0% (as in the case of the current model), the function given for the specific heat of concrete with siliceous or calcareous aggregates may be modelled by a constant value ($c_{p.peak}$) situated between 100 °C and 115 °C with linear decrease between 115 °C and 200 °C. Therefore, the values that define the peak of specific heat are the following:

$c_{p.peak}$ = 1470 (J/kgºC) for moisture content of 1.5% of concrete weight

$c_{p.peak}$ = 2020 (J/kgºC) for moisture content of 3.0% of concrete weight

Moreover, for other moisture contents European standard EN 1992-1-2 [1] defines that a linear interpolation is acceptable.

In the modelling, a higher value of 8.5% for the moisture content was defined according to the humidity conditions of the concrete specimens. Therefore, the $c_{p.peak}$ for the moisture content of 8.5% corresponded to 4040 J/kgºC. This specific heat peak is due to the fact that the evaporation of the free water from the concrete occurs through endothermic reactions. The evolution of the specific heat value in relation to the temperature adopted for the concrete used in the current investigation, based on the recommendations of Eurocode 2, part 1-2 [1], is described by the diagram shown in Figure 5.6.

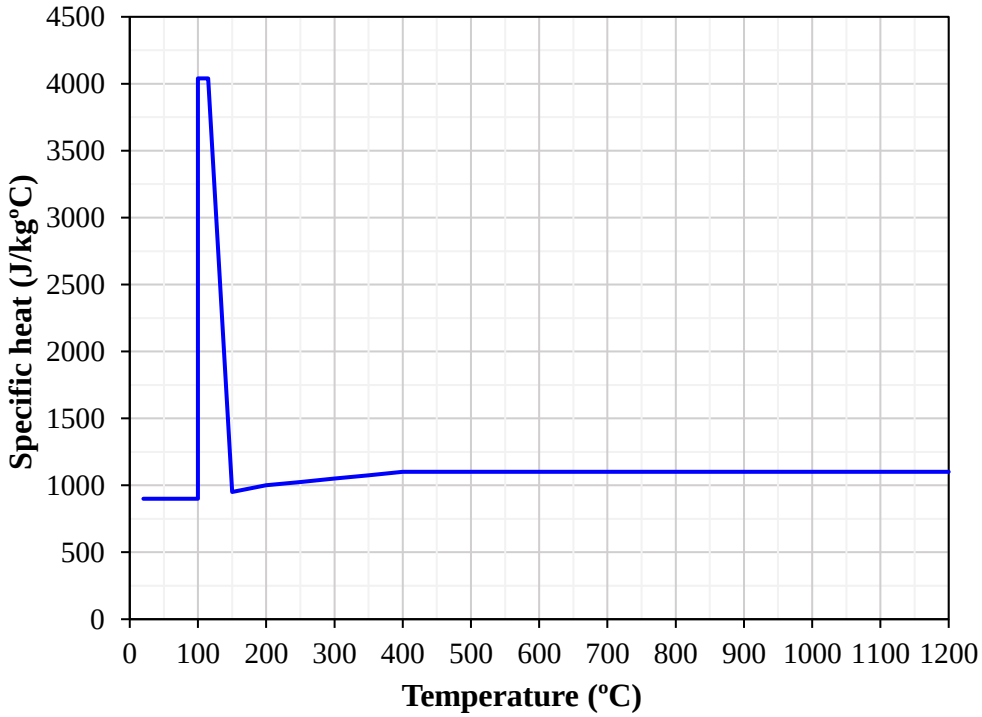

Figure 5.6 – Specific heat as function of temperature for siliceous concrete at a moisture content of 8.5% by weight according to EN 1992-1-2 [1]

5.4.1.1.2 Thermal conductivity

Eurocode 2, part 1-2 [1] proposes that the value of the thermal conductivity of ordinary concrete for a given temperature should be between an upper and lower limit. However, for a better representation of the fire behaviour of the concrete, a new thermal conductivity curve was proposed based on the expressions provided in National French Annex to NF EN 1992-1-2 [96], whose evolution with temperature is shown in Figure 5.7. This Annex [96] considers an initial curve based on the upper limit of the Eurocode 2, part 1-2 [1] for temperatures up to 140 °C with a linear drop to the lower limit for temperatures above 160 °C. This new formulation sought to represent the free and hydration water evaporation phenomenon of cement in a more realistic way, which when present increases the thermal conductivity of the concrete. Therefore,

the curve established by the French Annex [96] was selected to be applied to the developed model.

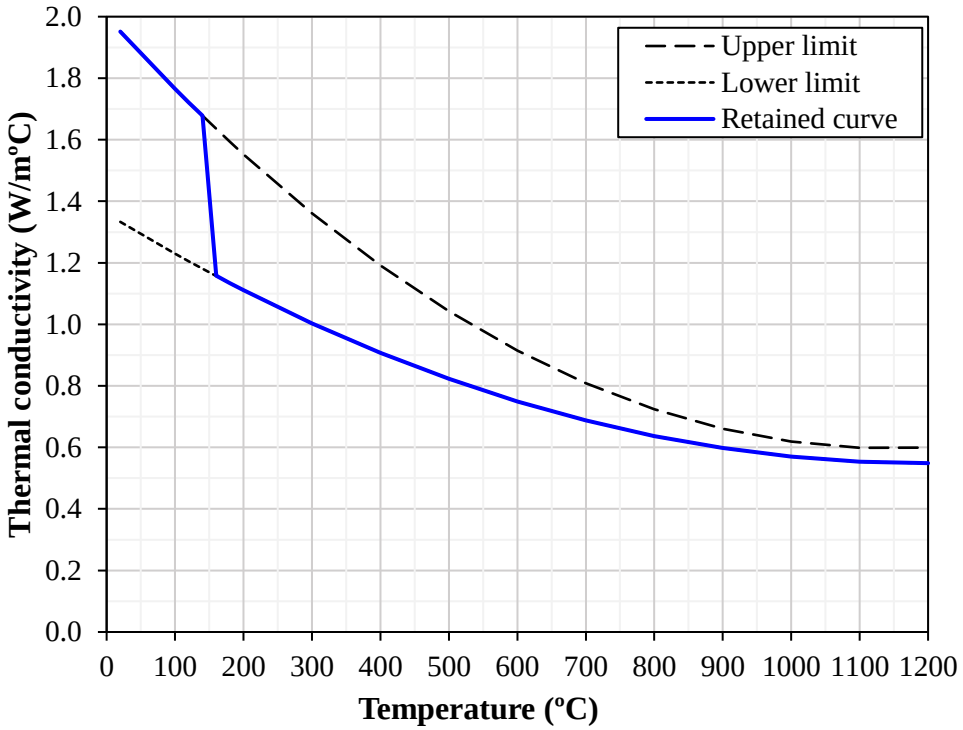

Figure 5.7 – Thermal conductivity of concrete as function of temperature according to National French Annex to NF EN 1992-1-2 [96]

5.4.1.1.3 Density

The variation of density (ρ) with temperature is influenced by water loss and is defined according to EN-1992-1-2 [1] by the following equations:

$$\rho(\theta) = \rho(20\ ^{o}C) \quad \text{for } 20\ ^{o}C \leq \theta \leq 115\ ^{o}C \tag{5.5}$$

$$\rho(\theta) = \rho(20\ ^{o}C)\cdot(1 - 0.02(\theta - 115)/85) \quad \text{for } 115\ ^{o}C < \theta \leq 200\ ^{o}C \tag{5.6}$$

$$\rho(\theta) = \rho(20\ ^{o}C)\cdot(0.98 - 0.03(\theta - 200)/200) \quad \text{for } 200\ ^{o}C < \theta \leq 400\ ^{o}C \tag{5.7}$$

$$\rho(\theta) = \rho(20\ ^{o}C)\cdot(0.95 - 0.07(\theta - 400)/800) \quad \text{for } 400\ ^{o}C < \theta \leq 1200\ ^{o}C \tag{5.8}$$

In the current model, the usual density of the single concrete at 20ºC [ρ (20 ºC)] was defined as 2300 kg/m^3, as suggested in Eurocode 2, part 1-2 [1]. Thus, the above expressions can be represented in a diagram form, as shown in Figure 5.8.

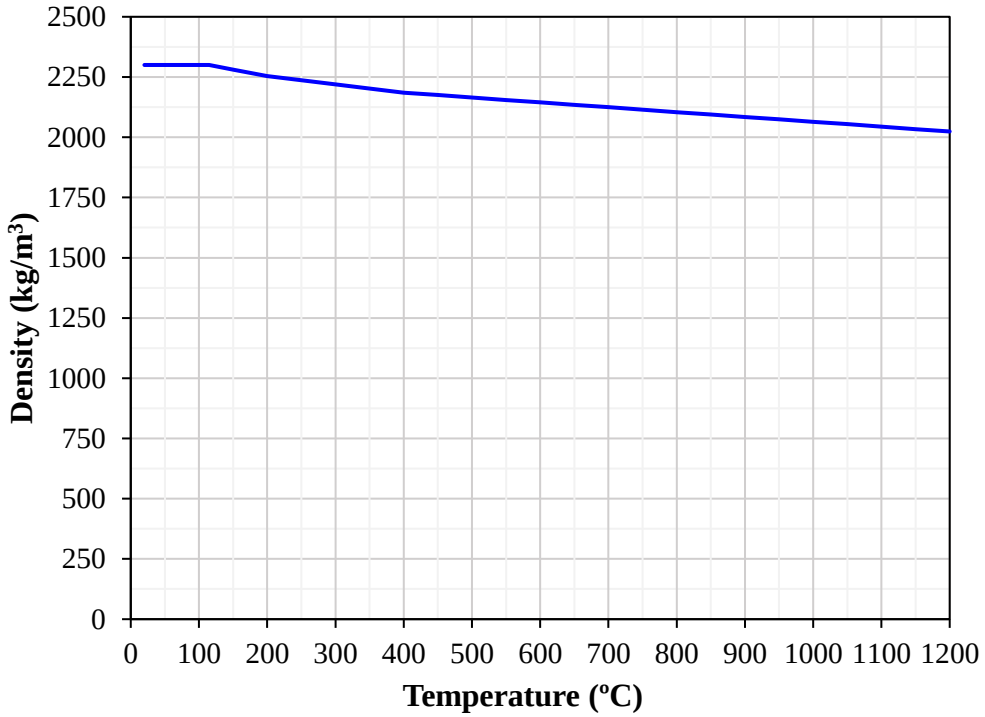

Figure 5.8 – Density of concrete as function of temperature according to EN 1992-1-2 [31]

5.4.1.1.4 Emissivity and convection

The emissivity of the concrete surface was defined as 0.7 and it was considered constant with temperature evolution, according to Eurocode 2, part 1-2 [1]. The radiative heat flux was calculated using the emissivity coefficients of the electric resistance of the furnace and of the concrete surface, both equal to 0.7, and it resulted in a value of 0.49. A convection coefficient of 15 W/m^2 ºC (also constant with temperature) was adopted as suggested in EN-1992-1-2 [1].

5.4.1.2 Steel reinforcement

In the case of steel reinforcement modelling, the thermophysical material properties were defined based on Eurocode 3, part 1-2 [97] recommendations.

5.4.1.2.1 Specific heat

The specific heat of steel reinforcement (c_s) at different temperatures in the numerical model was determined by the curve defined in EN 1993-1-2 [97], shown in Figure 5.9.

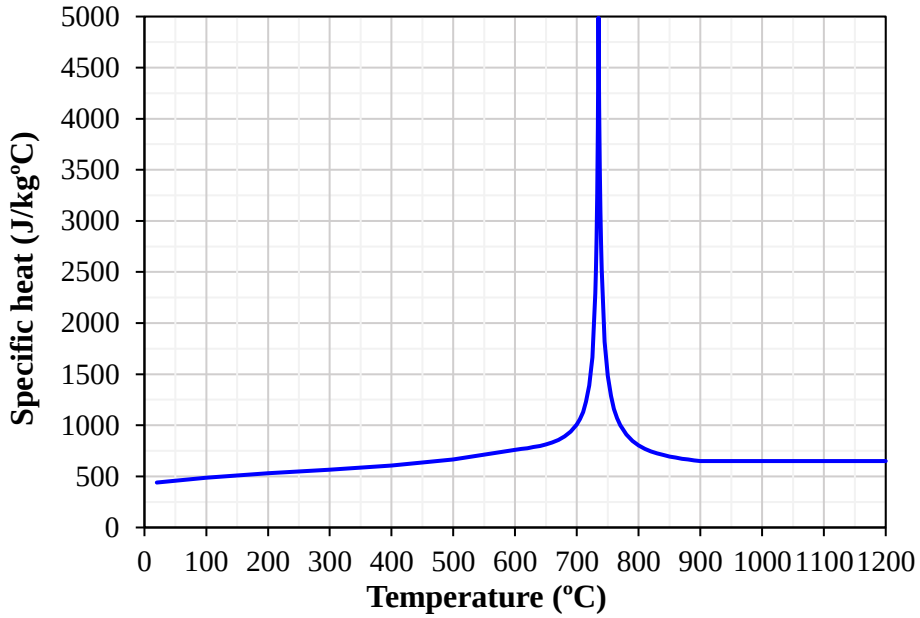

Figure 5.9 – Specific heat of carbon steel as a function of temperature according to EN 1993-1-2 [97]

5.4.1.2.2 Thermal conductivity

The thermal conductivity of the steel was also defined according to EN 1993-1-2 [97] and the variation of this magnitude with temperature is shown in the curve below on Figure 5.10.

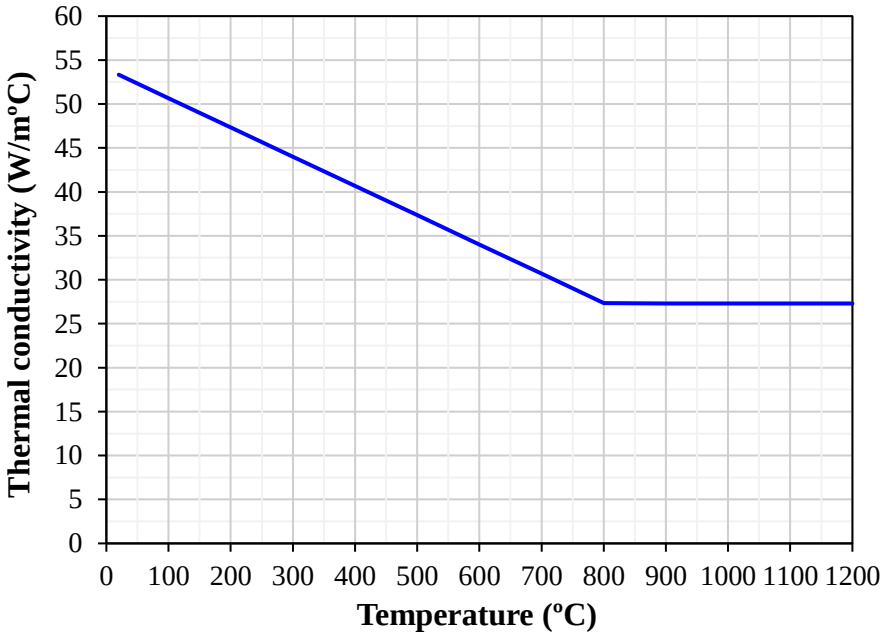

Figure 5.10 – Thermal conductivity of carbon steel as a function of temperature according to EN 1993-1-2 [97]

5.4.1.2.3 Density

According to Eurocode 3, part 1-2 [97], the steel reinforcement density (ρ_s) was defined constant with temperature, corresponding to 7850 kg/m^3.

5.4.1.3 CFRP laminate

The CFRP laminates were thermally characterized in the numerical model using experimental data from the literature [56,74]. In the sections ahead, these proposals suggested in the literature are presented in a graphical form.

5.4.1.3.1 Specific heat

The variation of the specific heat of CFRP laminates was modelled based on experimental data reported in the investigation by Griffis et al. [74]. Figure 5.11 illustrates the variation of the specific heat value of the CFRP in relation to temperature according to this researcher's proposal.

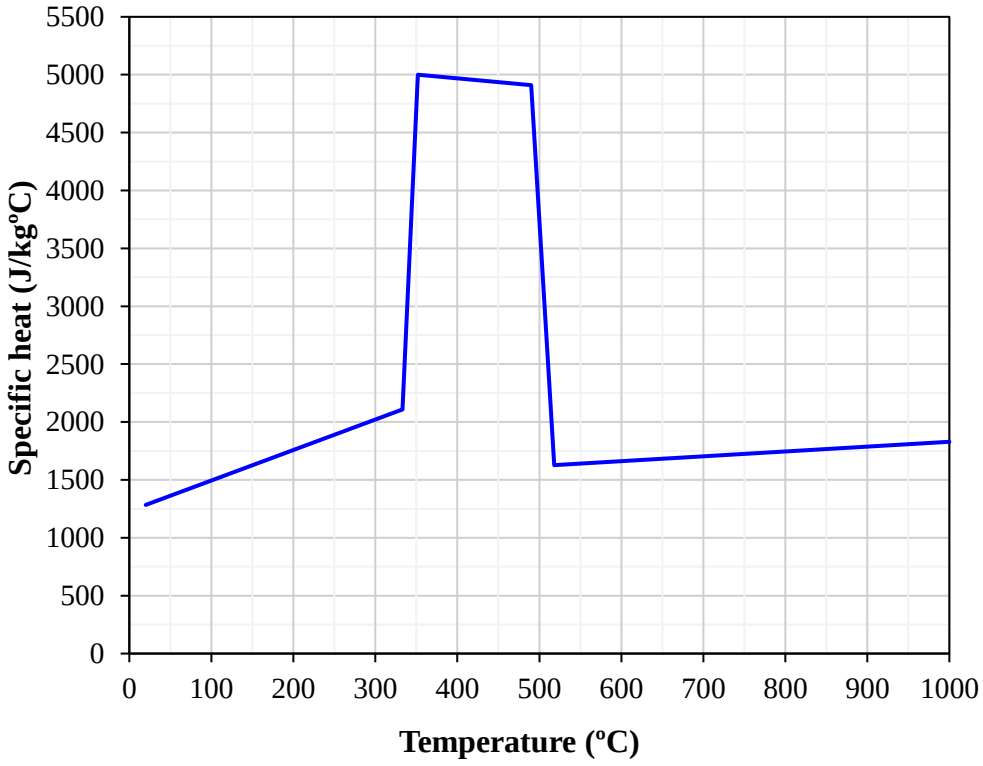

Figure 5.11 – Specific heat of CFRP laminate as a function of temperature according to Griffis et al. [74]

5.4.1.3.2 Thermal conductivity

Similarly to the specific heat variation, the proposal presented in Griffis et al. [74] for the evolution of the CFRP thermal conductivity in relation to temperature was adopted. The variation of the CFRP thermal conductivity value is shown in Figure 5.12, according to the Griffis et al. [74] proposal.

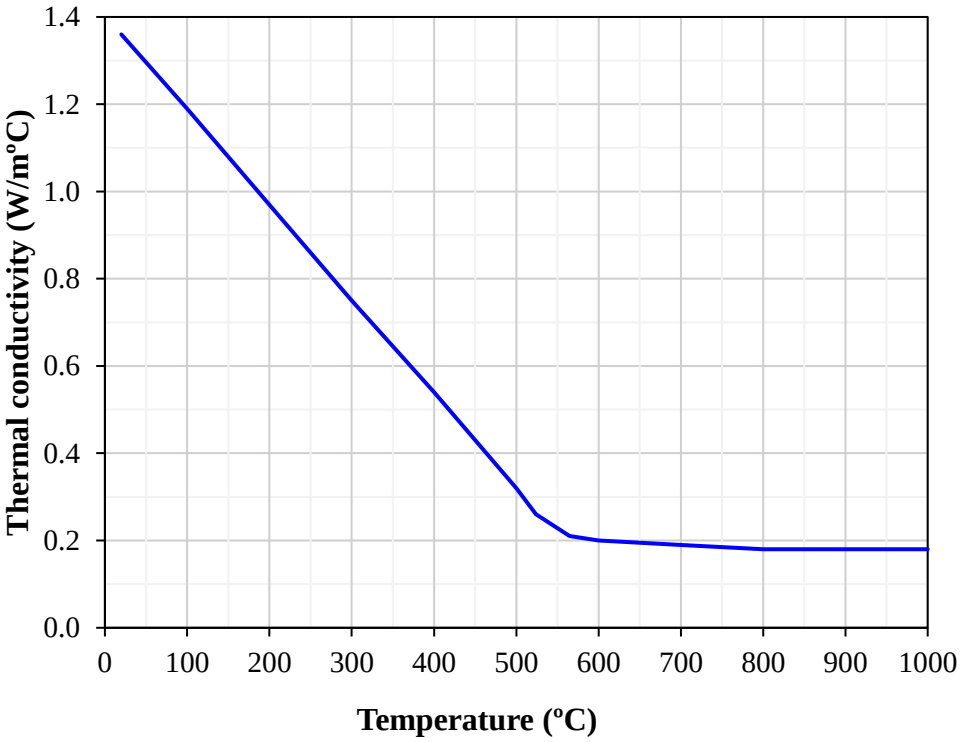

Figure 5.12 – Thermal conductivity of CFRP laminate as a function of temperature according to Griffis et al. [74] proposal

5.4.1.3.3 Density

The density of the CFRP was determined based on the relationship of the remaining mass with temperature according to results obtained by Thermogravimetric Analyses (TGA) performed by Firmo et al. [56]. Thus, considering the mass loss relationship determined in [56] and a density of 1550 kg/m^3 at ambient temperature according to the manufacturer [20], the variation of the density in relation to temperature is presented in Figure 5.13.

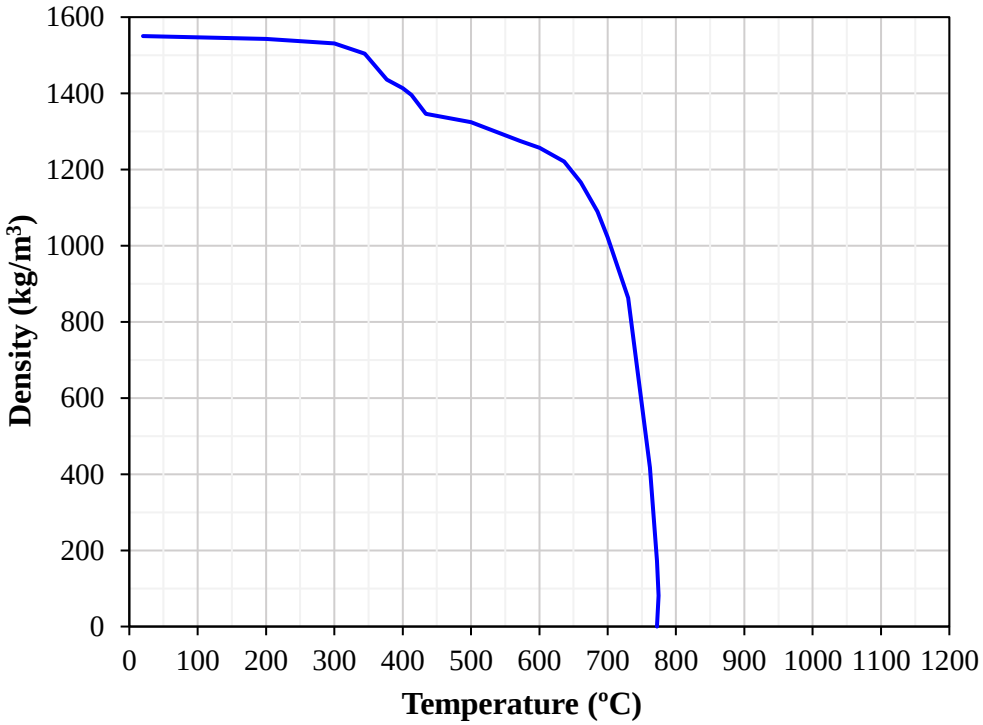

Figure 5.13 – Density of CFRP laminate as a function of temperature based on the mass loss relationship determined by Firmo et al. [56] and considering a density of 1550 kg/m^3 at ambient temperature [20]

5.4.1.4 Fire protection materials

Regarding the fire protection materials, their thermophysical properties variation with temperature was modelled based on experimental data from literature.

5.4.1.4.1 Specific heat

Thermal evolution of specific heat used in the modelling of the VP mortar properties was based on a study reported by Bai et al. [98]. Accordingly, the temperature-dependent specific heat capacities of the VP mortar ($c_{p,vp}$, in J/kgºC) were defined as follows:

$$c_{p,vp}(\theta) = 704 + 0.37\cdot\theta + 2.16\text{x}10^{-3}\cdot\theta^2 - 1.76\text{x}10^{-6}\cdot\theta^3 - 1.38\text{x}10^{-9}\cdot\theta^4 \quad (5.9)$$

Regarding the EC mortar, the experimental results from tests performed by MAXIT International, in Denmark [99] was used as reference to modelling their temperature-dependent specific heat capacities ($c_{p,ec}$). The OP mortar specific heat properties at elevated temperatures ($c_{p,op}$) were the same as those used for the concrete material (Section 5.4.1.1.1), according to

the recommendations of Eurocode 2, part 1-2 [1]. Figure 5.14 shows the specific heat *vs.* temperature diagram adopted for the different fire protection materials studied.

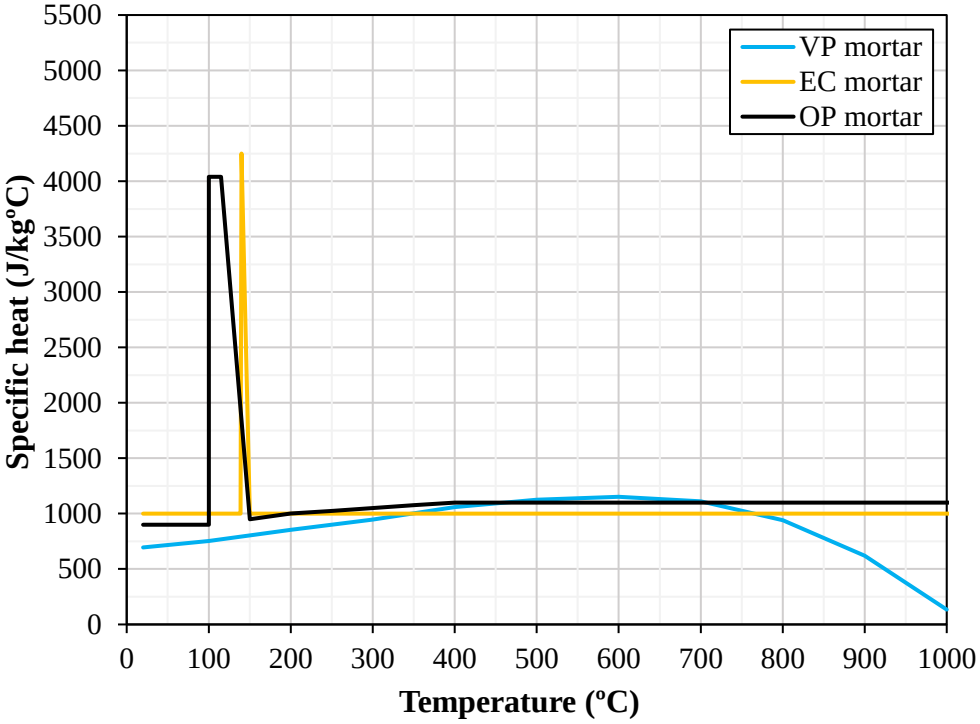

Figure 5.14 – Specific heat as a function of temperature for the fire protection materials composed by VP, EC and OP mortar according to Bai et al. [98], MAXIT International report [99] and Eurocode 2, part 1-2 [1], respectively.

5.4.1.4.2 Thermal conductivity

Similarly to specific heat variation, Bai et al. [98] proposal was adopted for the variation of the VP mortar thermal conductivity (λ_{vp}, in W/mºC). Thus, VP mortar thermal conductivity in relation to temperature was defined according to the following equation:

$$\lambda_{vp}(\theta) = 0.0581 + 9.209\text{x}10^{-5}\cdot(\theta - 20) \quad (5.10)$$

The study by MAXIT International [99] was also used in the modelling of the EC mortar thermal conductivity properties. National French Annex to NF EN 1992-1-2 [96] suggestions were used to define the thermal conductivity of the OP mortar, considering a thermal behaviour similar to the one of the concrete. Considering proposals of Bai et al. [98], MAXIT International report [99] and National French Annex [96], the thermal conductivity for the fire protection materials results in the diagrams illustrated in Figure 5.15.

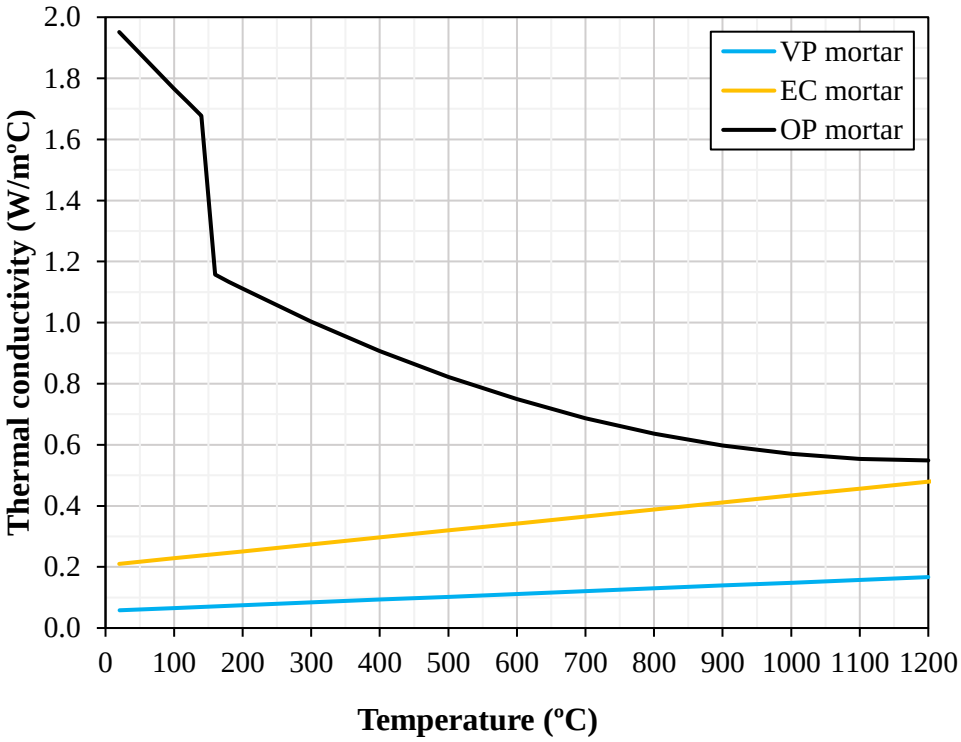

Figure 5.15 – Thermal conductivity as a function of temperature for the fire protection materials composed by VP, EC and OP mortar according to Bai et al. [98], MAXIT International report [99] and National French Annex [96], respectively.

5.4.1.4.3 Density

The density properties thermal evolution for the fire protection materials composed by EC and OP mortar were also defined in the model according to the experimental data reported in MAXIT International [99] and Eurocode 2, part 1-2 [1] suggestions, respectively. In addition, TGA measurements carried out by Firmo et al. [56] on fire protection materials were used as reference in the current study in order to determine the density variation as a function of temperature for the VP mortar. The density value at ambient temperature for the different fire protection materials was considered as reported by the manufacturers [89–91].

The density vs. temperature diagrams for both fire protection materials, based on the abovementioned references, are shown in Figure 5.16.

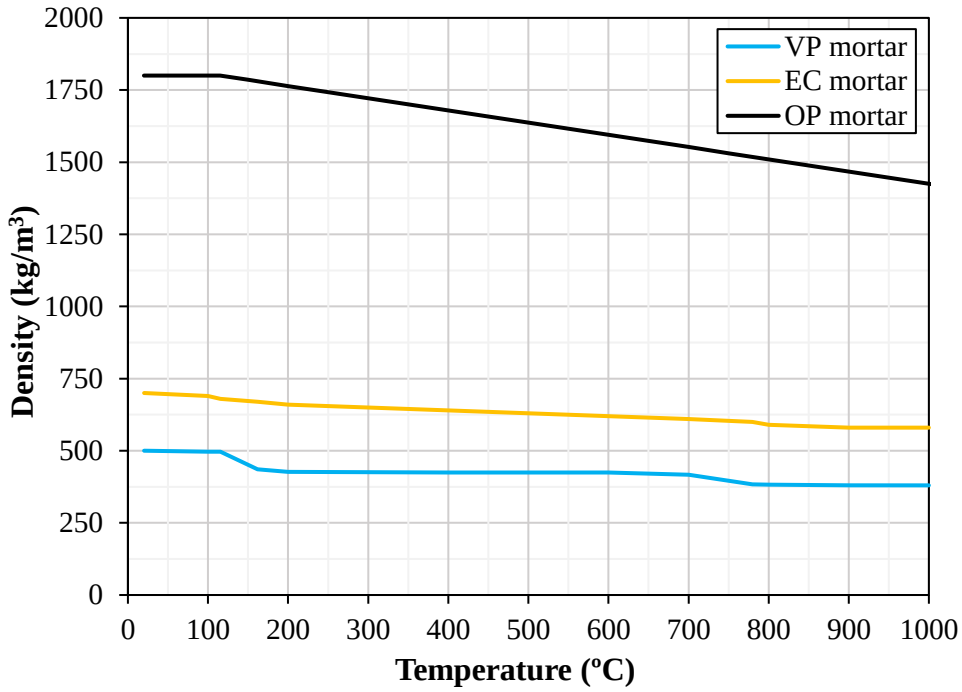

Figure 5.16 – Density as a function of temperature for the fire protection materials composed by VP, EC and OP mortar according to Firmo et al. [56], MAXIT International report [99] and Eurocode 2, part 1-2 [1], respectively.

5.4.2 Mechanical material properties

The continuous variations of the mechanical properties of the respective constitutive materials of the beams with the temperature influence necessary to a correct simulation of the thermomechanical behaviour of these structures in the developed FE models are shown in this section.

5.4.2.1 Concrete

The mechanical properties of the concrete at ambient temperature were experimentally determined and given in EN 1992-1-1 [33]. Thus, an average cube compressive strength of f_{cm}=30.1 MPa was experimentally obtained in this work by means of compressive strength tests. The average tensile strength (f_{ctm}) were defined as of 2.9 MPa according to [33]. Concerning the modulus of elasticity of concrete (E_{cm}), it was calculated for thermal actions (natural fire simulation) in accordance with a mathematical model for stress-strain relationships of concrete under compression at elevated temperatures proposed in EN 1992-1-2 [33]. The E_{cm} was calculated as 17.3 GPa (this value is generally lower than the one defined for concrete at ambient temperature).

The reduction of the mechanical properties of the concrete at elevated temperatures were obtained from the relationships suggested in EN-1992-1-2 [1] and EN 1994-1-2 [100]. The reduction factors with temperature for the compressive strength ($k_{c,c}$ (θ)), tensile strength ($k_{c,t}$ (θ)) and modulus of elasticity ($k_{E,c}$ (θ)) of concrete are presented in Figure 5.17, Figure 5.18 and Figure 5.19, respectively. The Poisson's ratio was defined equal to 0.2 and constant with temperature, according the Eurocode 2, part 1-1 [33] recommendation.

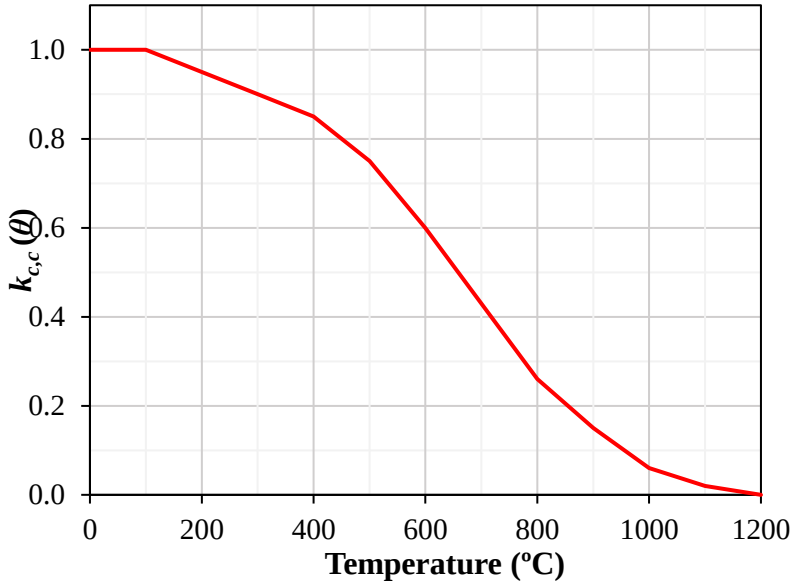

Figure 5.17 – Reduction factor for the compressive strength of concrete at elevated temperatures according to EN-1992-1-2 [1]

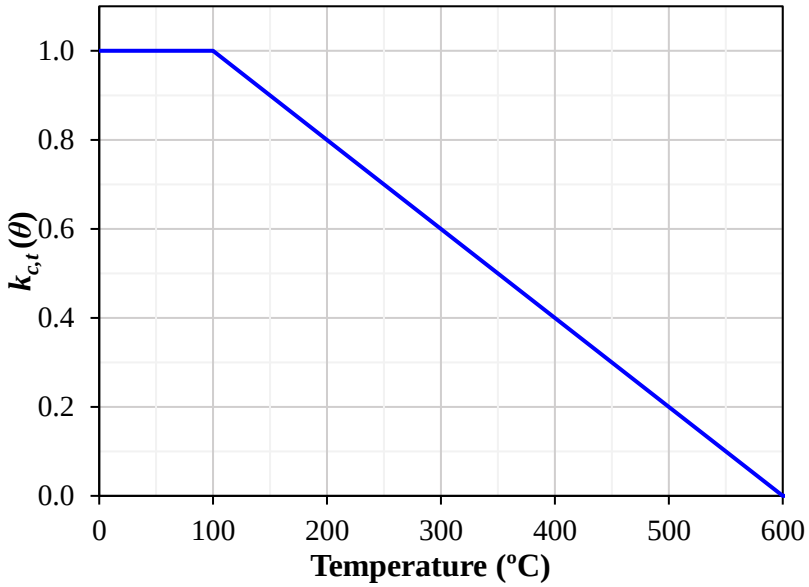

Figure 5.18 – Reduction factor for the tensile strength of concrete at elevated temperatures according to EN-1992-1-2 [1]

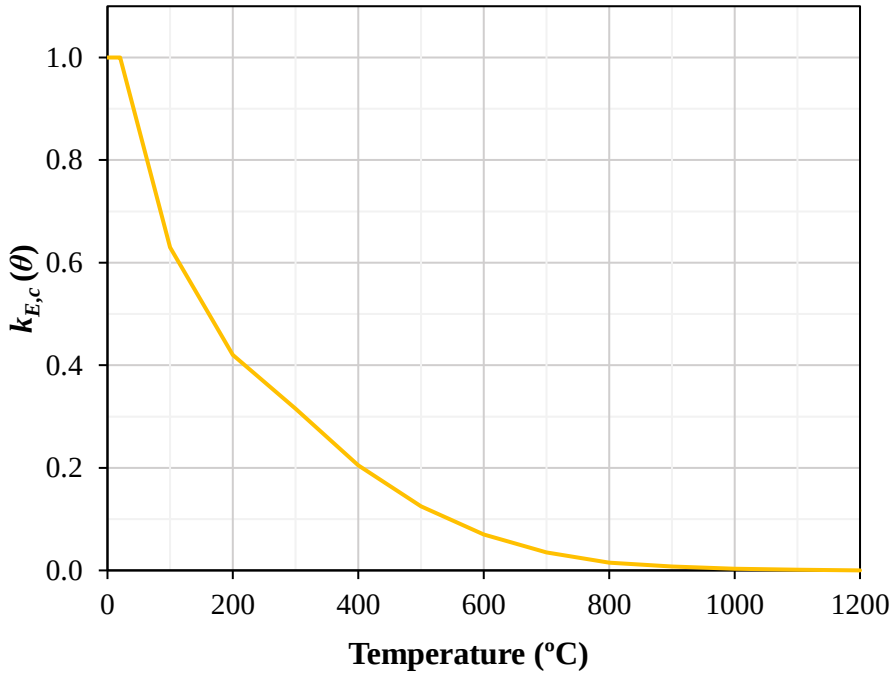

Figure 5.19 – Reduction factor for the modulus of elasticity of concrete at elevated temperatures according to EN 1994-1-2 [100]

5.4.2.2 Steel reinforcement

The mechanical properties of the steel reinforcement (B500 steel class) were defined according to Eurocode 3, part 1-2 [97]. The mechanical properties of the steel rebars at ambient temperature were as follows: yield stress of 500 MPa, modulus of elasticity of 210 GPa, ultimate tensile strength of 550 MPa and Poisson's ratio (v) of 0.3. The temperature-dependent behaviour of steel was also determined by part 1-2 of Eurocode 3 [97], following the reduction factor proposals presented in this standard. The diagrams of reduction factors in relation to temperature applied for the yield stress ($k_{s,y}(\theta)$), ultimate tensile strength ($k_{s,u}(\theta)$) and modulus of elasticity ($k_{Es}(\theta)$) of steel reinforcement are respectively presented in Figure 5.20, Figure 5.21 and Figure 5.22. Poisson's ratio was considered to be constant with temperature. The strain hardening effect on the steel at elevated temperatures was also accounted in the current numerical investigation and was calculated based on the calculation methods proposed by the part 1-2 of Eurocode 3 [97] (allowed by the stress-strain relationships for steel at elevated temperatures).

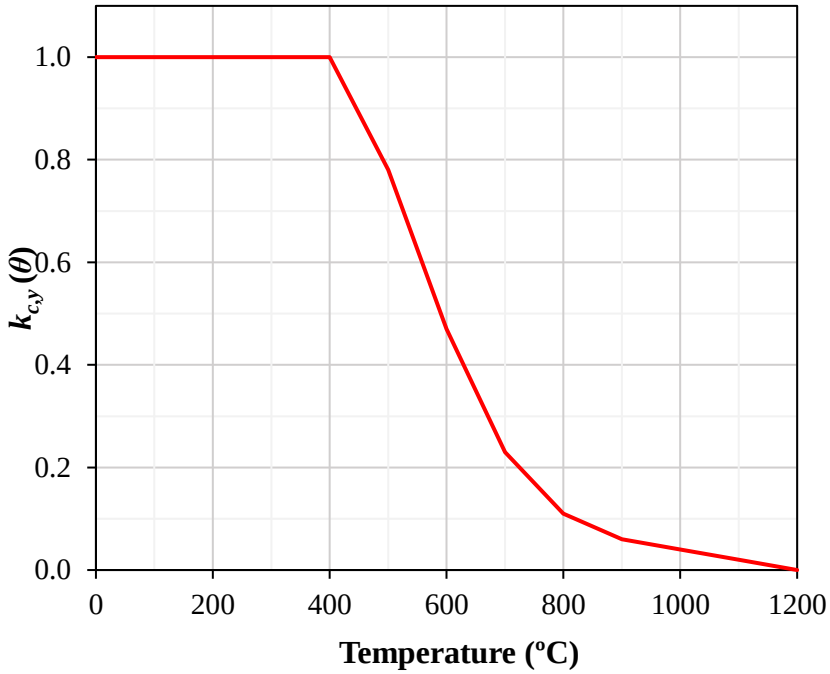

Figure 5.20 – Reduction factor for the yield stress of steel reinforcement at elevated temperatures according to EN 1993-1-2 [97]

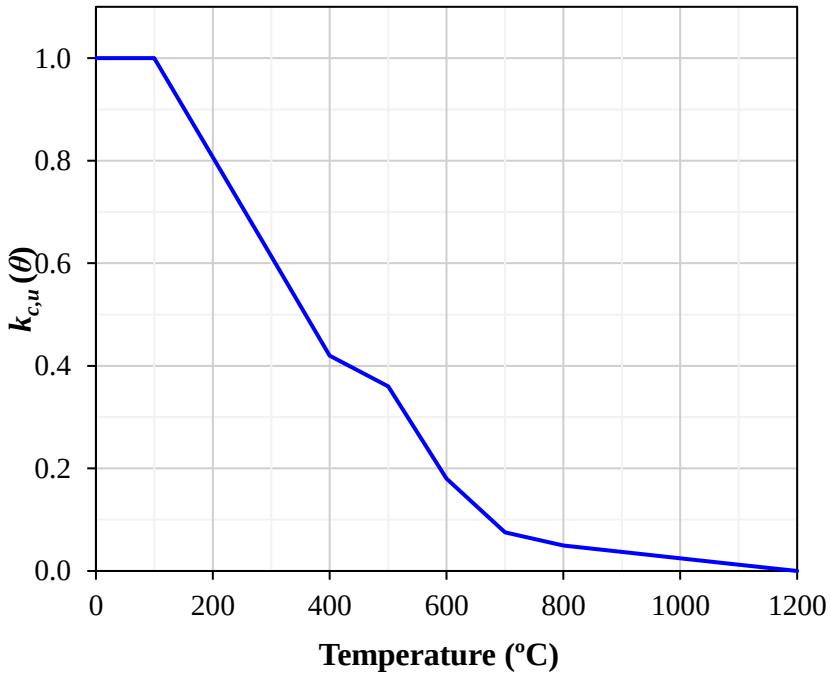

Figure 5.21 – Reduction factor for the ultimate tensile strength of steel reinforcement at elevated temperatures according to EN 1993-1-2 [97]

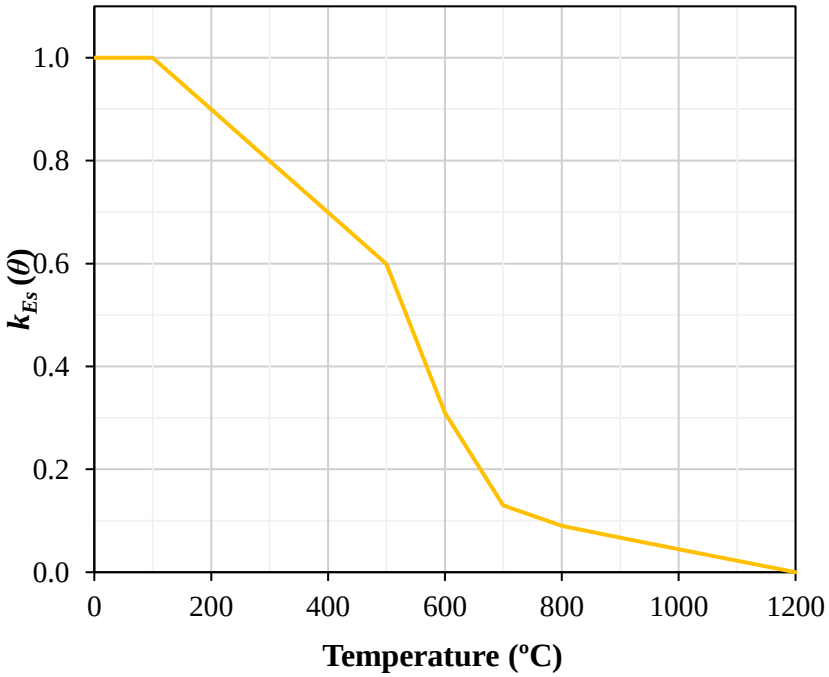

Figure 5.22 – Reduction factor for the modulus of elasticity of steel reinforcement at elevated temperatures according to EN 1993-1-2 [97]

5.4.2.3 CFRP laminate

Regarding the mechanical behaviour of the CFRP laminates, they behave essentially in the longitudinal direction in the present application, hence, as a simplification, the CFRP was modelled as linear elastic isotropic. The temperature influence on mechanical behaviour of CFRP laminate in the current model was based on the relations proposed by Wang et al. [101] and Bisby [102] for the tensile strength and modulus of elasticity, respectively. The laminates have an average tensile strength of 2800 MPa, modulus of elasticity of 170 GPa and ultimate strain of 16.0‰ at ambient temperature, according to manufacturer [20]. The Poisson's ratio is 0.3 (constant with temperature).

The variation of the CFRP-concrete bond mechanical properties at elevated temperatures was based on the temperature-dependent results obtained from the Single lap Shear Tests carried out in the current research (see Section 3.5).

Concerning the fire protection systems, their mechanical contribution was not considered since it is expected to be negligible.

5.5 Finite Element Mesh

The finite element size significantly influences the behaviour of the CFRP-strengthened RC beams. In an analysis based on the finite element method, the accuracy of the results is closely related to two aspects: first, the use of appropriate elements for each type of analyses, based on the structure geometry or material, interpolation degree and integration scheme; second, the correct model discretization defined from a sensitivity study, where a comparison of meshes with different arrangements or densities must be performed.

In the current research, three different mesh densities were studied in order to verify the effect of the finite element size on the behaviour of the unstrengthened and CFRP-strengthened RC beams. The meshes were defined (for both type of beams) based on a relatively coarse, intermediate and finer refinement level, corresponding to the densities (for the largest element) of 35 x 35 mm, 25 x 25 mm and 15 x 15 mm. Figure 5.23, Figure 5.24 and Figure 5.25 present the different finite element meshes studied in the finite element analysis (FEA) for the maximum densities of 35 mm, 25 mm and 15 mm, respectively. This study was proposed for ambient temperature conditions.

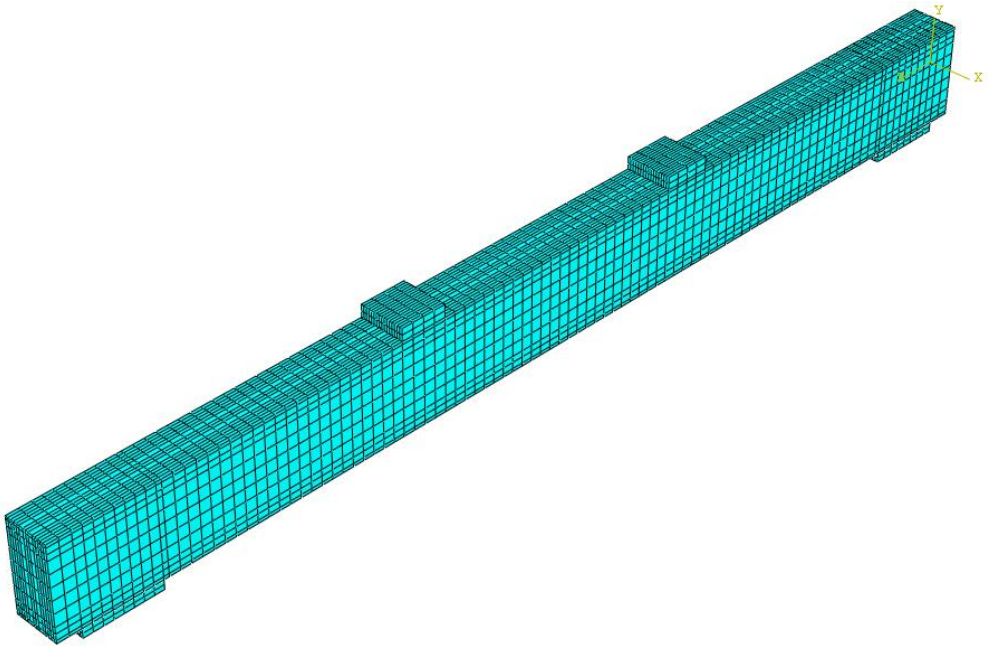

Figure 5.23 – Finite element meshes studied for the CFRP-strengthened and unstrengthened RC beam with maximum densities of 35 mm

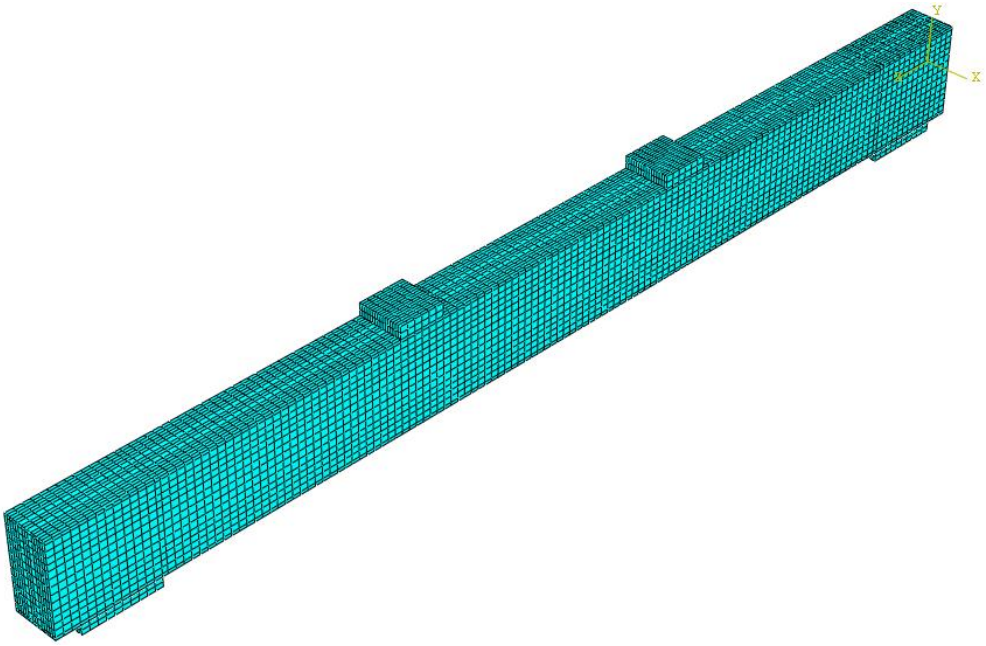

Figure 5.24 – Finite element meshes studied for the CFRP-strengthened and unstrengthened RC beam with maximum densities of 25 mm

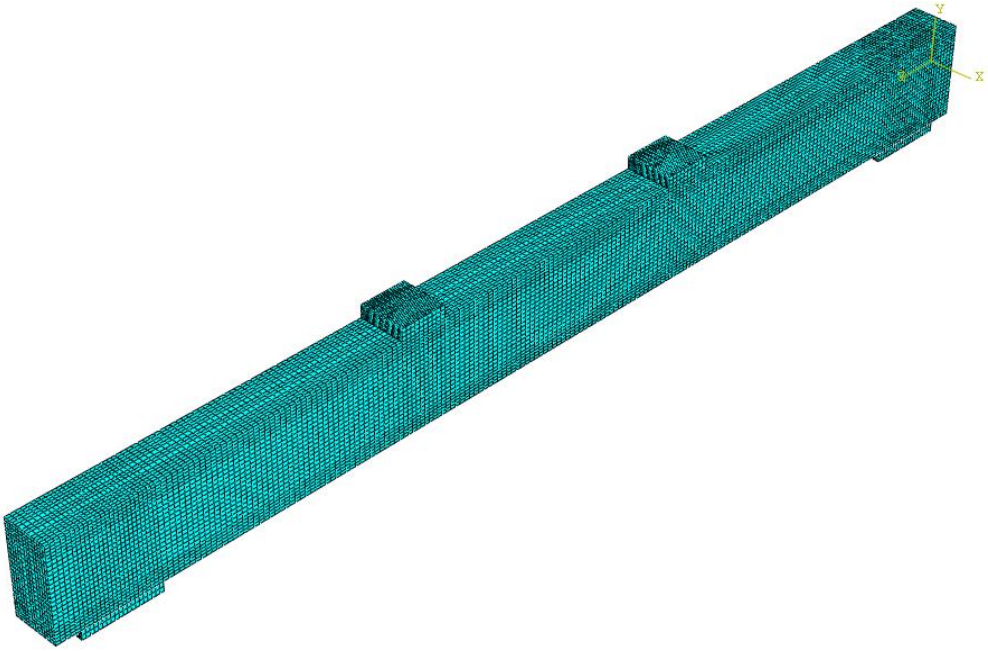

Figure 5.25 – Finite element meshes studied for the CFRP-strengthened and unstrengthened RC beam with maximum densities of 15 mm

The predicted load as a function of the vertical displacements at the mid-span obtained for different studied meshes are shown in Figure 5.26 and Figure 5.27 for the unstrengthened and CFRP-strengthened RC beam, respectively.

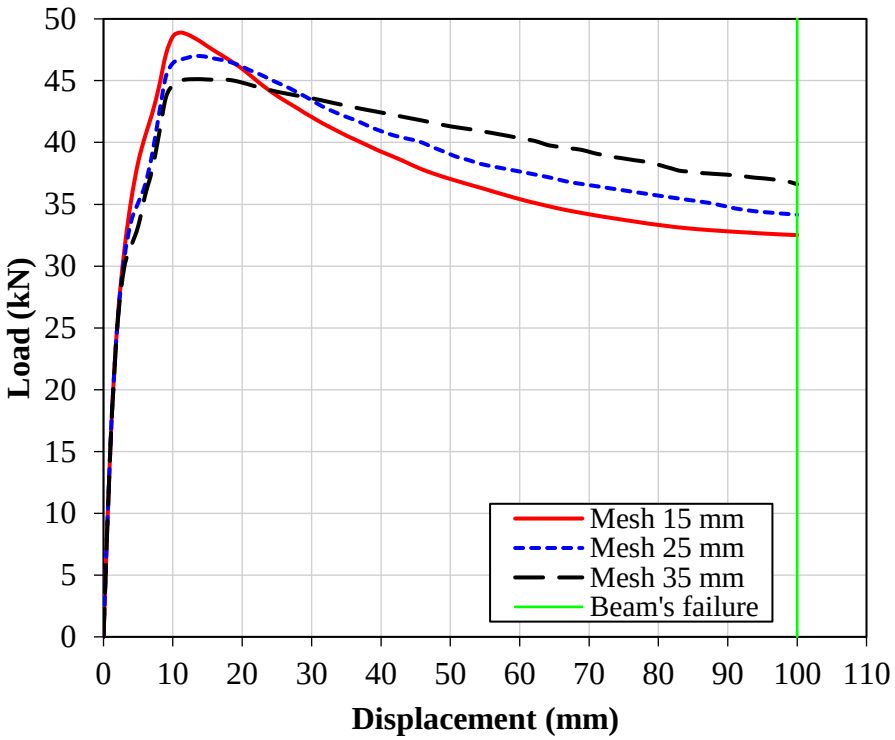

Figure 5.26 – Predicted load as function of displacements at mid-span for the unstrengthened RC beam by FEA at ambient temperature considering the different studied meshes

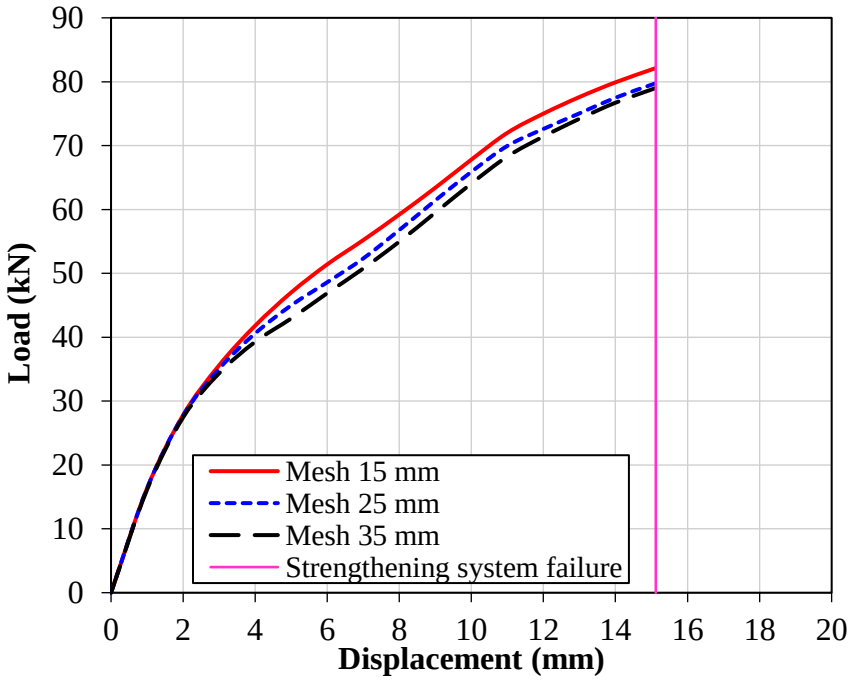

Figure 5.27 – Predicted load as function of displacements at mid-span for the CFRP-strengthened RC beam by FEA at ambient temperature considering the different studied meshes

Regarding the sensitivity analysis performed on unstrengthened RC beams (Figure 5.26), it can be concluded that the three studied densities had similar tendency during the elastic phase of the beams, i.e., until the peak load (ultimate load capacity result). The finite element size did not demonstrate significant impact on the ultimate load capacity. A difference of 1.9 kN was noticed between the peak loads for the meshes of 15, 25 and 35 mm, corresponding to 45.1 kN, 47.0 kN and 48.9 kN, respectively. It was also observed that the increase of the mesh size led to a relative increase of the final stiffness of the beam, more precisely in the non-linear plastic phase (corresponding to the yielding plateau of the lower steel reinforcement). Also, in this phase a similar behaviour was noticed for the densities of 15 and 25 mm, whereas for the density of 35 mm an uncommon tendency was obtained, with a higher stiffness and a smoother and more uniform evolution.

The mesh study on CFRP-strengthened beams presented a high similarity between the different densities, as shown in Figure 5.27. The evolution of the predicted load as function of the vertical displacements until the 2 mm displacement were practically the same for the three mesh densities. For higher displacement values a small difference was noticed between the meshes, but this is not relevant. This proximity can be noticed by the predicted load results at the instant of strengthening failure, where values of 82.1 kN, 79.7 kN and 79.0 kN was obtained for densities of 15, 25, and 35 mm, respectively. For this type of beam, the predicted load vs. displacement evolution for the different studied meshes were presented until the strengthening failure instant only. Results obtained after this instant were not presented in this thesis since they are not relevant to the FE numerical analysis.

Finally, an excellent similarity and simulation stability between the predicted load vs. displacement evolution was obtained by using finite element meshes of 15 x 15 mm and 25 x 25 mm for both types of beam. To save computational time, finite element meshes of 25 x 25 mm (Figure 5.24) was adopted in all models simulated in this research.

5.6 Boundary, Loading and Contact Conditions

A 3D numerical model (see Figure 5.1) was used to describe the fire behaviour of CFRP-strengthened RC beams under simply supported flexural conditions observed in the experimental tests. The representation of the cross-sections of the different beams, the support and loading systems were modelled in detail to allow accurate predictions by the numerical analyses. As shown in Figure 5.28, the axis system of the model is such that Z axis lies in the longitudinal direction of the beam while X and Y axes lie in the minor and major axes of the cross-section of the beam, respectively. As it was observed in the real test set-up, the supports

of the beam and the loading were also applied on rigid plates attached to the beams so as to distribute possible concentrated forces on them.

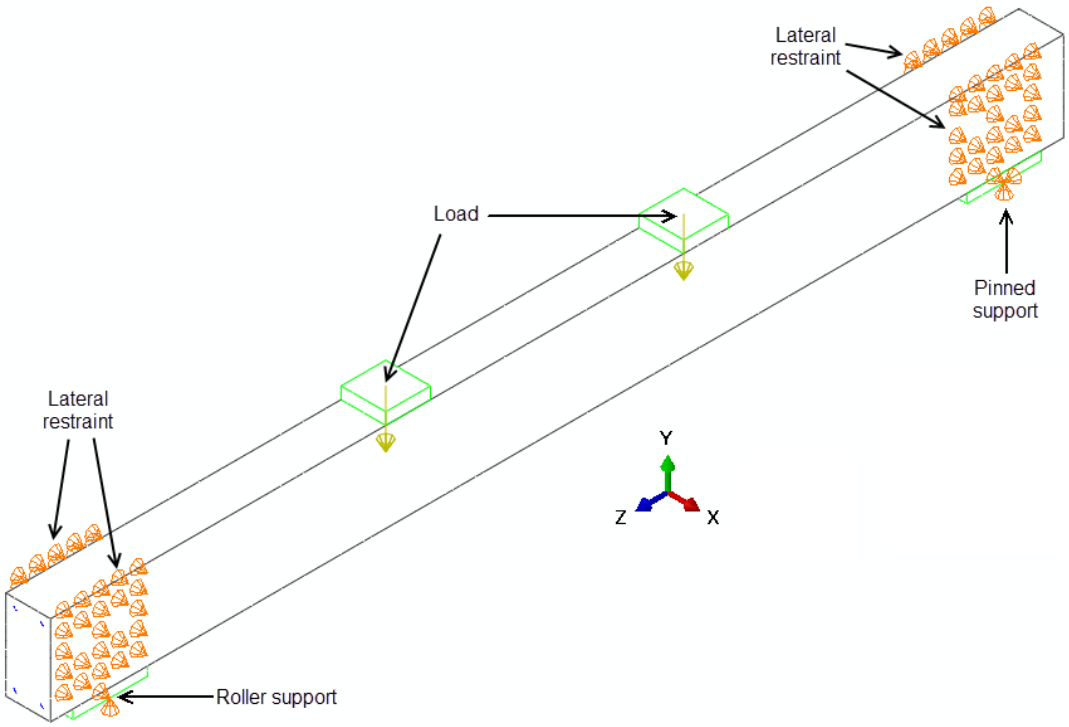

Figure 5.28 – Boundary and loading conditions of 3D numerical models used in the finite element analysis

The models were subjected to a fixed mechanical load (*P*) applied to the direction -Y at the centre of the rigid plates and each one was at a distance of 1.0 m from the nearest beam support, i.e., the loading were applied in a four-point bending configuration (see Figure 5.28) as used in the experimental tests. The preload applied in the simulations was defined based on the recommendations of EN 1992-1-1 (2004) [33] and correspond to 70% of the design value of the loadbearing capacity of the RC beam at ambient temperature (24.0 kN) as defined in the experimental test procedure (Section 4.4).

Regarding the support system, all degrees of freedom of the nodes located on the bottom surface and at the middle of the respective rigid plate were constrained to simulate the pinned support, whereas for the roller support only the translations in the directions X and Y were constrained. In addition, all nodes located at each end of both supports were constrained to translations in the direction X in order to prevent their lateral deformation (Figure 5.28).

In order to simulate the contact between the concrete beam and the fire protection materials, supports, loading points and also between them and the CFRP laminate (Figure 5.29), the

surface-to-surface contact method was used in the analyses. This method gives a good convergence rate and it is much less sensitive to the choice of master and slave surfaces [94]. According to Selamet and Garlock [103], the surface-to-surface contact conditions are enforced in an average sense, rather than at discrete points such as node-to-node discretization. Such averaging technique provides more accurate and smooth contact state transition. Small-sliding formulation was used in the contact tracking algorithm between the beams and the CFRP laminates. This formulation establishes the relationship between the slave nodes and the master surface at the beginning of the simulation, determining which segment on the master surface will interact with each node on the slave surface. This methodology maintains these relationships throughout the analysis, preventing changes in the interaction between the master surface segments and the slave nodes. In this case the geometric nonlinearity is included in the model, so the small-sliding algorithm accounts for any rotation and deformation of the master surface and updates the load path through which the contact forces are transmitted. In addition, two more assumptions were introduced in these analyses exclusively for modelling the contact behaviour between the concrete and the CFRP laminates. A penalty method (damage) was defined as the cohesive contact property between the concrete and CFRP surfaces. Thus, two bond damage criteria were adopted: maximum nominal stress and fracture energy. These values (temperature-dependent) were inputted in the FE model based on the experimental data obtained from the SST tests performed in this investigation (discussed in detail in the Chapter 3).

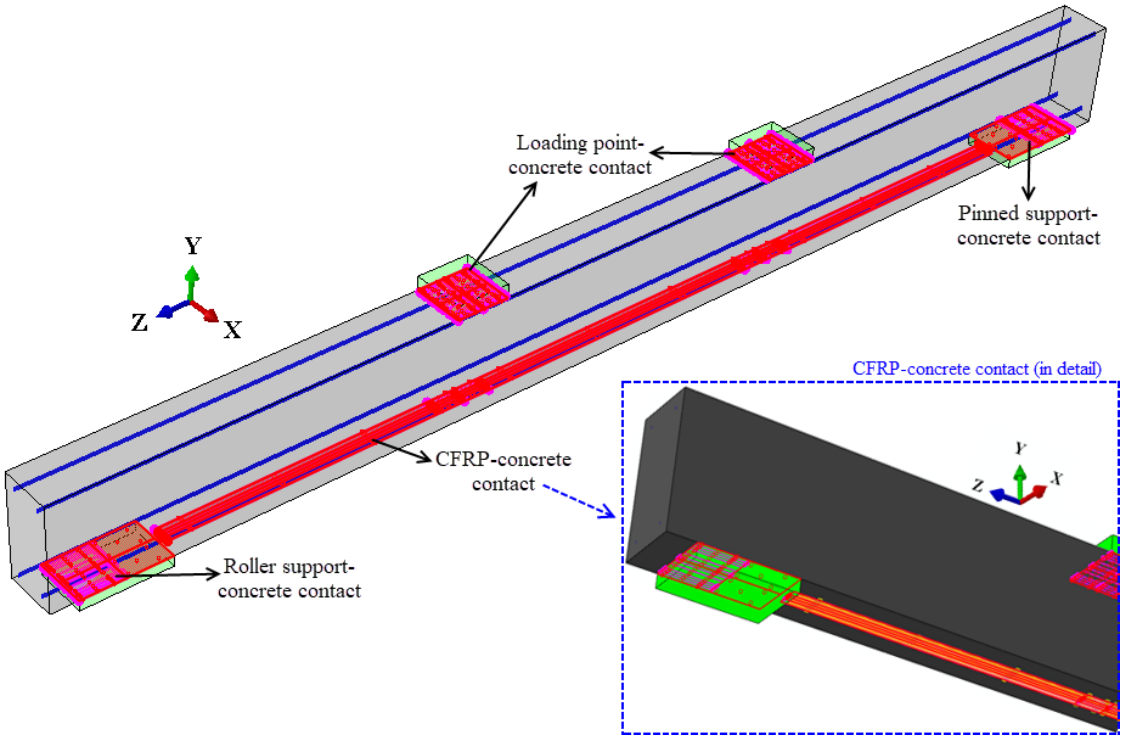

Figure 5.29 – Contact conditions of 3D numerical models used in the finite element analysis

Finally, the fire action was applied in the 3D model. The heat transfer step was applied after the preloading of the model (as defined in the experimental test procedure – Section 4.4) and performed according to the furnace temperatures registered in the experimental tests in order to validate the FE model. In Abaqus software the fire action was done by means of two types of surface, namely, "film condition" and "radiation to ambient", corresponding respectively to heat transfer by convection and radiation. In these simulations, a 4-node linear heat transfer quadrilateral element (DC2D4) was chosen and a 2D numerical model (described in Section 5.8.4) was developed to estimate the temperature distribution in the cross-sections of the beams. In order to accurately simulate the test conditions adopted in the experimental campaign, the bottom and lateral surface of the models of the beams (see Figure 5.30) were directly exposed to the heating. The upper face of the beam in the model was superposed by a surrounding concrete slab which in turn was submitted to a constant ambient temperature, as adopted in the experimental tests. This system was intended to reproduce, as faithful as possible, the effects arising from a real surrounding structure, such as the heat transfer reactions and the shading effect. The initial temperatures of the models were defined based on the measurements recorded in the experimental tests. Radiation and convection heat transfer modes were considered on both lateral and bottom surfaces. The resultant emissivity was taken as 0.49, considering the emissivity coefficients of the electric resistance of the furnace and the beams both equal to 0.7. A convection coefficient of 15 W/m^2 ºC (constant with temperature) was adopted since the temperatures of the furnace were an input data, as suggested in EN-1992-1-2 [1].

Three types of passive fire protection materials (ordinary Portland, ordinary Portland with expanded clay and vermiculite-perlite cement-based mortar) were modelled in the lateral and bottom surfaces along the fire-exposed length of the strengthened beams. Actually, these boundary conditions correspond to the thermal exposure of simply supported beams in contact with surrounding concrete slabs and fire-protected by different passive systems, as well as those adopted in the experimental test set-up. It is worthwhile to mention that the beam temperatures registered in the experimental tests were considered as an input in the numerical simulations, since the temperature distribution along the beam presented some irregularities, in other words the distribution was not perfect, as discussed in Chapter 4. Hence, it was assumed that the temperatures in the cross-section were uniform and equal to the respective thermocouples, meaning that the temperatures recorded by the thermocouples located in Section S1 were uniform along the entire longitudinal length of the beam, including sections S2 and S3 (Figure 5.30). Exclusively at the regions of CFRP-concrete interface, CFRP laminate and fire protection material surfaces of the strengthened beams, the temperature was inputted along the section length of the model by an interpolation between the measurements of four cross-sections S1,

S2, S3 and SM_{1-3}, since these zones is relevant and very sensitive to thermal variation and more accurate data are needed.

A constant and uniform temperature corresponding to ambient temperature was defined at beam supports and at loading application points.

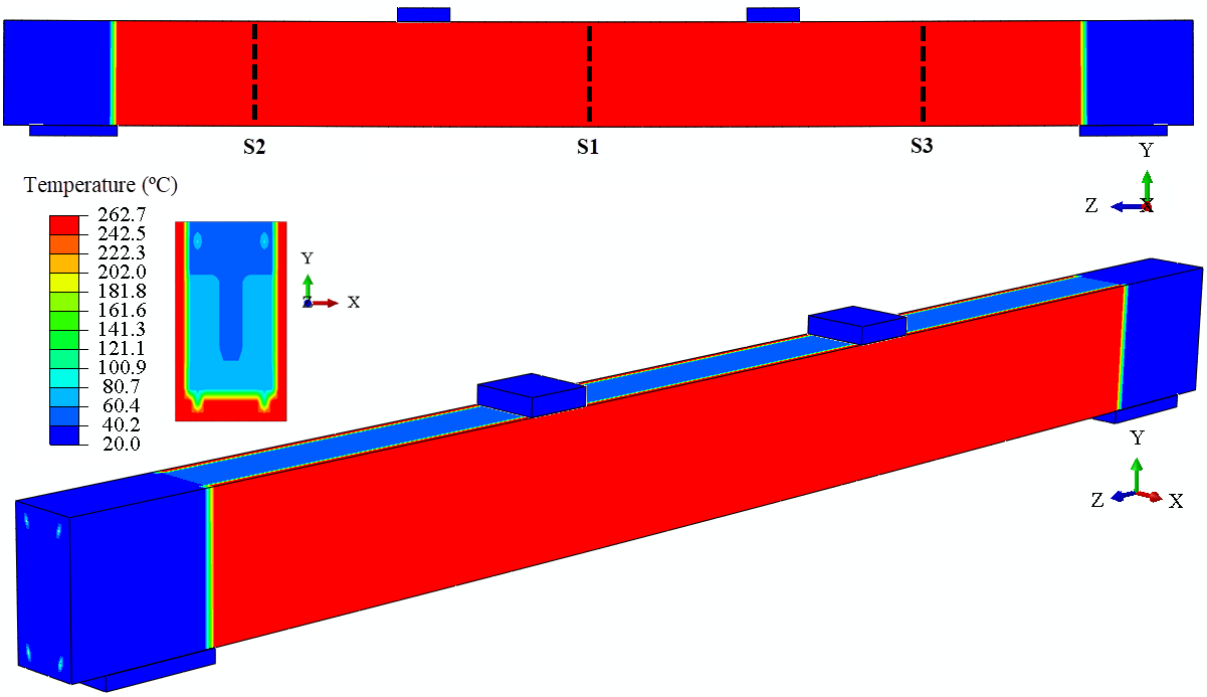

Figure 5.30 – Temperature distribution introduced in Abaqus of the RC test beam at 34 minutes of simulation run

For the validation of models at ambient temperature conditions only a mechanical analysis was performed, loading the beams under displacement control until collapse in accordance with experimental tests.

5.7 Analysis Method and Procedure

Geometrical and material non-linear analysis were employed in the developed FE model. The non-linear equations were solved iteratively using the Newton Raphson's Method. The main advantage of Newton's method is its quadratic convergence rate when the approximation at iteration is within the "radius of convergence", i.e., when the gradients defined by matrix provide an improvement to the solution. The method disadvantage is due to the fact that Jacobian matrix has to be calculated, and this same matrix has to be solved. The solution of the Jacobian matrix can be a problem due to the computational effort involved. The direct solution

to linear equations can dominate the entire computational effort, as the complexity of the problem increases. Despite the high computational effort required, Moltubakk [104] states that this method needs few iterations to reach the convergence capable of establishing the final solution.

A sequentially uncoupled thermo-mechanical analysis was adopted to simulated the fire behaviour of the CFRP-strengthened RC beams. A heat transfer analysis was first performed to obtain the temperature distributions along the cross-section of the beam by 2D FE models, followed by a 3D mechanical analysis that considered the thermal data influence provided in the previous step. Therefore, in the Abaqus software the thermo-mechanical response of the specimens (allowed after the uncoupled analysis) was simulated by a two-step analysis. In the first step, the desired loading was applied under displacement control to the FE model at ambient temperature and it was fixed afterwards, inducing an initial deflection (as occurred in the experimental model). The loading step was explicitly defined in the Abaqus. In the second step, the temperature distributions in relation to time (previously determined in the thermal analysis) were imposed to the loaded beams for a duration similar to that observed in the fire resistance tests (discussed in the Chapter 4). In the case of validation of models at ambient temperature, only a structural analysis was performed with the purpose of simulating the behaviour of unstrengthened and CFRP-strengthened RC beams up to failure.

5.8 Validation of Finite Element Model

5.8.1 Mechanical response at ambient temperature

Numerical simulations of the flexural tests at ambient temperature previously performed in this investigation (cf. Section 4) on an unstrengthened and EBR-CFRP-strengthened beams (referred as RC_AT and CFRP_AT, respectively) were performed to assess the ability and accuracy of the FE models described above in predicting the mechanical response of these beams. Figure 5.31 shows a comparison of the load vs. vertical mid-span displacement curves for the unstrengthened and CFRP-strengthened RC beams obtained from the experimental tests (Exp.) and FEA (Num.).

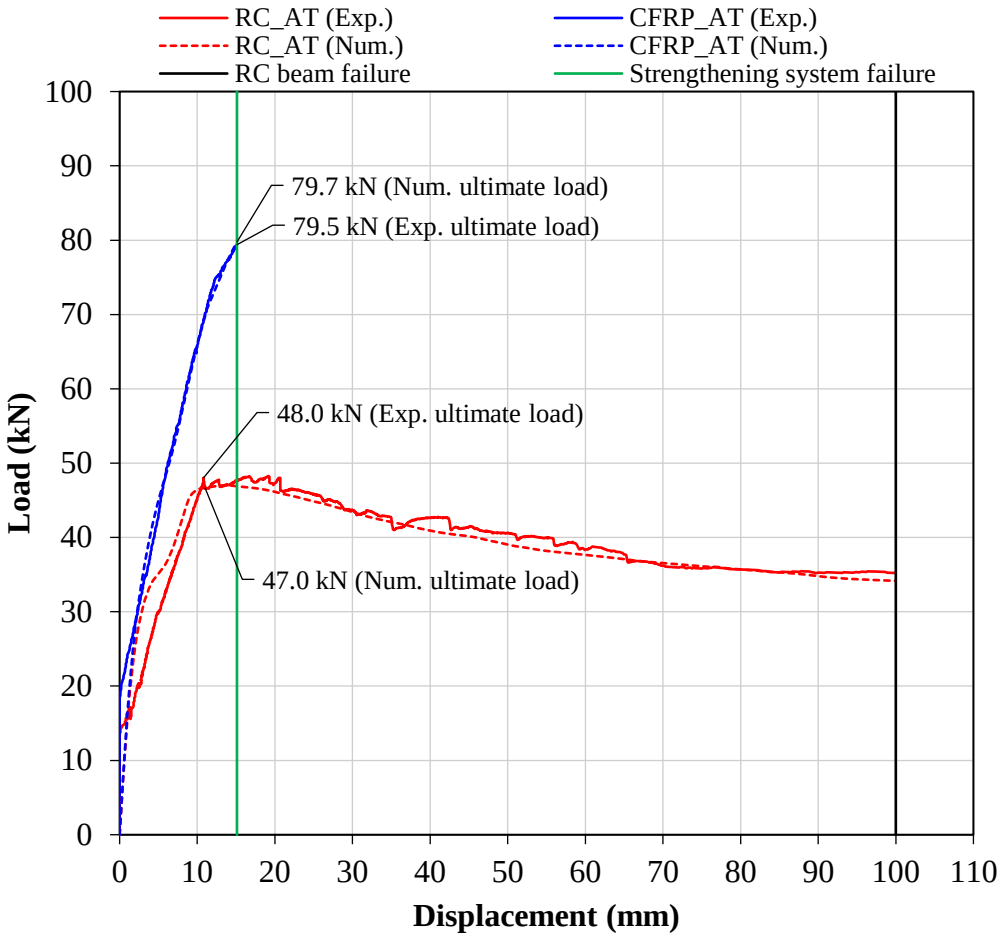

Figure 5.31 – Experimental (Exp.) and predicted (Num.) load vs. mid-span displacement curves for the unstrengthened and CFRP-strengthened RC beams at ambient temperature

Figure 5.31 reveals that all predicted results generally fit closely with the experimental curves for both specimens, especially for obtained peak loads (ultimate load). The ultimate predicted load of the RC_AT and CFRP_AT beams was 47.0 kN and 79.7 kN, respectively. The ultimate load experimentally obtained for the unstrengthened and CFRP-strengthened beams was 48.0 and 79.5, respectively. These results were very similar to those obtained numerically for both specimens. Therefore, the values of the predicted-to-experimental loading capacity ratios (P_{NUM} / P_{EXP}) for the RC_AT and CFRP_AT beams corresponds to 0.98 and 1.00, respectively, as shown in Table 5.1.

Table 5.1 – Experimental and numerical loading capacity of the beams

Test reference	Experimental loading capacity (P_{EXP}) – (kN)	Numerical loading capacity (P_{NUM}) – (kN)	Loading capacity ratio (P_{NUM} / P_{EXP})
RC_AT	48.0	47.0	0.98
CFRP_AT	79.5	79.7	1.00

Finally, an excellent agreement and accuracy between the experimental and numerical results was noticed, ensuring a strong validity of the developed FE model in predicting the mechanical response of both RC beam flexurally strengthened with EBR-CFRP laminate and unstrengthened RC beam at ambient temperature. Moreover, the good accuracy of the results also provided reliable and safe models in the case of a future parametric study (as suggested in Section 6.4).

5.8.2 Mechanical response under fire conditions

The experimental results from fire resistance tests carried out on the CFRP-strengthened beam EC-35 were used to validate the mechanical response of the 3D numerical model under fire conditions (see Figure 5.33). The beam EC-35 was chosen because it presented more accurate results in comparison to the other simulated beams during the heat transfer analyses (Section 5.8.4). Furthermore, for the mechanical validation of the FE model that represents the RC beam subjected to fire (see Figure 5.32), the experimental data from the unstrengthened specimen (RC) were assigned for comparative purposes. The comparison of the displacement-temperature curves of the simply supported RC and CFRP-strengthened beams obtained from the experimental tests and FEA are presented in Figure 5.32 and Figure 5.33, respectively. It is important to note that an initial deflection induced to the specimens was due to the pre-loading stage, as exhibited in the figures below. Moreover, the results of the RC beam are presented until its final collapse ("beam failure" in the figure legend – 100 mm deflection) in Figure 5.32, while for the CFRP-strengthened beam the results are presented until the CFRP strengthening debonding ("strengthening failure" in the figure legend).

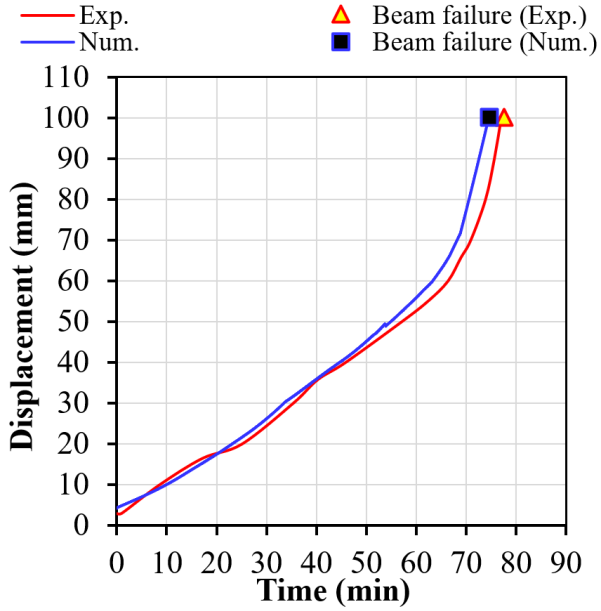

Figure 5.32 – Experimental (Exp.) and predicted (Num.) displacement-temperature curves for the RC beam

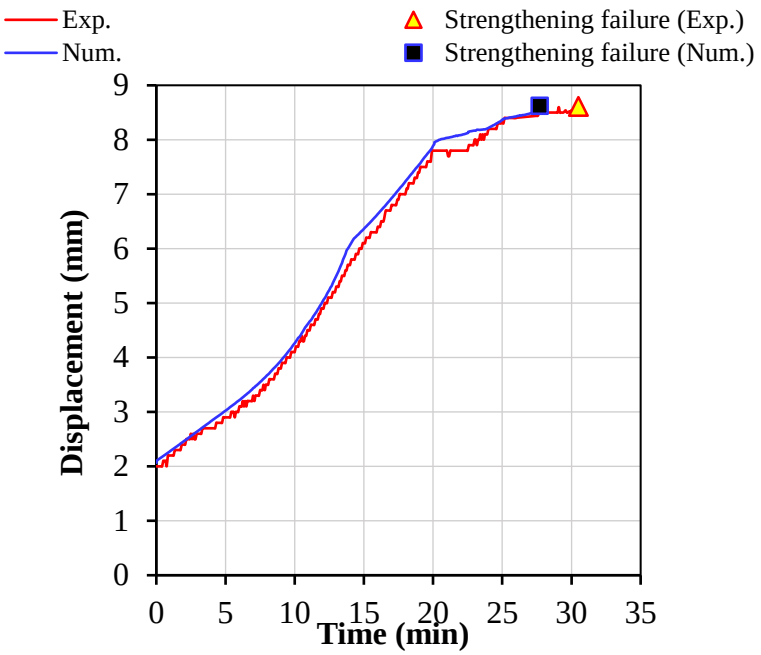

Figure 5.33 – Experimental (Exp.) and predicted (Num.) displacement-temperature curves for the CFRP-strengthened beam

Similar tendencies with an equivalent slope were obtained from the FEA in comparison with the experimental results for both RC and CFRP-strengthened RC beams (specimens RC and EC-35, respectively). The experimental curves presented a slightly higher stiffness than the numerical ones.

A good agreement between the FEA (Num.) and experimental (Exp.) analysis in terms of critical fire resistance time of the RC beam (FR_{time}) was obtained, as shown in Table 5.2. The failure instant of this beam (when achieved a deflection of 100 mm) was experimentally achieved at 78.2 min of fire exposure, while for the numerical model a fit close and slight conservative time of 74.5 min was noticed. In the case of strengthened beam, a satisfactory convergence of results between the models was also obtained. The fire resistance time at the CFRP debonding instant ($FR_{time,CFRP}$) for the strengthened beam was quite similar for both experimental and numerical models, corresponding to 30.5 and 27.7 min, respectively, as showed in Table 5.3. Therefore, the results showed that the differences between experimental and numerical fire resistance times were less than 5% and 10%, respectively for unstrengthened beam and CFRP strengthening system (Table 5.2 and Table 5.3, respectively). In addition, a relationship between the fire resistance times (FR_{time} or $FR_{time,CFRP}$) at different displacements obtained by the numerical and experimental analysis for both type of beams was also presented in Table 5.2 and Table 5.3.

Table 5.2 – Experimental (Exp.) and numerical (Num.) FR_{time} at different deflection levels of unstrengthened RC beam

FR_{time} at 50 mm displacement (min)		FR_{time} at 75 mm displacement (min)		FR_{time} at beam failure instant (min)		FR_{time} ratio at failure instant of the beam
Exp.	Num.	Exp.	Num.	Exp.	Num.	
57.0	54.9	72.3	69.5	78.2	74.5	0.95

Table 5.3 – Experimental (Exp.) and numerical (Num.) $FR_{time,CFRP}$ at different deflection levels of CFRP-strengthened beam

$FR_{time,CFRP}$ at 5 mm displacement (min)		$FR_{time,CFRP}$ at 8 mm displacement (min)		$FR_{time,CFRP}$ at CFRP failure instant (min)		$FR_{time,CFRP}$ ratio at failure instant of the CFRP system
Exp.	Num.	Exp.	Num.	Exp.	Num.	
12.2	11.8	23.0	20.1	30.5	27.7	0.91

Notwithstanding the slight differences abovementioned, the models presented general good agreement and accuracy between the experimental and numerical results of the RC and CFRP-strengthened beams. All these results indicate that the estimated data is generally accurate. The satisfactory agreement and accuracy between the experimental and numerical results confirm the validity of the developed finite element models and attest to their ability to simulate the mechanical response of simply supported RC and CFRP-strengthened beams under fire conditions.

5.8.3 Failure mode analysis

The numerical failure modes of the tested specimens under four-point bending configuration and at ambient temperature conditions obtained from the FEA are illustrated in Figure 5.34a to Figure 5.37a and they are compared to the experimental failure modes as shown in Figure 5.34b and Figure 5.37b.

The bending failure mode characterized by excessive deflections and flexural cracks at mid-span, without lateral displacements, due to tensile rupture and excessive elongation of the bottom rebars that were responsible for the collapse of the experimentally tested unstrengthened RC beams were also clearly identified in the predicted failure modes. Figure 5.34 and Figure 5.35 show two views of (a) numerical and (b) experimental deformed shape of the RC beam at the failure instant. Moreover, the cracking along the cross-section of the beam was also registered and a good similarity was achieved between the numerical and experimental models, as shown in Figure 5.36a and Figure 5.36b, respectively, for a perspective view; and in Figure 5.37a and Figure 5.37b, respectively, for a mid-span approximated view.

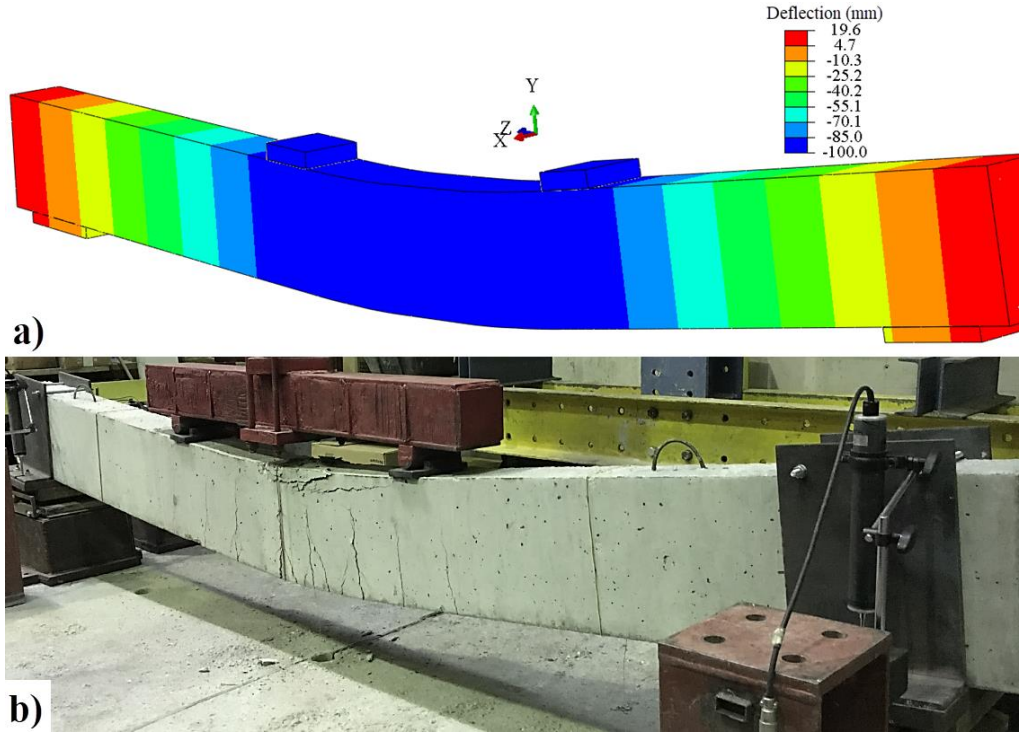

Figure 5.34 – (a) Numerical (b) and experimental deformed shape for the unstrengthened RC beam (specimen RC_AT) at the failure instant: view 1

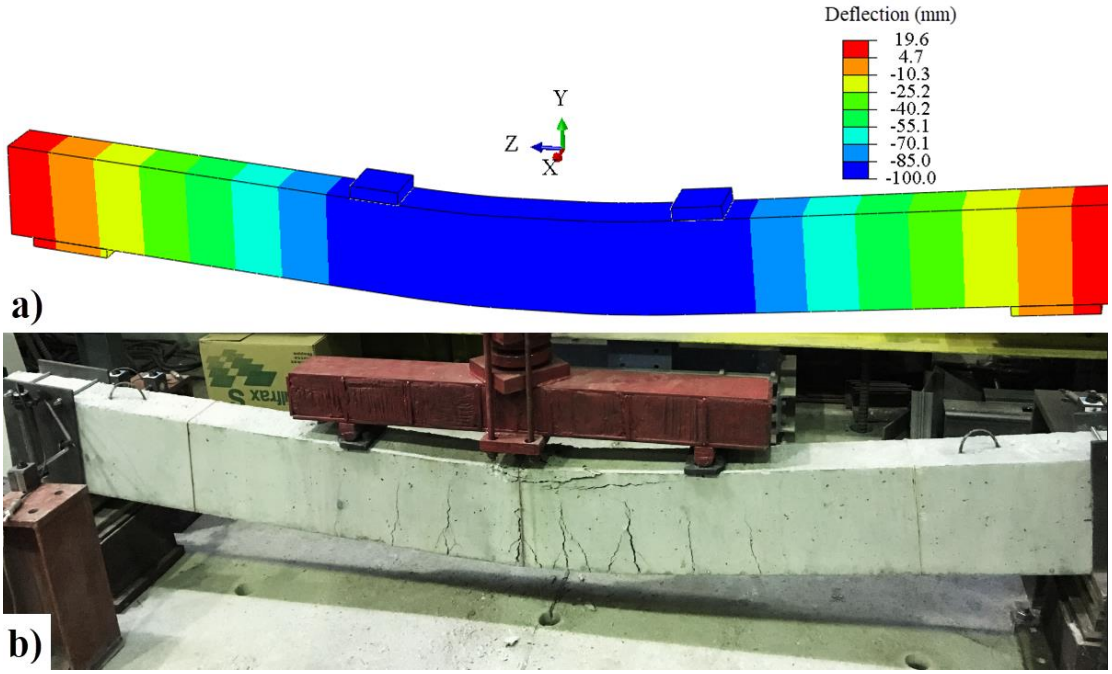

Figure 5.35 – (a) Numerical (b) and experimental deformed shape for the unstrengthened RC beam (specimen RC_AT) at the failure instant: view 2

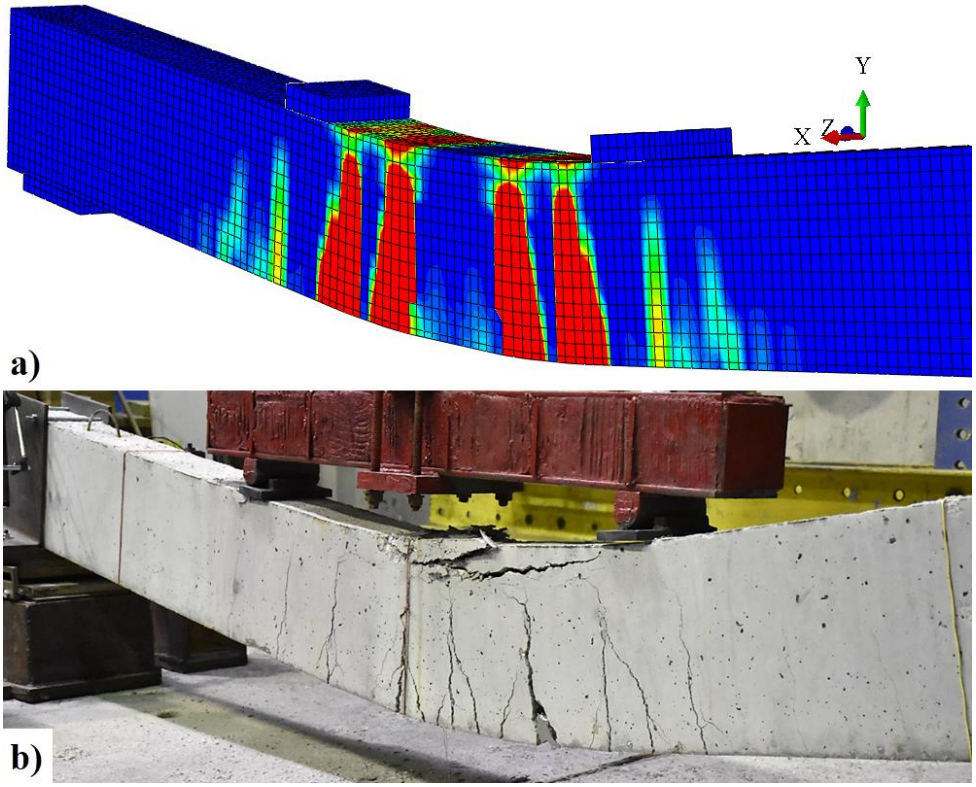

Figure 5.36 – (a) Numerical (b) and experimental cracking along the cross-section of the unstrengthened RC beam (specimen RC_AT) at the failure instant: perspective view

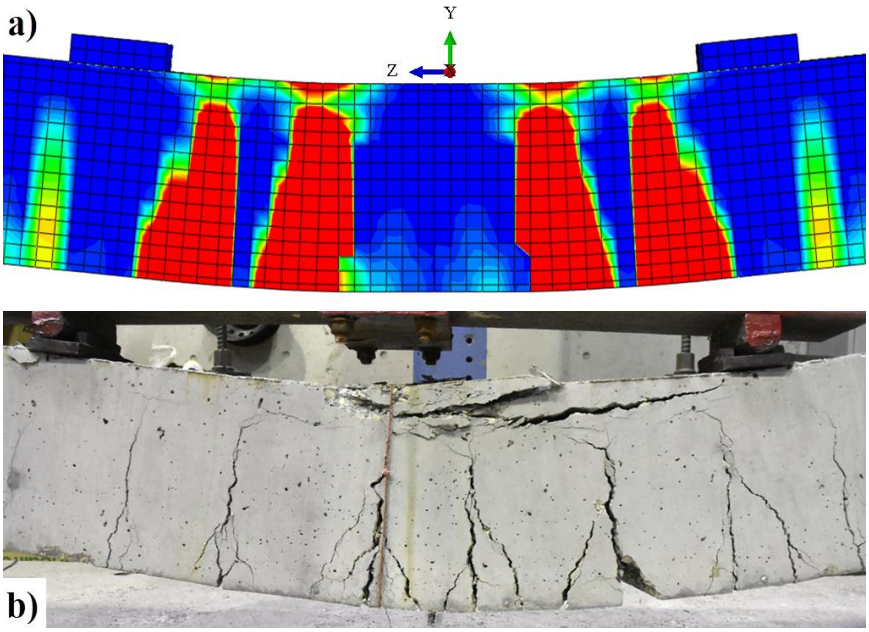

Figure 5.37 – (a) Numerical (b) and experimental cracking along the cross-section of the unstrengthened RC beam (specimen RC_AT) at the failure instant: mid-span detail view

The stress concentrations and excessive elongation on the bottom steel reinforcement verified at the mid-span region of the flexurally tested RC beam (see Section 4.5.1.2) was also noticed in the numerical model deformed shown in Figure 5.38. At the beam failure instant (at 100 mm deflection), the rupture of the bottom rebars by tensile was imminent since the maximum stress values registered in the numerical model was quite close to the yield stress limit of the steel (Figure 5.38).

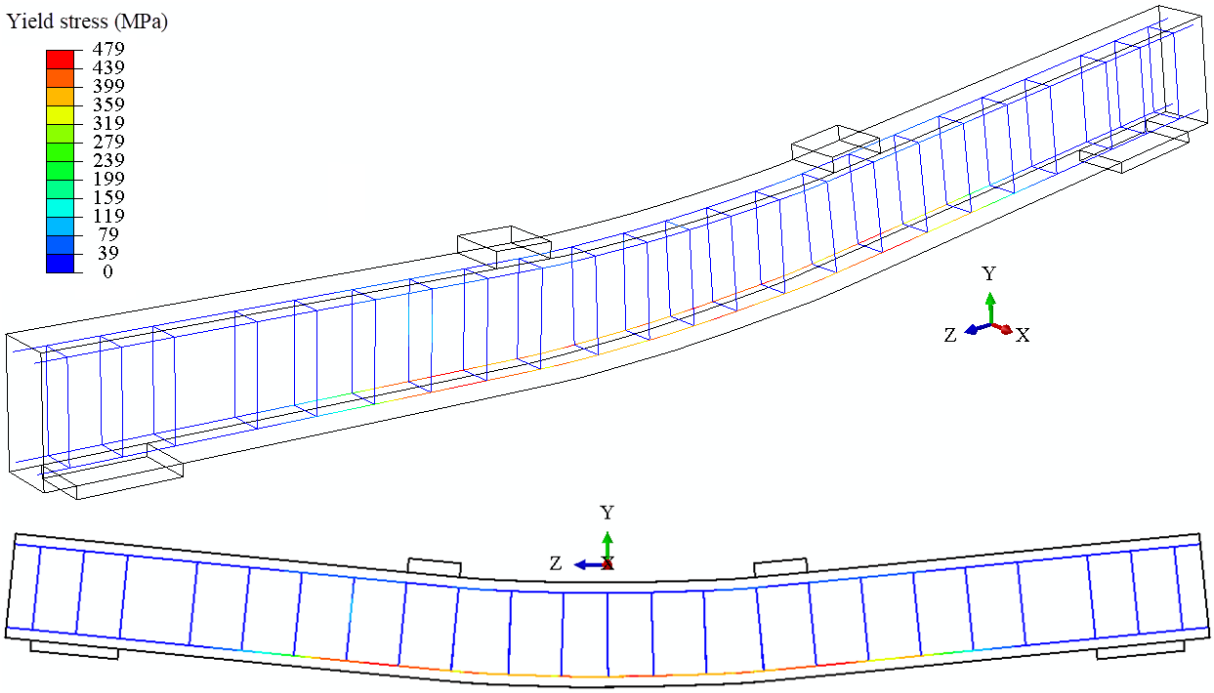

Figure 5.38 – Numerical stress results of the bottom steel reinforcement for the unstrengthened RC beam (specimen RC_AT) at 100 mm deflection

Regarding the failure modes of the CFRP-strengthened beam at ambient temperature, that was characterized by the debonding of strengthening system in the CFRP-concrete bond region, a good agreement between the numerical and the experimental failure modes was noticed, as shown in Figure 5.39a and Figure 5.39b, respectively. Furthermore, the deformed shape of the strengthened beam at the CFRP failure instant was precisely predicted by the FE model, as noticed in Figure 5.40. Similarities regarding the cracking along the cross-section of the strengthened specimen were also numerically estimate successfully as shown Figure 5.41.

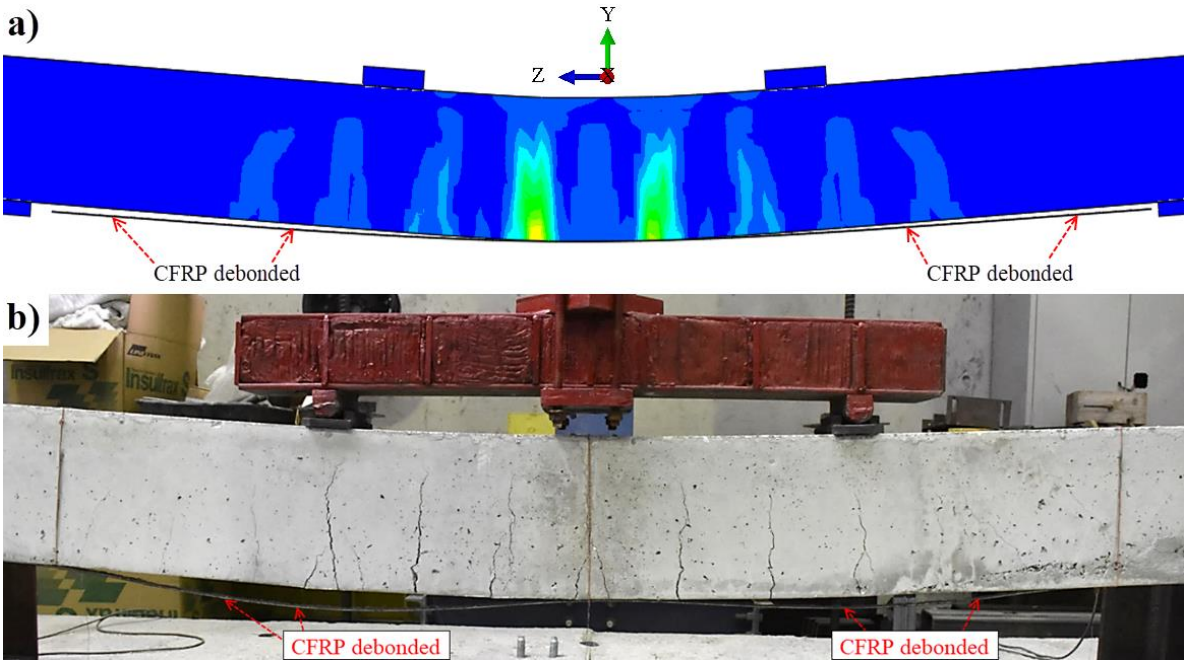

Figure 5.39 – (a) Numerical (b) and experimental failure modes for the CFRP-strengthened RC beam (specimen CFRP_AT) after the laminate collapse

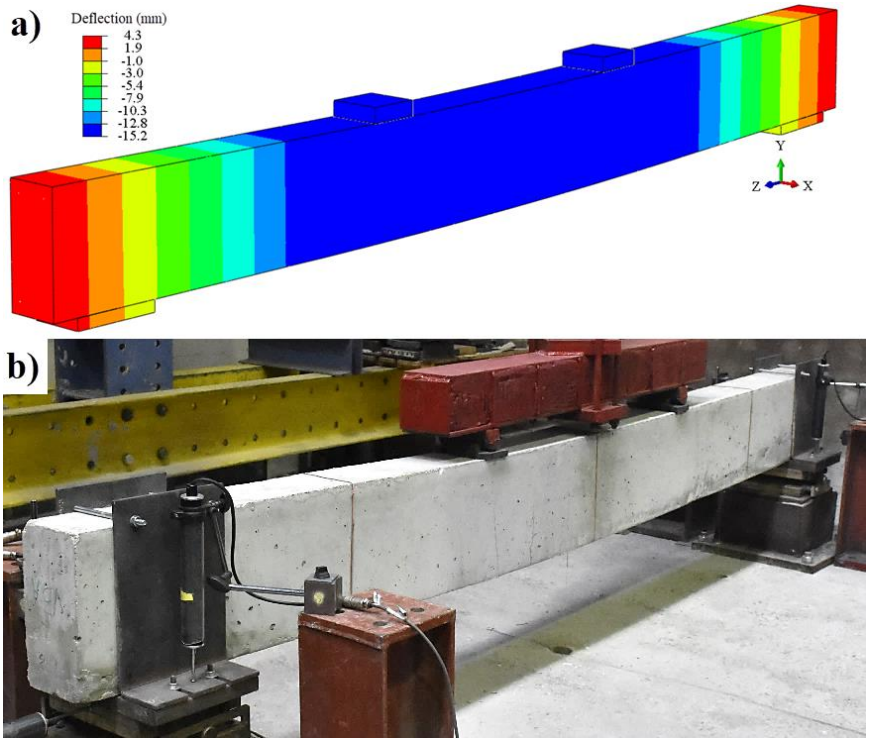

Figure 5.40 – (a) Numerical (b) and experimental deformed shape for the CFRP-strengthened beam (specimen CFRP_AT)) at the CFRP failure instant

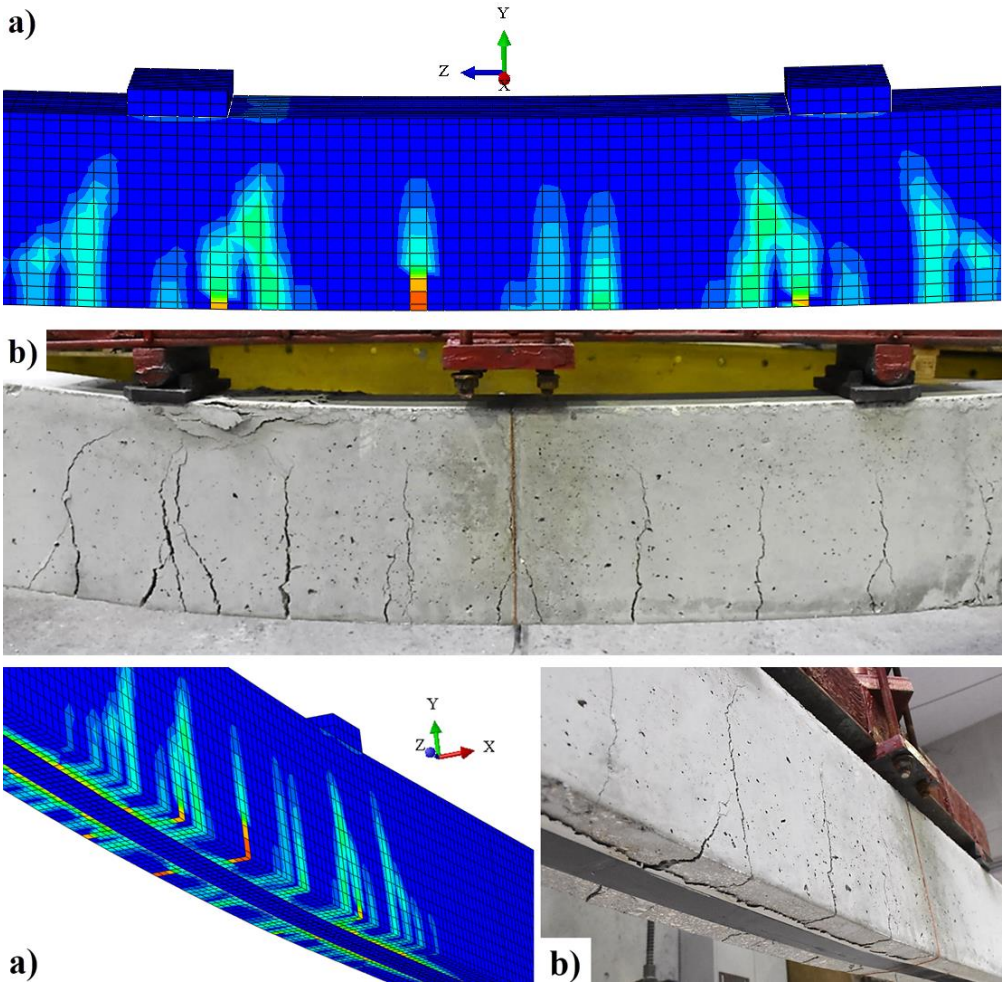

Figure 5.41 – (a) Numerical (b) and experimental cracking along the cross-section of the CFRP-strengthened beam at the CFRP failure instant

The results above presented confirm that the finite element models predicted the failure modes of unstrengthened and CFRP-strengthened beams with good precision, attesting their consistency to simulate the mechanical response of this type of structures at ambient temperature. Furthermore, the mechanical validation of the model at ambient temperature allowed to assess the FE model to mechanical analyses under fire conditions (Section 5.8.2).

5.8.4 Heat transfer analysis

The suitability of 2D thermal models developed using the heat transfer option available in Abaqus was assessed in this section. The purpose of this numerical approach was to determine the appropriate modelling parameters, in particular, especially the input thermal boundary conditions and material thermal properties, so that standard fire resistances tests of unstrengthened and CFRP-strengthened RC beams can be simulated.

The 2D models were developed based on the tested cross-sections of the beams, including the modelling of the concrete slab cross-section in order to maintain the fidelity of the thermal interactions between the surrounding elements, as intended in the experimental study (cf. Section 4). Four representative heat transfer models (Figure 5.42a-d), analogous to the experimentally tested beams (including both unstrengthened and CFRP-strengthened beams, fire-protected by different passive materials) and corresponding to references RC, EC-35, OP-35 and VP-35 (listed in Table 4.2 of the Fire Resistance Test Program, Section 4.3.2), were numerically simulated under fire conditions. The predicted results of these simulations (Num.) were compared with the experimental data obtained in this investigation (Exp.) in terms of temperatures in relation to time of fire exposure at different locations of the mid-span cross-section (Section S1, cf. Figure 4.4). To allow comparison between results, the same thermocouples nomenclature and location used in the experimental study was defined in the current heat transfer analysis, as shown in Figure 5.43a and Figure 5.43b for the unstrengthened and CFRP-strengthened beams, respectively.

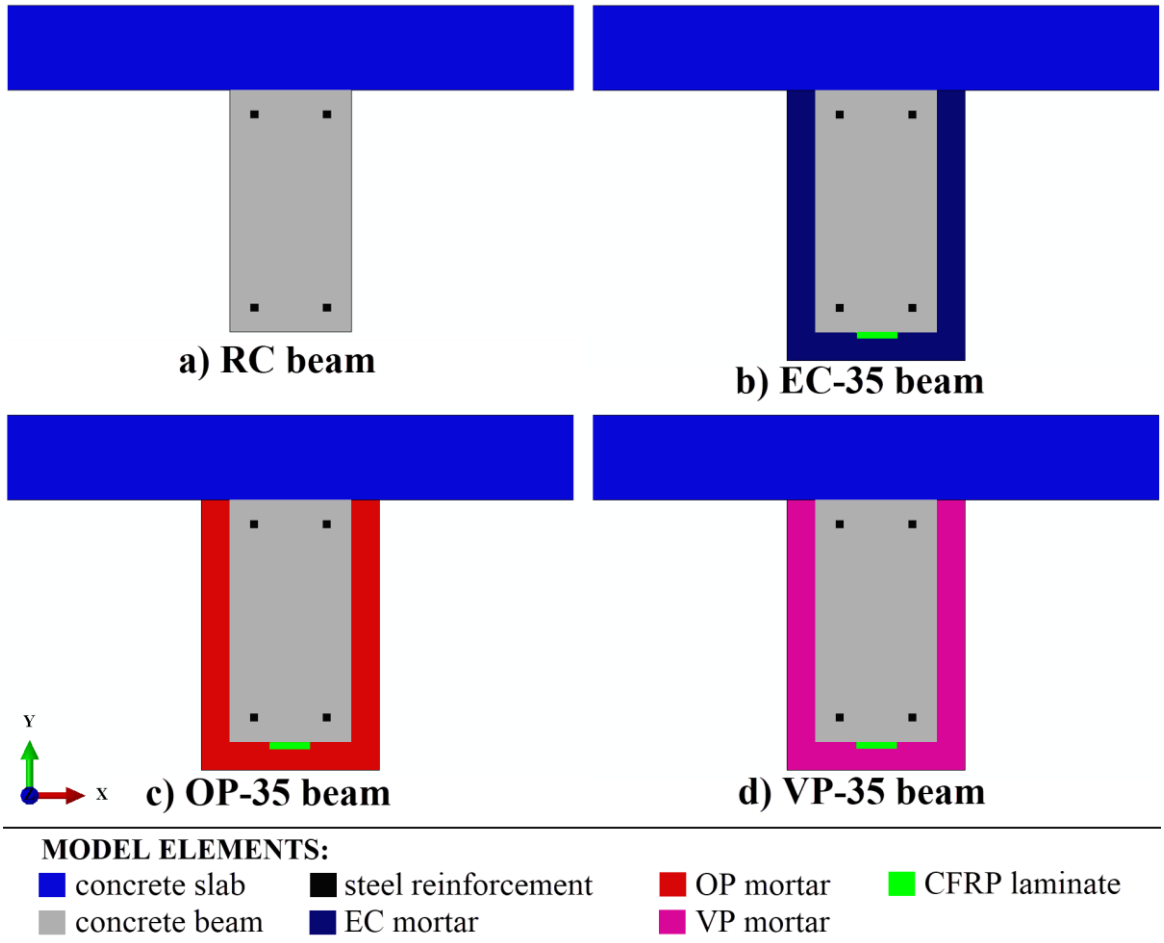

Figure 5.42 – Numerical models for heat transfer analysis: (a) RC beam, (b) EC-35 beam, (c) OP-35 beam and (d) VP-35 beam (not to scale)

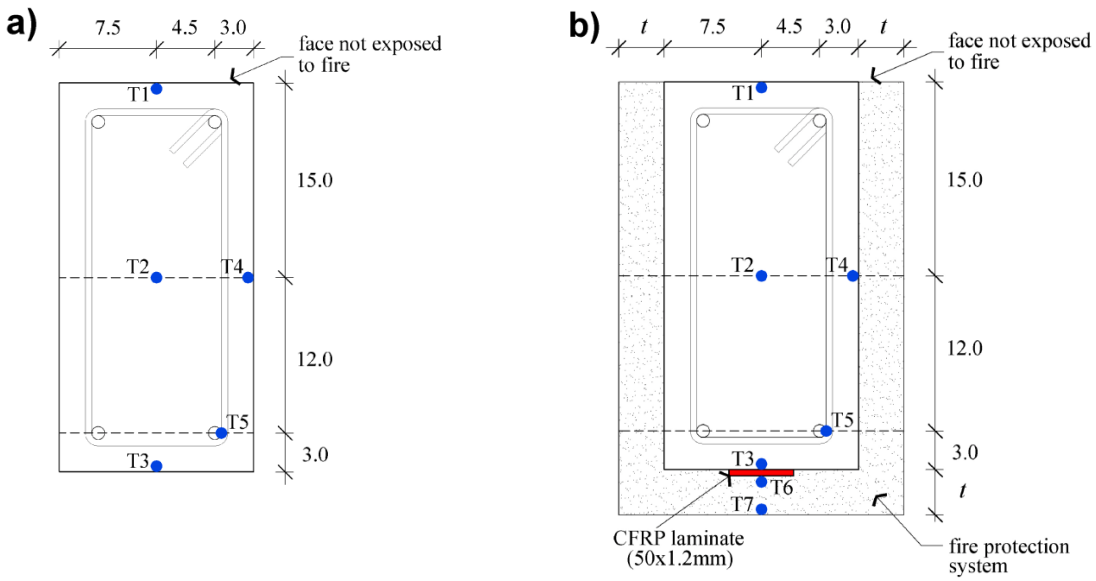

Figure 5.43 – Location and nomenclature of thermocouples at Section S1 of (a) unstrengthened and (b) CFRP-strengthened RC beams (not declared units in cm)

It should be also noted that a uniform temperature distribution along all beam length was intended for the validation study, in contrast to the tested beams in the Laboratory. Moreover, in order to calibrate FE model for fire simulation of CFRP-strengthened RC beams, the furnace fire curve data registered from the FR tests (cf. Section 4) were used. Note that the emissivity, the heat transfer and the thermal contact conductance coefficients were constant with temperature evolution. The radiative heat flux was calculated as 0.49 using an emissivity of 0.7 for fire and 0.7 for the concrete surface. The Stefan-Boltzmann constant was defined as 5.67×10^{-8} W/m^{2}K^4.

Figure 5.49, Figure 5.50 and Figure 5.51 show respectively the comparison between experimental (Exp.) and predicted (Num.) temperatures as a function of fire exposure time for the different thermocouples at mid-span (cf. Figure 5.43b) of the CFRP-strengthened beams fire-protected by 35 mm thick of EC, OP and VP mortar (referred as EC-35, OP-35 and VP-35, respectively). The temperature vs. fire exposure time evolution for the different thermocouples (cf. Figure 5.43a) of the unstrengthened and unprotected RC beam (referred as RC) is shown in Figure 5.48. In addition, the numerical temperature gradients (thermal fields) in the aforementioned sections of the beams at (a) 5 and (b) 20 minutes of simulations are shown in Figure 5.44, Figure 5.45, Figure 5.46 and Figure 5.47. The thermal fields at (c) collapse instant of the beam (in the case of RC beam; Figure 5.44c) or the respective fire protection material (in the case of the strengthened beams; Figure 5.45c, Figure 5.46c and Figure 5.47c) are also illustrated in the figures below.

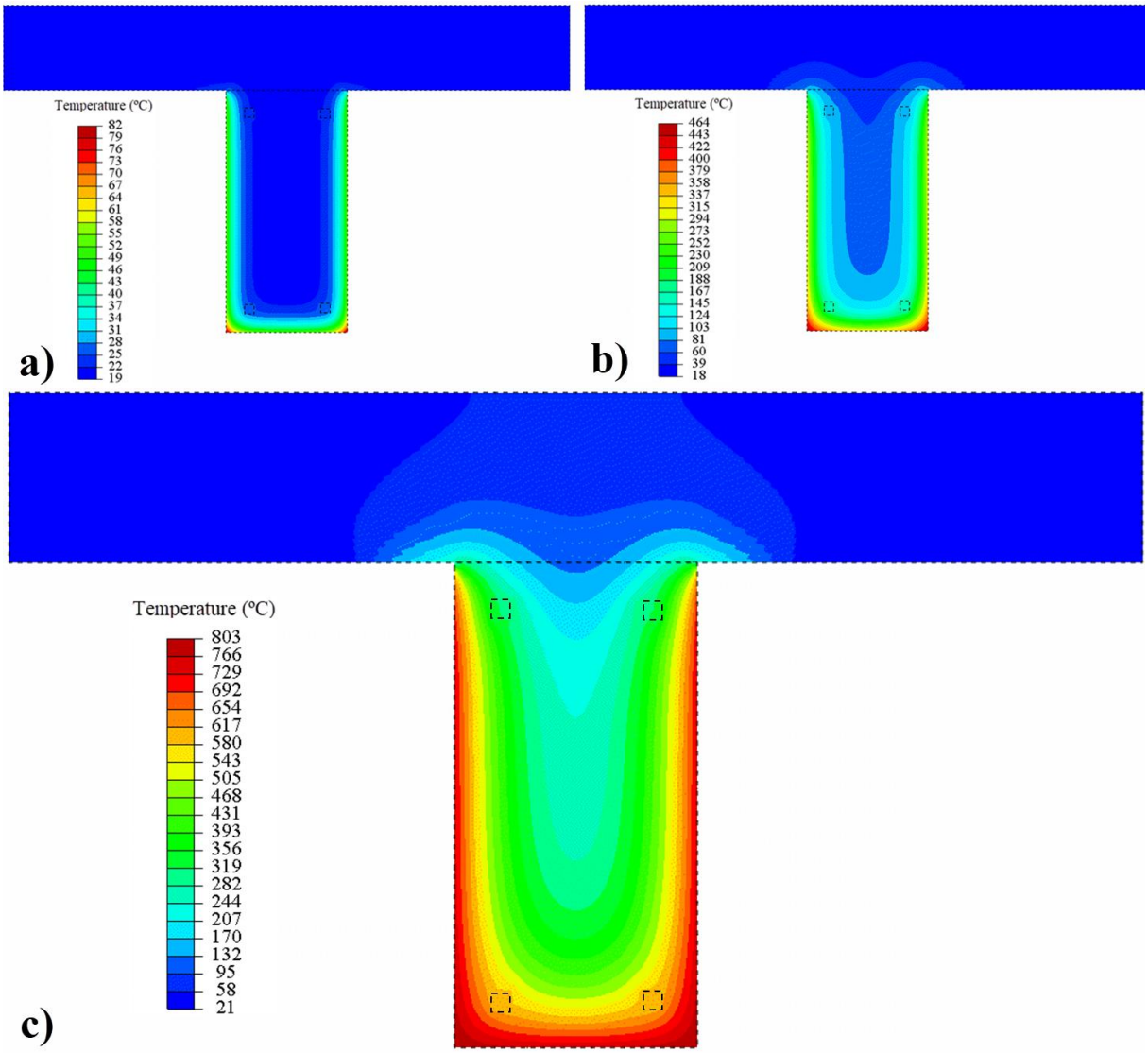

Figure 5.44 – Numerical thermal fields in the cross-section of the RC beam for a fire exposure time of (a) 5 min, (b) 20 min and at (c) the failure instant of the beam (78.2 min)

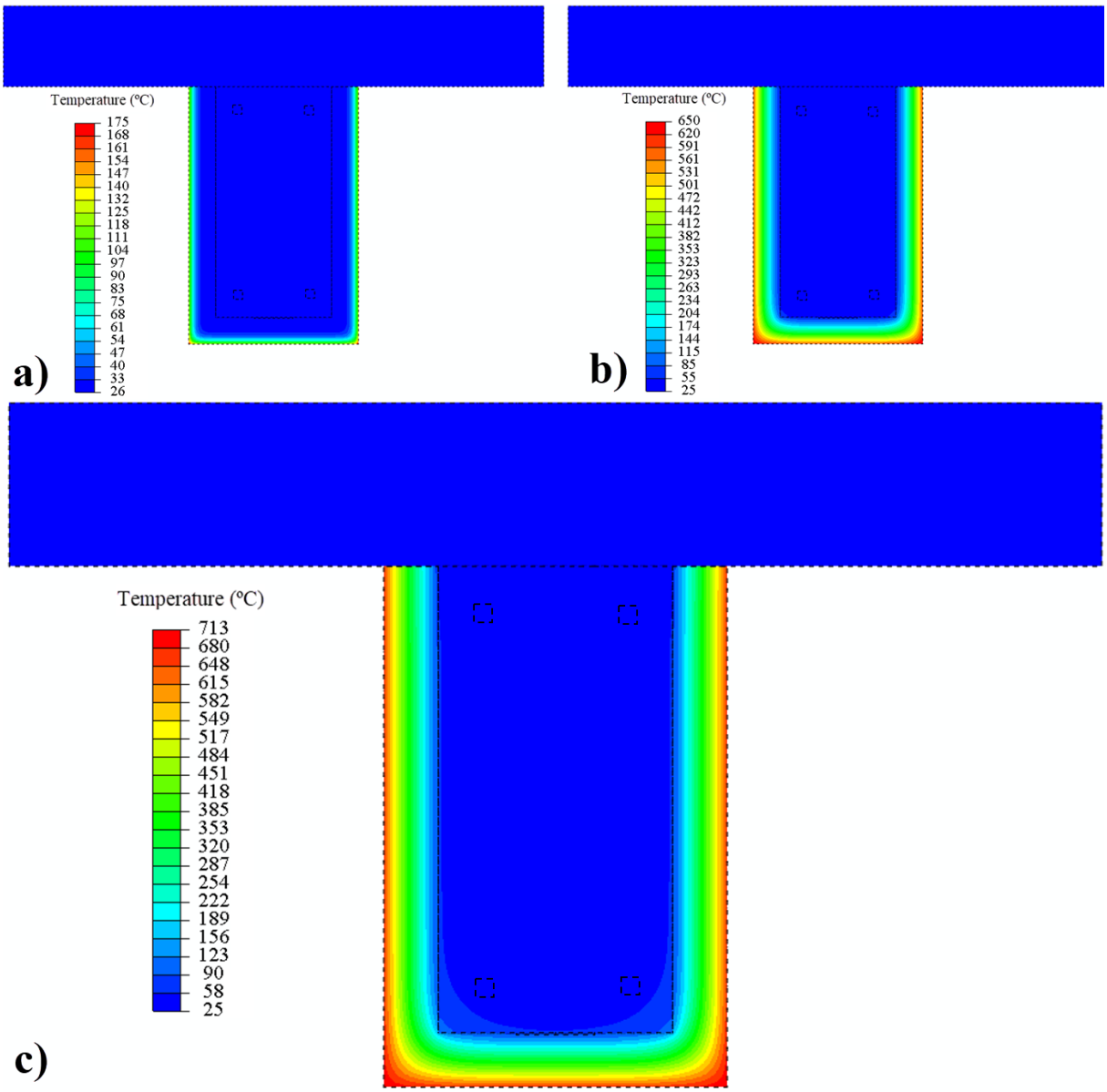

Figure 5.45 – Numerical thermal fields in the EC-35 beam's cross-section for a fire exposure time of (a) 5 min, (b) 20 min and at (c) the failure instant of protection system (25.9 min)

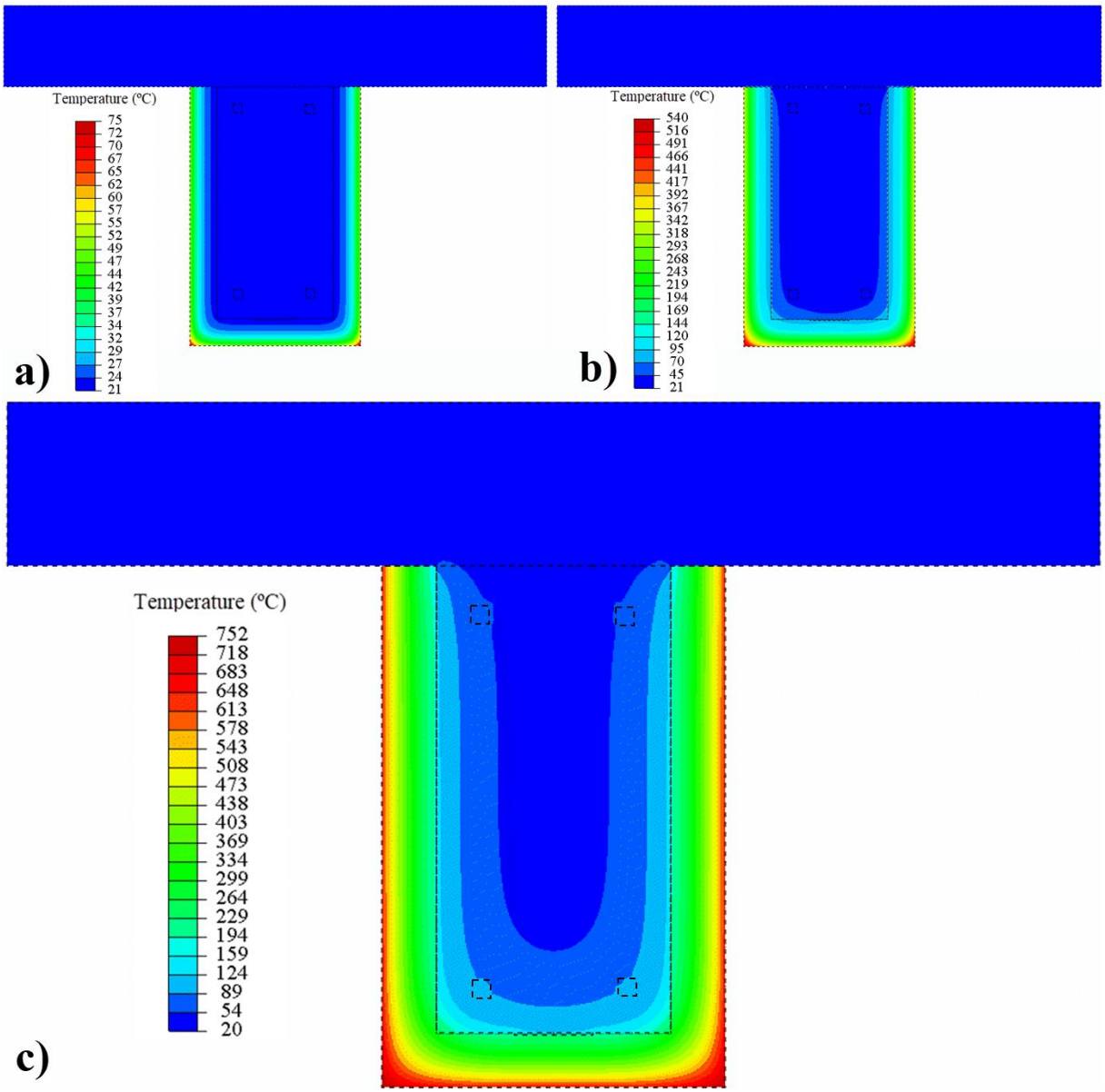

Figure 5.46 – Numerical thermal fields in the OP-35 beam's cross-section for a fire exposure time of (a) 5 min, (b) 20 min and at (c) the failure instant of protection system (39.8 min)

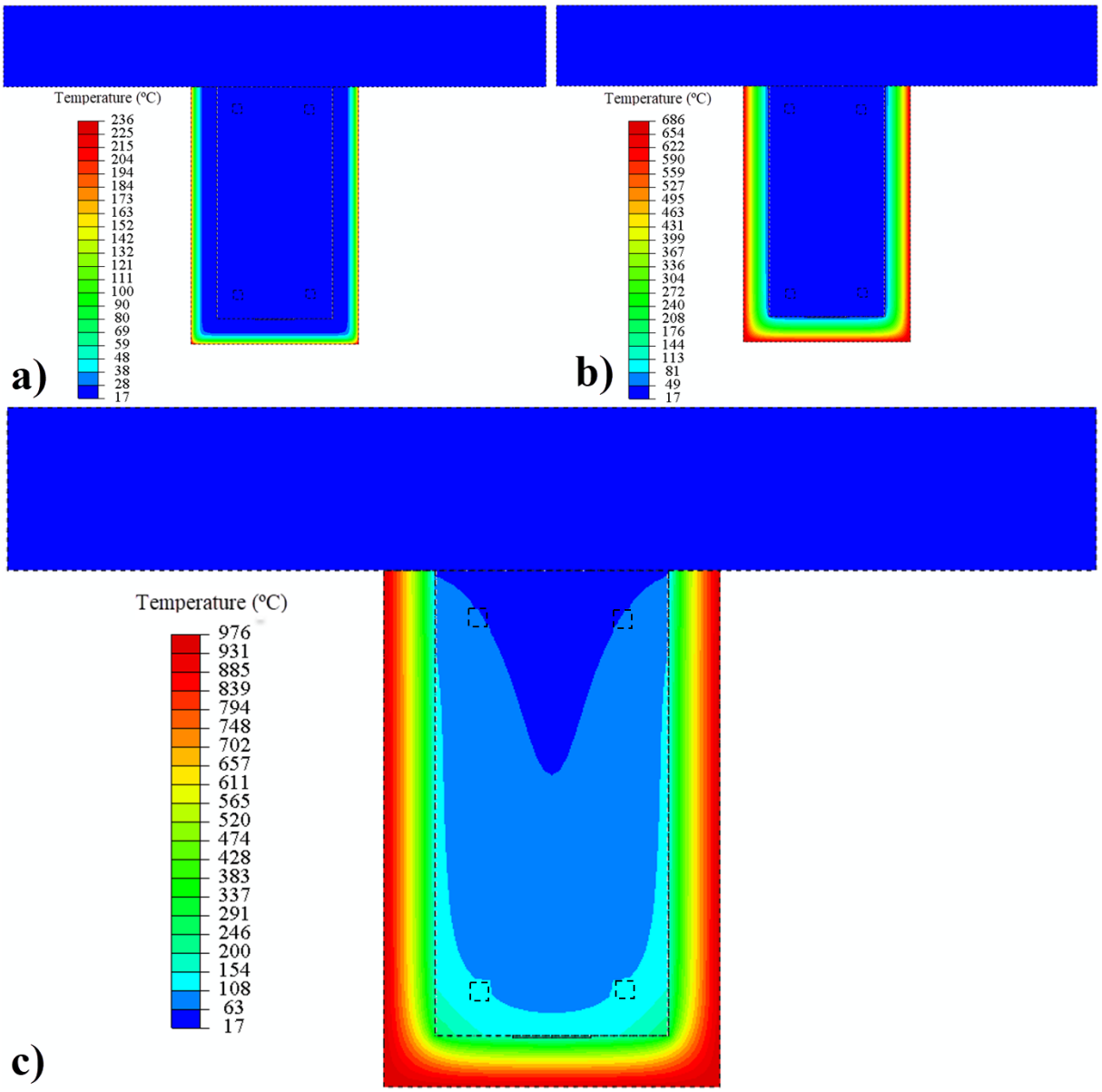

Figure 5.47 – Numerical thermal fields in the VP-35 beam's cross-section for a fire exposure time of (a) 5 min, (b) 20 min and at (c) the failure instant of protection system (84.9 min)

For an exposure time of 20 min, a large temperature gradient was obtained in all models especially at the ends of the beams with a lower and uniform temperature in the interior region of the cross-section, as it can be seen in Figure 5.44-Figure 5.47. This gradient is consistently higher at longer exposure times, i.e., near to the collapse instant of the beam or fire protection system. For example, in VP-35 beam, considering a fire exposure time of 84.9 min (protection system failure instant), the temperature gradient was of 959 ºC. The difference is quite notable mainly at the region between the external surface and near the end of concrete cover. The gradient was also elevated for the other strengthened beams that were protected by EC and OP

mortar, corresponding to 688 ºC and 732 ºC at the protection system failure instant, respectively. These large temperature gradients were due to the fact that the effectivity of the fire protection system in avoiding heat dissipation to the interior of the beams and, especially in the case of the RC beam, due to the concrete thermal performance. In the RC beam, the thermal gradient was also elevated (782 ºC), but with a smoother and more uniform distribution along the cross-section, since in this case there was no passive fire protection.

It is worthwhile mentioning that the temperature evolution in the CFRP-strengthened RC beams was presented in Figure 5.49, Figure 5.50 and Figure 5.51 only until the collapse instant of the respective fire protection material (cf. tf_{ps} in Table 4.3), since the results after that time are negligible for the purpose of this numerical study. Regarding the RC beam, the results were plotted in Figure 5.48 until the collapse of the beam.

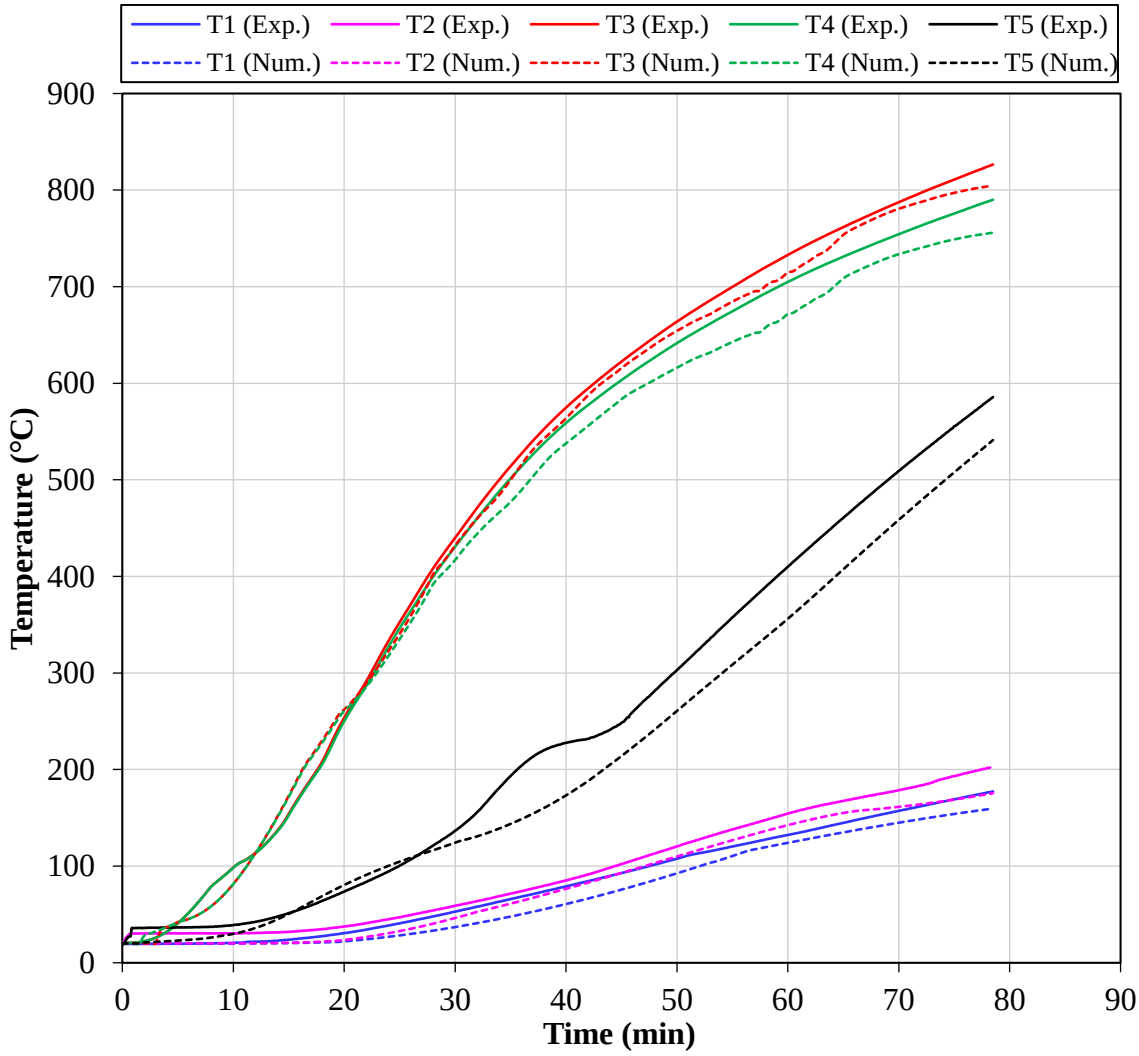

Figure 5.48 – Experimental (Exp.) and predicted (Num.) temperatures vs. fire exposure time curves at different points of the RC beam's mid-span cross-section

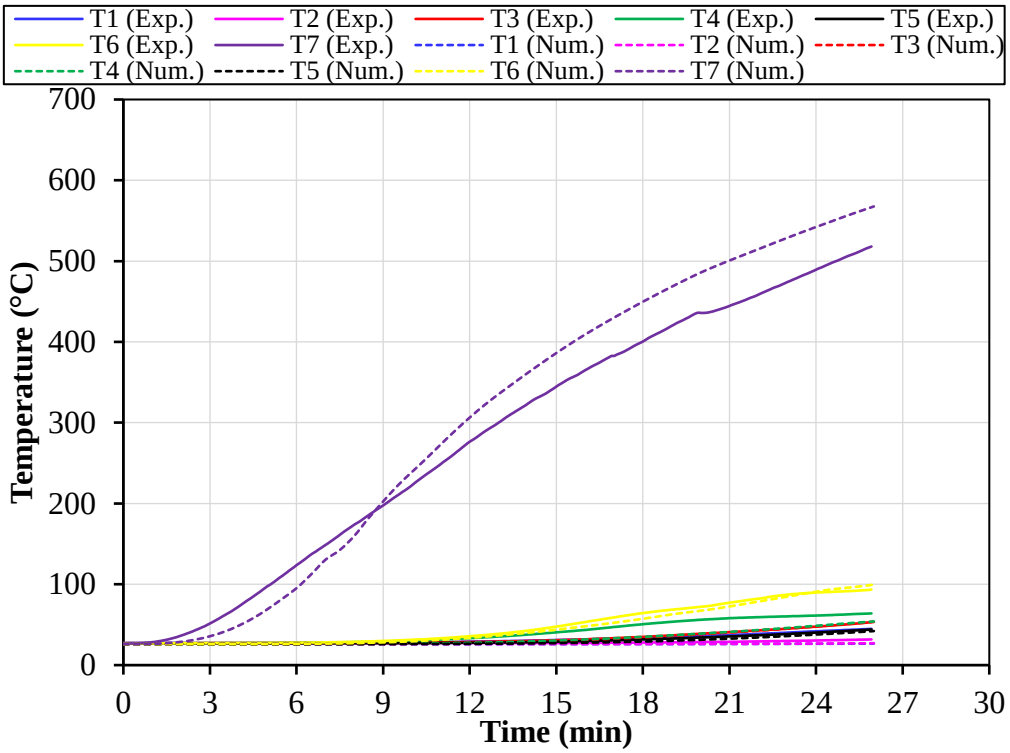

Figure 5.49 – Experimental (Exp.) and predicted (Num.) temperatures vs. fire exposure time curves at different points of the EC-35 beam's mid-span cross-section

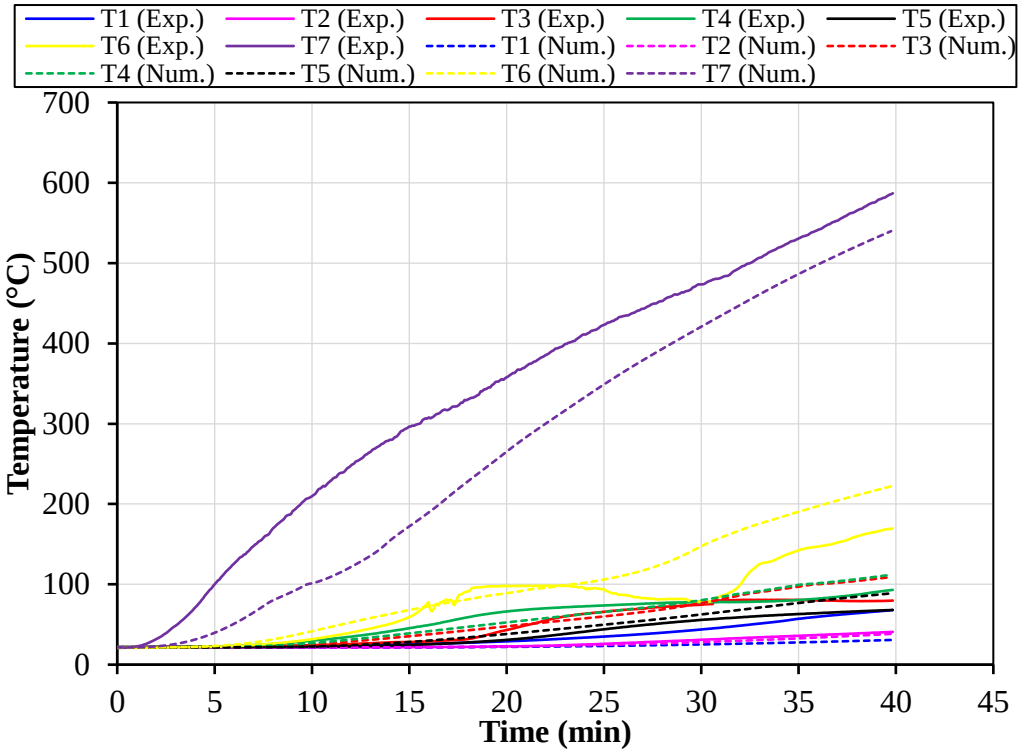

Figure 5.50 – Experimental (Exp.) and predicted (Num.) temperatures vs. fire exposure time curves at different points of the OP-35 beam's mid-span cross-section

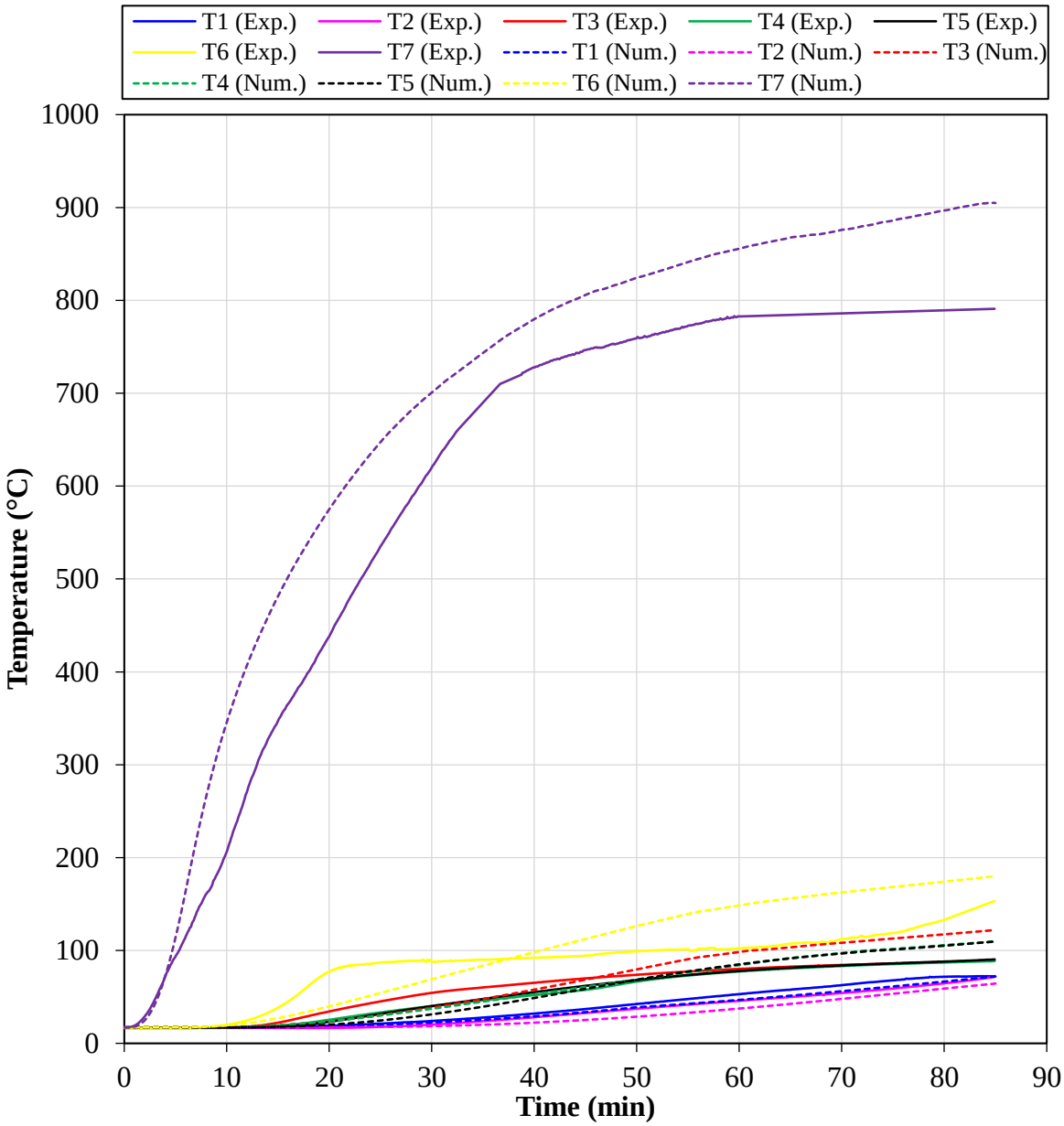

Figure 5.51 – Experimental (Exp.) and predicted (Num.) temperatures vs. fire exposure time curves at different points of the VP-35 beam's mid-span cross-section

Overall, all FE models provided a good agreement with the experimental results of the temperatures evolution in the corresponding beams, as noticed in the Figure 5.48 to Figure 5.51.

With exception of thermocouples T6 and T7 (positioned on the bottom surfaces of the laminate and the fire protection material, respectively) for the strengthened beams protected by OP and VP mortar, all other temperature distribution at different points of the cross-section were accurately predicted by the models. Relative (small) deviations between experimental and

numerical temperatures in T6 and T7 of the OP-35 and VP-35 beams were observed, as depicted in Figure 5.50 and Figure 5.51. This may be due to differences between the actual thermal properties at elevated temperature of the particular materials used in the beams (concrete, CFRP laminate, fire protection materials) and those considered in the FE models. In addition, the interaction of these materials with hot air and in contact with each other, such as the contact concrete-CFRP-fire protection material, makes an accurate numeric representation for temperature evolution at these specific section points more difficult. The divergence can also be attributed to the high heat consumption during the evaporation of free water in the concrete and other materials (common in fire situations) and this effect is often difficult to capture by the (input) thermal properties of the numerical model. In spite of that, the FE models were still able to simulate the thermal behaviour tendency with a relative consistency in the above-mentioned thermocouples. Concerning the strengthened EC-35 and RC beams (Figure 5.48 and Figure 5.49, respectively), the numerical temperature results by the heat transfer analysis presented an excellent convergence with the experimental measurements for all thermocouples.

The comparison between the predicted and experimental results of the temperatures at the CFRP-concrete interface when the fire protection system collapsed (Tf_{PS}) were described in Table 5.4. An excellent accuracy was obtained from the heat transfer analysis for the CFRP-strengthened beam fire-protected by EC mortar (EC-35 specimen) compared to the experimental results. In the experimental model, the fire protection system failed when the temperature at the CFRP-concrete interface achieved 53.3 ºC, while a fit close temperature of 53.4 ºC was predicted for the numerical model. These results corresponded to a precision of 100% of the FE the models to predict the Tf_{PS}. However, significant deviations between the experimental and numerical results were noticed in the beams protected by the OP and VP mortar (OP-35 and VP-35 specimens, respectively). A Tf_{PS} of 79.8 ºC and 109.1 ºC was experimentally and numerically achieved for the OP-35 beam, respectively. For the VP-35 beam, the Tf_{PS} values were 89.7 and 122.0 for the experimental and numerical models, respectively. Therefore, an error around 35% between the experimental and numerical models for Tf_{PS} results of both OP-35 and VP-35 beams was noticed. The deviations observed in the specimens OP-35 and VP-35 probably were due to the significant differences in thermal proprieties found in the contact between the CFRP and fire protection materials since their accurately representation in numerical modelling is a challenge.

Table 5.4 – Experimental (Exp.) and predicted (Num.) temperatures at the CFRP-concrete interface when the fire protection system collapsed (Tf_{PS})

Test reference	Tf_{PS} (ºC)		Tf_{PS} ratio at failure instant of the fire protection system
	Exp.	Num.	
EC-35	53.3	53.4	1.00
OP-35	79.8	109.1	1.37
VP-35	89.7	122.0	1.36

To sum up, the tools of Abaqus program for the application of thermal actions allowed simulating the phenomenon of heat transfer between hot air and composite structural elements with satisfactory results. Despite the above-mentioned deviations, all models overall provided a good estimate between the experimental and numerical results, confirming the ability of the FE models to accurately simulate the thermal response of unstrengthened and EBR-CFRP-strengthened RC beams subjected to fire, even when using complex and different fire protection materials.

5.8.5 Final Remarks

A numerical investigation into the behaviour of CFRP-strengthened and unstrengthened RC beams under flexural conditions at ambient temperature and subjected to a combined state of flexural loading and fire have been presented here. The main purpose of the numerical modelling was to simulate as faithfully as possible the mechanical and thermal response and the failure modes of this type of beams such as the ones observed in the beams previously tested by the author in Laboratory.

As noticed in this chapter, a good agreement between the experimental and numerical results was obtained in terms of mechanical response under ambient and fire conditions as well as between the respective failure modes of the beams. Moreover, the application of thermal actions also allowed simulating the phenomenon of heat transfer between air and structural elements, as well as with the surrounding building slab initially proposed in the experimental phase, presenting satisfactory results. The use of elements with finite element mesh of 25 x 25 mm provided very accurate results, as well. Therefore, these satisfactory results proved that the developed finite element models may be a reliable tool to predict accurate results.

Finally, it is also concluded that the use of material and geometric nonlinear finite element analysis is required for solving such highly nonlinear problems involving composite structures, high temperatures and contact. The behaviour of such members or structures may be very

complex, especially in case of fire and under particular boundary conditions. The computational modelling has thereby a strong role to play in the research and design of such structures.

6 CONCLUSIONS AND FUTURE WORK

6.1 Experimental Analysis on CFRP-concrete Bond

An experimental investigation on the bond behaviour between the concrete and a CFRP strengthening system at ambient and elevated temperatures have been presented and discussed in the current research. The specimens were subjected to different temperature series, addressing heating levels below, near, higher or much higher than the T_g of the adhesive (quoted as 75 ºC). A total of twenty-one SST tests at elevated temperatures and under steady state conditions were performed. Based on the results, the following conclusions may be drawn:

- Regarding the bond strength, a continuous reduction with the increasing temperature was observed. A reduction of 5% was observed at 40 °C, 40% at 65 °C (near the T_g of the adhesive), 66% at 90 °C (above T_g), 79% at 115 ºC and 89% at 140 ºC (much higher than T_g) was noticed. However, a significant residual bond strength was observed for temperatures of the bond interface higher than the T_g, where a retention of 34%, 21% and 11% was obtained for the temperature series of 90 °C, 115 °C and 140 °C, respectively. These results confirmed that an important residual bond strength was retained for temperatures considerably higher than the glass transition of the epoxy adhesive. Therefore, based on these results it can be concluded that the T_g cannot mean the ultimate temperature of the CFRP-concrete interface. For practical applications, these results indicate that it could be possible to define a temperature limit for the adhesive in the CFRP-concrete interface much higher than the T_g for service conditions in the current concrete structures (depending on the stress level installed on the strengthening system). Results observed for the fire resistance tests carried out on CFRP-strengthened RC beams under flexural conditions (in Section 4) confirm this conclusion. The debonding of the strengthening system occurred in these tests for temperatures above the T_g of the adhesive.

- The axial strains along the CFRP-concrete bonded length were significantly affected by the temperature. A typical non-linear behaviour of the axial strains at the bond was noticed for specimens at normal temperatures (ambient and 40 °C) and a smoother and more uniform evolution (close to linear) were observed for specimens exposed to elevated temperatures (65 °C to 140 °C). The stiffness reduction of the adhesive with increasing temperature explains this observation, promoting a more uniform distribution of shear stresses along the bonded length.

- The increasing temperature affected the transfer stress length on the specimens. At ambient temperature, it corresponded to the bonded length, while for temperatures series varying from 40 °C to 140 °C it exceeded the bonded length.

- All tested specimens presented a load-displacement evolution approximately linear with an initial non-linear elastic domain in the shear behaviour. The failure load and the maximum deflection was continuous and severally affected by the increasing temperature. Moreover, the specimens presented a brittle rupture, losing completely and immediately their strength at failure.

- After the SST tests, the failure modes of the specimens at ambient temperature and 40 °C occurred in the concrete substrate along the bonded length area. For the specimens exposed to higher temperatures (65 °C to 165 °C) the failure mode occurred in the adhesive at the CFRP-concrete interface.

- These experimental results along with the ones for CFRP-strengthened RC beams provide data for validating the numerical models that were developed by the authors and are described in detail in Chapter 5 of this thesis.

- Finally, the results achieved in this investigation are fundamental to a better understanding of the CFRP-concrete bond behaviour at elevated temperatures, particularly concerning to its behaviour at temperatures above T_g of the adhesive. It can be concluded that residual bond strength phenomenon noticed in the current investigation at temperatures higher or much higher than T_g is very relevant in the effectiveness of the CFRP strengthening system and must be considered in their fire design. In addition, these results confirm the conservatism of the current standards in this regard, where they merely define the critical temperature of the system by the T_g of the adhesive or, in an oversimply way, recommend not consider the effectiveness of the strengthening system in a fire situation. These reported experimental data are valuable and can be useful for the review and improvement of the mentioned standards or still for creating new rules, documents or calculation methods for guiding the fire design of these structures.

6.2 Experimental Analysis on CFRP-strengthened RC beams

This thesis presented and discussed the results of an experimental investigation on the flexural behaviour of CFRP-strengthened RC beams subjected to fire. A total of twelve four-point bending tests under ambient and high temperatures has been carried out, including

unstrengthened and CFRP-strengthened beams. Based on the results the following conclusions may be drawn:

- The fire resistance tests on specimens confirmed the vulnerability of the CFRP strengthening systems when directly exposed to fire. This could be observed by the sudden failure of the strengthening system immediately after the collapse of the fire protection system. This fact confirmed the limited fire behaviour of the bond in these systems and the need of their fire protection, which in turn is a zone very sensitive to thermal variation.

- The CFRP strengthening system failed at temperatures above T_g of the adhesive. The bond between the CFRP and the concrete is severely affected for this temperature conditions (ranging from 85 to 110 ºC), losing its bond strength.

- The use of passive fire protection delayed the increase of temperature in the CFRP-concrete interface confirming its importance in the increasing of the fire resistance of the beams. It was observed that in all fire protection systems tested the thicker insulations were more effective in the thermal response of the specimens, keeping the effectiveness of the CFRP strengthening system for a longer period of fire exposure. As a result, the mechanical resistance of the strengthening system and the assembly had their capacity extended.

- The VP mortar was significantly more effective than the EC and OP mortars in the fire protection of the CFRP strengthening system, preserving their integrity for longer periods of time. For the same thickness of fire protection material, the beam VP-50 (50 mm thick) presented 120.3 min of fire protection to the strengthening system, while the beams OP-50 and EC-50 (both also with 50 mm thick) presented 51.7 min and 31.2 min, respectively. This represented an increase on fire resistance of CFRP system of 133% and 286% in comparison to the beams OP-50 and EC-50, respectively. Similar result was observed for the other thicknesses tested. The better performance of VP mortar in terms of fire resistance compared to the others tested was due to the low thermal conductivity of the vermiculite-perlite material and the good mechanical properties of the mortar. Regarding the EC mortar, in what concerns to the fire protection of the strengthening system, a premature loss of effectiveness occurred in comparison with the other systems. This was due to low capacities of its mechanical properties and surface adherence, although this material has a quite low thermal conductivity. Although this system failed early, it presented an excellent fire behaviour during its serviceability period, maintaining the temperatures low and at a heating rate almost null in the cross-section of the

specimens. For this reason, it is important to foresee a technical solution in order to avoid the premature fall of the protection, particularly if the thickness of the fire protection is important. The use of a steel wire netting or the incorporation of steel or polymeric fibres into the mortar composition as a mechanical as mechanical improvement could be a good solution to delay this phenomenon and could validate this material as a high-performance fire protection system, but new tests would be needed to confirm this hypothesis.

- After failure of the strengthening system, the beams remained resisting to the applied load and, subsequently, they presented a mechanical behaviour similar to that of a RC beam once again.

- The CFRP-strengthened RC beam had a significantly higher resistance to the fire exposure than the RC beams. This is justified by the insulation provided by the passive fire protection materials.

- An important contribution in the flexural capacity of the RC beam was provided by the CFRP strengthening system, preserving its serviceability condition to higher loading levels compared to the unstrengthened RC beams.

- The final deformed shape of the specimens after fire test has occurred predominantly at mid-span of the beams due to tensile rupture and excessive elongation of the bottom rebars. These results confirmed a typical behaviour in fire of an axially non-restrained RC beam.

- The surrounding slab may have exerted an influence on the thermal heating and mechanical response of the tested beams. The concrete slab promoted an almost adiabatic surface which altered the heating and temperature profiles on the cross-section of the tested beams. The contact of the beam with the concrete slab generated thermal gradients in the cross-section of the beam that may have influenced the results of the tf_{CFRP} and tf_{beam}. Therefore, the effects of the contact of the strengthened elements with the surrounding building elements should be taken into account in their behaviour in case of fire.

- Finally, these experimental tests provided valuable data for the validation of the numerical models which were developed by the authors.

6.3 Numerical Analysis

The structural behaviour of RC beams flexurally strengthened with CFRP laminates bonded according to the EBR technique and unstrengthened RC beams was numerically investigated in this thesis. Finite element models capable of simulating the mechanical and thermal response of simply supported unstrengthened and CFRP-strengthened RC beams both under ambient and fire conditions were developed and described in the current research. The thermal interaction of these specimens with the different fire protection systems as well as with a building surround element was taken into account in the fire simulations. A series of numerical simulations using the finite element software Abaqus has been performed. The results obtained from the numerical study presented herein allow to draw the following conclusions:

- The thermal response of the fire-protected CFRP-strengthened RC beams subjected to high temperatures was accurately predicted by the FE models, similarly to the heat transfer analysis of the unprotected and unstrengthened RC beam. Moreover, the modelling of the surrounding building slab allowed to represent the thermal interactions and influence between the elements as faithful as possible, providing a better predicting of the experimental results and, consequently, more realist.

- Concerning the prediction of the mechanical response at ambient temperature, the 3D models presented a satisfactory accuracy for both unstrengthened and CFRP-strengthened RC beams, especially for estimating the ultimate load capacity.

- The developed finite element models also estimate with precision the mechanical response of unstrengthened and CFRP-strengthened RC beams simultaneously subjected to a flexural load and high temperatures. An accuracy of about 91% and 95% was respectively achieved by the numerical models that represents the RC and CFRP-strengthened RC beams, compared to the experimental results in terms of failure instant.

- The FE models confirmed that the materials used as fire protection system contributing to the fire performance of the CFRP-strengthened RC beams, either by preservation of CFRP-concrete bond for longer exposure time or by keeping lower temperatures in the interior of the beams and steel reinforcement zones. As a result, it increased the mechanical effectiveness of the EBR-CFRP strengthening system, as proved in the simulations at high temperatures.

- The failure modes of the beams and the aspects after test were also estimated with accuracy by the finite element models. The predictions of deformed shape, failure and

cracking aspects, stresses on the steel reinforcements and, especially, the CFRP failure aspect in the strengthened beams, were very similar to the ones observed in the experimentally tested models.

- Finally, the presented results confirmed the validity of the developed FE models and strongly guarantee an accurate prediction of the mechanical response of both strengthened and unstrengthened RC beams at ambient and high temperatures. They also confirmed the capacity of the models to estimate the thermal performance of these structures along with the use of different fire protection materials. Furthermore, it is still possible to stated that this developed FE models can be used as a valuable auxiliary tool for the design of fire protection systems for CFRP-strengthened RC structural members or in parametric studies outside the bounds of experimental field, as well as provide safe and economical structural solutions for these type of structures in fire situations.

6.4 Future Work

The use of different types and dimensions of CFRP, adhesives with different T_gs, types and geometries of passive protection systems, imperfections and the high sensitivity of the CFRP-concrete bond, as well as the interaction between these different elements, make the full understating of the mechanical and thermal behaviour of reinforced concrete structures externally strengthened with CFRP materials a great challenge to researchers. In the previous sections of this chapter, the most important conclusions of the research were presented. However, some aspects addressed there, if investigated in greater depth, could contribute to a better understanding of the fire response of this type of structures and to the development of more effective protection systems. This PhD thesis is a step in the right direction, but there is still much more to be done and discovered. Some relevant aspects that may be considered or in-depth in future work, along with the gaps in this field of knowledge that need further investigation are addressed below:

- The FE models developed in this thesis has the potential to be used in parametric studies, testing several other factors that were not used in the experimental models and that potentially affect the fire behaviour of the CFRP-strengthened RC beams as follows: the load level and rate applied on the specimens, the different type and thickness of the fire protection materials, the effect of surrounding elements and boundary conditions, the geometry of the beams, the fire performance of strengthening and adhesive materials, among others.

- The author also suggests as future work the development of a suitable analytical guidance in the fire design of CFRP-strengthened RC beams based on the experimental and numerical data reported in the current thesis and the results of new parametric studies. The numerical simulations will enable the development of design methods and possibly best application techniques for these strengthening systems.

- Experimental tests of EC mortar in CFRP-strengthened beams combined with the use of steel wire netting or the incorporation of steel or polymeric fibres into the mortar composition as a mechanical enhancement could validate this material as a high-performance fire protection system, since it has a good fire performance and low mechanical capacity as noticed in fire resistance tests. The development of new fire protection materials is also important to contribute to the advance of technology and fire performance of buildings and to promote increased fire safety of structures in the future.

- It is also important to promote an extensive investigation of existing and recent bonding adhesives with the purpose of developing a standard for these materials. As a result of this study, it would be possible to create working temperature classes for the different adhesives found in civil construction based on the minimum T_g values and their respective mechanical properties at this temperature. Although CFRP-strengthened structures' fire design is more complex than simply focusing on a single component of the strengthening system, the abovementioned suggestion would provide greater clarity and safety in fire designs by engineers and could provide interesting data for review of the current design rules.

- Finally, all these studies might contribute to a future revision and improvement of the standards relative to the fire design of the CFRP-strengthened concrete elements, such as EN 1992-1-2 [1], or to the creation of a new document associated with these standards, fulfilling a gap in the structural concrete engineering.

REFERENCES

[1] EN 1992-1-2. Eurocode 2: Design of concrete structures - Part 1-2: General rules - structural fire design. vol. 2. Brussels, Belgium: European Committee for Standardization (CEN); 2004.

[2] FIB. Bulletin 14: Externally bonded FRP reinforcement for RC structures. Lausanne, Switzerland: International Federation for Structural Concrete (FIB); 2001.

[3] ACI 440.2R-17. Guide for the design and construction of externally bonded FRP systems for strengthening existing structures. Farmington Hills, MI, USA: American Concrete Institute; 2017.

[4] Correia JR. Perfis pultrudidos de fibra de vidro (GFRP) - Aplicação de vigas mistas GFRP-betão na construção. MSc thesis. Instituto Superior Técnico, 2004.

[5] Abdul-salam B. Behaviour of shear critical FRP reinforced concrete one-way slabs. PhD thesis. University of Sherbrooke, 2014. doi:10.13140/RG.2.1.2783.1844.

[6] Liu Y, Zwingmann B, Schlaich M. Carbon fiber reinforced polymer for cable structures-a review. Polymers 2015;7:2078–99. doi:10.3390/polym7101501.

[7] Bakis CE, Bank LC, Brown VL, Cosenza E, Davalos JF, Lesko JJ, et al. Fiber-Reinforced Polymer Composites for Construction—State-of-the-Art Review. Journal of Composites for Construction 2002;6:73–87. doi:10.1061/(ASCE)1090-0268(2002)6:2(73).

[8] Marsh G. Material trends for FRP boats. Reinforced Plastics 2003;47:23–34. doi:10.1016/S0034-3617(03)00931-7.

[9] Ed Coates Collection. No. 3879. Duramold F-46 (NC19131 c/n 5000) 2015. http://1000aircraftphotos.com/Contributions/Coates/3879.htm (accessed July 14, 2018).

[10] Gibson AG. The cost effective use of fibre reinforced composites offshore. 2003. doi:ISBN 0717625915.

[11] Schreiber R. The Stout Scarab – An Art Deco Automotive Artifact That Was Ahead of Its Time. The Truth About Cars 2014.

[12] Silva JDP da. Comportamento ao fogo de vigas de betão armado reforçadas à flexão com laminados de fibras de carbono (CFRP). MSc thesis. Instituto Superior Técnico, 2013.

[13] Halliwell S, Reynolds T. Effective Use of Fibre Reinforced Polymers Materials in Construction. United Kingdom: FBE Report 8, Centre for Composites in Construction, BRE Press; 2004.

[14] Firmo JP. Fire protection systems for reinforced concrete beams strengthened with CFRP laminates. MSc thesis. Instituto Superior Técnico – Technical University of Lisbon, 2010.

[15] Flickr. Hinder Ibach Bridge over the Muota River, Schwyz, Switzerland 2011.

[16] ARTIS Kreativ. Le Corbusier - die einzigartige Persönlichkeit 2017.

[17] Sonnenschein R, Gajdosova K, Holly I. FRP Composites and their Using in the Construction of Bridges. Procedia Engineering 2016;161:477–82. doi:10.1016/j.proeng.2016.08.665.

[18] S&P Clever Reinforcement Ibérica Lda. Basicis for S&P FRP-Systems. Seewen, Switzerland: 2018.

[19] Alkhrdaji T. Strengthening of Concrete Structures Using FRP Composites. STRUCTURE Magazine 2015:18–20.

[20] S&P C-Laminate. Carbon fiber polymer plates for structural reinforcement: product technical specifications. Seewen, Switzerland: 2018.

[21] S&P Clever Reinforcement Ibérica Lda. Case study_2015_01: reinforcement of columns with S&P C-Sheet 240. Zug, Switzerland: 2015.

[22] EasyComposites. Carbon fibre sheet. 2018 n.d.

[23] Global Sources Ltd. Carbon fiber rod. Global Sources Ltd, 2018.

[24] Vieira JD, Liu T, Harries KA. Flexural stability of pultruded glass fibre-reinforced polymer I-sections. Proceedings of the Institution of Civil Engineers - Structures and Buildings 2017:1–12. doi:10.1680/jstbu.16.00238.

[25] Yu B, Kodur VKR. Fire behavior of concrete T-beams strengthened with near-surface mounted FRP reinforcement. Engineering Structures 2014;80:350–61. doi:10.1016/j.engstruct.2014.09.003.

[26] A. S. F, Barros JAO, Padaratz IJ. Vigas de betão armado reforçadas com laminados de CFRP inseridos no betão de recobrimento. vol. 110. 2002.

[27] Mouritz AP, Mathys Z, Gibson AG. Heat release of polymer composites in fire. Composites Part A: Applied Science and Manufacturing 2006;37:1040–54. doi:10.1016/j.compositesa.2005.01.030.

[28] Correia JR, Branco FA, Ferreira JG. The effect of different passive fire protection systems on the fire reaction properties of GFRP pultruded profiles for civil construction. Composites Part A: Applied Science and Manufacturing 2010;41:441–52. doi:10.1016/j.compositesa.2009.12.002.

[29] Dodds N, Gibson AG, Dewhurst D, Davies JM. Fire behaviour of composite laminates. Composites Part A: Applied Science and Manufacturing 2000;31:689–702. doi:10.1016/S1359-835X(00)00015-4.

[30] Mouritz AP, Gibson AG. Fire properties of polymer composite materials. Dordrecht: Springer; 2006.

[31] Mohammadi M, Barghian M, Mostofinejad D, Rafieyan A. Alkali and temperature long-term effect on the bond strength of fiber reinforced polymer-to-concrete interface. Journal of Composite Materials 2018;52:2103–14. doi:10.1177/0021998317740201.

[32] Tadeu AJB, Branco FJFG. Shear Tests of Steel Plates Epoxy-Bonded to Concrete under Temperature. Journal of Materials in Civil Engineering 2000;12:74–80. doi:10.1061/(ASCE)0899-1561(2000)12:1(74).

[33] EN 1992-1-1. Eurocode 2: Design of concrete structures - Part 1-1 : General rules and rules for buildings. vol. 1. Brussels, Belgium: European Committee for Standardization (CEN); 2004.

[34] ISO 834-1. Fire resistance tests – elements of building construction, Part 1: general requirements. Geneva, Switzerland: International Organization for Standardization (ISO); 1999.

[35] ABAQUS CAE. Finite element analisys, Version 6.14-5. SIMULIA TM; 2015.

[36] Blontrock H. Analysis and modeling of the fire resistance of concrete elements with externally bonded FRP reinforcement. PhD thesis. Ghent University, 2003.

[37] Klamer EL, Hordijk DA, Janssen HJM. The influence of temperature on the debonding of externally bonded CFRP. Proceedings of 7th International Symposium on Fiber Reinforcement Polymer Reinforcement for Concrete Structures (FRPRCS-7), 2005, p. 1551–70.

[38] Klamer E-L. Influence of temperature on concrete beams strengthened in flexure with CFRP. PhD thesis. Eindhoven University of Technology, 2009. doi:10.6100/IR656177.

[39] Firmo JP, Correia JR, Pitta D, Tiago C, Arruda MRT. Experimental characterization of the bond between externally bonded reinforcement (EBR) CFRP strips and concrete at elevated temperatures. Cement and Concrete Composites 2015;60:44–54. doi:10.1016/j.cemconcomp.2015.02.008.

[40] Ferrier E, Agbossou A. Temperature effects on the shear capacity of external bonded fiber reinforced polymer on concrete. Construction and Building Materials 2017;152:333–44. doi:10.1016/j.conbuildmat.2017.07.002.

[41] Wu Z, Iwashita K, Yagashiro S, Ishikawa T, Hamaguchi Y. Temperature Effect on Bonding and Debonding Behavior between FRP Sheets and Concrete. Journal of the Society of Materials Science, Japan 2005;54:474–80. doi:10.2472/jsms.54.474.

[42] Gamage JCPH, Wong MB, Al-Mahadi R. Performance of CFRP strengthened concrete members under elevated temperatures. Proceeding of the International Sysposium on Bond Behaviour of FRP in Structures (BBFS 2005), International Institute for FRP in Construction; 2005, p. 113–8.

[43] Leone M, Matthys S, Aiello MA. Effect of elevated service temperature on bond between FRP EBR systems and concrete. Composites Part B: Engineering 2009;40:85–93. doi:10.1016/j.compositesb.2008.06.004.

[44] Dai J-G, Gao WY, Teng JG. Bond-Slip Model for FRP Laminates Externally Bonded to Concrete at Elevated Temperature. Journal of Composites for Construction 2013;17:217–28. doi:10.1061/(ASCE)CC.1943-5614.0000337.

[45] Dai J, Ueda T, Sato Y. Development of the Nonlinear Bond Stress–Slip Model of Fiber Reinforced Plastics Sheet–Concrete Interfaces with a Simple Method. Journal of Composites for Construction 2005;9:52–62. doi:10.1061/(ASCE)1090-0268(2005)9:1(52).

[46] Gao WY, Teng JG, Dai J-G. Effect of temperature variation on the full-range behavior of FRP-to-concrete bonded joints. Journal of Composites for Construction 2012;16:671–83. doi:10.1061/(ASCE)CC.1943-5614.0000296.

[47] Gamage JCPH, Al-Mahaidi R, Wong MB. Bond characteristics of CFRP plated concrete members under elevated temperatures. Composite Structures 2006;75:199–205. doi:10.1016/j.compstruct.2006.04.068.

[48] Arruda MRT, Firmo JP, Correia JR, Tiago C. Numerical Modelling of the bond between concrete and CFRP laminates at elevaded temperatures. Engineering Structures 2016;110:233–43. doi:http://dx.doi.org/10.1016/j.engstruct.2015.11.036.

[49] DIANA FEA BV. User's manual, Version 9.1. Delft, Netherlands: 2005.

[50] Strand7. User's manual, Version 2.2.5. Strand7 Pty Ltd; 2003.

[51] Gamage JCPH, Wong MB, Al-Mahadi R. Bond performance of CFRP plated concrete members at elevated temperatures. Proceedings of Australian structural engineering conference (ASEC), Newcastle, Australia: 2005.

[52] Gamage JCPH, Al-Mahaidi R, Wong MB. Effect of insulation on the bond behaviour of CFRP-Plated concrete elements 2005:119.

[53] AS1530.4. Methods for fire tests on building materials, components and structures - Part 4: Fire-resistance tests of elements of building construction. Sydney, Australia: Standards Australia; n.d.

[54] ABAQUS CAE. Analisys standard user's manual, Version 6.11. Rhode Island, USA: Dassault systèmes; 2011.

[55] Ahmed A, Kodur V. The experimental behavior of FRP-strengthened RC beams subjected to design fire exposure. Engineering Structures 2011;33:2201–11. doi:10.1016/j.engstruct.2011.03.010.

[56] Firmo JP, Correia JR, França P. Fire behaviour of reinforced concrete beams strengthened with CFRP laminates: Protection systems with insulation of the anchorage zones. Composites Part B: Engineering 2012;43:1545–56. doi:10.1016/j.compositesb.2011.09.002.

[57] Firmo JP, Correia JR. Fire behaviour of thermally insulated RC beams strengthened with EBR-CFRP strips: Experimental study. Composite Structures 2015;122:144–54. doi:10.1016/j.compstruct.2014.11.063.

[58] Williams B, Kodur V, Green MF, Bisby L. Fire endurance of fiber-reinforced polymer strengthened concrete T-Beams. ACI Structural Journal 2008;105:60–7.

[59] Adelzadeh M, Green MF, Bénichou N. Behaviour of fibre reinforced polymer-strengthened T-beams and slabs in fire. Proceedings of the Institution of Civil Engineers - Structures and Buildings 2012;165:361–71. doi:10.1680/stbu.11.00014.

[60] Deuring M. Brandversuche an Nachtraglich Verstarkten Tragern aus Beton. Research Report EMPA No 148, 795 1994.

[61] Grace N, Bebawy M. Fire protection for beams with fiber-reinforced polymer flexural strengthening systems. ACI Structural Journal 2014. doi:10.14359/51686729.

[62] Blontrock H, Taerwe L, Vandevelde P. Fire tests on concrete beams strengthened with fibre composite laminates. Proceedings of the Third PhD Symposium, Vienna, 2000 2000;Volume 2:151–61.

[63] ASTM E119. Standard test methods for fire tests of building construction and materials. West Conshohocken, USA: American Society for Testing and Materials; 2002.

[64] ASTM D4065. Standard practice for plastics: dynamic mechanical properties: determination and report of procedures. West Conshohocken, USA: American Society for Testing and Materials; 2006.

[65] Hawileh RA, Naser M, Zaidan W, Rasheed HA. Modeling of insulated CFRP-strengthened reinforced concrete T-beam exposed to fire. Engineering Structures 2009;31:3072–9. doi:10.1016/j.engstruct.2009.08.008.

[66] Ahmed A, Kodur VKR. Effect of bond degradation on fire resistance of FRP-strengthened reinforced concrete beams. Composites Part B: Engineering 2011;42:226–37. doi:10.1016/j.compositesb.2010.11.004.

[67] Dai JG, Gao WY, Teng JG. Finite Element Modeling of Insulated FRP-strengthened RC Beams Exposed to Fire. Civil Engineering 2010. doi:10.1061/(ASCE)CC.1943-5614.0000509.

[68] Firmo JP, Arruda MRT, Correia JR. Numerical simulation of the fire behaviour of thermally insulated reinforced concrete beams strengthened with EBR-CFRP strips. Composite Structures 2015;126:360–70. doi:10.1016/j.compstruct.2015.02.084.

[69] Firmo JP, Arruda MRT, Correia JR, Rosa IC. Three-dimensional finite element modelling of the fire behaviour of insulated RC beams strengthened with EBR and NSM CFRP strips. Composite Structures 2018;183:124–36. doi:10.1016/j.compstruct.2017.01.082.

[70] ANSYS. Finite element computer code, Version 11. Canonsburg, USA: ANSYS, Inc.; 2007.

[71] Kodur VKR, Ahmed A. Numerical Model for Tracing the Response of FRP-Strengthened RC Beams Exposed to Fire. Journal of Composites for Construction 2010;14:730–42. doi:10.1061/(ASCE)CC.1943-5614.0000129.

[72] GangaRao HVS, Taly N, Vijay P V. Reinforced Concrete Design with FRP Composites. Boca Raton, USA: CRC Press; 2007.

[73] ABAQUS CAE. Analisys standard user's manual, Version 6.8. Rhode Island, USA: Dassault systèmes; 2008.

[74] Griffis CA, Masumura RA, Chang CI. Thermal response of graphite epoxy composite subjected to rapid heating. Journal of Composite Materials 1981;15:427–42. doi:10.1177/002199838101500503.

[75] FIB. The FIB Model Code for Concrete Structures, Model Code. Lausanne, Switzerland: International Federation for Structural Concrete (FIB); 1990.

[76] Firmo JP, Arruda MRT, Correia JR. Contribution to the understanding of the mechanical behaviour of CFRP-strengthened RC beams subjected to fire: Experimental and numerical assessment. Composites Part B: Engineering 2014;66:15–24. doi:10.1016/j.compositesb.2014.04.007.

[77] TML Tokyo Sokki Kenkyujo Co., Ltd. TML Strain gauges: product technical specifications. Tokyo, Japan: 2017.

[78] TML Tokyo Sokki Kenkyujo Co. L. Operation manual of TML strain gauge adhesive type NP-50B. Tokyo, Japan: 2018.

[79] EN 206-1. Concrete - Part 1: Specification, performance, production and conformity. Brussels, Belgium: European Committee for Standardization (CEN); 2000.

[80] CIMPOR. Cimento Portland de Calcário - CEM II/A-L 42,5R: ficha técnica. Lisbon, Portugal: 2014.

[81] BASF Construction Chemicals España, S.L. MasterPozzolith 7002: ficha técnica. Barcelona, Spain: 2017.

[82] S&P Clever Reinforcement Ibérica Lda. S&P Resin 220: epoxi adhesive. Seewen, Switzerland: 2018.

[83] RESCOLL Société de Recherche. Dynamic Mechanical Analysis (DMA) to determine the glass transition temperature of the RESIN 220HP: test results, Pessac, France: Analysis Bulletin no. 1705283b; 2017, p. 1–4.

[84] ASTM-E1640. Standard test method for assignment of the glass transition temperature by dynamic mechanical analysis. West Conshohocken, USA: American Society for Testing and Materials; 2013.

[85] Leone M, Matthys S, Aiello MA. The Influence of Service Temperature on Bond between FRP Reinforcement and Concrete 2006:1–11.

[86] Palmieri A, Matthys S, Taerwe L. Bond behavior of NSM FRP bars at elevated temperatures. Proceedings of First Middle East Conference on Smart Monitoring Assessment and Rehabilitation of Civil Structures (SMAR 2011), Dubai: 2011, p. 8.

[87] Firmo JP, Correia JR, Bisby LA. Fire behaviour of FRP-strengthened reinforced concrete structural elements: A state-of-the-art review. Composites Part B: Engineering 2015;80:198–216. doi:10.1016/j.compositesb.2015.05.045.

[88] Firmo JP, Correia JR, Pitta D, Tiago C, Arruda MRT. Bond Behavior between Near-Surface-Mounted CFRP Strips and Concrete at High Temperatures. Journal of Composites for Construction 2015;19:4014071. doi:10.1061/(ASCE)CC.1943-5614.0000535.

[89] Perlita y Vermiculita, SL. Biofire: product technical specifications. vol. 1. Barcelona, Spain: 2008.

[90] Secil Martingança, SA. RHP manual interior: product technical specifications. Leiria, Portugal: 2013.

[91] Argex – Argila Expandida SA. ARGEX® 0-2: product technical information. vol. 3. Aveiro, Portugal: 2008.

[92] EN 1363-1. Fire resistance tests - Part 1: General requeriments. Brussels, Belgium: European Committee for Standardization (CEN); 1999.

[93] ABAQUS CAE. Abaqus analisys user's guide, Version 6.14. Rhode Island, USA: Dassault systèmes; 2015.

[94] Laím L, Paulo J, Rodrigues C, Simões L. Experimental and numerical analysis on the structural behaviour of cold-formed steel beams. PhD thesis. University of Coimbra, 2013.

[95] ABAQUS CAE. Abaqus theory guide, Version 6.14. Rhode Island, USA: Dassault systèmes; 2015.

[96] Annexe Nationale à la NF EN 1992-1-2. Eurocode 2 : Calcul des structures en béton - Partie 1-2: Règles générales - Calcul du comportement au feu. vol. 2. Saint-Denis, France: Association Française de Normalisation (AFNOR); 2007.

[97] EN 1993-1-2. Eurocode 3: Design of steel structures - Part 1-2: General rules - structural fire design. vol. 2. Brussels, Belgium: European Committee for Standardization (CEN); 2010.

[98] Bai Y, Keller T, Correia JR, Branco FA, Ferreira JG. Fire protection systems for building floors made of pultruded GFRP profiles - Part 2: Modeling of thermomechanical responses. Composites Part B: Engineering 2010;41:630–6. doi:10.1016/j.compositesb.2010.09.019.

[99] MAXIT International. Thermal properties at high temperatures of clay concrete, Internal Report. Denmark: 2005.

[100] EN 1994-1-2. Eurocode 4: Design of composite steel and concrete structures - Part 1-2: General rules - structural fire design. Brussels, Belgium: European Committee for Standardization (CEN); 2005.

[101] Wang K, Young B, Smith ST. Mechanical properties of pultruded carbon fibre-reinforced polymer (CFRP) plates at elevated temperatures. Engineering Structures 2011;33:2154–61. doi:10.1016/j.engstruct.2011.03.006.

[102] Bisby LA. Fire behaviour of FRP reinforced or confined concrete. PhD thesis. Queen's University, 2003.

[103] Selamet S, Garlock M. Guidelines for modeling three dimensional structural coneection models using finite element methods. Proceedings of the International Symposium on Steel Structures: Culture and Sustainability 2010:351–60.

[104] Moltubakk ØT. Nonlinear analysis of fibre reinforced concrete beams: Influence of fibre orientation and density. MSc thesis. Norwegian University of Science and Technology, 2014.

APPENDIX A PHOTOS OF THE FAILURE MODES OF CFRP-STRENGTHENED CONCRETE BLOCKS AT AMBIENT AND ELEVATED TEMPERATURES

A.1 TA Series Specimens

Figure A.1 – Failure mode in the concrete substrate for the TA-1 specimen tested at ambient temperature (perspective view on the left and front view on the right)

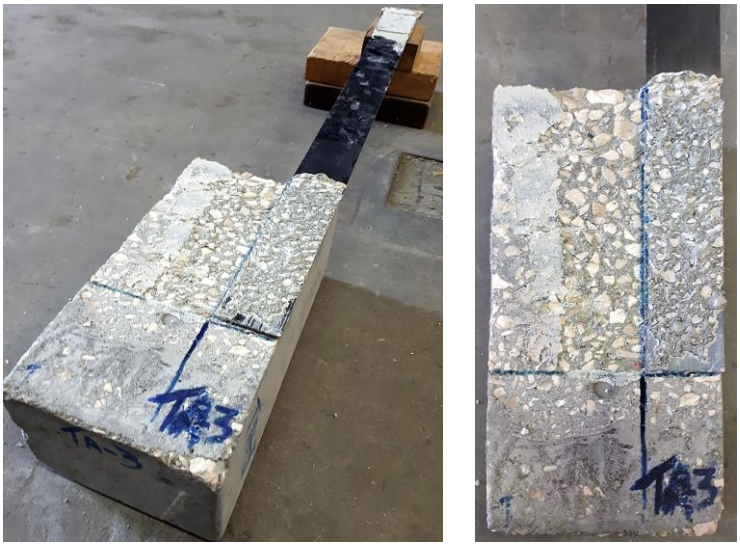

Figure A.2 – Failure mode in the concrete substrate for the TA-3 specimen tested at ambient temperature (perspective view on the left and front view on the right)

A.2 T40 Series Specimens

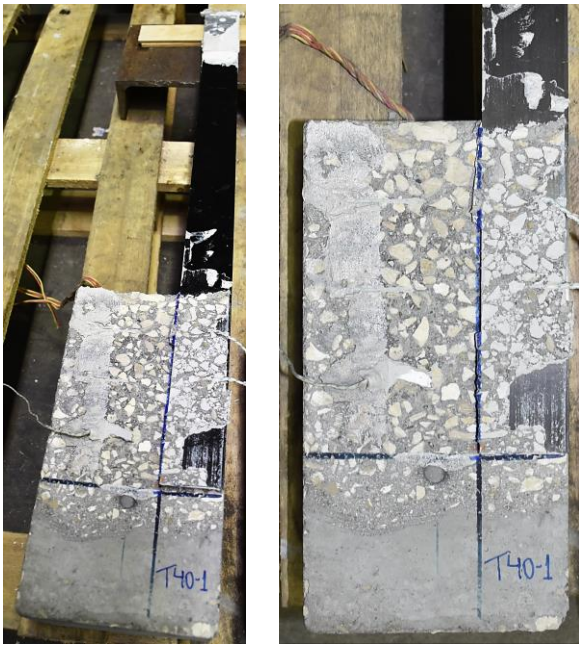

Figure A.3 – Failure mode in the concrete substrate for the T40-1 specimen tested at 40º C (perspective view on the left and front view on the right)

Figure A.4 – Failure mode in the concrete substrate for the T40-3 specimen tested at 40º C (perspective view on the left and front view on the right)

A.3 T65 Series Specimens

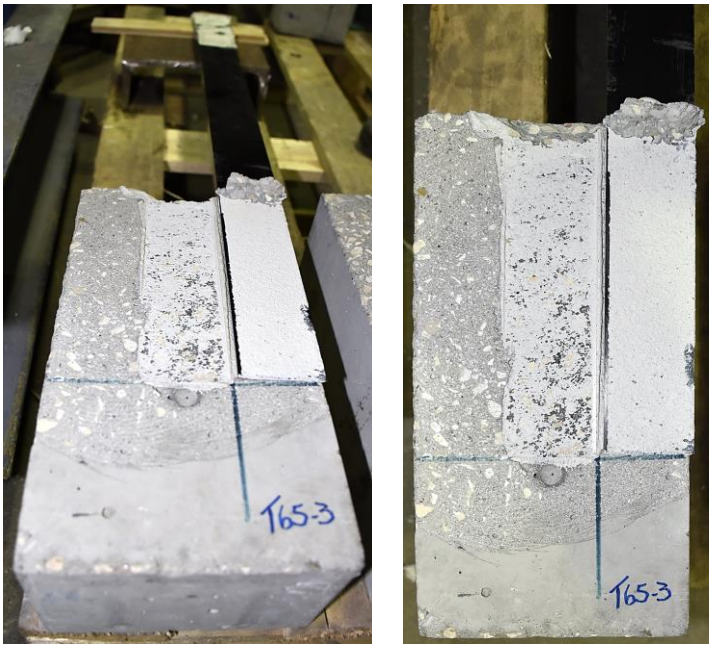

Figure A.5 – Failure mode in the adhesive at the CFRP-concrete interface for the T65-3 specimen tested at 65º C (perspective view on the left and front view on the right)

A.4 T90 Series Specimens

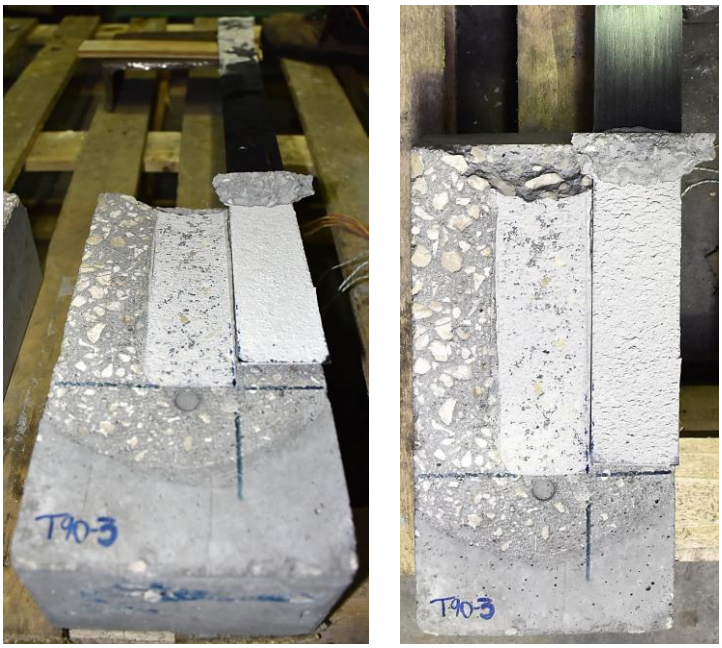

Figure A.6 – Failure mode in the adhesive at the CFRP-concrete interface for the T90-3 specimen tested at 90º C (perspective view on the left and front view on the right)

A.5 T115 Series Specimens

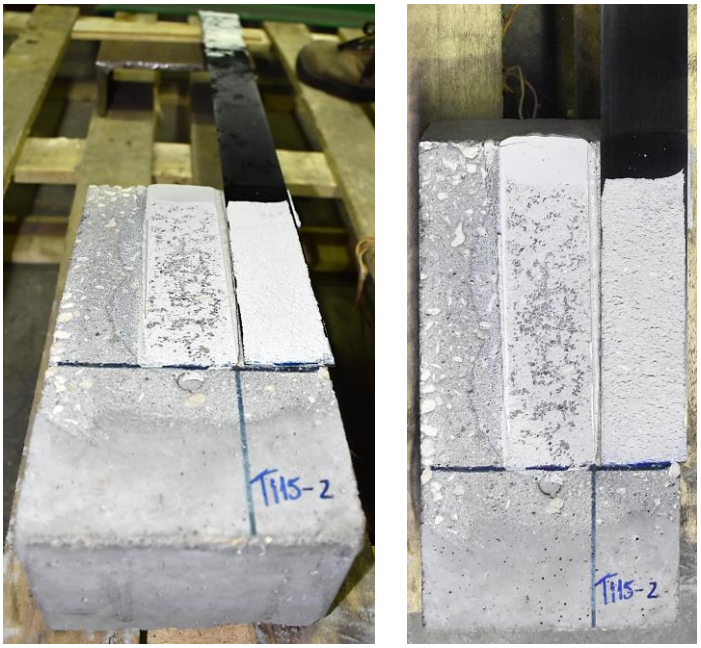

Figure A.7 – Failure mode in the adhesive at the CFRP-concrete interface for the T115-2 specimen tested at 115º C (perspective view on the left and front view on the right)

A.6 T140 Series Specimens

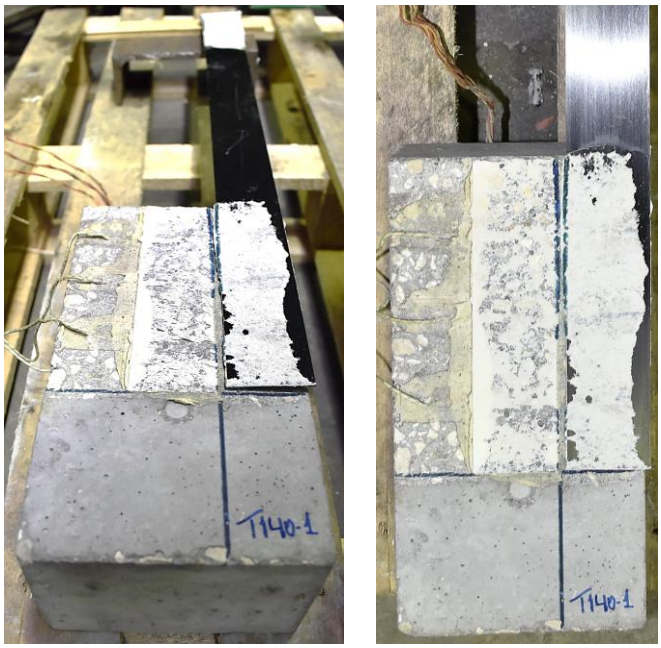

Figure A.8 – Failure mode in the adhesive at the CFRP-concrete interface for the T140-1 specimen tested at 140º C (perspective view on the left and front view on the right)

A.7 T165 Series Specimens

Figure A.9 – Failure mode in the adhesive at the CFRP-concrete interface for the T140-1 specimen tested at 140º C (perspective view on the left and front view on the right)

APPENDIX B PHOTOS OF THE FAILURE MODES OF CFRP-STRENGTHENED AND SIMPLE RC BEAMS SUBJECTED TO FIRE

B.1 Simple RC Beam

Figure B.1 – Failure mode of the RC beam after fire resistance test (front view)

B.2 CFRP-strengthened Beams

B.2.1 EC-20 Beam

Figure B.2 – Failure mode of the EC-20 beam after fire resistance test

B.2.2 EC-50 Beam

Figure B.3 – Failure mode of the EC-50 beam after fire resistance test

B.2.3 OP-20 Beam

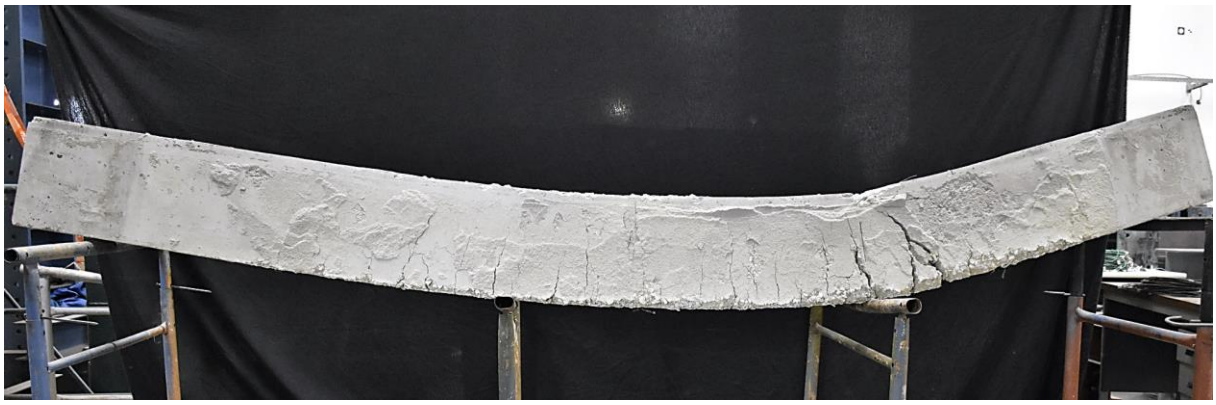

Figure B.4 – Failure mode of the OP-20 beam after fire resistance test

B.2.4 OP-50 Beam

Figure B.5 – Failure mode of the OP-50 beam after fire resistance test

B.2.5 VP-20 Beam

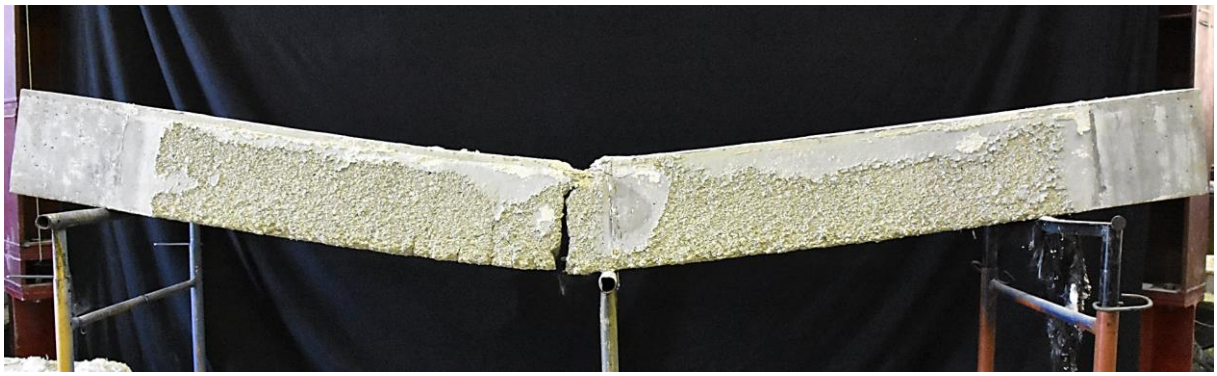

Figure B.6 – Failure mode of the VP-20 beam after fire resistance test

B.2.6 VP-35 Beam

Figure B.7 – Failure mode of the VP-35 beam after fire resistance test

B.2.7 VP-50 Beam

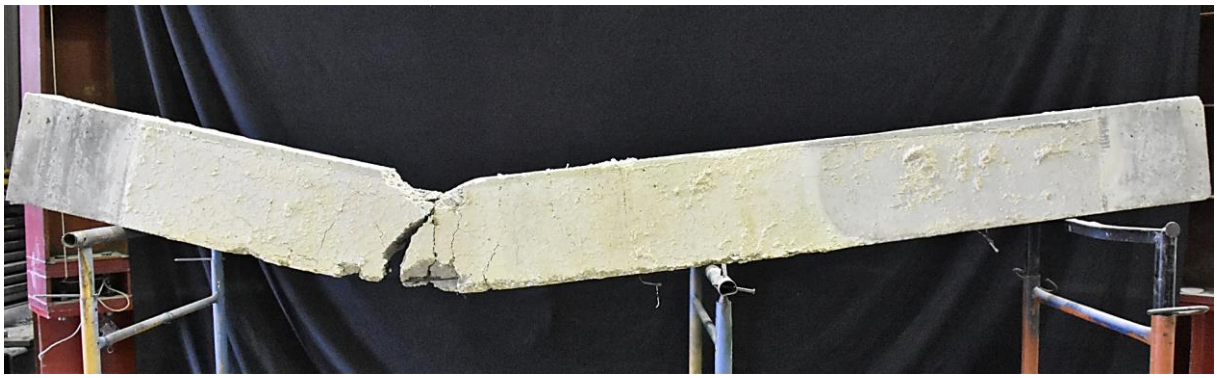

Figure B.8 – Failure mode of the VP-50 beam after fire resistance test